Biomechanical Design Prognosis and Preclinical Assessment of Bone Plates Used to Treat Extracapsular Femoral Fractures

Thesis submitted to

Indian Institute of Technology Guwahati

for the award of the degree

of

Doctor of Philosophy

by

Pratik Nag

(Roll Number: 176106027)

Under the supervision of

Dr. Souptick Chanda

Department of Biosciences and Bioengineering

Indian Institute of Technology, Guwahati.

Guwahati 781039, Assam, India

March, 2023

"Dive deep into yourself,
for this is the way which leads
you to the knowledge of all soul
and to the love of all beings."

~ Swami Swarupananda
(His Holy Words)

For

Pratima Nag, mother

and

Dilip Kumar Nag, father

DECLARATION

I declare that

a. the work contained in this thesis is original and has been done by me under the guidance of my supervisors.
b. the work has not been submitted to any other Institute for any degree or diploma.
c. I have followed the guidelines provided by the Institute in preparing the thesis.
d. I have conformed to the norms and guidelines given in the Ethical Code of conduct of the Institute.
e. whenever I have used materials (data, theoretical analysis, figures, and text) from other sources, I have given due credit to them by citing them in the text of the thesis and giving their details in the references. Further, I have taken permission from the copyright owners of the sources, whenever necessary

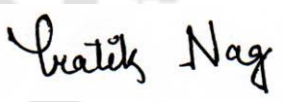

Pratik Nag

CERTIFICATE OF APPROVAL

Thesis submitted on
Date: 26.07.2022

Certified that the thesis entitled '**Biomechanical Design Prognosis and Preclinical Assessment of Bone Plates used to Treat Extracapsular Femoral Fractures**' submitted by **Patik Nag** to **Indian Institute of Technology Guwahati**, is a record of an original research work carried out by him under my supervision and guidance. The thesis has fulfilled all requirements as per the regulations of the institute and in my opinion has reached the standard needed for submission. The findings embodied in this thesis have not been submitted to any other University or Institute for the award of any degree or diploma

Signature:

Dr. Souptick Chanda
Assistant Professor
Department of Biosciences and Bioengineering
Indian Institute of Technology Guwahati
Guwahati-781039, Assam, India

Dr. Souptick Chanda
Assistant Professor
Department of Biosciences and Bioengineering
Indian Institute of Technology Guwahati
Guwahati-781039, Assam, India

Acknowledgement

A PhD journey is often no less than a roller coaster ride. But as it is rightly said “all is well that ends well” and by God’s grace when all the cumulative efforts get paid off, joy knows no bound. Therefore, with great pleasure, I take this humble opportunity to express my sincere and heartfelt gratitude to my supervisor Dr. Souptick Chanda for believing in me and providing his valuable guidance and encouragement throughout the course of my Ph.D. work. Apart from his consistent instructions and positive outlook regarding work, his perspective towards life and philosophy and many a time the discussions revolving around them kept my motivation going, making this journey altogether memorable and enriching. His continuous support, constant availability for related discussions has generated in me a spirit of adventure in regard to research.

I would like to sincerely acknowledge my Doctoral Committee, Dr. Cota Navin Gupta from Department of Bioscience and Bioengineering, Prof. Debabrata Chakraborty and Dr. Atanu Banerjee from Department of Mechanical Engineering for their insightful observations and suggestions at various stage of the research study. I am indebted to Dr. Bhaskar Borgohain, Head of the Department, Department of Orthopedics, NEIGRIHMS (Shillong) for being an active collaborator and sharing his valuable experience from time to time. His expertise contributed to the design and fabrication of the novel implant (DODO) for NE people of India. I owe a huge debt of gratitude to Prof. Gautam Biswas, Professor, Department of Mechanical Engineering, IIT Kanpur whose spellbound dedication towards research ignited the light of research in me. His inspiration and motivation made sure I stay focus to research only. He continues to inspire us, through his hard-work and passion for science and research, to lend our best efforts. I am sincerely thankful to Prof. Amaresh Dalal, Department of Mechanical Engineering, IIT Guwahati for always taking care of me in my Ph.D. journey and providing various fruitful suggestions related to work and life. I am thankful to the Ministry of Education (formerly MHRD) for awarding me with the Prime Minister Research Fellowship (PMRF) during my doctoral degree. I also wish to place on record the use of some sophisticated facilities at Central Instrumental Facility, IIT Guwahati and Harvard University, USA for the research work. Further I express my sincere gratitude to the Heads and authorities of the Department of Bioscience and Bioengineering for their cooperation and various help. I would also like to thank all the technical staff of the department for providing me all the assistance for the completion of my work. I am fortunate enough to have some real good friend and seniors to

resolve any queries and problems. I would like to convey my sincere thanks to Sambit Majumder, Pallab Banik, Chandi Charan Patra, Bipra Chatterjee, Neeraj Kumar for their continuous support and various help related to the research work. I also wish to thank all of my friends, especially Dibyojyoti, Sagnik, Parnab, Tanmoy, Supratik, Kaustabh, Pratik, Ekramul, Anurag, Ajit and many more, who helped me in different ways and encouraged me during the critical phases of the study. In addition, a heartfelt thanks to my lab mates Rahul, Jaideep, Soumyadeep, Rajdeep, Ankan and others for all their supports. My special thanks to Mrs. Titir Chanda, wife of Dr. Souptick Chanda and Mrs. Soumita Dalal, wife of Dr. Amaresh Dalal for being gracious hosts and taking care of me like family during my stay at IIT Guwahati.

I express my sincere gratitude and my heart-felt love to my cousins, sister-in-law, my nephew Aumee, and my relatives for their love and affection. My mother, Pratima Nag, stood like a rock with me and supported all my decisions. She continues to make sure I perform the best through her prayers and suggestions. My father, Dilip Kumar Nag, has been a constant source of inspiration to me. He instilled into me a strong character which is helping me every day on both personal and professional level. Also, worth mentioning my in-laws, Mr. Gautam Bose and Mrs. Geetanjali Bose, for their continuous support, love and good wishes. I would like to express my appreciation to my elder brother, Deepayan Nag, who continues to guide me and had been part of infinite long discussions related to the work and life. Finally, I would like to specially mention the contributions of my wife, Devleena Bose, who has been my constant support and a true critic of my work and my companion through thick and thin. Without her moral support and constant encouragement, the thesis wouldn't have been possible to complete in time and in high spirit.

Abstract

The incidence of extracapsular femoral fracture is increasing with relatively high mortality, which requires immediate surgical interventions. The aim of surgical treatment is to provide initial fixation/rigidity such that the broken bones re-join through secondary bone healing. Such healing usually involves the need for fixation devices, e.g., bone plates, nails, external fixators etc. However, attaching such stiff, metallic fixation devices leads to excessive stress shielding causing impediment to healing. Osteoporosis and subsequent cortical thinning are the adverse outcome of stress shielding. Also, when a plate is in direct contact and pressed down to the bony surface, it can disturb blood flow to the underlying cortex. Thus, successful operative intervention depends on three crucial aspects, e.g., stability of fixation, bone fracture healing and post-operative cortical thinning. The concerned mechanical aspects and biological phenomena motivate to computationally predict the ideal implant for a particular patient. The thesis employs methods to biomechanically investigate the effect of different bone plates related to various fractures. Finite element (FE) models are used as tool to predict post-operative implant stability for different types of bone plates, fixated to proximal femoral fractures. The predicted results accorded well with various previous experimental observations. The present study vividly identified the different initial response in healing under different fixation stabilities. The investigation was able to forecast the regions of failure associated to implants under both physiological loading and extreme cases of fall and to highlight the probable reasons. Further, the study proposed a novel design of implant considering regional morphometry of Northeast India. The prognosis of cortical thinning due to implantation and simulation of bone fracture healing studied in the thesis, different treatment strategies can be predicted, and the optimal strategy can be chosen, which then can reduce the healing time and lighten the economic burden and pain for the patients.

Keywords: proximal femoral fracture, finite element analysis, patient specific implant, bone remodelling, cortical thinning, tissue differentiation, fuzzy logic.

Contents

List of symbols and abbreviations

Most of the symbols and abbreviations are defined as they occur in the thesis. Some of the mostly used symbols and abbreviations are listed below.

Symbols

E	Young's Modulus
ρ	Apparent density of bone
S_i	Strain energy density of the i^{th} node
S_{ref}	Reference strain energy density
b_i	Normal displacement of surface node
$\mu\varepsilon$	micro-strain
R	Correlation coefficient
σ_i	Principal stress in the respective direction
τ_{ij}	Shear stress in the ij plane
b	Regression Slope
N_{neigh}	Nearest neighbouring elements
v	Poisson's ratio

Abbreviations

2D	Two Dimensional
3D	Three Dimensional
AO	Association of Osteosynthesis
BC	Boundary Condition
BW	Body Weight (in kg)
CAD	Computer Aided Design
CAGR	Compound Annual Growth Rate
CT	Computed Tomography
DCP	Dynamic Compression Plating
DHS	Dynamic Hip Screws
DIC	Digital Image Correlation
EF	External Fixations
EM	Extra Medullary
Eq.	Equation
FE	Finite Element
Fig.	Figure
HU	Hounsfield Unit
IM	Intra Medullary
LP	Locking Plate
NE	Northeast
PE	Percentage Error
PFF	Proximal Femoral Fractures
PFLP	Proximal Femoral Locking Plate
PMMA	Polymethyl metacrylate
PSP	Patient Specific Plate
ROI	Region of Interest
SD	Standard Deviation

SE	Standard Error
SED	Strain Energy Density
SFF	Subtrochanteric Femoral Fracture
Ti	Titanium
UTM	Universal Testing Machine
VA-DHS	Variable Angle Dynamic Hip Screw

List of figures

List of tables

Chapter 1

Introduction and Review of Literature

1.1 Introduction

The incidences of femoral fractures have increased significantly in recent decades. Extracapsular femoral fracture, commonly known as hip fracture, accounts for a large proportion of hospitalisation in trauma cases. It occurs at the proximal end of the femur (thigh bone), near the hip. In the vast majority of cases, these fractures occur due to a fall or minor trauma in someone with weakened osteoporotic bone. This has been closely linked to the global rise in the elderly population since most fracture occurs predominantly in older people, and the frequency of incidence increases with advancing age (Sartori et al., 2017; Wilson, 2007). The total number of incident fragility fractures is estimated to be 9 million annually worldwide (Johnell et al., 2006). In the United States alone, the number of osteoporotic fractures was estimated to exceed 2 million in 2005, and the total costs of these fractures were estimated to be around $17 billion (Burge et al., 2007). Nonvertebral fractures, which typically occur in cortical bone (e.g., fractures of the hip, legs, upper arms, and forearms), were estimated to account for 73% of the total number of fractures and 94% of the health care costs. Thoracic and lumbar vertebral fractures are common from low-impact or high-impact trauma and are estimated at 27% of fragility fractures (Burge et al., 2007). While around 1.3 million hip fractures were reported globally in 1990, the number is estimated to range between 7.3 and 21.3 million by 2050 (Gullberg et al., 1997). Osteoporotic fragility fractures, specifically proximal femoral fractures (PFFs), occur in increasing numbers due to the ageing of the population, with over 500,000 annual cases in Europe (Borgström et al., 2020). Worldwide, PFFs will reach 2.6 million cases per year by 2025 and 6.25 million by 2050 (Cooper et al., 1992; Borgström et al., 2020). The Asian region would account for over half of the hip fractures by the end of 2050 (Cooper, 1992). Hip fracture characteristics included intertrochanteric fractures (nearly 60%), followed by femoral neck fractures (almost 30%) and subtrochanteric fractures (almost 10%) (Bishnoi, 2018). More than 90% of all hip fractures are due to sideways fall (Nevitt, 1989).

Elderly patients afflicted by decreased visual acuity and muscle imbalance may slip and fall, resulting in such fractures. A report on India in 2004 estimated an annual incidence of 600,000 osteoporotic hip fractures (Kanis, 2014), which is supposed to increase significantly by 2026, as the share of people over 60 years rises to 12.4% of the 1.36 billion population (Government of India report, 2015). Comorbidities are high in patients with PFFs, with 50% of PFFs occurring in people with pre-existing nursing care needs (Rapp, 2019).

If the fracture happens to be in normal bone, then it is primarily due to high energy trauma such as car accidents, falling from a height or sports injury. These fractures are treated by orthopaedic surgery, which involves implanting some orthopaedic devices. The healing process may continue for anytime between 4-6 months. Treatment of such fracture is based on the attempts to achieve anatomic reduction, which will allow early functional therapy and rehabilitation. Owing to patients' advanced age and multiple comorbidities, fracture of the proximal femur is often life-threatening: in the first postoperative year, mortality rates may be as high as 30% (Kraus, 2011).

The growth in demand for the orthopaedic device market is mainly due to rising elder populations, innovations in surgeries, increasing accidents and sports-related injuries, growing obesity and expanding average weight of the population. The global orthopaedic device market size was USD 53.44 billion in 2019 and is forecasted to reach USD 68.51 billion by 2027, exhibiting a CAGR of 6.6% during the period (Fortune Business Insight, 2020). However, high coast associated with clinical procedures involving orthopaedic implants treatment and stringent government policies restricts the growth. Though emerging economies having well developed healthcare infrastructures, large medical reimbursement coverage fuelled the growth of market in near future. In a study conducted by Allied Market Research, in the forecasted period of 2019 to 2026, the hip orthopaedic devices are projected to be the fastest growing segment. North America was the leading contributor in the global orthopaedic device market and is anticipated to continue the trend (Allied Market Research, 2020; Fortune Business Insight, 2020). Europe is the second largest market mainly due to the growing awareness towards modern orthopaedic device and increase in healthcare expenditure by the population in the region. Asia Pacific is projected to register a comparatively higher CAGR during the period 2019 to 2027 owing to large patient pools and the expanding healthcare spending. In India, the orthopaedic device market was valued at around USD 1540.41 million in FY2020 and is expected to grow at CAGR of 7.71%.

In another report, it was forecasted that the Indian orthopaedic device market is expected to grow around 20% a year for the next decade to reach $2.5 billion (Rs. 16,000 crore) by 2030 (Sathguru Management Consultant Reports, 2016). The Indian orthopaedic devices market is worth around $375 million or Rs. 2,400 crores, of which knee and hip joints constitute alone a staggering 54%. The market is further expected to rise due to increase in healthcare expenditure through FY2026. The joint reconstruction product segment mainly dominates the market. Among the entire India, South India is expected to dominate the market due to better healthcare infrastructure and health awareness among the people.

1.2 Anatomy and Biomechanics of the hip joint

1.2.1 Anatomical planes and terminology

Typical orientations of the different anatomic planes are presented in Fig. 1.1 and discussed.

- Frontal (Coronal) plane: A plane perpendicular to the ground dividing the body into an anterior (front) and a posterior (ventral and dorsal) portion.
- Transverse (Axial or Horizontal) Plane: A plane which is parallel to the ground, dividing the body or limbs into upper and lower parts.
- Sagittal (Median) Plane: A plane which is perpendicular to both the transverse and coronal plane, running from front to back (Anterior-Posterior), dividing the body into right and left parts.

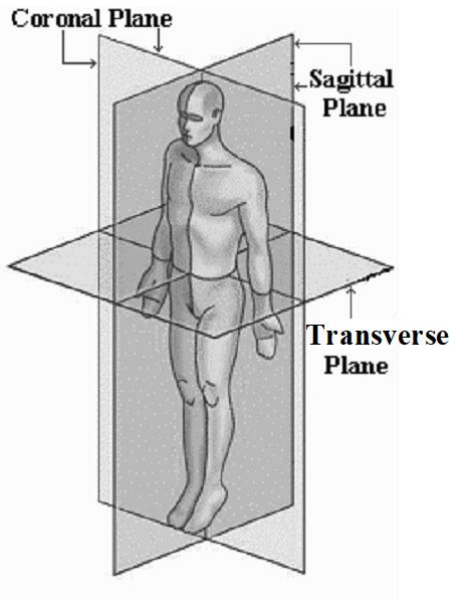

Fig. 1.1: Sketch showing the anatomical planes of reference.

- *Anterior (Ventral):* Towards the front.
- *Posterior (Dorsal):* Towards the back.
- *Superior:* Towards the head.
- *Inferior:* Towards the feet.
- *Proximal:* Closer to the trunk.
- *Distal:* Farther from the trunk.
- *Lateral:* A point or area more distant from the median plane.

- *Medial:* A point or area that is closer to the median plane.

While considering a four-legged animal, the zoologists refer to the head as anterior, the tail as posterior, the animal back as dorsal and under the belly side as ventral. Anatomists, while considering the human body refer to the head as superior, the feet as inferior, the front of the body as anterior or ventral and the back of the body as posterior or dorsal.

1.2.2 Hip Anatomy

The hip articulation is a diarthrodial ball and socket style joint formed from the head of the femur as it articulates with the acetabulum of the pelvis. The primary connection between the bones of the trunk and lower limbs of the human skeletal system is formed by the hip joint. The hip joints mainly transfer the load from the trunk to the lower limb besides supporting the body weight. The main part of the joint constitutes a ball (femoral head) and a hemispherical socket (acetabulum). The femoral head is situated at the top of the thigh bone (femur), and it fits into the acetabulum of the pelvis by means of bands of tissue called ligaments (hip capsule). The ligament provides stability to the joint. A smooth, durable cover of articular cartilage (a protein substance) cushions the end of the bone between the two bone surfaces (femoral head and acetabulum) and enables them to move easily. The motions concerned with the hip are shown in Fig. 1.2 and discussed:

- *Flexion:* Forward and upward movement of the femur at the hip occurs at the sagittal plane about a medial-lateral axis.
- *Extension:* Upward movement towards the rear of the body of the femur at the hip occurring at the sagittal plane.
- *Abduction:* Movement of the femur on the hip in the

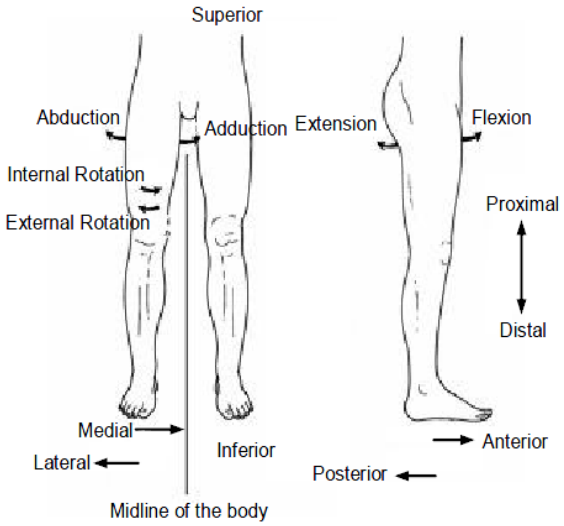

Fig. 1.2: Anatomical directions and movements of the hip joint (Martini and Bartholomew, 2000).

direction away from the midline of the body in the frontal plane.

- *Adduction:* Movement of the femur on the hip in a direction towards the midline of the body in the transverse plane.
- *Internal rotation:* Rotation of femur towards the midline of the body in the transverse plane.
- *External rotation:* Rotation of femur away from the midline of the body in the transverse plane.

1.2.3 Structure of Femur

The thigh bone, also called the femur, is the longest of all bones in the human skeletal system and the toughest. It is the single bone of the thigh region and accounts for approximately one-quarter of a person's total height. The proximal part of the femur has a head, a neck, a greater trochanter and a lesser trochanter (Fig. 1.3). The head forms two-thirds of a sphere and is directed upward, medially, and slightly forward. The Greater trochanter is the large, upward, bony projection located above the base of the neck. Multiple muscles across the hip joint are attached to the greater trochanter, because of which its projection from the femur gives additional leverage to these muscles. The narrowed region below the head is the neck of the femur, a common area for fractures in the femur. The lesser trochanter is a small, bony prominence that lies on the medial aspect of the femur, just below the neck. Each epiphysis is connected to the diaphysis through a conical region called metaphysis. The diaphysis is mainly composed of hard cortical bone with a small, spongy core, while the epiphysis and metaphysis contain mostly cancellous or spongy bone within a thin shell of cortical bone. The elongated shaft of the femur has a slight anterior bowing or curvature. The distal end of the

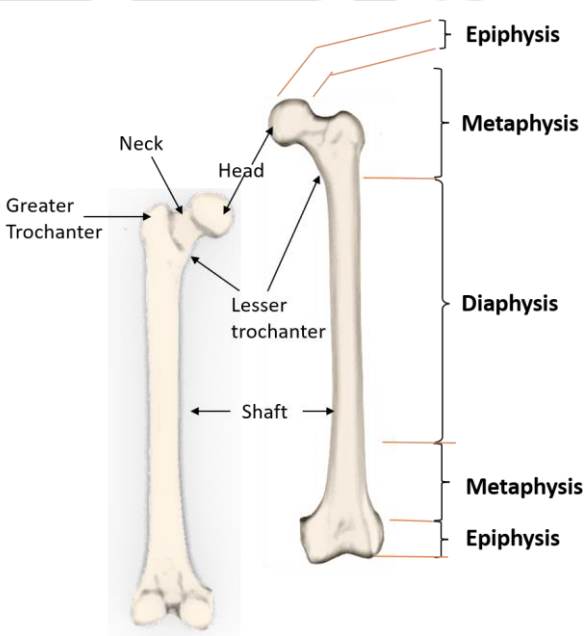

Fig. 1.3: Anatomy of human femur.

femur has medial and lateral bony expansions known as medial (condyle of the femur) and lateral condyle of the femur, respectively. The roughened area covering the outer surfaces of both medial and lateral condyles is known as the medial or lateral epicondyle of the femur, respectively.

1.2.4 Human Gait Cycle

Bipedal locomotion in humans, i.e., walking on our two feet, is probably the most practised physical activity in the world. It is one of the significant features of humans that largely involves both motor ability and adaptability. Though the nature of gait is different from individual to individual, it typically follows a common pattern: it is bipedal and biphasic. The two distinct but interconnected phases that constitute the gait cycle are the stance phase and swing phase. These phases can be further sub divided into eight different phases, as described in terms of the gait cycle. In the stance phase, which is approximately 60% of the normal walking cycle, the foot remains in contact with the ground. The cycle begins with the heel contact at the start of the right foot stance phase. The right foot then comes in flat contact with the ground before the heel rises. Lifting the toe off the ground marks the end of the stance phase. The remaining 40% of the gait cycle is known as the swing phase when the foot moves in the air. During the right swing phase, the left leg solely supports the body. The swing phase ends with heel contact, and the cycle repeats itself. The same cycle applies to the left leg with a phase difference. The duration when both feet remain in contact with the ground is known as the double support.

1.2.5 Musculoskeletal loading of the hip joint

Musculoskeletal loading is known to play a significant role in the biological process of fracture healing, bone remodelling and primary stability of an implant. The movements of the hip joint are facilitated by a total of twenty-one muscle forces. However, not all of them play a major role in load transmission (Nordin and Frankel, 2001). The muscles are grouped primarily as flexors, extensors, abductors and adductors, based on the movements (Fig. 1.4) they produce. Given the complexity of the nature by which the human musculoskeletal system works and the present computational capabilities, it is not feasible to simulate an individual entire system. The simulation system, therefore, should take into account the site of interest. In static analysis, the system must have zero degrees of freedom on the macro scale. This is accomplished by constraining the nodal degrees of freedom within a defined region. While modelling the femur, if

loading is applied at the hip joint, the knee joint interface on the distal condyles must be constrained.

In a cohort study using four patients, Bergmann et al. (2001) measured the hip contact forces during most-frequent daily activities, such as normal walking and stair climbing, and calculated the average joint forces. The average value of the peak hip contact force reported in the study was roughly 238% of body weight (BW) during walking (at a speed of 4 km/h). However, during stair climbing and going downstairs, the average measured hip contact forces were reported to be higher, 251% and 260% BW, respectively.

Both computational and *in vitro* studies indicated that the hip contact force and abductor muscle forces have the greatest influence on the strain distribution within the proximal femur during walking and stair climbing. The other significant contributors are the vastus (medialis and lateralis), tensor fasciae latae and iliotibial tract. Musculoskeletal hip loading data of Bergmann et al. (2001) and Heller et al. (2001) have been extensively used in most of the recent investigations on the proximal femur (Fig.1.4). The hip contact force acts at a distributed area on the surface of the femur head acting at an angle with the vertical axis in the frontal plane. However, both the force and the angle vary during gait. Abductor muscle force also acts parallel to the hip contact force, albeit along an opposite direction and at a different location of attachment (P1) in the greater trochanter region. Surrounding the area around the point P1 attached is the iliotibial tract (proximal and distal) and the muscle tensor fascia latae (proximal and distal). The respective attachment sites for vastus lateralis and vastus medialis are P2 and P3.

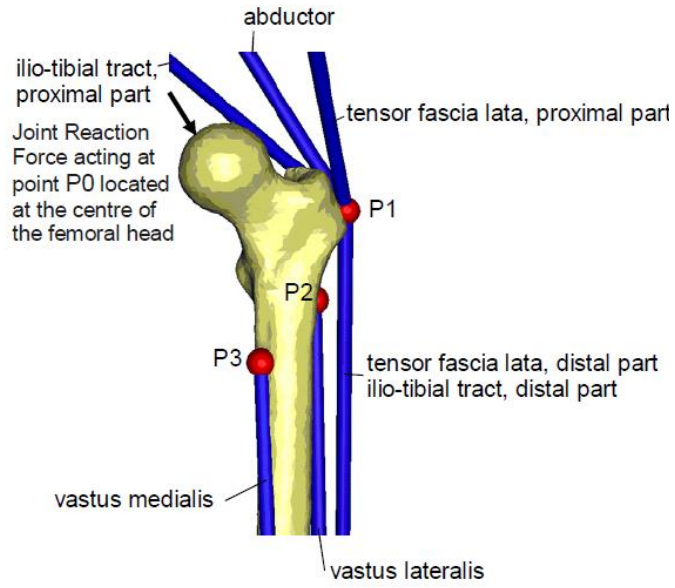

Fig. 1.4: Major group of muscles and their attachment points: P1, P2 and P3 are the attachment sites of the muscles (Bergmann, 2001; Heller, 2001).

Musculoskeletal loading conditions for normal walking comprise the hip contact force and the muscle forces of the abductor, tensor fascia latae (proximal and distal) and vastus lateralis (Bergmann, 2001; Heller, 2001). The loading conditions for stairs climbing include the additional effects of the iliotibial tract (proximal and distal), and vastus medialis, along with the hip contact force and the muscle forces applied during normal walking.

1.3. Bone structure and properties

The skeletal system comprises of rigid framework that provides support and protection to soft tissues. The primary function of the bone, however, is to bear the load. From an engineering perspective, bone is an anisotropic, non-homogenous and visco-elastic material. In dry weight, bone is composed of roughly 65 % of inorganic mineral, mostly impure hydroxyapatite, which provides resistance to compressive stresses, and 35% of organic constituents that includes bone cells, fluids and the organic bone matrix, composed of 90% of type collagen and 10% non-collagen proteins (Jee, 2001).

Macroscopically, bone exists in two bone forms depending on their relative densities or volume fraction of solids: cortical and cancellous (Gibson, 1985). Cortical bone is denser, comprising around 80% of the mass of a bone and has 3-4 % porosity. Cancellous bone, on the other hand, consists of a mesh of trabeculae (rod and plate-like shape) and is 70-80% porous. The distribution of cortical and cancellous bone varies significantly between individual bones. For example, the ulna is 92% cortical and only 8% cancellous bone, while a typical vertebra consists of 62% cortical and 38% cancellous bone.

Microscopically bone can be structurally classified into woven and lamellar bone. Woven bone is premature and typically found in foetus, at younger ages and during fracture healing of bones. Lamellar bone is more regularly arranged, and the growth rate is not as fast as in woven bone. The collagen fibres in woven bone are comparatively loosely packed and randomly oriented compared to lamellar bone. The outer and inner surfaces of the bone are covered by a thin membrane of connective tissue, the periosteum and endosteum, respectively. The periosteum contains nerves and provides nourishment from blood flows. The endosteum, which has similar functions, is the internal interface with the medullary cavity and lies on the inner cortical bone and trabecular structures (Jee, 2001).

Long bones are divided into three different sections: a) the diaphysis, a central cylindrical structure mainly composed of cortical bone, and b) the epiphysis; a wider structure located at both longitudinal ends of the bone and surrounded by articular cartilage that lies on the joint surface and c) the metaphysis; transition between epiphysis and diaphysis. Cancellous bone is primarily present within the last two sections.

1.3.1 Bone cells

Bone has four main types of bone cells that are present in its biological milieu, which can be classified according to their functions.

a) *Osteoclasts:* Their function is associated with demineralising the bone with acid and dissolving collagen with enzymes releasing minerals and other molecules stored in the bone matrix to the systematic circulation (Blair, 1998). These cells originate from bone marrow.

b) *Osteoblasts:* These are the differentiated mesenchymal cells that produce bone. They are created at the periosteum layer or stromal tissue of bone marrow. Osteoblast can be eventually trapped within the newly mineralised matrix, differentiating into osteocytes or adopting a flattened configuration upon filling a cavity, becoming lining cells.

c) *Bone lining cells:* They are inactive osteoblasts that are not buried in the new bone. It can be found in all external surfaces of bone, i.e., periosteum, cortical endosteum and trabecular endosteum whenever they are in a quiescent state. They also form a connected network mediated by gap junctions, continuous to the osteocyte network and are thought to contribute to correct resorptive and appositional functions of osteoclasts and osteoblasts (Everts et al., 2002), haematopoiesis, and control calcium and phosphate homeostasis (Miller, 1989).

D) *Osteocytes:* They are bone lining cells, former osteoblasts that are buried in the bone matrix. They are located in lacunae and communicate with the rest of the cells via canaliculi.

1.3.2 Material properties of bone tissue

In general, bone exhibits anisotropic elastic modulus in different anatomic directions. For example, the elastic modulus in the longitudinal direction of a long bone (17.4 GPa for human bone and 20 GPa for bovine bone) is larger than in the transverse direction

(9.6 GPa for human bone and 11.7 GPa for bovine bone). An orthotropic or transversely isotropic constitutive relation describes cortical bone properties fairly well (Edward Guo X, 2001). Cancellous bone is a complex material with significant heterogeneity. Its elastic and strength properties vary across anatomic sites, with ageing and diseases. Cancellous bone is classified from an engineering material perspective as a composite, anisotropic open porous cellular solid like many biological materials. It displays visco-elastic behaviour, as well as damage susceptibility during cyclic loading (Crob, 2006). It has been established, both theoretically (Gibson, 1985) and experimentally (Carter and Hayes, 1977, Dalstra et al., 1995), that the Young's modulus of cancellous bone was strongly dependent on the bone's apparent density.

In cortical bone, an elastic modulus in the range of 17 GPa was found in the initial linearly elastic region. In the intermediate region, the bone exhibits nonlinear elastoplastic behaviour (Fig. 1.5). This region is characterised by bone yielding with a yield strength value reported to be around 110 MPa. The final region exhibits linear plastic behaviour with a strain hardening modulus of 0.9 GPa.The bone was found to have fractured when the tensile stress was 128 MPa and the corresponding tensile strain was 0.026 (Özkaya and Nordin, 1999). The elastic moduli and strength values of a bone specimen depends on the strain rate, indicative of the viscoelastic property of thebone (Özkaya and Nordin, 1999).

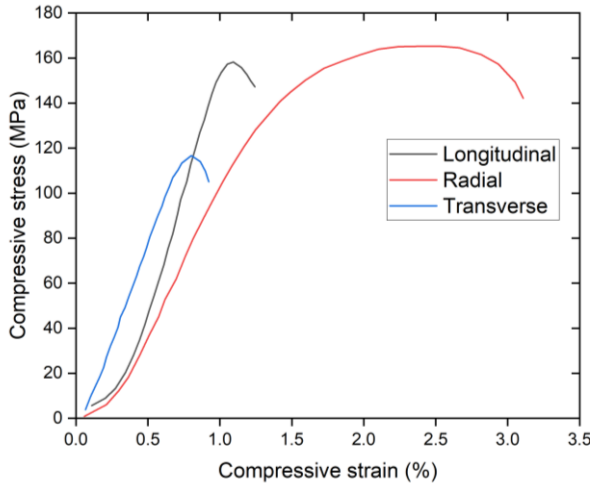

Fig. 1.5: Stress-strain curve for Cortical bone (Villette et al., 2018).

The stress-strain curve of cancellous bone has three distinct phases of behaviour (Fig. 1.6).

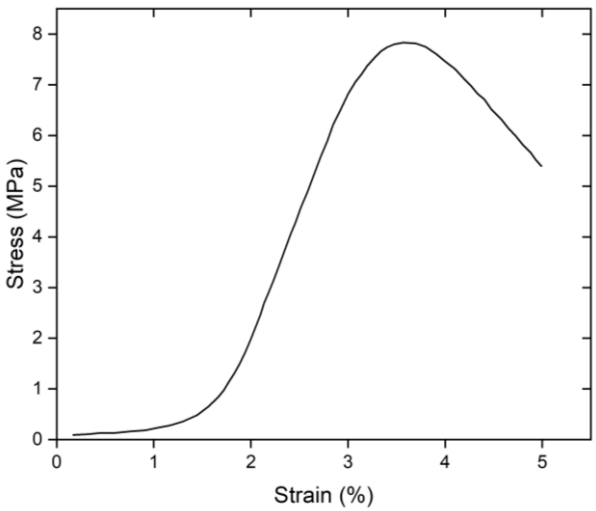

Fig. 1.6: Stress-strain curve for Cancellous bone (Villette et al., 2018).

Phase 1: Behaviour is linear elastic as the cell walls bend or compress axially.

Phase 2: Eventually, at high enough loads, the cells collapse by elastic buckling, plastic yielding or brittle fracture of the cell walls. This second phase of collapse progresses at a roughly constant load until the cell walls meet and touch.

Phase 3: Once this happens, the resistance to load increases, giving rise to a final increasingly steep portion of the stress-strain curve.

1.4 Literature review

1.4.1 Fracture Types

Proximal femoral fractures, commonly known as hip fractures can be classified into three types based on the anatomical site of the fracture: 1. Femoral head fracture, 2. Femoral neck fracture, 3. Trochanteric fracture. Head and neck fractures are clinically referred to as Intracapsular fractures, whereas the trochanteric fracture fall within the category of extracapsular fractures (Fig. 1.7). An overwhelming majority of the patients suffering this type of fracture (>90%) are aged above 50 years (Zuckerman, 1996). The incidence of such fractures is 2-3 times more in females as compared to the male population (Zuckerman, 1996).

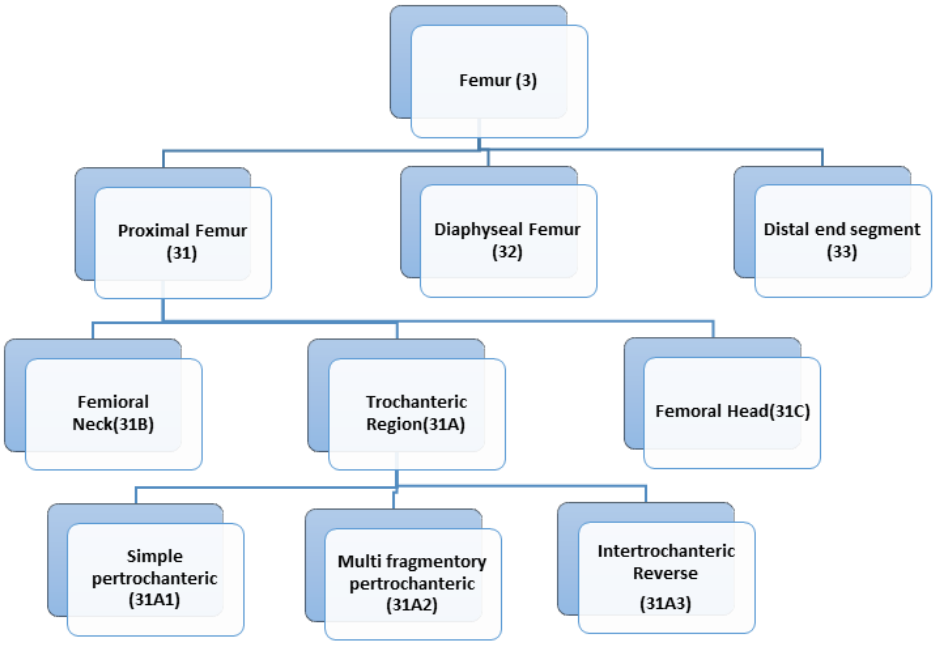

Fig. 1.7: AO/OTA fracture and dislocation classification long-bone fractures.

Classification of femoral fracture is based on the anatomical location of the fracture. The region of interest of this study in general is proximal femur and in specific

the trochanteric region. Therefore, the classification about the fractures at the femoral shaft and distal end will not be elaborated.

Trochanteric Fracture: Any fracture centered below the intertrochanteric line and above the lesser trochanter region (Fig. 1.8).

Subtrochanteric fracture: Those fractures that occurs in a zone extending from the lesser trochanter to 5 cm distal to lesser trochanter (Fig. 1.8).

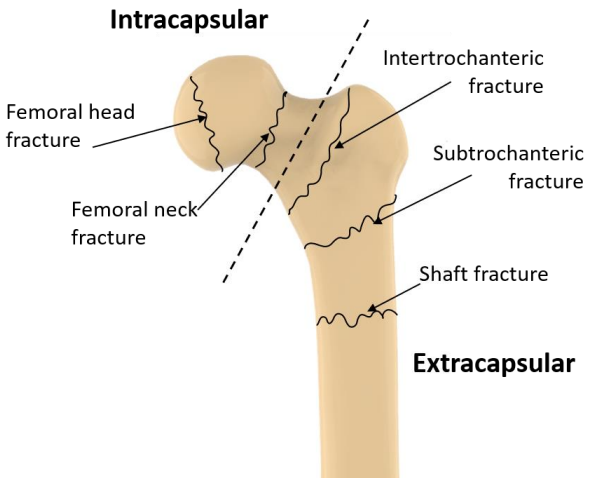

Fig. 1.8: Different types of fracture zone in the proximal femur.

1.4.2 Types of Implants/ Fixation techniques

Treatment of femoral fracture can be achieved either by conservative or non-conservative methods. Conservative method of treatment of fracture, e.g., cast, splint, traction etc. involves repositioning of the bone fragments, wound closure (if necessary) and application of a cast or a splint to hold the bone in place. This type of treatment is

(a) **(b)** **(c)**

Fig. 1.9: Examples of non-conservative methods: (a) Plates, (b) Screws, (c) IM rods. (Source: www.indiamart.com).

generally reserved for children and in rare exceptions in elderly patients. Immobilisation facilitates the joining of the fragments along with the healing process. It requires early callus formation and gradual transformation of the primitive tissue to bone. Early mobilisation should be achieved as early as possible to prevent stiffening of the joints. Further complications may be due to poor blood circulation due to dressings that are too tight or an increased risk of thrombosis and embolism caused by

immobilisation of lower extremities. In non-conservative method, achieved through surgical treatment using fixation devices or implants such as plate, screws, Intra medullary (IM) rod and nails etc., the fracture site is held more securely to provide greater stability (Fig. 1.9). This may result more rapid healing and bone healing processes can even skip some of the early stages.

Fixation implants can be either internal or external. External fixation (EF) device is a simple, quick and safe procedure to stabilise fracture in poly traumatised patients. First stage in orthopaedic treatment involves fracture stabilisation in order to reduce blood loss and facilitate patient management (Lavini, 2007). A useful method for assessing the seriousness of such trauma is the injure severity score (ISS). An ISS > 20, usually indicates the necessity of immediate stabilisation treatment through EF (Pape, 2000).

Generally femoral fractures are treated with internal fixation devices. They provide simpler overall management by offering numerous advantages such as early weight bearing and good stability. Despite being disruptive to the biologic environment, patients are usually comfortable with internal fixation after surgery. Internal fixation can be done by means of wires, pins, screws, nails or rod and plates. There are various devices available for surgical fixation of trochanteric fracture. But broadly they can be divided into two groups namely intramedullary and extramedullary devices.

Operative intervention generally includes IM (e.g., Proximal femoral nail anti-rotation (PFNA); Proximal femoral nails (PFN); Intramedullary hip screw (IMH); Gamma nail (GN); InterTan nail (TN)) or extramedullary (EM) fixation techniques (e.g. Proximal femoral locking plate (PFLP); Dynamic hip screw (DHS); Compression hip screw (CHS)). Intramedullary nails are stronger than extramedullary devices for the fixation of trochanteric fractures with subtrochanteric extension. IM fixations are extensively used by clinicians all over, given their less operating time, less blood loss, reduced hospital stay, small incisions, and better biomechanical strength (Sharma, 2007; Yeganeh, 2016). However, certain disadvantages associated with IM fixations include iatrogenic comminution, technical difficulties in the insertion of the nail, particularly in an obese and highly muscular patient or in femurs with an excessive bow, and difficulty in removal of the nail after fracture healing due to bone formation into the medullary canal (Bombaci, 2003; Aneja, 2014). Also, there is a high rate of general complications in case of prolonged overall recovery time. The overall failure

rate for such fixations is reported to be around 3-16.5% (Haentjens, 1994; Davis, 1990). Moreover, IM devices are significantly costlier implants than the EM, with almost similar outcomes (Sharma, 2007). Radiation exposure was also found to be higher in the case of IM fixation as compared to EM fixations (Sathish Kumar, 2017). In recent times, the use of EM plating techniques is being advocated owing to the advent of some new-age plating techniques (Ramachandra, 2019). The EM techniques do not intervene largely inside the structure of the femur and keep the bone anatomy intact (reserved) and support total bone healing (osteosynthesis) at the fracture location. Though complicated in implantation, plating techniques are beneficial in long-term results, especially where the bone anatomy of the patient needs to be retrieved through osteosynthesis. Bone plates are the most frequently used among all these implants (Stiffler, 2004). Bone plates resist well against tension, compression, shearing, rotational forces and bending forces (Stiffler, 2004). In critical trauma condition of patients, a combination of two methods, a first stage EF is used as an emergency procedure to stabilise followed by secondary stage of intramedullary nailing.

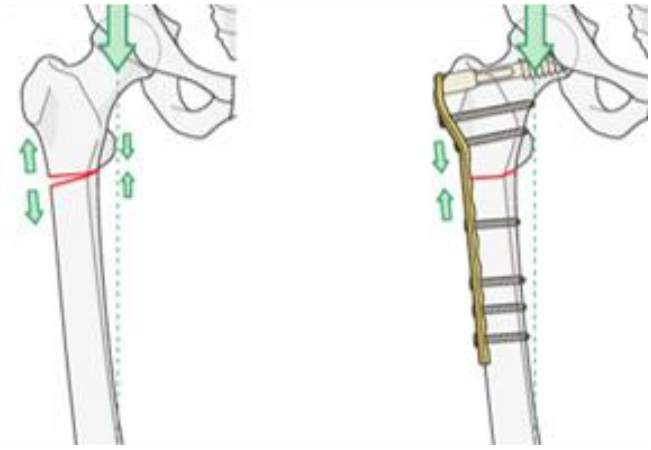

Fig. 1.10: Dynamic compression plating technique.

Internal bone plate fixations differ primarily in the screw design. Conventional plating technique, Dynamic compression plating (DCP), involves the use of compression screws that relies on preloading of several interfaces in the construct (Gardner, 2004) (Fig. 1.10). The tightening of the screws results in generation of force at the screw thread-bone interface, and predominantly between the bone and plate (Perren, 1979). Newer type of plate, locking plate (LP), has expanded the ways of screw-

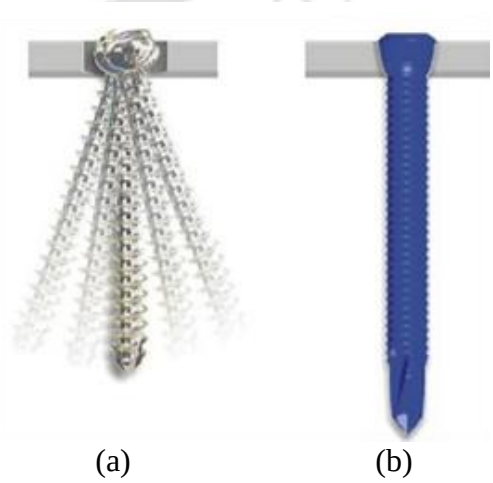

(a) (b)

Fig. 1.11: Screw arrangements in bone plate: (a) conventional. (b) locking.

plate fixation. LP involves locking screws having threaded head that allow the screw to fasten into the plate as well as into the bone (Perren, 2002) (Fig. 1.11). The biomechanical environment achieved using LP is totally different from that obtained through DCP (Perren, 2002). The surrounding environment of the screws in DCP is governed by a mix of effects contrary to LP, whose mechanics is simple like that of unilateral external fixation device. The bony fragments are not compressed and the fracture surfaces exhibits small amount of elastic motion. As compared to DCP, LP are less rigid and forms fixed angle between the plates, screws and bone fragments. The fixed angle eliminates the requirement for compression or contact between the plate and bone. This suggests that the plate can be offset from the bone, thereby preserving the periosteum and avoiding necrosis. Various authors have observed that LP performs better than DCP in older or weaker bone (Gardner, 2004; Yánez, 2010; Wagner, 2004). Few other biomechanical studies found LP to have more stiffness and superior failure load compared to other implants (Aminian, 2007; Crist, 2009; Floyd, 2009). Uhl et al. found that DCP provides inherently more stability than LP. Gap closure and bone-to-bone load transfer resulted in better mechanical performance of DCP over LP during axial compression (Uhl, 2008). A comparative evaluation between LCP and the traditional DCP) was undertaken based on periprosthetic femoral fracture using a parameterised FE model (Moazen, 2012). The computational results highlighted that changing the bridging length had more influence on the stiffness and fracture movement than varying other parameters. Despite limitations with regards to the simplistic nature of the model, the computational approach demonstrated the potential of such preclinical techniques to compare the stiffness and fracture movement of different fixation constructs in order to determine the optimum fixation method for proximal femoral fractures. To further understand the underlying biomechanics between these two types of fixations, FE modelling of tibial bone of varying quality was carried out (MacLeod, 2015). The bone properties considered in this study include orthotropy, inhomogeneity, cortical thinning and periosteal apposition associated with osteoporosis. The findings provided a biomechanical basis for the reported improved performance of locking plates in poorer bone quality.

DHS is considered to be gold standard fixation for extracapsular femoral fracture and yielded good results in patients with stable intertrochanteric fractures (Jonnes, 2016). At lower costs and simple technique with a high rate of bone union and good to

excellent functional level make the DHS preferable for stable intertrochanteric fracture. The DHS is designed to provide strong and stable internal fixation of a variety of intertrochanteric, subtrochanteric with minimal tissue irritation (Fig. 1.12). The number of screw holes per plate length is maximised, without compromising plate strength. This allows an increased number of fixation points with a small incision. The DHS plates have a low-profile design, reducing the risk of trochanteric bursitis. Holes in the DHS side plate allows angulation of 4.5 mm cortex screws for lag screw fixation of medial fragments and axial compression and multiple screw fixation of the main fragment in subtrochanteric fractures with shaft extension. Variable angle dynamic hip screw (VA-DHS) is another modification of the traditional DHS, which allows for relative angular variation of the lag screw concerning the plate.

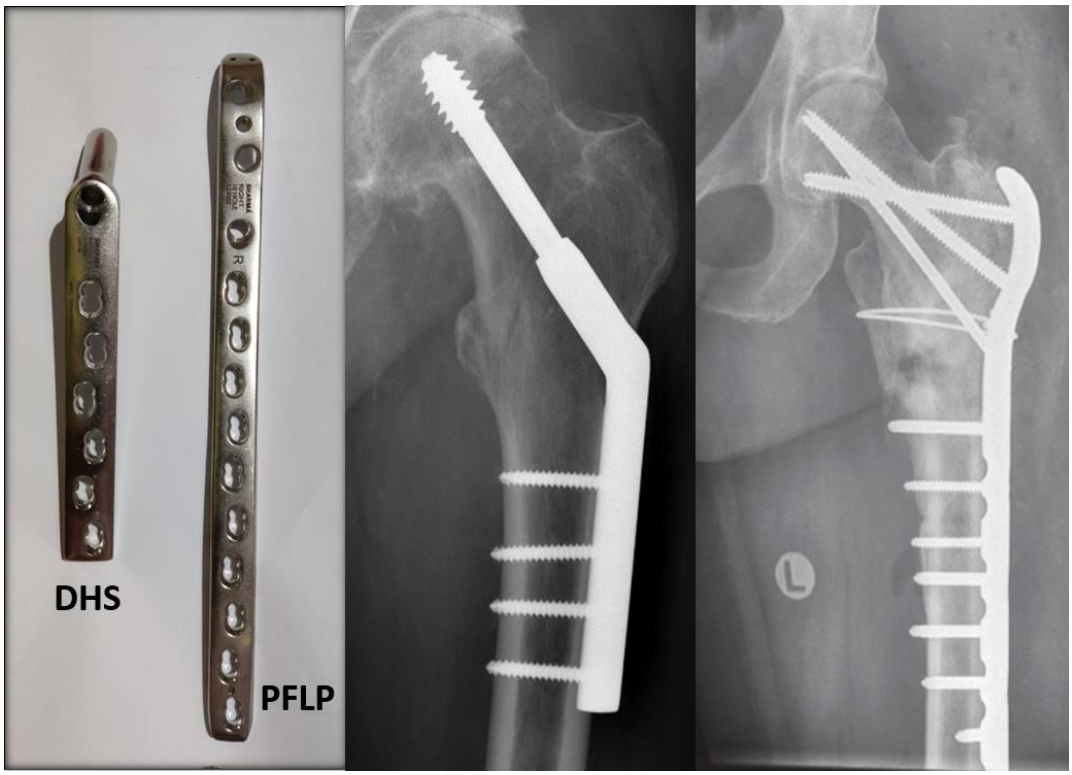

(a) (b) (c)

Fig. 1.12: Two commercial bone plates: (a) DHS and PFLP, (b) Xray image of a femur implanted with DHS (Sunku, 2015), (c) Xray image of a femur implanted with PFLP (Viberg et al., 2017).

Since its inception in 2007, the Proximal Femoral Locking Compression Plate (PF-LCP) 4.5/5 (PF-LCP, Synthes, West Chester, PA, USA), a new extramedullary implant which is anatomically precontoured, offered greater angular stability that improved the osteosynthesis of peritrochanteric, intertrochanteric and subtrochanteric fractures of femur (Gautier, 2003; Wagner, 2003) (Fig. 1.12). PFLP merges locking screw technology with conventional plating technique. The convergent angle design (95 /120/ 135) and the locking interface of the proximal cannulated locking screws (First and

second screws 7.3 nm, third screw 5.00 nm) improves the PF fixation stability especially in osteoporotic patients. The remaining screw holes (4-16) are located distally at plate shaft are LCP combined holes allowing placement of either cortical (4.5 nm) or locking head (5.0 nm) screws. PFLP are minimally invasive fixation device that offers optimum fixation for comminuted and highly unstable fractures. Zhong et. al. (2014) suggested that PFLP as a better fixation device than DHS in subtrochanteric fracture in terms of significantly shorter operative times, less blood loss, shorter bone union times, higher excellent to good functional level and fewer complications. However, they found no difference between PFLP and DHS fixation for intertrochanteric fractures.

Wirtz et al. (2013) indicated that in trochanteric fracture there is a high failure rate in PFLP due to small size and less number of proximal stress to provide stable fixation to proximal fragment. Also, the long lever arm of the plate and thin proximal screws cannot guarantee a sufficient contact surface for early partial weight bearing, leading to cut-out and loss of reduction. Streubel et al. (2013) also reported that locking plate fixation for unstable intertrochanteric femur fracture is associated with a high rate of screw 'cut-out', proximal breakage of screws, screw loosening with varus deformity and plate fractures. Naiyer et al. (2016) studied the complication rate and analysed the functional outcome of PF-LCP and DHS, but they found no significant difference. Various other studies reported complications and failure rates with the use of angled plates, proximal femoral nails, and DHS in unstable intertrochanteric fracture ranges from 3 to 26 % (Yong, 2009; Sehat, 2005; Saarenpaa, 2009; Fogagnolo, 2004). Hodel et al. (2017) showed the application of the PF-LCP may be justified for its superior abilities to restore and maintain the anatomy especially for the younger sub-group of patients. However, if anatomical reduction is not achieved and patient compliance is low, the usage of PF-LCP should be carefully weighed against other implants especially in unstable intertrochanteric or subtrochanteric fractures.

1.4.3 Stability assessment of fracture plates

1.4.3.1 Biomechanical studies

There are a few clinical and biomechanical studies in relation to the outcome of PFLP method as compared to other fixation methods. In femoral neck fracture, two biomechanical studies showed that PFLP had higher axial stiffness (Nowotarski, 2012; Aminian, 2007). However, DHS was found to register the highest failure load in one

study (Nowotarski, 2012), whereas PFLP was found to have the highest failure load in the other (Aminian, 2007). Only one clinical study included femoral neck fracture and found a complication rate of 37% (Berkes, 2012).

Clinical investigations on both intertrochanteric and subtrochanteric fractures and their post-surgical evaluations can also be found in the literature. The outcome, however, varied markedly; 5 studies found complication rates of 25–53% (Wieser, 2010; Floyd, 2013; Mardani, 2013; Wirtz, 2013; Johnson, 2014). The study by Chalise et al. (2012) showed a combined low complication rate of 6% for intertrochanteric and subtrochanteric fractures. The largest study, with 98 intertrochanteric fractures, reported a 2% revision rate, but it was not clearly defined as being prospective or retrospective (Zha, 2011). The study by Zhong et al. (2014) did not give any clear overall complication rate.

Although no biomechanical studies were found for intertrochanteric fracture fixation, few such studies dealing with subtrochanteric fractures are worth mentioning here. Out of them, 2 used cadaveric bone (Forward, 2012; Wang, 2014) and 3 used synthetic bone (Crist, 2009; Floyd, 2009; Latifi, 2012). In the 2 studies that used cadaveric bone, PFLP was found to have lower failure load than PFN and DHS (Forward, 2012; Wang, 2014). In the 3 studies that used synthetic bone, a PFN was not used for comparison and PFLP registered higher failure load than an angled blade plate (ABP) in all three studies (Crist, 2009; Floyd, 2009; Latifi, 2012).

Experimental analysis is required for validating the FE analysis results. Practically, the credibility of numerical modelling technique can be established only by comparing the result with experimental data obtained in similar conditions (Hefzy and Singh, 1997). A FE model is fully qualified only when the level of mesh refinement and contact stiffness are assigned after several iterations and all parameters' physical significance is identified with previous independent experiments. Experimental analysis generally requires the measurement of the deformation on the bone for a particular load, or the stain field generated for that load. Most of the experiments on the femur used strain gauge for measuring the deformations, until last decade, when Digital Image Correlation (DIC) and Digital Volume Correlation (DVC) came to existence. The restricted area of interrogation associated with strain gauges is considered to be a limitation of the technique

DIC is a non-contact full-field optical technique that evaluates the deformation field of given complex surfaces of an object subjected to external loads (Kahn-Jetter, 1990). The technique was first put forward independently by Yamaguchi (1981) and Peters et al. (1982) in the early 1980s. As digital technology continues to rise over the last two decades, the application of DIC is becoming further widespread. The technique at foremost involves obtaining digital images of the specimen at different loading conditions using digital imaging devices and then analysing those images with correlation based matching algorithms followed by numerical differentiation approach to predict deformation and strain responses (Peters, 1983). DIC effectively tracks the movement of the naturally occurring, or applied surface pattern during the test or experiment. This is done by analysing the displacement of the patterns within discretised subsets or facet elements of the whole image. The maximum correlation in each window corresponds to the displacement, and this gives the vector length and direction for each window. DVC is a novel technique for full 3D strain and deformation measurements. The technique imports volume images of the component in reference and deformed states and is able to calculate the full 3D displacement and strain map. DVC is a powerful non-intrusive technique for the identification of sub-surface material deformation and is capable of identifying defects, discontinuities or other material characteristics. DVC is an extension of 2D DIC, which measures in-plane surface displacements only. DVC is also distinct from 3D DIC, which uses 2D images to measure both in-plane and out-of-plane displacements but only on the surface of a material. In contrast, DVC measures 3D displacements inside a material.

In DIC, optical metrology method is used to extract full-field deformation measurements of objects subjected to external loads (Cofaru, 2013; Kahn-Jetter and Chu, 1990). It is particularly useful for measuring deformations in complex geometries with inhomogeneous material properties, like human bone, by finding spatial correspondences between different digital images (Grassi, 2013). Use of DIC can further avert reinforcement effects associated with strain gauging, which originate from the stiffness of the sensor mounted onto (or embedded into) the tested material (Ajovalasit, 2010; Beatty and Chewning, 1979; Perry, 1986). Recently, a series of investigations has been carried out using DIC to measure strain over bone surfaces (Moerman, 2009; Sztefek, 2010; Dickinson, 2011).

Whilst several studies have employed full-field experimental strain measurements to validate computational predictions and to verify bone constitutive laws and fracture criteria, there is a dearth of full-field experimental strain studies on intact and implanted femurs, to support computational predictions of implant-induced long-term bone response. Nevertheless, despite its strong potential, the use of DIC has largely been restricted to FE validation purposes in experimental biomechanics. Moreover, only a handful of such investigations were carried out on the femur, either using composite (Tayton, 2010; Dickinson, 2011; Grassi, 2013) or cadaver specimens (Op Den Buijs and Dragomir-Daescu, 2011). A few recent studies on human cadaver femora have used DIC to investigate femur fracture (Gilchrist, 2013; Grassi, 2014; Helgason, 2014). Chanda et al. (2015) measured the surface strains in intact and implanted composite femurs using DIC in order to (1) validate the full-field numerical strains predicted by the corresponding FE models and to (2) quantitatively assess the implant-induced surface strain changes across seven defined Gruen zones of cementless femoral stem fixation.

1.4.3.2 Finite Element (FE) studies

FE Analysis has been extensively used in the design and evaluation of fixation plates and screws to overcome the most drawback of the current fixation devices: fatigue failure of the device and stress shielding of the bone. A 3-D analysis is necessary to take into account the complex geometry of the plate system and predict stress distribution in the bone. FE is a numerical approach that provides approximate solutions to differential equations that form a boundary value problem. FE based technique was established in the 1960s, but was introduced in bone research in the 1970s. To allow the analysis of complex geometries, boundary conditions and material properties the overall structure is arranged as a set of discrete problems. The geometric representation consists in a mesh of element connected at nodal points, whose displacements are calculated from applied boundary conditions and mapped intro local strains and stresses of the whole structure.

Despite the prevalence of experimental study related to the biomechanics of femur fractures and plated construct, the computational modelling of supporting osteotomies has been scarce. A few studies, however, included FE based numerical models, albeit simplistic, to assess the outcome of various fixation plates. Using a hierarchical nonlinear hyperelastic FE analysis, Latifi et al. (2012) predicted higher stability and

durability with PFLP fixation for subtrochanteric fracture, as compared to that obtained with DCS and ABP. The effect of stress shielding was assessed using a 3D, quarter-symmetric FE model based on a canine femur diaphysis plated with a metal/polymer hybrid design (Ferguson, 1996).

FE can be used to study the underlying mechanics of different biological tissues, for instance, to understand how these structures will respond to different loading conditions or constraints. It can also be employed to study the mutual correlation between Biology and Mechanics, ranging from cell level studies (Barreto, 2013) to whole organ study (Geralds and Phillips, 2014). Bone remodelling is extensively studied by using FE analysis. When the bone tissue is subjected to load, the mechanical environment in the bone tissue changes and the tissue responses by generating local mechanical stimuli. These predictive algorithms are often implemented in a feedback loop fashion, where the properties of the model updates after each iteration. Practically, the credibility of numerical modelling technique can be established only by comparing the result with experimental data obtained in similar conditions (Hefzy and Singh, 1997). When the experimental validations could not be done, any source of error calls for proper addresal using multiple meshes and multiple exploratory runs. Bernakicwicz. et al. (2002) concluded in their study that using a FE model it is possible to carry out predictions without a direct experimental validation of the model. Stress residuals, convergence tolerance and contact compenetrations can be used to define an upper boundary for the model error, in combination with the necessary sensitivity analyses on the parameter uncertainties. FE model helps us to understand the mechanical behaviour of orthopaedic devices and also has the potential to provide additional information about individual patient to guide the orthopaedic surgeon in decision making before a surgery.

1.4.4 Post-operative phenomena

1.4.4.1 Post-operative complications

Primary endpoints defined as radiological fracture healing are union, delayed-union, non-union, post-operative ambulatory status and post over complications. Clinically, fracture union is acquired when there is no pain or motion at the fracture site in response to physiological stress, and/or the patient can exercise with full, pain-free weight bearing without additional support. Fractured non-union or delayed union prolongs morbidity and delays the normal functioning of the fractured limb. The localised effect

of plating i.e., directly beneath the plate determine the extent of osteopenia following plating. Secondary varus collapse, implant failure, screw cut out are some of the post-operative complications that are generally reported. Further implant associated complications such as malrotation and symptomatic impingement of the hip can also occur. The disadvantages associated with secondary surgery is the removal of the implant after the reunion of fracture bones. This may even lead to bone refracture due to the temporary weakening of the bone after implant removal. Though relatively rare, corrosion of a metallic implants is not a negligible concern. Also, metallic implants interfere with post-operative CT scans, MRI images or radiography. Brief descriptions of the above-mentioned complications are discussed below:

- *Varus:* Deviation towards the midline in the anatomical position.
- *Valgus:* Deviation away from the midline in the anatomical position.
- *Delayed Union:* Missing in radiological fracture healing after 6 months or no progressive signs of fracture healing in between the 3-6month control (Ferolke, 2007)
- *Non-Union:* Missing radiological fracture healing after 9 months or no signs of progression of fracture healing in between 3-6 months control.
- *Avascular necrosis:* Death of bone tissue due to blood supply. Osteonecrosis can lead to tiny breaks in the bone and bone eventually collapse. A broken bone or dislocated joint can interrupt the blood flow to a section of bone.

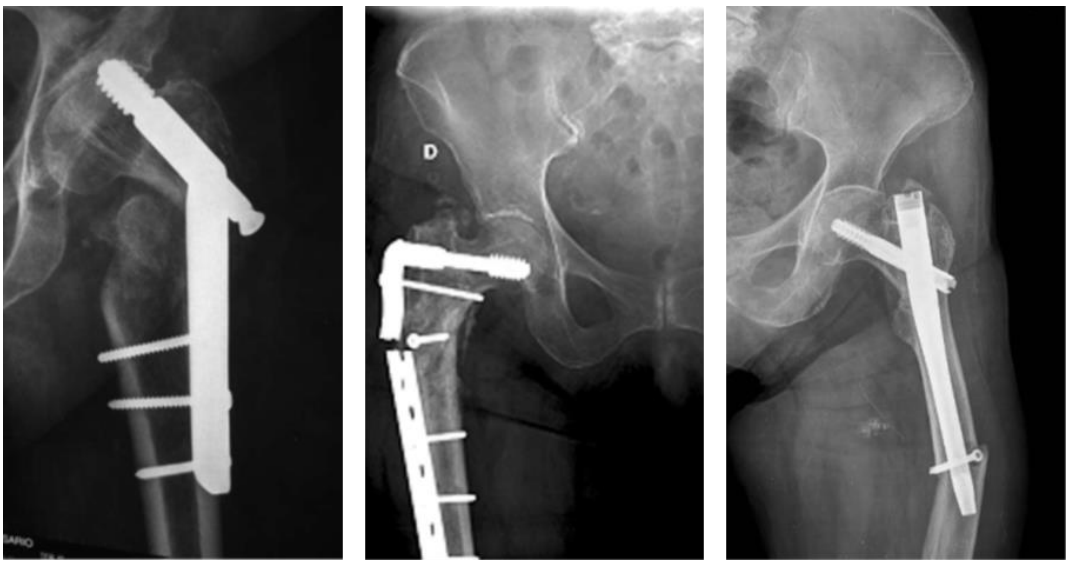

(a) **(b)** **(c)**

Fig. 1.13: Complications extracapsular fracture: (a) Screw cut out, (b) Implant failure, (c) Femoral fracture in intramedullary nail (Carpintero, 2014).

- *Osteoporosis:* It is a bone disease that occurs when the body loses too much bone, make too little bone or both. Osteoporosis means porus bones.
- *Osteopenia:* It is the decrease in bone density but not to the extent of osteoporosis

There are two major complications following treatment of an intracapsular fracture by osteosynthsis: non-unions and avascular necrosis. Factors influencing the appearance of non-unions include patient age, degree of displacement, fracture line, degree of comminution and quality of reduction; non-unions re reported in between 10% and 45% of patients undergoing osteosynthesis (Blomfeldt, 2005). Avascular necrosis of the femoral head occurs at 9%-18% of patients, between two- and eight-years post fracture; risks factors include the degree of fracture displacement, patient age and delay in surgical treatment (Lu-Yao, 1994).

1.4.4.2 Complications in extracapsular fracture

The three most common complications reported for extracapsular femoral fractures are screw cut out, femoral shaft fracture and implant failure. Screw cut out (Fig.1.13a) is the phenomenon where the screw comes in contact with the surrounding tissues and cuts it. It is a major cause of implant failure in the fixation of proximal femoral fractures and cause several injuries. It occurs in between 1.1% and 6.3% of patients treated for extracapsular fracture, and accounts for 85% of fixation failure (Lorich, 2004). The main causes of cut out are fracture instability and especially the incorrect placement of the lag screw. Implant failure usually appears as a result of poor fracture reduction, mechanical stress or fracture instability, but may also be caused by technical error. Implant failure is more common when there is greater rigidity of the fraction fixation device (Carpintero, 2014) (Fig.1.13b). Femoral shaft fracture occurs much more frequently in patients treated with intramedullary nails, and particularly with first-generation nails with a larger distal diameter; according to one meta-analysis, these nails were associated with a femoral fracture rate of 5.3% (Parker, 1996) (Fig. 1.13c). Special mention should be made of reverse obliquity intertrochanteric fractures, in which extramedullary devices are associated with a failure rate of 36%, compared to only 5% for intramedullary nails, since the latter offer improved load-bearing capacity (Sadowski, 2002). It should be borne in mind that reverse obliquity fractures of the proximal femur have biomechanical characteristics different from those of other intertrochanteric fractures.

1.4.4.3 Bone healing

The biology of fracture healing is complex biological process that depends on specific regenerative patterns and involves change in the expression of several thousand genes. Fracture healing is biology of repair at the fracture site that proceeds through a series of stages successfully. Bone healing generally takes place either by primary or secondary bone healing. Primary bone healing involves a direct attempt by the cortex to re-establish itself after interruption without the formation of a fracture callus. It is, however a rarity that all the edges conform exactly and hence this type of healing is less seen. Secondary bone healing involves the classical stages of injury, haemorrhage, inflammation, primary soft callus formation, callus mineralisation and callus remodelling (Fig. 1.14).

Soon after occurrence of fracture, a haematoma is formed from the raptured blood vessels in the bone, periosteum and soft tissues adjoining to the fracture site. The haematoma mainly constitutes of platelets and macrophages, which releases cytokines and growth factors responsible for recruiting the inflammatory cells. The cytokines involved in this process mostly indulge in angiogenesis i.e., restoring of blood supply through formation of new blood vessels from existing intact vessels. After few days post-fractured, the haematoma is restored mainly due to Osteoclasts, leaving a loose aggregate of cells known as granulation tissue. The inflammation phase is followed by repair phase of secondary bone healing. During this phase, both soft and hard calluses

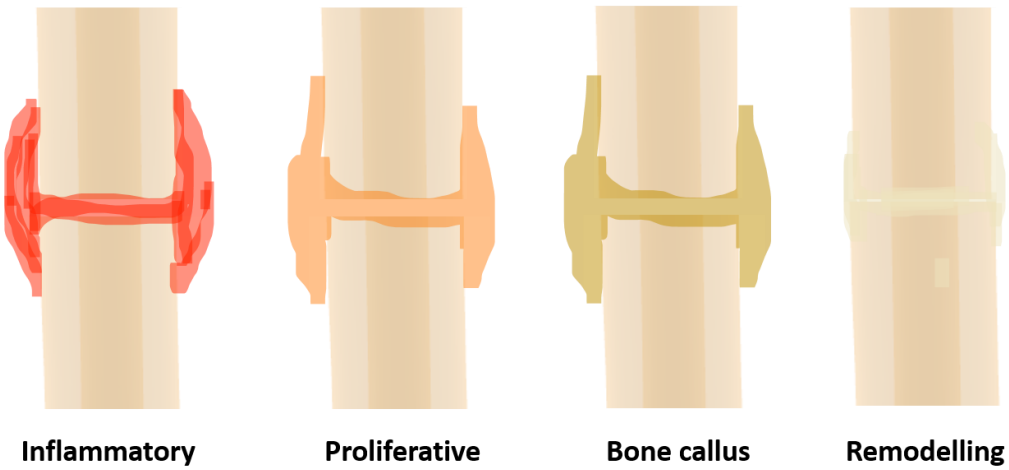

Fig. 1.14: Stages of secondary bone healing.

are formed through a combination of endochondral and intramembranous ossification. Intramembranous ossification response generates a hard callus of woven bone predominantly at the periphery of the callus (Yuasa et al., 2014; Childs et al., 2016;

Marsell and Einhorn, 2011). This type of ossification is mainly observed in the regions where periosteum and vascularisation are less disturbed along with low tissue strain (Claes et al., 2012). Contrary, the soft cartilaginous callus is calcified gradually through the process of endochondral ossification till bone has bridged the fracture site. As the process continues, both stiffness and stability of the fracture increases due to increase in callus volume and tissue calcification (Harwood et al., 2010; Marsell and Einhorn, 2011) . Finally, bony bridging will occur where the fracture callus will compose entirely of woven bone. However, woven bone contains collagen fibre unlike those in normal lamellar bone and hence further remodelling is required to restore the original structure (Harwood et al., 2010).

Absolute stability allows direct bone healing. Absolute stability is the fixation of the fracture fragments in such a way that there is virtually no displacement of the fracture surface under physiological load. Relative stability results in indirect healing by callus. In relative stability the fixation or support construct allows small amount of motion in proportion to the load applied. Goodship et al. (1993) concluded that more flexible fixation may lead to excessive interfragmentary motion whereas more rigid fixation may impair callus formation contributing to non-union.

1.4.4.4 Bone Adaptation

Bone being a living material functions in building the skeleton and therefore enabling protection and locomotion of the organism. Bone does not behave like inert engineering material. It undergoes definite changes in shape, structure and composition depending on the mechanical and physiological environment. It removes older bone and replaces it with newly formed bone gradually. By doing so it repairs the microscopic damages which can lead to fatigue failure. It is also hypothesised that bone tune itself in such a way to achieve maximum mechanical efficiency.

Mechanical cues are site specific factors which play a significant role in skeletal maintenance and adaption. Bone structure can lose its bone mass while still capable of holding strenuous loads. In 17th century, the famous Italian physicist, Galileo Galilei first predicted a certain relationship between mechanical forces (body weight) and bone morphology (Treherne, 1981; Carter 1984). Thereafter in 1982, a notable contribution came from Wolff, who further developed the theory of functional adaptation originally conceived by Roux (Roester, 1981; Roux, 1881). Roux concluded in his study that the

combination of bone apposition and resorption is a biological controlled process that depends on the local state of stress (Roux, 1881).

According to Wolff's hypothesis, "Every change in the form and function of bone is followed by certain definite change in their internal architecture and equally definite secondary altercation in their external geometry, based on certain mathematical laws" [Wolf, 1892]. This 'law of bone transformation' by Wolf was later referred to as 'Wolff's law'. Classical example of this adaptive capability of bone, in humans, are bone loss during bed rest confinement and bone mass gain due to strenuous physical exercise (Issekutz et al. 1966, Haapasalo et al. 2000).

Frost in 1963 identified two separate mechanisms by which bone responds to altercations in the mechanical environment: Bone modelling and Bone remodelling. Bone Modelling can be understood as the long bone grows, it is not enough just to add material to make the bone organs longer and larger but also to shape it in various ways. That calls for removal of bones in some places while adding in other. This sculpting, combining osteoblastic activity (bone formation) in others, has come to known as modelling (Frost, 1990).

Contrary, remodelling (Frost, 1990), is lifelong continuous process by which bone renews itself, replacing woven or old bone by new lamellar bone. Bone turnover is operated by coupled action of osteoblasts and osteoclasts, forming temporary anatomical structures known as Basic Multicellular Unit (BMU). Thus, modelling and remodelling are distinguished in several ways:

i. Modelling involves independent action of osteoblasts and osteoclasts. Remodelling involves sequential, coupled actions by the two types of cells.

ii. Modelling is a very active process during early life stages, fundamental in the early growth processes, and less present after skeletal maturity. Remodelling is independent of age and occurs throughout life, although it substantially reduced after growth stops.

iii. Modelling result in change of bone size, shape or both. Remodelling does not usually affect size and shape.

Bone adaptation in material properties and in shape at the apparent level are often referred to in biomechanics as internal and external remodelling respectively, despite of the fact that cortical adaptation is more relatable to Frostian modelling rather than

Frostian remodelling. Internal bone remodelling refers to change in internal morphology, whereas external remodelling is described as occurring relative to periosteal geometry. Internal remodelling, thus, is expressed as change of density or porosity of the cancellous bone (Carter, 1989; Huiskes, 1987), whereas the geometric (or shape) changes of the cortical bone are referred to as external remodelling (Hart, 1984). For an adult the cancellous bone usually has a higher rate of metabolic activity and hence, appears to respond more rapidly to changes in mechanical loads than the cortical bone (Garcia, 2002). Therefore, the geometry changes are considerably less in comparison to internal adaptation or internal remodelling of the bone. The combined effect of internal and external remodelling models has been investigated by several researchers. (Huiskes, 1987; Weinans, 1993).

Few studies have thoroughly examined the spatial arrangement of adapted cortical bone across the entire bone in relation to the mechanical field. In addition, simulations of cortical bone thinning are often tested against experimental data with the representation of a few cross sections, with the calculation of bulk quantities, such as minimum moment of area (Chennimalai, 2011) or remodelling rate (Malachanne, 2011). These approaches lack a thorough spatial representation of in vivo and simulated cortical adaptation. Animal study correlating site-specific distribution of new bone apposition with mechanical signals was limited to single cross sections (Roberts, 2009). A new approach with higher spatial resolution is required to fully assess the predictive ability of phenomenological models.

1.4.4.5 Stress shielding effect and cortical thinning thereof

Surgical reconstruction of bone with prosthesis alters the mechanical environment within the bone by changing the load transfer mechanism. As a result, the prosthesis starts to share the joint load in the implanted situation which otherwise was carried exclusively by the bone in the pre-operative stages. This leads to a major post-operative problem known as stress shielding. Bone requires continuous stress for its growth. Stress shielding occurs when two or more components with different moduli from one mechanical system. The component with higher modulus bears most of the load and protects the other component (Ferguson, 1996). Similar things happen in case of rigid fixation devices. At the initial phase, rigid fixation devices help in the restoration or healing of the fragmented parts of the fractured bone by sharing most of the load itself. But in the later stages of healing, it may lead to osteoporosis with decreased bone

strength (Tonino et al., 1984). Stress shielding as reported by several in-vivo studies results from the use of rigid internal fixation plates. On the other hand, if flexible plates with inadequate strength are used, it may result in non-union of the fracture and thus causing pain. So, a trade-off should be reached between strength and stiffness. Ideally, as the fracture heals, the stiffness of the fixation device should decrease as the bone strength increases. Uhtoff et al. (1981) studied fracture healing using stainless steel plate and less rigid titanium alloy plates. The titanium plates were as strong as the steel plate, but were half as stiff. Less stress shielding induced bone loss were observed in the femur plated with titanium. Ferguson et al. (1996) mentioned that increasing flexibility of the fixation plate reduces the effects of stress shielding beneath the plate. Stress concentration at the edges of the screw holes after plate removal can lead to refracture of the bone. Also, the isolated bone screws would lead to bone resorption at the side of the screw holes and new bone formation at the end of the holes. On removal of the screws, the stress concentration at the side of the hole will act on bone which is already weaken by the remodelling process, further increasing the chances of fracture. Complications arising from femoral fractures are fairly common, and vary depending on whether the fracture is intracapsular or extracapsular. Generally, the problems related to intracapsular fractures are biological: vascularisation of the femoral head, and lack of periosteum- a major contribution to fracture healing in the femoral neck. Contrastingly, in extracapsular fracture the problem is mechanical and is related to load bearing.

1.4.5 Patient specific plates

Data obtained from the morphometric study of the proximal femur demonstrated that femoral morphometry had regional features and social differences (Mahaisavariya et al., 2002; Su et al., 2015). Patient specific plates (PSPs) are pre-contoured fracture fixation plates based on the anatomy of the patients. This customised plate promotes fast anatomy recovery, optimise the biomechanical conditions of the fractured sites and improves the success rates of the surgery. The need of PSP rises from the difference in the anatomy and variability of fractures, it is sometimes challenging for surgeons to select a well fit plate from existing variety of plates. It is a longstanding belief among the Indian and Asia-Pacific arthroplasty surgeons that the currently available prosthetic components do not meet the requirements of these anthropometrically smaller ethnic groups. Surgeons need to deform (e.g., bend and/or cut) the proximal plate manually before operations to achieve an optimal fit (Chen, 2018). Such deformations may

compromise the mechanical stability of the plate-bone construct, delay surgery or cause higher rate of complications (Strauss, 2008). Though various studies related to PSPs were reported for femoral hip stems (Chanda, 2015; Ruben, 2012; Huiskes and Boeklagen, 1989) and its consequent shape optimisation of the implant but only few studies are available related to femur fracture. Chen (2018). studied the parametric design of patient specific fixation plates for distal femur fractures. In their study, PSPs were created and edited by parameterising the features of the plate and femur. PSP development usually includes the stages of digital data acquisition of patients followed by restoration of the fracture segment, thereafter parameterisation and creation of the plate model based on fracture information and finally performance evaluation and design optimisation of the bone plate structure.

1.5 Motivation of the study: research gaps observed in the current state of the art

The clinical outcome of the different bone plate fixation techniques is debatable since there is hardly any consensus on their relative superiority as an internal fracture fixation device. There is no clear biomechanical parameter based on which a comparative stability assessment of these extramedullary implants can be made. There is a lack of rigorous preclinical assessment that takes into account the physiological loading conditions of the osteotomies. Also, there is ample evidence that incidences of sideways fall constituted majority of fragility related hip fractures, and hence it becomes pertinent to analyse the condition in implanted femurs. Most of the previously published studies considered loading at quasi-static or at constant displacement rate, which neglects the physics of actual fall. The input loads need to be improved for accurate modelling of the injury itself, which is a result of the dynamic event. Further, there is barely any comparative investigation concerning intact vis-à-vis plated femur based on their response to vibrational effect for sideways fall. Though a number of numerical models of bone fracture healing have developed over the last few decades to predict quantitively tissue differentiation, no modelling approach addressed the influence of screw-type in determining the overall progression of fracture healing. Furthermore, most of these investigations relied on 3D primitive models instead of realistic bone and implant geometries. Moreover, computational studies concerning stress shielding and subsequent bone adaptation in the form of external remodelling of fracture fixated femur have been limited. Most of the commercially available implants in the market

are developed based on the data of the Caucasian population of western countries, and thus they may not be an ideal fit for Indian patients due to anatomic variations.

1.6 Objectives and scope of the thesis

The present study aims to obviate the limitations as discussed in section 1.6, by incorporating an in-depth state-of-the-art biomechanical assessment, which includes simulation of time-dependent post-surgery bone adaptation. This will give a clinical perspective to the design of the bone plates. In the first phase of the study, in vitro dynamic compression tests of a bone-plate construct are performed for damage analysis using femur bone analogues. Furthermore, the influence of the screw arrangement for improved post-surgery behaviour of the implant is endeavoured. For the purpose of validating an *in silico* model (FE based) of a similar construct, a full-field strain measurement using DIC is carried out. Once validated, the *in silico* modelling technique is extended to CT based bone models, thereby addressing the variability in bone quality and fracture pattern. A rigorous preclinical assessment of implant-induced stress shielding is attempted to predict longer term bone adaptation. The present investigation includes the following objectives, which collectively contributed towards achieving the goal of the study.

- **Objective 1:** *In silico* assessment and *in vitro* validation of bone plates for extracapsular femoral fracture under static loading
- **Objective 2:** Dynamic impact analysis on plated femur models to assess implant strength on sideways fall
- **Objective 3:** Phenomenological modelling of post-operative secondary healing for plated femur
- **Objective 4:** *In silico* evaluation of external bone adaptation due to extramedullary fixation plates
- **Objective 5:** A novel design of hip osteosynthesis plate for Northeast (NE) Indian population

1.7 Structure of the thesis

The purpose of this research is to expand knowledge in the field of computational biomechanics and implant design. The research work was carried out with the primary objective that the theoretical findings of the study would be translated into a product that can benefit the public healthcare sector. Technology is a blessing for healthcare sector. Incorporating modern technology in the traditional healthcare strategies can

offer a cost effective, better diagnosis, fast and optimized patient specific solution. Overall, the work has been conceived in 8 chapters. Chapter 1 provides a comprehensive review of the literature and current state of the art related to the field of implant biomechanics and bone healing. Further, the research gaps were discussed, and the objective for the present study was outlined.

Chapter 2 deals with the biomechanical assessment of two different bone plates for subtrochanteric femoral fracture under static loading. The work provides a comparative preclinical assessment between two standard fracture fixation techniques: DHS and PFLP, by employing FE-based in silico models. Two physiological load cases replicating maximum loads during the stance phase of normal walking and stair climbing were considered to simulate daily life activities. Stress based failure characteristics were assessed for the implanted constructs. Experimental validation of the intact femur was conducted to impart confidence in the FE model generation technique. Hoffman failure criteria was used to predict the damage properties of cancellous bone, taking into consideration of the differing tension and compression that characterises the brittle behaviour. The study attempts to evaluate and compare the two implants on following biomechanical behaviours: (1) stress variation on the femur and implant, (2) axial displacement of the fixated femur constructs, (3) postoperative stress shielding and longer-term external remodelling of the host bone.

In Chapter 3, *in vivo* study is carried out using DIC to validate the *in silico* models based on full-field strain measurements. Two commercial implants, e.g., PFLP and VA-DHS were chosen to carry out the FE-based preclinical assessments on a simulated Evans type-I intertrochanteric fracture. The study has been conducted in two parts. In the first part, the 3D in silico osteotomies, intact and implanted (PFLP), was validated based on full-field surface strain measurements using the 2D DIC technique. Once validated, the virtually implanted constructs were assessed under physiological static load cases, and conclusions were made on their relative biomechanical performance. The aim of Chapter 4 is to compare the dynamic response of the implants: intact vis-à-vis plated femurs, in a sideways fall scenario. Further, the investigation explores on the understanding of femur resonance frequency and associated mode shapes excited by dynamic loads. Also, the chapter investigated the performance of the implant in terms of energy loss and predicted the failure zones associated with each implant under sideways fall scenarios.

Chapter 5 implements a fuzzy logic-based algorithm to address the bone fracture healing in the callus region associated with two different techniques of implant in a subtrochanteric femoral fracture. The study applies 3D dynamic fracture healing scheme modelled on a subtrochanteric femur fracture, regulated by both FE analysis and Fuzzy logic control in order to understand the spatio-temporal healing phenomena for both LP and DCP. The study specifically examines the influence of the two screw fixation mechanisms in determining the comparative progression of fracture healing. The simulation of the healing phenomenon in the callus region can be described as an initial value problem involving two mechanical (invariants of strain tensor) and five biological state variables (local tissue composition and vascularisation). The problem is solved iteratively in several healing steps running in loop and accordingly, the local tissue concentrations and material properties are updated. A linguistic fuzzy rule-based algorithm simulated the tissue differentiation phenomenon inside the callus region.

Chapter 6 presents *in silico* assessment for a comparative longer-term performance evaluation of the two extramedullary fixation techniques: DHS vis-à-vis PFLP, in order to conclude their relative superiority. The longer-term performance was evaluated based on the relative extent of the external remodelling predictions. A physiological loading regime was introduced for a more realistic assessment of the osteotomies. External bone adaptation was modelled mathematically using stress analysis coupled with a growth model, in which SED acted as the feedback control variable.

Chapter 7 proposes a a novel design, double oblique device for osteosynthesis of hip (DODO), for the NE population of India, and its performance was compared to that of the conventional implants. This study employs FE analysis to compare the biomechanical outcome of the new device with that of PFLP and variable angle VA-DHS on a femur having an Evans type-I intertrochanteric fracture. Further, dynamic impact load mimicking the sideways fall scenario and secondary bone healing analysis is carried out on NE patient specific femur implanted with DODO.

Chapter 8 summarises and discuss on the salient findings of the present work. Future scope of the study is also outlined to advance the knowledge in the field of computational biomechanics and implant design.

Chapter 2

Preclinical Assessment of Two Extramedullary Fixation Devices for Subtrochanteric Femur Fracture Based on Biomechanical Failure Criteria

2.1 Introduction

Subtrochanteric femoral fracture (SFF) accounts for major proportion (almost up to 34%) of the trauma cases associated with femoral fractures (Koval, 2006; Medda, 2020). It requires immediate surgical intervention usually with a fracture fixation device or implant. The role of the implant is to bridge the fracture site and provide stability to allow early load bearing, while being flexible enough to promote secondary bone healing. DHS and PFLP are two extramedullary implants that are used to fix SFF. DHS comprises primarily of dynamic proximal screw that provides compression along the femoral neck. Low cost, high rate of bone union albeit being a simpler technique and good to excellent functional behaviour make DHS a preferred choice (Swift et al., 2010). However, its outcome remains uncertain for comminuted and highly unstable intertrochanteric and subtrochanteric fractures, and a high failure rate besides causing excessive impaction have been reported in the literature (Glassner et al., 2011; Streubel, 2013). Moreover, the long incision needed for DHS fixation may lead to significant blood loss and soft tissue damage (Morris and Zuckerman; 2002). Some studies associated DHS fixation to longer surgical time, re-fracturing after implant removal, instability of the medial part of the subtrochanteric region (Madsen et al., 1998; Setiobudi et al., 2011).

PFLP, on the other hand, employs locking screw technology with pre-contoured plate that fits well to the contralateral surface of the proximal femur. Theoretically, this technique offers optimum fixation of comminuted and highly unstable fractures associated with higher shearing and pull-out forces (Glassner et al., 2011; Streubel, 2013; Sommer et al., 2003). The pre-contoured plate allows for improved stability by the convergent cannulated proximal locking screws, especially in osteoporotic bone (Tonino et al., 1976). Owing to the presence of multiple proximal locking screws, PFLP

provides better stability against proximal femoral rotation, which is a known limitation of a conventional DHS fixation. Patients having subtrochanteric fractures, fixated with PFLP was found to have shorter bone union time, less operation time and lower blood loss (Zhong et al., 2014). However, few other studies reported failures with this implant in the form of secondary varus collapse, screw cut out, implant failure etc (Glassner et al., 2011; Streubel, 2013). Several other investigations found PFLP as a successful fixation technique for complex femoral fracture and also for revision surgeries (Sommer et al., 2003). While the clinical outcome of the two techniques is still debatable, there is hardly any consensus on their relative superiority as internal fracture fixation device. In their FE analysis, Wang et al. (2020) speculated that PFLP offers greater stability for stable subtrochanteric fracture. Sowmianarayanan et al. (2008) however, predicted that the deflection of the DHS fixated femur to be closer to that of intact femur, though the magnitude of axial strains for DHS was less than that of the intact femur. Despite limitations with regards to the simplistic nature of some of these models, the computational approach demonstrated the potential of such preclinical techniques. Also, it has the ability to evaluate the risk of implant failure, since replicating in vivo conditions certainly allows pre-assessment of various biomechanical failure scenarios. Moreover, computational investigations with regard to stress shielding and subsequent bone adaptation in the form of external remodelling of fracture fixated femur have been limited.

The primary objective of the present study was to carry out a comparative preclinical evaluation of the two techniques: DHS and PFLP, by employing FE based in silico models. A physiological loading regime was introduced for more realistic assessment of the implanted osteotomies. Stress based failure characteristics were assessed for the implanted constructs. An experimental validation of the intact femur was also conducted to impart confidence into the FE model generation technique.

2.2 Materials and Method

2.2.1 FE model generation of intact and implanted construct

The 3D FE models of the implanted and the intact femur were generated using the manufacturer supplied CAD model of a left femur (Sawbones Europe AB, Malmo, Sweden, model# 3406). The CAD models were converted into faceted surfaces (STL file format) and imported into Rhinoceros v14.0 (Rhinoceros, Robert McNeel & Associates, Seattle, USA). All components of the implant were modelled separately and

virtually assembled later during implantation. A seven-hole DHS plate was modelled in NURBS modelling environment of Rhinoceros and virtually fitted with five screws (1 proximal locking and 4 dynamic) (Fig. 2.1 a,b). A seven-hole PFLP plate was also designed and fitted virtually with a total number of six bone screws (3 proximal locking and 3 dynamic) as per the surgical guidelines (DePuy Synthes®) (Fig. 2.1 c,d). A comminuted fracture, simulated as two-part fracture gap of 20 mm, was created in the subtrochanteric region of the implanted femur (Fig. 2.1 b,d) (Latifi et al., 2012; Floyd et al., 2009). All implant specifications are given in Table 1. The fracture surfaces were modelled as transverse gap. This transverse gap accounts for the misalignment in the mated ends of the broken bone during fixation. It may further be noted that the fracture gap was intentionally made large to simulate an extreme case of fracture, which enabled focussing on the biomechanical response of each implant fixation avoiding the interference from fracture itself or its opposing interfacial surfaces while subjected to different load cases.

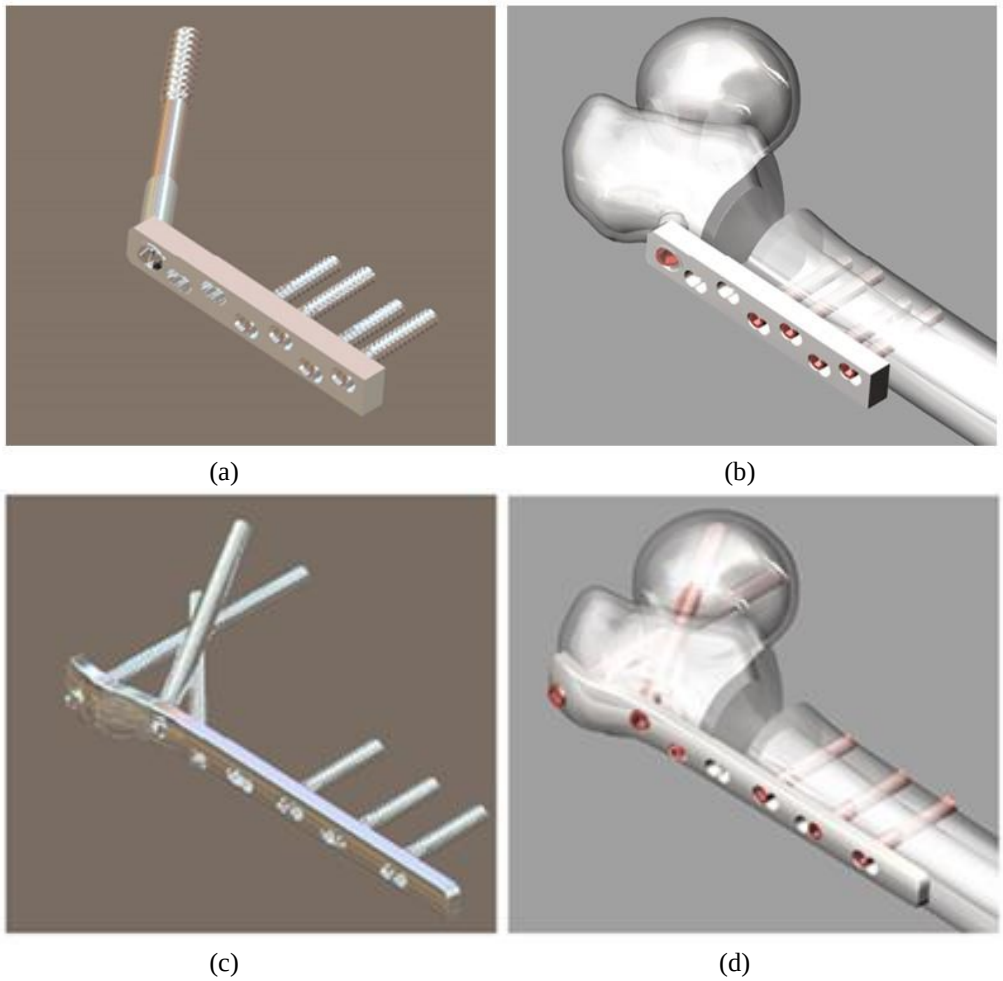

Fig. 2.1: Rendered CAD models of the implants and the implanted femur with a simulated non-comminuted subtrochanteric fracture gap of 20 mm: (a) DHS, (b) DHS fixated femur, (c) PFLP and (d) PFLP fixated femur.

Table 2.1: Specifications corresponding to DHS and PFLP models (DePuy® Synthes). All dimensions are in mm.

Implant	Plate thickness	Proximal locking screws		Dynamic screws	
		diameter	pitch	diameter	pitch
DHS	9.0	9.0	3.0	6.0	2.0
PFLP	4.5	7.0	2.0	6.0	2.0

Table 2.2: Applied forces, expressed in percentage of body weight corresponding to load cases, normal walking and stair climbing normalised for body weight of 80kg (Bergmann et al., 2001; Heller et al., 2001). The abbreviation m. stands for muscle.

Load cases	Types of force	F_x	F_y	F_z	Resultant F
Normal walking	hip joint	-15.3	-258.1	-83.6	271.7
	m. abductor	48.1	106.4	23.7	119.1
	m. tensor fascia lata, proximal part	5.5	13.7	15.9	21.7
	m. tensor fascia lata, distal part	3.2	-21.0	-4.5	21.7
	m. vastus lateralis	17.4	-106.8	2.6	108.3
Stairs climbing	hip joint	-19.8	-261.5	-116.4	286.9
	m. abductor	62.0	102.1	51.4	130.1
	Iliotibial tract, proximal part	9.3	16.8	-0.5	19.2
	Iliotibial tract, distal part	2.8	-18.6	-4.2	19.2
	m. tensor fascia lata, proximal part	2.9	2.8	6.2	7.4
	m. tensor fascia lata, distal part	1.1	-7.2	-1.6	7.4
	m. vastus lateralis	24.3	-154.6	-1.3	156.5
	m. varus medialis	62.9	-302.2	-7.3	308.8

The tessellated surface models were subsequently imported into Ansys ICEM CFD v15.0 (ANSYS Inc., PA, USA) to generate a volumetric mesh comprising of 4-noded unstructured tetrahedral elements. Thereafter, the volumetric mesh was imported into Ansys Mechanical v15.0 (ANSYS Inc., PA, USA) and converted into 10-noded tetrahedral mesh. An important advantage of quadratic tetra meshes other than numerical accuracy is its great ability to approximate the 3-D geometry, which is particularly useful for complex geometries, such as the femur in this study (Viceconti et al., 1997). A mesh size study was carried out to check the numerical convergence of

the cortical model (intact) using three different FE meshes containing ~70,000, ~150,000 and ~520,000 elements respectively, and a comparison between their predicted von Mises stress. The maximum difference in peak von Mises stress was predicted to be ~5% between the coarse and the medium meshes, and ~2% between the medium and fine meshes. Therefore, considering the computational efficiency and accuracy, the medium sized mesh was judged to be sufficiently accurate (Chanda et al., 2015). The femur models (implanted and intact) were oriented laterally by 10° in the frontal plane and dorsally by 10° in the sagittal plane as described for fatigue testing (ISO 7206-4:2010). A condition of zero displacement was applied at distal femoral surface nodes sufficiently away from point of application of load. Two physiological load cases replicating maximum loads during stance phase of normal walking and stair climbing were considered to simulate daily life activities (Bergmann et al., 2001; Heller et al., 2001). Musculoskeletal loading conditions for normal walking comprise of hip contact force and muscle forces of abductor, tensor fascia latae (proximal and distal) and vastus lateralis. The loading conditions for stairs climbing include additional effects of iliotibial tract (proximal and distal) and vastus medialis, along with the hip contact force and the muscle forces applied during normal walking. All muscle forces were normalized for a body weight of 80kg, as shown in Table 2.2. An equal weightage was given to each load case while calculating the results. It may be noted that muscle attachment points were slightly adjusted to make way for the implant, though the arrangement was kept identical and clinically admissible for both fixations.

Table 2.3: Material property data (based on ASTM D1621[*], D695[**], D638[***] & 308[#]).

Material	**Young's modulus (MPa)**	**Poisson's ratio**
Cancellous	155[*]	0.3
Cortical	16,700 (*compressive*)[**] 10,000 (*transverse tensile*)[***]	0.3
Plate & screw (stainless steel)	193,000[#]	0.3

The material models for bone and implants were considered as per Table 2.3. Linear elastic, isotropic and homogenous material properties were applied to cancellous bone, whereas orthotropic material properties were applied to the cortical bone based on the data provided by the manufacturer (Biomechanical products catalog Sawbones).

The material for the plate and screw was considered to be stainless steel (SS). Poisson's ratio for all material was set as 0.3. In order to simulate the locking behaviour of the screws, the interface between the proximal locking screws and the bone, however, was considered to be bonded under all conditions. Screw plate interface was assumed to be bonded for PFLP fixation to mimic the locking plate characteristic whereas it was assumed to be in contact for DHS fixation with coefficient of friction set as 0.3. In both models, distal dynamic screws were assumed to be in contact with bone having a coefficient of friction of 0.3. The interface between the cortical and cancellous bones is considered to be bonded under all conditions. It may be noted that by defining bonded interface in an FE simulation, the geometry was treated as though it was perfectly connected, like one solid piece. Hence, no relative movement, frictional or otherwise, is allowed at the interface. Augmented Lagrange Method with standard (surface-to-surface) contact behaviour was considered as the contact algorithm (Eberle et al., 2007; Devika et al., 2012). For convergence, values of penalty stiffness and penetration tolerance were set as 10 and 0.1, respectively.

2.2.2 Hoffman Failure Criterion

Hoffman failure criteria (Eq. i) was used to predict the damage properties of cancellous bone taking consideration of the differing tension and compression that characterize the brittle behaviour (Hoffman, 1967). Subscript 1, 2 and 3 indicates the three principal directions of the model respectively.

$$C_1(\sigma_2-\sigma_3)^2 + C_2(\sigma_3-\sigma_1)^2 + C_3(\sigma_1-\sigma_2)^2 + C_4\sigma_1 + C_5\sigma_2 + C_6\sigma_3 + C_7\tau_{12}^2 + C_8\tau_{13}^2 + C_9\tau_{23}^2 = 1 \quad \text{... (2-1)}$$

C_1, C_2, C_3, ..., C_9 are the material properties constant, the values of which were determined from literature (Reilly et al., 1975). σ_1, σ_2 and σ_3 are the principal stresses along the respective principal direction. τ_{ij} are the shear stresses in the ij plane (i,j = 1 to 3). The calculation of the Hoffman failure values was done by using a custom MATLAB script (MATLAB v19a, The MathWorks, Inc., Natick, Massachusetts, United States). Any state of stress lying outside the Hoffman envelope suggests damage initiation or failure at that point.

2.2.3 Experimental validation through *in vitro* testing

Physical model of an analogue femur bone having similar dimensions and properties of the CAD model (4th generation composite femur, model# 3406, Sawbones Inc.) was

procured for in vitro testing under a universal testing machine (UTM) (Fig. 2.2). The cortex of this composite bone was made of short fiber-filled epoxy and the cancellous core made from 17 pcf polyurethane foam. For testing, the intact bone specimen was potted inside a cast iron pot by means of custom-made metal fixtures (Al, Grade HE30), as shown in Fig. 2.2. The custom-made fixture was introduced in order to provide sufficient distal constraint one-third along the shaft from the distal end while tilting the bone laterally by ∼10° in the frontal plane and by ∼10° dorsally in the sagittal plane (Fig. 2.2). This orientation is similar to that described for fatigue testing of hip prostheses (ISO 7206-4:2010), designed to represent typical gait load at heel strike. The potted osteotomy was then fixed at the base of the UTM (ZwickRoell Z005TN, Germany) which was equipped with 5kN load cell (Fig. 2.3 a). An identical orientation was maintained for the FE models as well (Fig. 2.3 a).

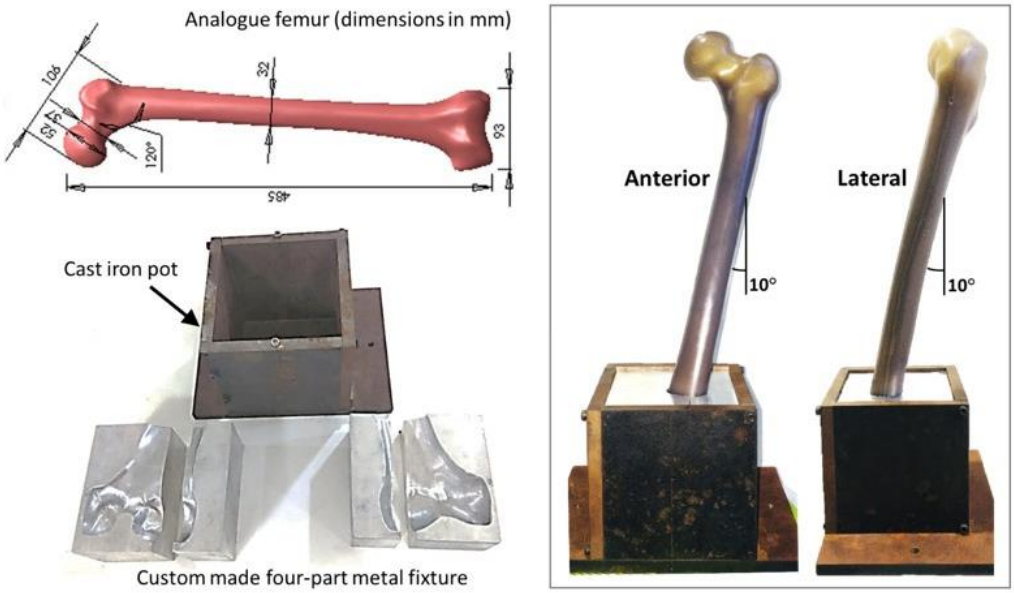

Fig. 2.2: Sample preparation for experimental test set up: (*Left*) analogue femur model (4th generation composite femur, model# 3406, Sawbones Inc.) with dimensions and a custom-made four-part metal fixture (Al, Grade HE30) with cast iron pot; (*right*) anterior and lateral views, respectively, of the potted intact femur. The orientation of the femur was based on ISO 7206-4:2010.

The sample was subjected to axial compressive load acting vertically downward through the load cell to the femoral head (Fig. 2.3 a). The set up was initially calibrated with a minimum load which was then increased quasi-statically up to 2kN at a constant displacement rate of 5 mm/min. The deformation characteristic of the specimen was measured using displacement of the load cell of the UTM and used to calculate the stiffness as the slope of the force–displacement curve (TestXpert, ZwickRoell). For one-to-one validation with respect to the in vitro osteotomy, however, muscle forces

were not considered in the FE model of the intact femur. For all other in silico analyses, muscle forces were considered as per Table 2.1.

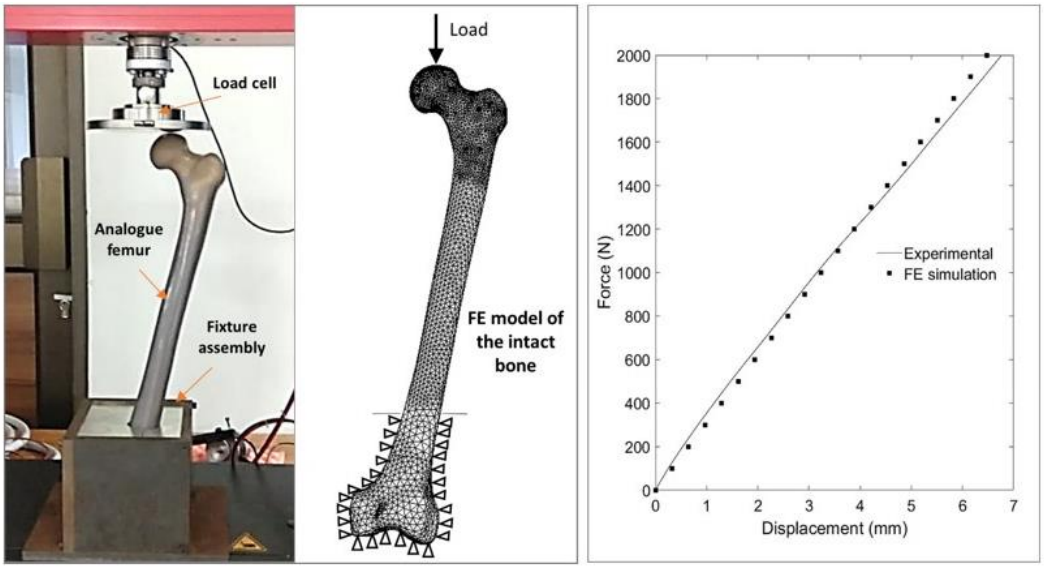

(a) (b)

Fig. 2.3: Experimental validation of the FE model of intact femur under compressive load: (a) the potted test specimen under UTM and the representative FE model; (b) the force-displacement characteristic plots for compressive test and that obtained during FE simulation.

2.2.4 Statistical analysis for correlation between measured and FE predicted values

In order to verify the degree of correlation between the FE predicted and the measured data, a Student's t-test was conducted. The null hypothesis states that there exists no significant correlation between the measured and the predicted values. The correlation coefficient (R), standard error of estimate (SE), percentage error (PE) and 'test statistics' value (t-statistic) of the regression slope (b) were used to evaluate whether a significant relationship existed between the DIC measured and FE predicted strain, assuming the data points were normally distributed (95% confidence interval). The percentage error was calculated as the ratio of 'SE of b' to the slope of the regression line, 'b'. There are standard methods in statistics to calculate P value, which is nothing but the area under the probability curve. The entire statistical analysis was performed and interpreted with the help of IBM SPSS Statistics package (V20).

2.3 Results

The FE model of the intact femur was validated based on experimental data obtained from the force-displacement characteristics under compressive load. The cut-off compressive load was chosen as 2kN because hip joint reaction force under the musculoskeletal loading regime for an 80-kg subject (Table 2.1) was close to 2kN. The

Student's t-test revealed significant correlation between the measured and the predicted dataset (R^2 = 0.9989) (Fig. 2.3 b). The regression slope (b = 0.934, PE of b = 0.3%) was indicative of a strong linear relationship between the measured and FE predicted values (95% confidence interval). The overall validation outcome imparted significant confidence into the FE model generation procedure and model calibration to counter error due to artifacts. The calibration was done through the calibration interface of standard software (TestXpert, ZwickRoell) where the residual force value was cleared before the start of test.

In order to carry out a comprehensive preclinical assessment of the two implants, the musculoskeletal loading regime, as described in Table 2.1, was applied in the representative FE models under static condition. The axial displacement for the DHS fixated femur was found to be 14 mm, which was closer to that predicted for intact femur (8 mm). However, the PFLP construct deflected almost twice as much as the DHS counterpart, thereby exhibiting lesser structural stiffness. Fig. 2.5 illustrates the distribution of von Mises stress on intact, DHS and PFLP fixated femur (cortex) in anterior, medial and posterior aspects, respectively. In both DHS and PFLP fixated bone, a major portion of the proximal femoral head and the region adjoining to the plate under the fracture site were stress shielded (Fig. 2.4). Proximally above the fracture, the stress shielding was predicted to be 27% for DHS and 31% for PFLP fixated bone. However, the corresponding values were found to be 43% and 37%, respectively, in the distal femur below the fracture gap. The maximum stress values in the DHS fixated femur were identified around the medial side of the screw hole just under the fracture region. However, for PFLP fixated femur, the lateral side of the 3rd screw hole (from top of plate) in the femoral head was associated with maximum stresses. The PFLP plate was subjected to higher degree of bending stresses as compared to the DHS plate (Fig. 2.5). The hip screw in DHS predicted higher amount of stresses than the three proximal locking cross-screws in PFLP. Among distal screws, the first dynamic screw for both implants predicted maximum stresses, although this stress magnitude was 30% less for PFLP as compared to DHS.

Fig. 2.6 shows the Hoffman failure envelope for the two bone-implant constructs along with the stress planes indicating the ultimate strength limits for tension and compression in all three directions. The intersection between these three mutually perpendicular planes and the envelope is the effective working zone.

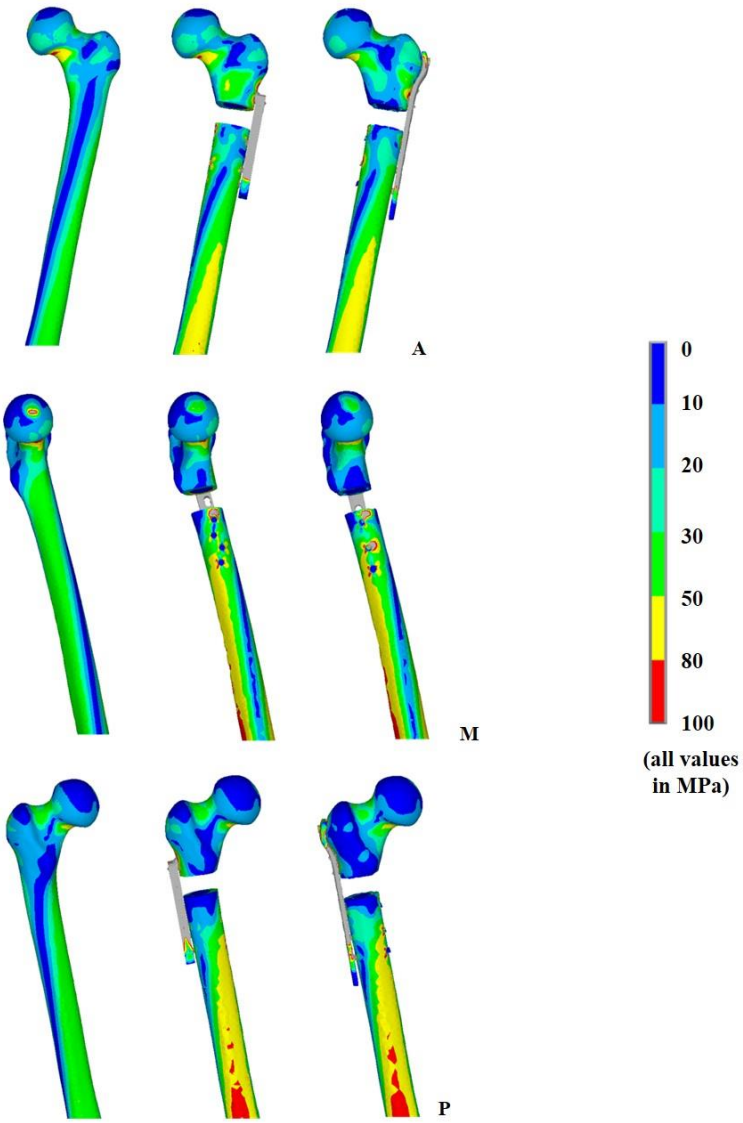

Fig. 2.4: The von Mises stress distribution in anterior (**A**), medial (**M**) and posterior (**P**) aspects of intact, DHS and PFLP fixated femur, respectively. An equal weightage was given to each load case of normal walking and stair climbing, considering body weight of 80 kg, while calculating the results.

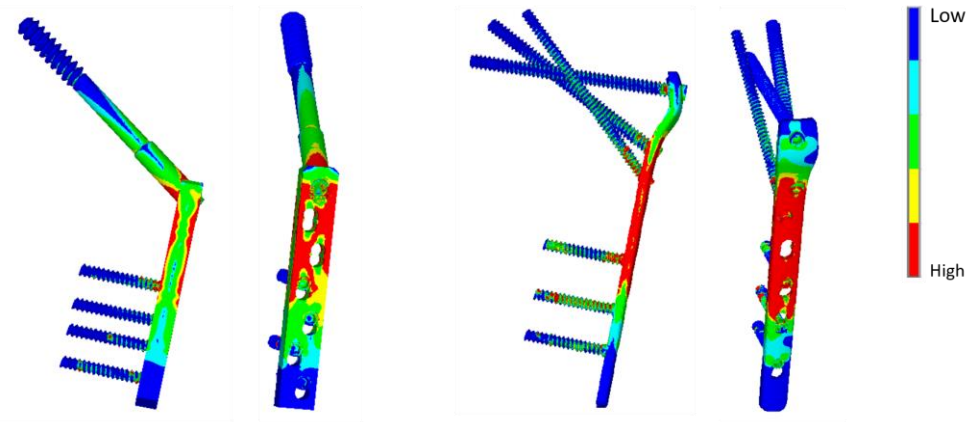

(a) (b)

Fig. 2.5: The von Mises stress distribution at various aspects in corresponding bone plates (a) DHS, (b) PFLP. An equal weightage was given to each load case of normal walking and stair climbing, considering body weight of 80 kg, while calculating the results.

For DHS construct, the state of stress of all bonded interfacial nodes was found to lie inside the effective working zone (Fig. 2.6 a). However, the state of stress of some interfacial nodes corresponding to PFLP construct was found to lie outside the working zone, thereby indicating possible chances of debonding (Fig. 2.6 b).

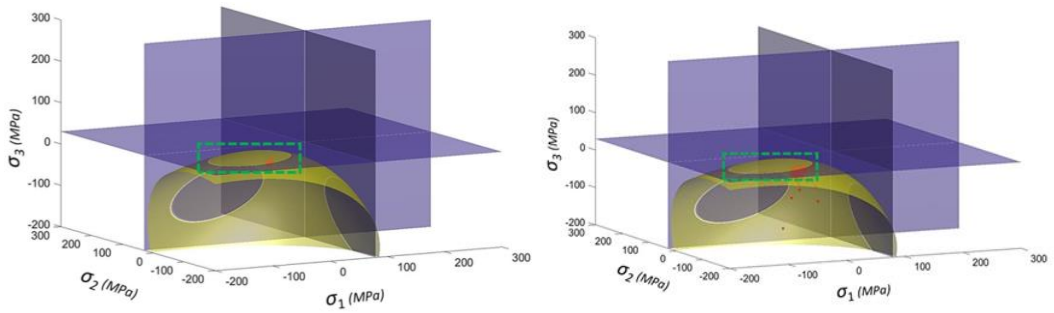

(a) (b)

Fig. 2.6: 3D Hoffman failure envelope for (a) DHS and (b) PFLP fixated bone. The effective working zone (as indicated by the dotted green rectangle) is the intersected portion of the elliptic paraboloid (yellow) with the stress planes (violet).

2.4 Discussion

In the present study, the interface strength was assessed preclinically for subtrochanteric fracture treated with two extramedullary devices, e.g., DHS and PFLP. The structural rigidity of the FE based osteotomies was tested under physiological loading. The FE modelling scheme was validated based on in vitro testing of an intact analogue femur subjected to compressive load. Three successive tests were performed for reproducibility. Linear regression analysis indicated close agreement between the measured average and FE predicted values with a high correlation coefficient (R^2 = 0.9989), low PE in the regression slope (0.3%) and statistically significant results ($P < 0.0001$). However, an intercept of +60N of the regression equation may be ascribed to the non-linear deformation characteristic of the analogue bone, which further requires supportive constitutive modelling for the FE analysis. Further, a full-field surface strain measurement would have been more revealing with regards to validation of the *in silico* models (Chanda et al., 2015). This may be posed as a limitation of the study.

Contrary to the overall uniform load distribution in the intact bone, the load flow pattern in a laterally plated bone is predominantly mediolateral (Fig. 2.4). Consequently, distal to the fracture site, the load is passed on from the plate to screw and then finally to the bone. Proximally above the fracture site, the load flow pattern, however, is reverse since the same is transferred from bone to the device. As a result,

the hip screw in DHS receives more load from the head of femur than that shared by the three cross-screws in PFLP. The higher degree of bending stresses in PFLP as compared to the DHS plate, is suggestive of risk of mechanical failure. Thus, necessitating the importance of imparting post-operative rigidity, especially to a comminuted fracture like this. Moreover, the present study also predicted that the pre-contoured proximal bend in PFLP and multiple cross-screws serve little in terms of proximal stress shielding (Fig. 2.5). Biomechanical studies involving cadaveric bone also showed that PFLP had lower failure load than DHS (Wang et al., 2014; Forward et al., 2012).

2.5 Summary of the findings

The above findings altogether indicate that, however superior the plating strategy may be in terms of less invasive nature and more anatomic loading in PFLP, it may still lead to compromised rigidity unless the screws are not arranged judiciously and in sufficient numbers. Contrarily, the preclinical prognosis of DHS fixation revealed rigid mechanical support, owing much to its thicker plate geometry, with admissible longer term external adaptation. Nevertheless, it goes without saying that the results may be vastly differential depending on the nature of fracture, screw positioning, surgical paraphernalia and patient specificity. The post-operative von Mises stress distribution was predicted to be non-uniform for both DHS and PFLP fixated cortical bone as opposed to an intact femur, though stress shielding was slightly higher for DHS in the distal bone fragment (by ~6%). Although the two fixation devices are simulated in an artificial femur, the preclinical biomechanical assessment performed here can also be successfully applied to compare fixation techniques in patient-specific models.

Chapter 3

Static Strength Assessment of Extramedullary Plates for Intertrochanteric Femur Fracture: a Comparison Based on Validated Models

3.1 Introduction

Hip fracture accounts for a large number of hospitalizations and is associated with high mortality, morbidity, and substantial economic burden (Braithwaite et al., 2003). Intertrochanteric fracture accounts for about 50% of all hip fractures that are caused by trauma (Ahn and Bernstein, 2010). The risk of intertrochanteric fracture increases with osteoporosis, typically seen in the elderly population, predominantly in women (Haentjens et al., 2007). Elderly patients afflicted by a decrease in visual acuity and muscle imbalance may slip and fall, resulting in such fractures. In the younger population, such fractures may be caused by high-velocity injuries, e.g., road traffic accidents or injuries related to sports (Nieves et al., 2010; Hasenboehler et al., 2007).

Surgical treatment for intertrochanteric fracture can involve intramedullary or extramedullary fixation of the femur. Contrary to the intramedullary types, extramedullary plates bridge the fracture site by attaching superficially with the bone by means of bone screws. Introduction of VA-DHS facilitates in optimum placement of dynamic hip screw, which otherwise is difficult with DHS. It further allows angular adjustment of side plate barrel to conform to different shaft angle. Also, the adjustable nature of the plate accommodates the variability of screw plate in femoral head (Chaim et al., 2002). PFLP is a relatively newer type of extramedullary plate, which merges locking screw technology with conventional plating techniques, as discussed in the previous chapter. Several studies reported success with PFLP fixation for complex femoral fractures, especially for revisions subsequent to failure of other implants (Sommer et al., 2003; Zha et al., 2011; Saini et al., 2013; Hasenboehler et al., 2007). Nevertheless, whether PFLP has better biomechanical outcomes than DHS or VA-DHS with regards to non-comminuted intertrochanteric fractures remains debatable.

Strain gauges (SGs) are considered to be the gold standard for measuring the in vitro strain fields (Katz et al., 2020). This technique has been employed in various long bone FE model validation studies and also to access local deformation of composite femurs (Gupta et al., 2004; Schileo et al., 2007; Bettamer et al., 2017). However, the major limitations associated with the SGs are the need for detailed surface preparation and its inability to provide full-field strain information since strain results are available only at the site of application of the SGs (Yang et al., 2007). Further disadvantages include the necessity of plane and smooth surface of the specimen to bond the gauge and non-availability of 3D component of strain (Diaz et al., 2000). Moreover, for heterogeneous, natural composites such as bone, the material inhomogeneity often leads to considerable strain variation across its structure. This calls for full-field data-rich strain measurement technique. In recent years, digital image correlation (DIC) has garnered extensive popularity in the field of experimental biomechanics owing chiefly to its full-field strain measurement capability apart from detailed resolutions and greater tolerance to complex test specimens (Dickinson et al., 2012; Ghosh et al., 2012; Peters et al.,1982; Kahn-Jetter et al.,1990).

Typically restricted to FE validation purposes, DIC has been predominantly used in the field of orthopaedic biomechanics to measure surface strain fields both in cadaveric and composite femur. DIC was employed to find the differences in strain pattern of the medial cortex of composite femurs implanted with femoral prostheses of different material stiffness (Tayton et al., 2010). Thomson et al. (2007) used DIC to investigate the local distribution of mechanical strain within regenerating soft tissue section []. Dickinson et al. (2011) validated their FE model using DIC on composite proximal femur under quasi-static loading. Chanda et al. (2015) compared the DIC measured strain data corresponding to seven gruen zones of the intact and implanted femur analogues to the FE predicted strain field.

In recent years, Grassi et al. (2013) in their study validated FE models of human femora against experimental data from three cadaveric femora using full-field strain distribution collected via DIC. The drawback in their study was low sample size and single loading condition. Bettamer et al. (2017) employed DIC to validate their 2D FE model based on quasi brittle damage law under quasi static loading condition till complete fracture occurs. Another study conducted DIC measurements on five frozen femurs to validate their quantitative computed tomography-based FE (QCT/FE) analysis and compared the results with SG measurements using both strain and

displacement mapping (Katz et al., 2020). Repeatability of the DIC measurements during compressive testing of composite femurs was evaluated by another study (Väänänen et al., 2013). Rossman et al. identified the fracture initiation region within the femur using DIC with high strain rate application and subsequently validated the representative QCT/FE models (Rossman et al., 2017).

The objectives of the present study have been achieved in two parts. In the first part, the 3D in silico models, intact and PFLP implanted, were validated based on full-field surface strain measurements on composite femurs using the 2D DIC technique. Once validated, the implanted FE constructs – PFLP and VA-DHS – were assessed in toto under static compressive loading, and conclusions were made on their relative biomechanical strength vis-à-vis the intact femur.

3.2 Materials and Method

The entire methodology starting from specimen preparation for the DIC study till the FE model generation has been described piecemeal in the following subsections.

3.2.1 Specimen preparation and DIC experimental setup

Two large-sized synthetic left femurs (Sawbones, Europe AB, Malmo, Sweden, model# 3406) were procured and prepared as a two-part intertrochanteric fracture (clinically known as Evans type-I) by an experienced orthopaedic registrar. Sawbones are artificial bone analogues that mimic natural bone both in terms of geometry and material properties (Biomechanical products catalog Sawbones). The fracture simulated bone analogues were subsequently fixated with a PFLP and a VA-DHS implant (Fig. 3.1). Full specifications of the PFLP and VA-DHS implants are mentioned in Table 1. One such femur was kept intact to use as a control reference for the implanted construct (PFLP) during the experiment. Only the PFLP and intact femur were considered for experimental analysis. Both the PFLP fixated and the intact femur were painted matt white followed by spraying of black speckles (using airbrush) on identifiable locations to generate a high contrast random speckle pattern (Fig. 3.1). The average speckle diameter was kept at less than 5 pixels to adhere to the recommended guidelines (Chanda et al., 2015). After removing the lower condylar section, the femur specimens were subsequently potted one-third along the shaft from the distal end to a custom-made aluminium rig using a dimensionally stable dental tray material (Bosworth FastrayTM) (Fig. 3.1). An identical upright orientation of the analogue bone specimens ensured ease of comparison during the experiment.

The 2D DIC experiment was carried out under a universal testing machine (MTS 858 Bionix-Test System, MTS Systems Corp., MN, USA) by applying quasi-static compression through the head by ramping the load to 3 kN at a speed of 10 N/s (Fig. 3.2). A load relaxation of 3s after every 500 N was used to capture deformed speckle

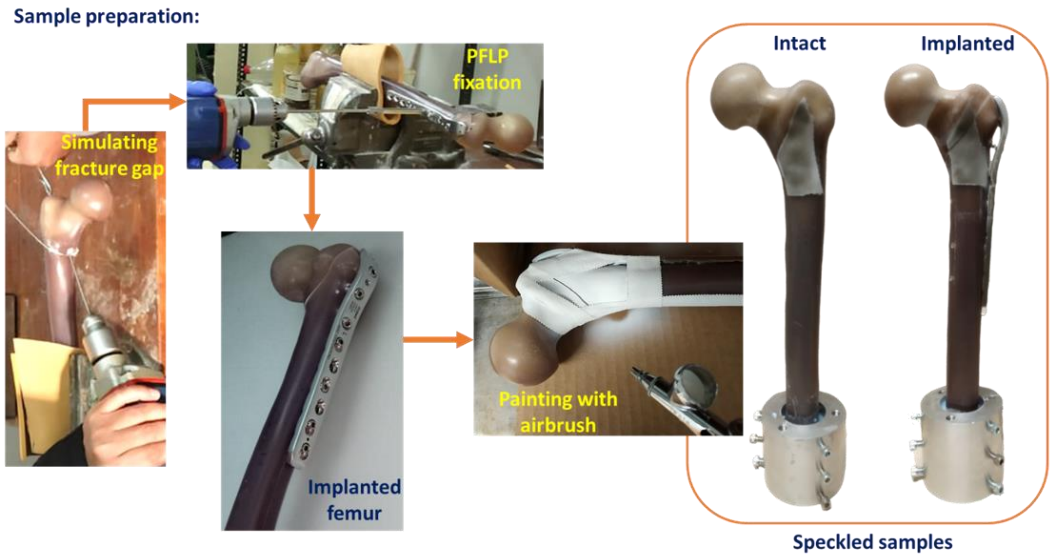

Fig. 3.1: Sample preparation starting with simulating fracture gap, PFLP fixation, generation of speckle pattern on the two constructs and finally constraining distally via a custom fixture.

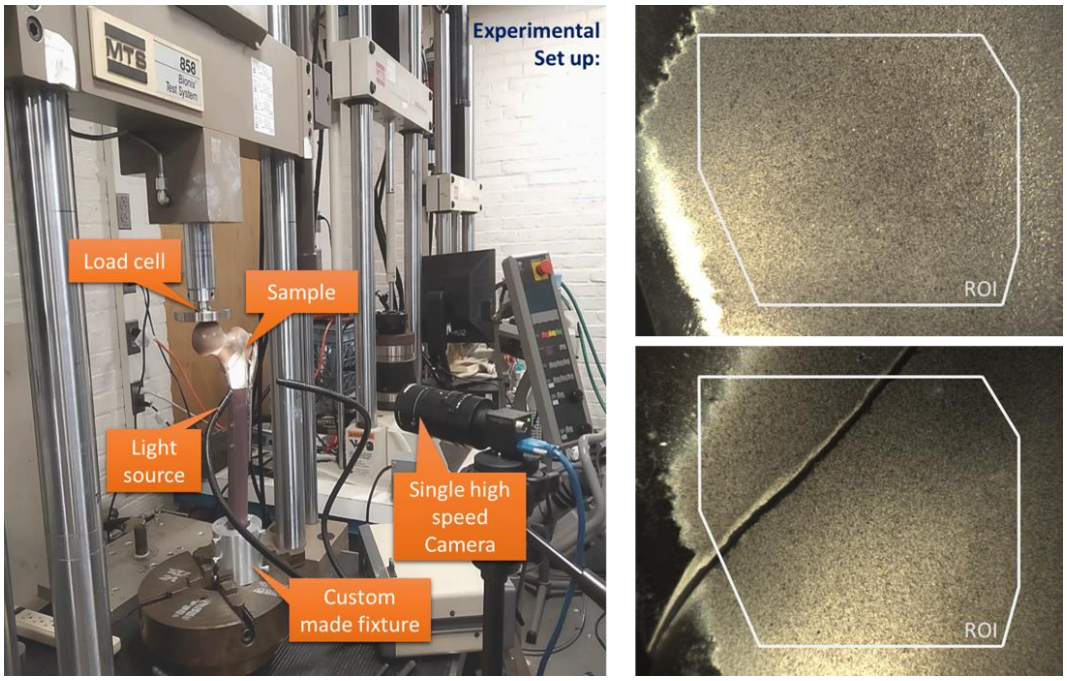

Fig. 3.2: Experimental set up along with the region of interest (ROI) on the speckled part of the construct for DIC experiment on intact and PFLP implanted femur.

patterns using a digital camera (LIMESS Messtechnik u. Software GmbH, Krefeld, Germany). The position of the solo camera was kept fixed, both for the implanted and intact case, in order to have a one-to-one comparison of the measured data. The rate of

image acquisition was set at 1 fps. The duration of the experiment in both the case was 2 min 43 secs. Also, the sampling rate for the experimental data was 104 samples/sec. GOM Correlate, an open-sourced image correlation software, was used to measure the strain field at the region of interest (ROI) for both specimens by post-processing the recorded data – deformed vis-à-vis undeformed (Fig. 3.2). In order to eliminate any mechanical slack in the system, a small preload (N) was introduced. Necessary preconditioning was conducted to ensure 'steady state' stiffness of the constructs is reached. It is worth noting, however, that such quasi-static testing may not represent many clinical conditions, e.g., impact injuries, but it is a widely accepted non-destructive technique for comparative assessment (Hensley et al., 2017; Dickinson et al., 2011; Katz et al., 2020).

Table 3.1: Specifications corresponding to PFLP and VA-DHS.

		PFLP	**VA-DHS**
Screw	proximal	3	1
	distal	4	4
Profile (l,b,t) (mm)		195,19,6	109,19,5.8
Holes		6 (Combi)	5
Angulation of screws	proximal locking	96º, 115º, 130º	115º
	distal dynamic	90º, 90º, 90º, 90º	90º, 90º, 90º, 90º
Diameter of screws (mm)	proximal locking	6.5	12.5
	distal dynamic	5	5

3.2.2 FE modeling and analysis

The 3D FE models corresponding to the PFLP and VA-DHS constructs were created from CT scan dataset using medical image processing program Simpleware™ (Synopsys Inc., Mountain view, USA) (Fig. 3.3). The CT scans (512 x 512 resolution, 120 kVp, 1.0 mm slice thickness and 0.64 mm layer spacing) were performed by an experienced radiologist and obtained from a precision scanner (SOMATOM Definition AS+, SIEMENS). The FE model of the intact bone, however, was generated from the manufacturer-supplied CAD model of the left femur. The 3D models were then imported into Ansys ICEM CFD v15.0 (ANSYS Inc., PA, USA) to generate volumetric meshing comprising of 10-noded tetrahedral elements (Nag et al., 2021). It may be noted that 10-noded quadratic tetra elements are known to predict more accurate results than 4-noded unstructured tetra mesh. Geometric non-linearity was considered for all FE analyses.

The loading of the specimens was kept identical to that during the experiment, to validate the FE models of intact and PFLP implanted femurs. The load (3kN) was applied vertically downward through the femoral head (Fig. 3.3). All the six degrees of freedom were arrested at distal femoral surface nodes to mimic the experimental arrangement (Fig. 3.3).

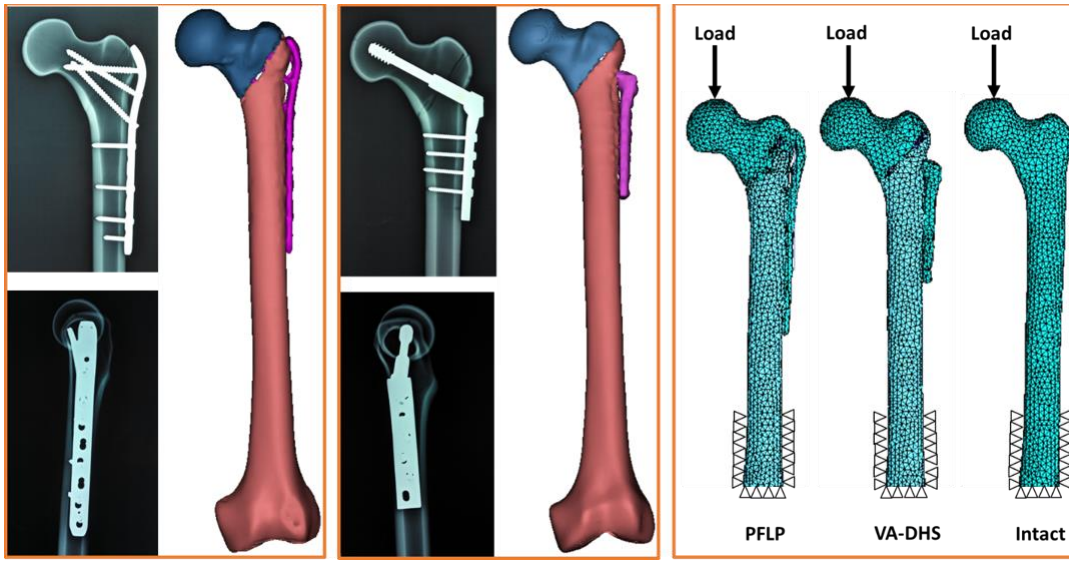

Fig. 3.3: Generation of the FE models: 3D reconstruction of (a) PFLP and (b) VA-DHS fixated femur was done using Simpleware® software package (Synopsys).

The material models considered for bone and implant are similar to that presented in Table 2.3. Isotropic and homogeneous material properties were applied to the cancellous bone, plate and screws whereas orthotropic material properties were considered for the cortical bone based on the data provided by the manufacturer (Biomechanical products catalog Sawbones). The material for the plate and screw were considered to be stainless steel. Poisson's ratio was set as 0.3 for all materials. All interfaces of the FE models were assumed to be bonded under all conditions.

3.2.3 Data interpretation and statistical analysis

The 2D DIC strain measurements were compared with the FE predicted strain field across the ROI to impart confidence into the numerical analysis (Fig. 3.4). A 2 mm × 2 mm gage area was conceived for obtaining the nodal averaged strain values across the ROI, resulting in a total of 304 points (values). A judicial selection of subset size and filter size ensured less bias and improved accuracy. For one-to-one correspondence between the DIC measured and FE predicted strain, an in-house image registration algorithm was employed. It may, however, be noted that some data noises especially at the fracture site have been neutralized for better correspondence. Moreover, the

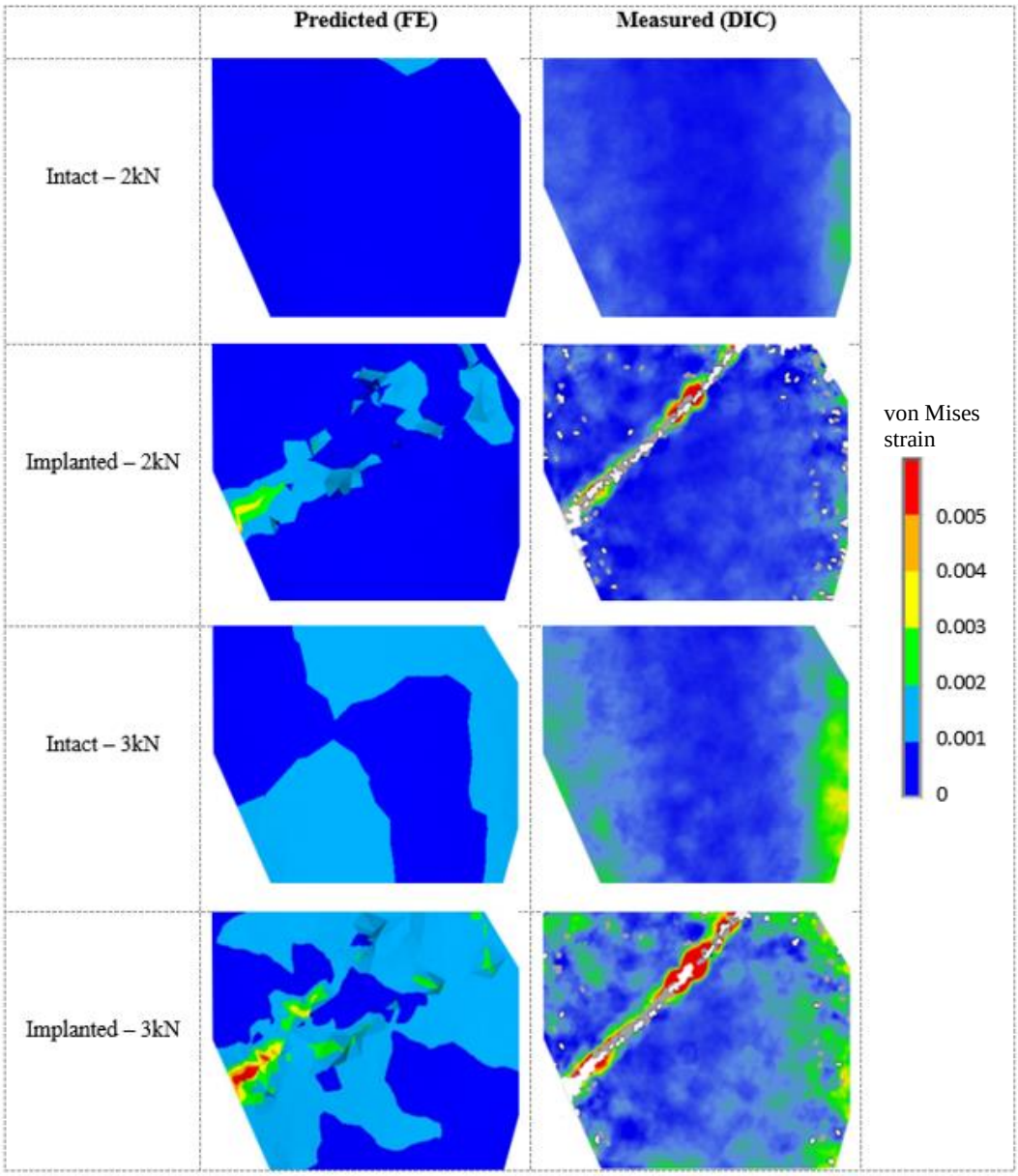

Fig. 3.4: The von Mises strain contours for the intact and implanted constructs when subjected to compressive load of 2kN and 3kN, respectively.

averaging technique also mitigated the effect of singularities present in the DIC images. The regression analysis was carried on the nodal averaged strain values across all 304 gage areas of the DIC measured and FE predicted values. The values of R, SE, PE, b and P-value were used to evaluate whether a significant relationship existed between the DIC measured and FE predicted strain. The percentage error was calculated as the ratio of 'SE of b' to the slope of the regression line (b).

3.3 Results

The von Mises strain contours – DIC measured and FE predicted – in the ROI for the intact and PFLP constructs under an axial compressive load of 2kN and 3kN are shown

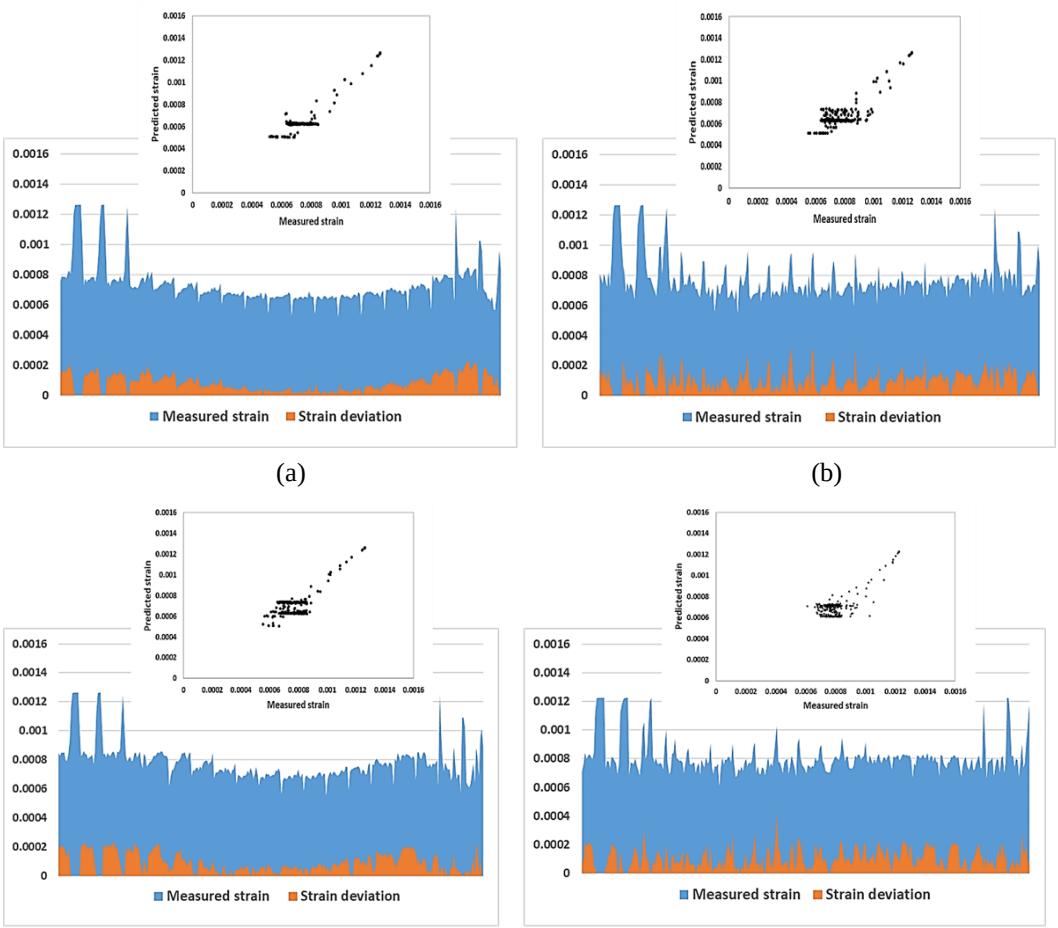

Fig. 3.5: The area plot representing absolute strain deviations against the measured strain data across all gauge areas starting from the top-left to the bottom-right gauge (taken vertically) for (a) intact – 2 kN, (b) implanted – 2 kN, (c) intact – 3 kN and (d) implanted – 3 kN constructs. On top of each plot, the corresponding correlation plot between measured (DIC) and predicted (FE) strain values is also shown.

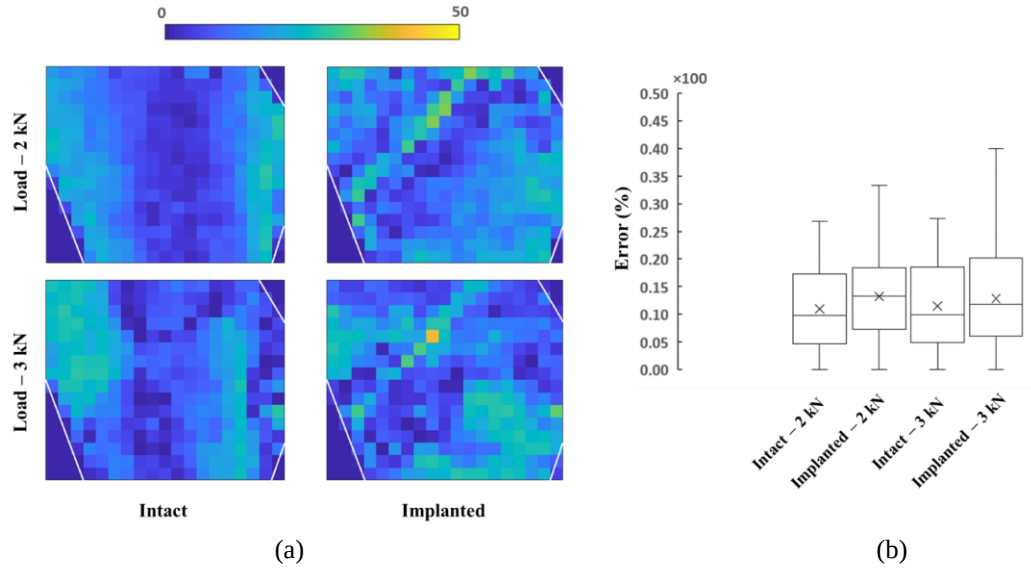

Fig. 3.6: Error analysis of the strain values obtained under static conditions – measured vs. predicted: (a) spatial distribution of error (%) for all four cases across the ROI shown by the polygonal region and (b) the error distribution (%) for all four cases. Mean values for the respective cases are shown by a cross sign.

in Fig. 3.4. The strain values ranged between 0 to 1400 με for both constructs. For 2kN loading, the mean values of strain for intact femur corresponding to FE predicted and DIC measured were found to be 650 με (SD) and 730 με (SD), respectively. For 3kN loading, the corresponding values were 700 με (SD) and 780 με (SD). The predicted and measured average strains for PFLP fixated femur were 670 με (SD) and 770 με (SD), respectively, under 2 KN load, and 710 με (SD) and 810 με (SD), respectively, under 3 kN load. In the ROI, the percentage of strain shielding in the PFLP fixated bone was measured to be 5.7% and 7.2% under 2kN and 3kN load, respectively. In contrast, the FE predicted strain shielding in the ROI was found to be 2.5% and 5.1%, respectively for the two loads.

Fig. 3.5 presents the correlation plots between DIC measured and FE predicted strain values along with the area plot representing absolute strain deviation (i.e., ||measured – predicted||) against the measured strain data obtained across all gage areas under 2 kN and 3 kN load. The linear regression analysis predicted a high correlation coefficient (R=0.90) and low standard error estimates (SE=18.71 με) for intact bone under 2kN loading. The corresponding t-test (95% C.I.) also indicated a significant correlation between the measured and predicted data (t-statistic=38.09). The regression slope, b=0.95 (PE of b=2.6%), was indicative of a strong linear relationship between the DIC measured and FE predicted strain. For the implanted specimen, the corresponding values were R=0.86 and SE=24.37 με, respectively. The t-test conducted on the same specimen dataset too yielded significant correlation (t-statistic=29.72, b=0.92, PE of b=3.3%). Under 3 kN load, the correlations were, however, slightly lower. For the intact femur, R=0.80 and SE=29.60 με were found along with a t-statistic score of 23.49 and the regression slope was b=0.87 (PE of b=4.25%). The correlation coefficient R was found to be 0.83 with low SE=29.60 με for the implanted specimen alongside a t-statistic score of 26.52. The corresponding regression slope was b=0.94 (PE of b=3.82%). The p-value associated with all t-tests was significantly small ($P<0.0005$).

It is, however, necessary to highlight the deviations in strain calculation from the measured strain data. Fig. 3.6a presents the spatial distribution of error (%) – DIC measured strain vs. FE predicted strain – across the ROI. This is calculated by dividing the abovementioned absolute strain deviations by the DIC measured strain. From the error distribution (Fig. 3.6b), it can be noted that although mean error remained below 15% for all cases, the values shot up by ~3% in the implanted cases. Maximum error

between measured and predicted strain was observed in the implanted case subjected to 3 kN compressive loading.

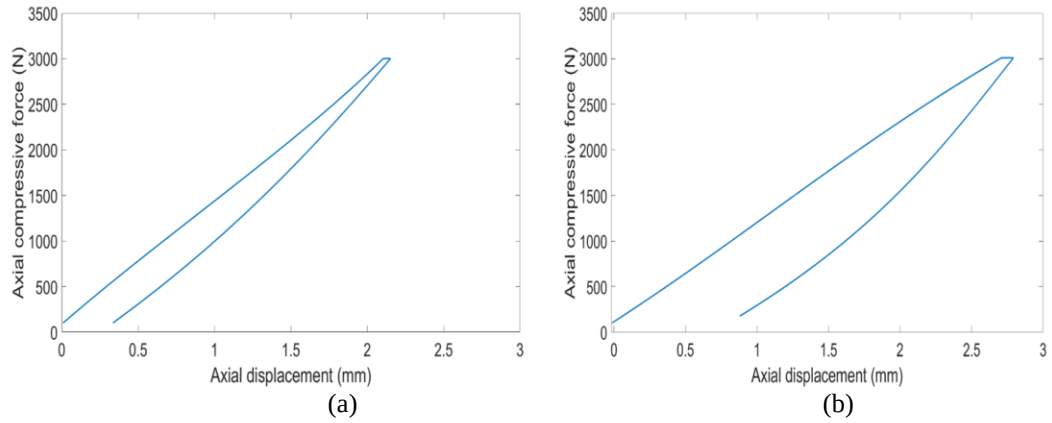

Fig.3.7: Force-displacement curve (loading and unloading) for (a) intact and (b) PFLP implanted femur obtained under quasi-static compressive test.

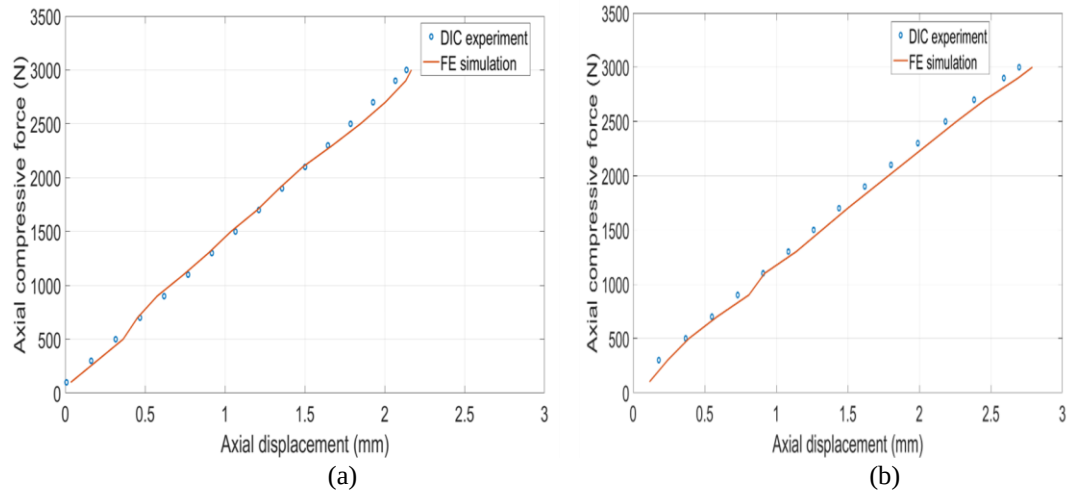

Fig. 3.8: The experimental data have been used for validation of static compression during FE simulation of (a) intact and (b) PFLP implanted construct.

Fig. 3.7a and 3.7b show the measured force-displacement curves corresponding to intact and PFLP fixated femur, respectively, under quasi-static loading-unloading. The maximum displacements at peak load of 3kN for intact and implanted constructs were found out to be 2.1 mm and 2.81 mm, respectively. The corresponding stiffness values were measured to be 1.5 kN/mm and 1.1 kN/mm, respectively. However, the gap between load and unload profiles may be attributed to some slippage of bone under the loading plate and implicit damping in the constructs.

The FE models of supporting osteotomies were validated based on force-displacement characteristics obtained under in vitro loading mentioned above (Fig. 3.8 a,b). The regression analysis and student's t-test, considering 16 data points,

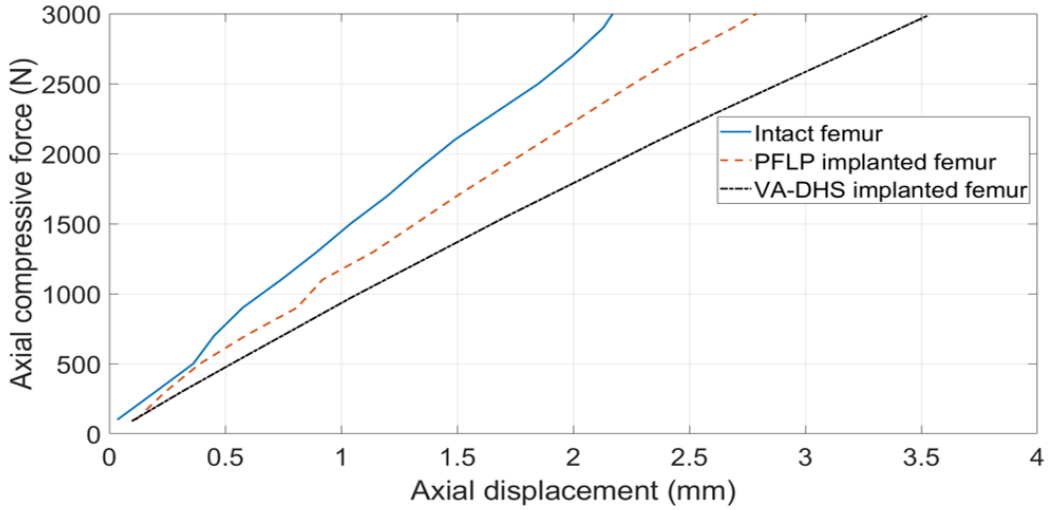

Fig. 3.9: FE predicted force-displacement characteristic of intact, PFLP and VA-DHS implanted femur.

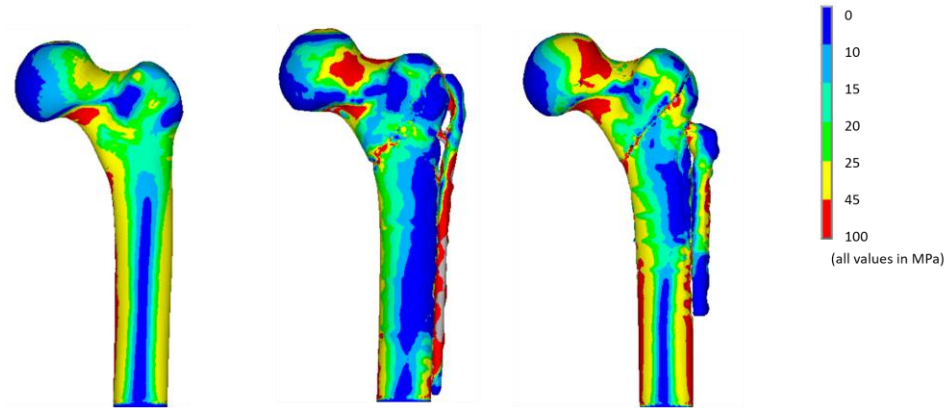

(a)

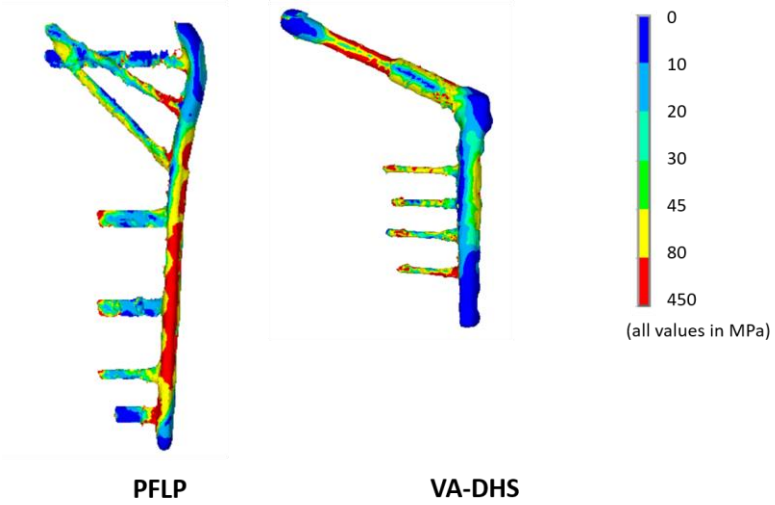

(b)

Fig. 3.10: The von Mises stress distribution in anterior aspect of (a) intact, PFLP and VA-DHS fixated femur (b) PFLP and VA-DHS implants.

revealed a significant correlation between measured and FE predicted curves. A high value of correlation coefficient (R=0.99) and low standard error of estimate (SE=0.02 mm) along with a regression slope, b~1.0 (PE of b=1.4%), and intercept of a = 0.022 were predicted for the intact femur (95% confidence interval). The PFLP construct also demonstrated a high correlation coefficient (R=0.99) and low SE (=0.009 mm) with a regression slope of b~1.0 (PE of b=0.67%) and intercept of a=-0.0317. The high degree of linearity with FE simulations (R^2>0.9) further foreclosed possibility of any permanent set occurring during the in vitro testing.

Fig. 3.9 shows the comparison between FE simulated stiffness models of the three constructs. While the maximum displacements (under peak load of 3kN) for PFLP and VA-DHS fixated femur were predicted to be 2.79 mm and 3.52 mm, respectively, the value was estimated to be 2.18 mm for the intact femur. The intact model demonstrated the highest axial stiffness (1.40 kN/mm) whereas the value for VA-DHS construct was predicted to be the least (0.85 kN/mm). The PFLP construct predicted a stiffness modality somewhere in between these two (1.07 kN/mm).

Fig. 3.10(a) illustrates the FE predicted von Mises stress distribution of intact, PFLP and VA-DHS implanted model (anterior aspect), respectively, under a compressive load of 3kN. Proximally in the femoral head, the stress shielding was predicted to be 37% for PFLP and 24% for VA-DHS models. However, the corresponding values were found to be 45% and 36%, respectively, in the distal femoral shaft. The PFLP plate was predicted to have high bending stress compared to VA-DHS (Fig. 3.10 b). Also, the proximal hip screw in VA-DHS had higher stress intensity than proximal locking screws of PFLP. The average von Mises stress at the calcar region of the PFLP and VA-DHS implanted femur was estimated to be 19.0 MPa and 27.6 MPa, respectively, as compared to 23.0 MPa in the intact model. The corresponding values in the distal femur were 14.5 MPa, 22.0 MPa and 23 MPa, respectively.

3.4 Discussion

The present study attempts to preclinically investigate the biomechanical strength parameters for extramedullary plates for simulated Evans type-I intertrochanteric femur fracture. Nonetheless, careful experimental validation of such in silico models is warranted a priori, wherever possible, before prediction models are employed in surgical decision-making or implant selection.

The DIC measured strain distributions across the ROI for all the specimens were observed to have a strong one-to-one correlation with respect to the FE predicted strain patterns. These results indicate that the overall DIC measured strain distribution was in good agreement with the FE predicted strain and further imparted confidence in the validity of the present in silico analysis. Strong correlations notwithstanding, certain deviations in strain values especially on the edge of the ROI can be attributed to curvature error resulting from the angle subtended by the region with the capturing lens of the camera in the viewing direction (Dickinson et al., 2011; Jetté et al., 2018). DIC measured strain values in the ROI were also overall found to be greater than FE predicted strain values. This can be ascribed to overestimated young's moduli values for cancellous and cortical bones used for simulation (Chanda et al., 2015). The absence of out-of-plane deformation – a known limitation of 2D DIC measurements – might have contributed adversely to the validation as well (Sutton et al., 2008). Nonetheless, a strong correlation between measured and predicted strain values imparted confidence into the present validation scheme.

Although there was a ~6 % increase in the average measured strain data in the intact femur when the load was increased from 2kN to 3kN (Fig. 3.5 a,c), the change was a bit subdued in the implanted femur (4%) (Fig. 3.5 b,d). Nonetheless, for both 2kN and 3kN loading, the implanted bone was found to have a higher average strain in the ROI. The reason for this may be the passing of the screw, resulting in a better load transfer in the ROI. However, the overall low magnitude of strain values in the ROI also suggests that greater strain intensities are more prevalent on the mediolateral aspect since the reactive force in femur under axial compression is predominantly in-plane bending (Nag et al., 2021). This is another reason behind choosing the ROI in the anterior plane. It can be noted here that PFLP provides additional support to counter the bending effect. The occasional spikes in strain values around the fracture region (Fig. 3.5 b,d) are suggestive of greater deformation/noise in and around the fracture gap.

The intact specimen demonstrated greater stiffness (1.5 kN/mm) as compared to PFLP construct (1.06 kN/mm), though the latter showed considerably greater strain energy (Fig. 3.7 a,b). This is consistent with some earlier findings where a comparable overall stiffness value of 1.7 kN/mm was reported for cadaver femora (Schileo et al., 2007; Link et al., 2003). Higher strain energy indicates greater toughness for the implanted bone albeit a slightly compromised rigidity. The separate unload profiles, as observed from Fig. 3.7 a and b, could have resulted from slippage of the head from the

load plate. However, a more pronounced separation for the implanted specimen suggests energy 'trapping' in the fracture plane and subsequent lag in strain during unloading (Thrun et al., 2021).

For the static axial load of 3kN, the FE predicted maximum displacement of PFLP implanted femur (2.79 mm) was found closer to that of the intact femur (2.18 mm). The corresponding value for VA-DHS was 3.53 mm (Fig. 3.9). The maximum displacement briefly explains the relative stiffness and stability of implanted femurs. The lateral fixation of the implants resulted in significant stress reduction in the femur, especially on the lateral side (Fig. 3.10). The fixated implants deprive the cortex of the lateral tensile stress due to bending, which is otherwise available sufficiently in an intact femur. The metallic implants are associated with higher modulus and consequently bears a major proportion of the physiological load (Ferguson et al., 1996; Tonino et al., 1980). In the proximal femur, significant stress shielding was associated with PFLP as compared to VA-DHS (Fig. 3.10 a) perhaps due to extra cross-screws. In the proximal segment, the load flows from the bone to the implant, contrary to the load flow from the implant to the bone in the distal part. This also justifies the reason for the greater intensity of stress in the proximal locking screw and distal-most screw of both the implants (Fig. 3.10 b). Also, the hip screw in VA-DHS receives more load in the proximal femur than that shared by the three cross-screws in PFLP. The higher bending stress in the mid and distal parts of the PFLP plate is also suggestive of the risk of mechanical failure.

There are, however, certain limitations in the present study. The mechanical testing was conducted on a bone analogue instead of cadaver bones. Although not an exact representation of native bone, the use of bone analogue is particularly advantageous for validation of FE models due to the degree of control and reproducibility of mechanical properties they offer. Consequently, they have a long history of use in biomechanical studies and have evolved to be a close and cost-effective surrogate for cadaver bone. Another limitation of this study is that, no muscle forces were considered in this study. The absence of out-of-plane components in principal strain estimations through 2D DIC might have a certain influence on the validation of the static case.

3.5 Summary of the findings

Strong one-to-one correlation between the DIC measured and the FE predicted strain fields were observed across the ROIs. Higher strain energy in the PFLP construct

indicates greater toughness as opposed to the intact femur. However, both measured and predicted data insinuate that overall rigidity of the former is lesser than the latter under axial compressive load. The axial stiffness of the VA-DHS construct, however, was predicted to be the least for the same fracture. This perhaps can be attributed to its shorter plate length. The above findings notwithstanding, the results may vary clinically depending on the fracture type, surgeon's skill, bone quality, screw fixation density and biological factors among other things.

Chapter 4

Dynamic and Impact Energy-Based Strength Assessment of Extramedullary Plates for Intertrochanteric Fracture

4.1 Introduction

More than 90% of all registered hip fractures are due to sideways fall (Grisso et al., 1991; Nevitt et al., 1989). The combination of high impact load associated with the sideways fall and the brittleness of the osteoporotic bone is the principal cause behind such fractures. Fracture occurs when the external force exceeds the physiological range or the strength of the femur. Femur is the longest and the strongest bone that supports the entire body weight. Because of the femur's load-bearing nature, the immediate aim of fracture treatment is to restore rigid stability at the fracture site. This goal is usually achieved by invasively supporting the bone by using screws, rods, pins, or plates.

Biomechanical studies examine the response of a construct when subjected to physiologically viable load (Burstein and Frankel, 1971). Although several such studies took time into account by loading the implant dynamically to test alteration in the construct over time, the number of cycles resembling post-operative patient movement varied significantly, making the studies difficult to compare (Crist et al., 2009; Forward et al., 2012). The biomechanical methodology was based on the implication that the construct would eventually break with the continuous cyclical loading. Although few biomechanical studies have employed mechanical testing and computational modelling to investigate the effect of sideways fall on proximal femur, they did not include structural dynamic characteristics (Aldieri et al., 2018; Gilchrist et al., 2014; Grassi et al., 2016; Link et al., 2003; Nevitt et al., 1989; Johnson et al., 2014; Rossman et al., 2017). Most of the previously published studies considered loading at quasi-static or at constant displacement rate, which neglected the physics of actual fall. The input loading needs to be chosen judiciously for accurate modelling of the injury itself, which is a result of dynamic event. Dynamic analyses consider the impact response of femur and highlight the load transfer mechanism of the lower extremity of the musculoskeletal system. The knowledge of femur resonance frequency and the associated mode shapes,

therefore, is critical for a better understanding of deformation patterns excited by various dynamic loads (Huang et al., 2000; Khalil et al., 1981). The clinical studies, on the other hand, were inherently confounded with subject-specific variations and biological parameters making it difficult to draw any clear conclusions on implant strength. This further underlines the gap between biomechanical and clinical studies.

The above studies notwithstanding, there is no clear biomechanical parameter based on which a comparative strength assessment of these extramedullary implants can be made. Since there is ample evidence that incidences of sideways fall constituted majority of fragility related hip fractures, it becomes pertinent to analyse the condition in implanted femurs also. There is hardly any study that has investigated dynamic analysis of sideways impact fall on full-scale implanted femurs. Further, there is barely any comparative investigation concerning plated femur based on their response to vibrational effect for sideways fall vis-à-vis the intact femur. In this study, it was hypothesized that the behaviour of the implant depends on the frequency and load magnitude of the forced vibration, and a rigid implanted construct will absorb less impact energy during sideways fall. Commercial implants, e.g., PFLP and VA-DHS were chosen to carry out the FE-based preclinical assessments on a simulated Evans type-I intertrochanteric fracture.

4.2 Materials and Method

4.2.1 FE modeling and analysis

The present study employs the 3D CAD model generated in Chapter 3 with the addition of polymethylmethacrylate (PMMA) cap in the femoral head and greater trochanter (Fig. 4.1). The sideways fall scenario was simulated by tilting the femoral shaft by 10º with respect to the ground, and the femoral neck was internally rotated by 15º similar to the analogous tests reported in the literature (Nishiyama et al., 2013; Schileo et al., 2014; Courtney et al., 1994) (Fig. 4.2). The distal femur was constrained such that it could rotate freely in the vertical plane, but was restrained distally against rotation about the diaphyseal axis (Fig. 4.2). The PMMA cap was simulated on the femoral head and the top surface of it was fixed in rotation as well as translation. The greater trochanter was protected by another PMMA cap to prevent local crushing and improve load distribution (Fig. 4.2). The simulation setup replicated typical in vitro mechanical test arrangements reported in various literature (Nishiyama et al., 2013; Schileo et al., 2014; Courtney et al., 1994; Abe et al., 2018; Villette et al., 2018).

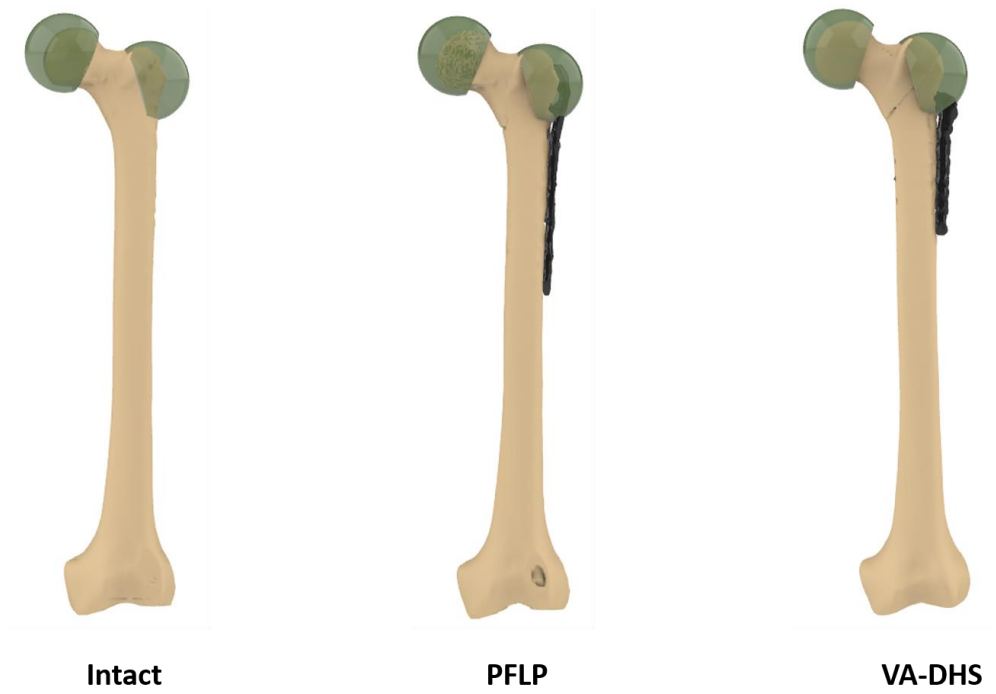

Fig. 4.1: 3D CAD models of intact and implanted femur with PMMA capping

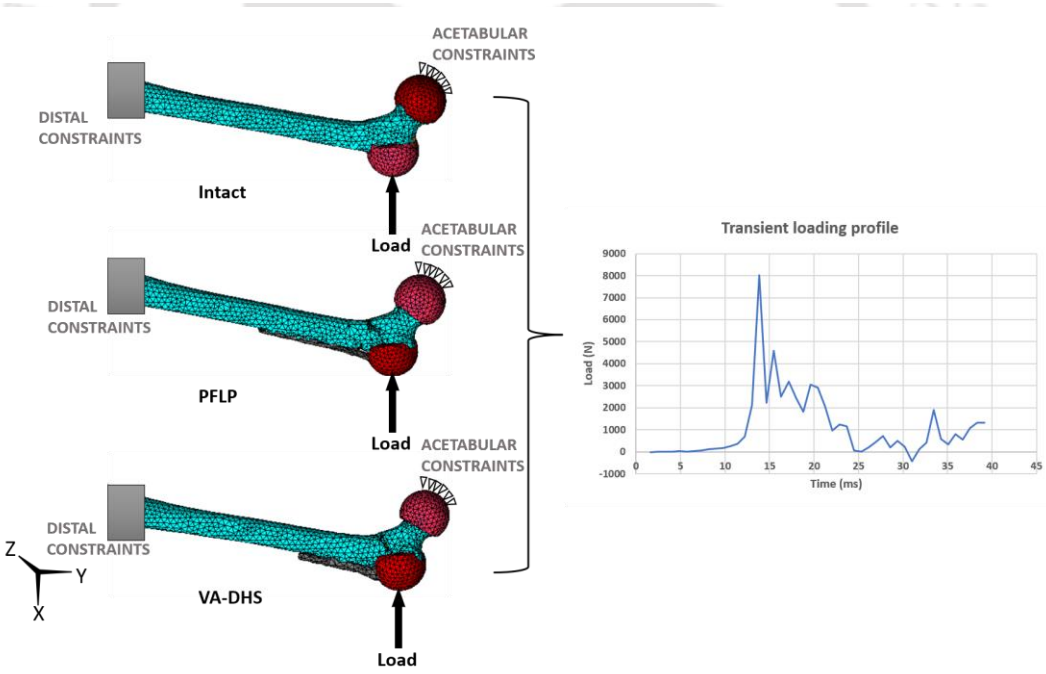

Fig. 4.2: Impact loading for simulated sideways fall and the transient load profile applied to the corresponding FE models.

The dynamic impact loading profile applied through the greater trochanter (PMMA cap) was refined using previous experimental data (Jazinizadeh et al., 2020). The average peak force was assumed to be ~11 times the body weight (i.e., ~8.8kN) (Lotz et al., 1995; Robinovitch et al., 1991). In the present study, FE simulations were performed by considering geometric non-linearity. In the non-linear FE analysis, stiffness was function of displacement in contrast to constant stiffness magnitude in

linear analysis. The non-linear analysis was conducted by employing piecewise linearity such that the load was split into small increments and stiffness matrix was updated after each incremental load application. The iterations were performed to ensure that equilibrium was satisfied at every load increment. In the process, Newton-Raphson method was used to solve the equations (Gokhale, 2008). A modal analysis was also performed to investigate the vibrational response of the intact and the implanted femurs in case of a sideways fall. This computational analysis was implemented using the Block-Lanchoz method owing to its efficient and robust algorithm (Reina-Romo et al., 2018). To avoid stress concentration, the input load was distributed over 20 nodes. The non-linear analyses were solved according to the concept of piece-wise linearity using the Newton-Raphson method.

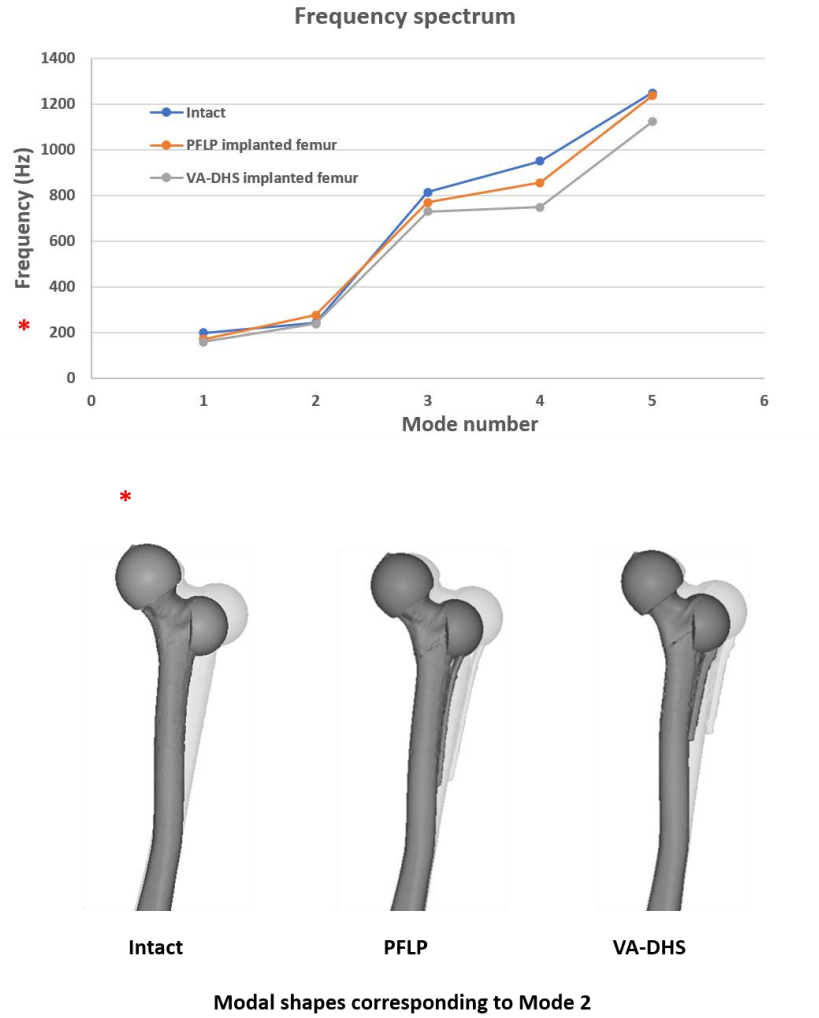

Fig. 4.3: Frequency values associated to various mode numbers for intact, PFLP and VA-DHS implanted femur. Modal shapes related to mode 2 has been described in details alongside. Mode 2 corresponds the effect of bending in the XY plane (frontal plane), where frequency of PFLP construct was found higher

The material models considered for bone and implant are similar to that presented in Table 2.3. Isotropic and homogeneous material properties were applied to the cancellous bone, plate, screws, and PMMA cap (E = 2500 MPa, ρ =1180 kg/mm^3), whereas orthotropic material properties were considered for the cortical bone based on the data provided by the manufacturer (Biomechanical products catalog Sawbones; Lewis et al., 1997). The density of cortical and cancellous bone was taken as 1640 kg/mm^3 and 270 kg/mm^3 respectively. The material for the plate and screw were considered to be stainless steel (ρ =7850 kg/mm^3). Poisson's ratio was set as 0.3 for all materials. All interfaces of the FE models were assumed to be bonded under all conditions.

4.3 Results

Modal analysis was used to predict the first five natural frequencies as well as their corresponding mode shapes corresponding to intact and implanted femurs for sideways fall (Fig. 4.3). The vibration analysis revealed the effects of bending, torsion, and tension/compression in the mode shapes. The first five natural frequencies for intact femur were predicted to be 199, 244, 814, 950, and 1248 Hz, respectively. The corresponding values for PFLP implanted femur were 172, 277, 770, 856, and 1237 Hz, whereas for VA-DHS the values were 158, 238, 729, 749, and 1122 Hz, respectively. The first modal shape corresponds to torsion in the X-Z plane. For the second mode, bending was observed in the X-Y plane (Fig. 4.3), followed by torsion and more complex modes, being a mixture of torsion and bending.

The displacement versus time curve corresponding to intact and implanted femurs for the sideways fall is presented in Fig. 4.4. The displacement corresponding to VA-DHS was found to be greater compared to intact and PFLP implanted femur. For intact and PFLP implanted femur, the values were closely associated. Maximum displacement corresponding to peak load of fall case was predicted to be approximately 10 mm, 9 mm and 13 mm for intact, PFLP and VA-DHS implanted femur, respectively. The energy losses were estimated by calculating the area of the stress versus strain loops using trapezoidal integration (Matlab v2019) (Fig. 4.5). Energy loss by PFLP implanted femur was found to be the least (43 J), followed by the intact (44 J) and VA-DHS construct (66 J). The yield stress of cortical bone is assumed to be 157 MPa and in general stress above 100 MPa are considered critical for the bone. Accordingly, fracture prone regions were earmarked when the FE predicted von Mises stresses

exceeded the yield strength of that region. Such regions could be associated more with VA-DHS implanted bone (Fig. 4.6). The peak von Mises stress in the intact cortex was predicted to be ~130 MPa, whereas the corresponding values were ~103 MPa and ~172 MPa, respectively, for PFLP and VA-DHS construct.

4.4 Discussion

FE models of femurs have been extensively used for fracture risk prediction and ideal implant selection. The present study attempts to preclinically investigate the biomechanical strength parameters of extramedullary plates for simulated Evans type-I intertrochanteric femur fracture subjected to sideways fall and strength predictions were made to gain insights into the relative rigidity of the constructs under impact loading thereof.

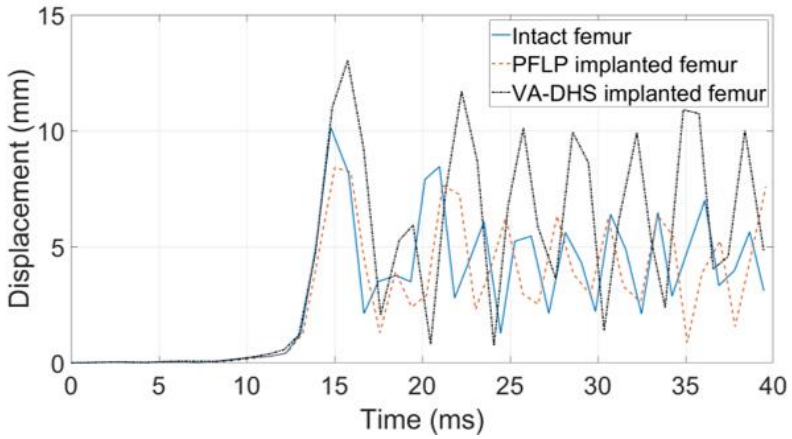

Fig. 4.4: Plot depicting displacement-time response related to intact, PFLP and VA-DHS implanted femur.

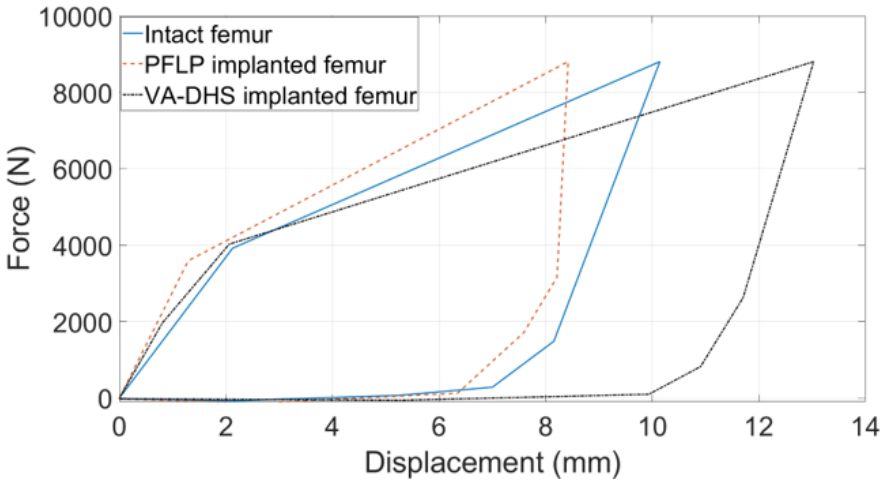

Fig. 4.5: Energy loss loop corresponding to intact, PFLP and VA-DHS implanted femur.

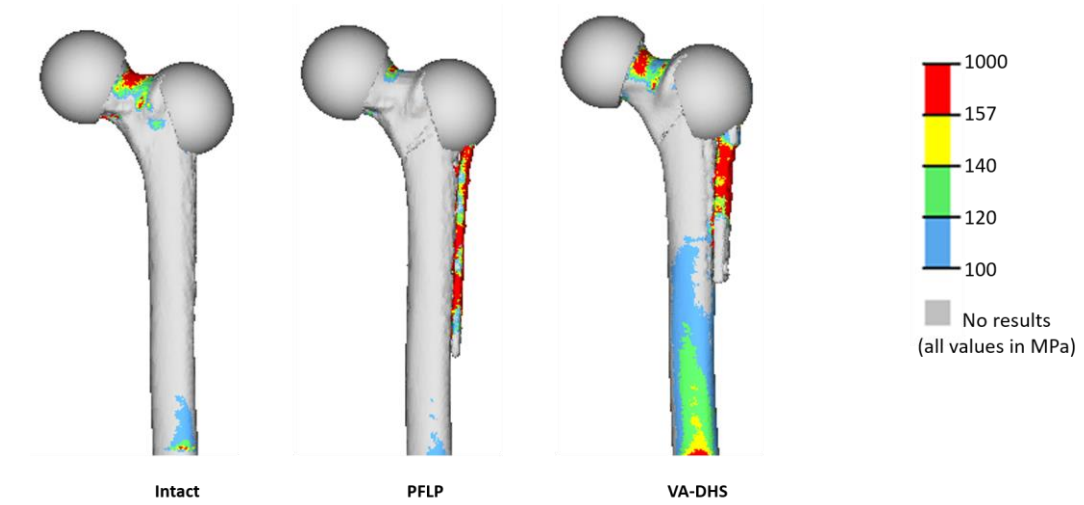

Fig. 4.6: Failure stress plot of intact, PFLP and VA-DHS implanted femur on sideways fall considering body weight of 80 kg.

Natural frequency distribution based on modal analysis is a non-invasive and non-destructive technique for assessing the stability of an implant. In the present study, the frequency analysis of the intact and implanted femur predicted the influence of different responses of the femoral construct on sideways fall. A few of these modes were difficult to detect in both physiological and experimental setup owing to limitations associated with instrumentation, soft tissue damping, and different wave propagation inferences (Pérez et al., 2013). PFLP implanted femur was found to have almost similar frequency distribution to that of the intact femur, though the frequency of intact femur was slightly greater for all the modes except mode 2 (Fig. 4.3). On the other hand, VA-DHS implanted femur was found to have the least frequency for all modes. For mode 2, which corresponds to the effect of bending in the X-Y plane (frontal plane), the frequency of PFLP construct was found to be higher. The effect of bending in the frontal plane could be seen when force was applied in the X direction in the greater trochanter, which was of special interest in this study as it replicated sideways fall. With reference to impact analysis, it may be noted that stiffer components result in higher stresses due to lower ability to accumulate elastic strain energy. However, from clinical perspective stiffer construct imparts an early load bearing and hence, is a better proposition. Greater accumulation of energy in the femur implicates greater deformation leading to clinical complications, e.g., bone or implant dislocation, screw pullout etc. PFLP, with greater mode 2 frequency, showcased greater stiffness than VA-DHS under sideways impact. In Fig. 10c it can be observed that the stress intensities are higher in the PFLP implant as compared to the host bone whilst relatively greater stress concentration was predicted for VA-DHS implanted femur in the neck region. This implies that PFLP was able to

shield the bone better from excessive stresses. However, inordinate stress shielding may cause adverse bone remodelling in the long run.

The displacement-time plot (Fig. 4.4), nonetheless, depicted an identical dynamic response to fall for intact and PFLP implanted femur. Both showed greater resistance to impact load indicating high bending stiffness. Conversely, VA-DHS predicted larger displacement throughout the loading period. A similar trend could be observed in the force-displacement loop (Fig. 4.5). The figure represents mechanical work done or energy absorbed during the impact force. Here, the signature of curve could be attributed to inertia in very short interval of time and consideration of geometric non-linearity in impact condition（Zhang et al., 2016). The authors also note that absorption of energy may be a desirable characteristic in case of flexible components, but not so much in case of rigid structures or where rigidity is desirable (Islam et al., 2011). Implanted bone should act as a rigid construct in order to avoid dislocation from joints. PFLP and intact femur were associated with low energy loss, whereas in VA-DHS the energy loss was the highest. This may be attributed to the difference in bridging length, the overall design as well as distal screw spacing (Bel, 2019). Bel (2019) advocated using screws alternately between empty holes and screws for better load distribution and to avoid fatigue fracture of the plate. Such arrangement of screws could be seen in the PFLP implanted femur.

It may be worth noting that the fixed boundary conditions were applied to the outer surface of PMMA cap and not directly applied to the femoral head. The material of PMMA is much softer compared to bone material. Therefore, it will not restrict the movement in sideways fall and will allow movement in the femoral head. The present situation describes realistic physiological loading scenario and only limitation may arise due to idealised equivalent material of soft tissue, i.e., PMMA. The dynamic impact loading profile in the present study was refined from a previous experimental study, in which the load was applied on the PMMA cap (Jazinizadeh et al., 2020). Hence, attenuation of the impact may not be necessary as the load was not applied directly on the greater trochanter. The location and magnitude of peak stress differed significantly in the case of sideways fall when compared to that under 3kN static axial load (section 3.3, Fig. 3.9a). A high magnitude of compressive stress was induced in the superior-posterior neck region under fall, whereas for static gait load the peak stresses were concentrated at the mid femoral shaft. For intact femur under fall, the peak stress magnitude was ~3.3 times greater than that under static gait loading of 3kN.

Lotz et al. also reported that the peak stress value at fall to be 4.3 times that present during gait albeit under a joint load of 1.5kN (Lotz et al., 1995).

Several studies have reported von Mises equivalent stress to be a good indicator for predicting bone failure, as it deals with the amount of energy that distorts a local volume of tissue under the peak fall load (Tomaszewski et al., 2010; Lotz et al., 1991; Keyak et al., 2001). VA-DHS implanted femur was found to be associated with more region having stress value greater than the yield limit of cortical bone (Fig. 4.6). The high stresses for both the intact and implanted femur were observed predominantly around the superior cortex region. This could be because the superior-lateral cortex region of the femoral neck is generally thinner as compared to the inferomedial cortex (Lotz et al., 1995; Mayhew et al., 2005). PFLP implanted femur predicted the least propensity to such adverse stress intensities, suggesting better structural rigidity and higher capacity in protecting the fractured femur against fall. In clinical terms, this means that the length of stay (LOS) in the hospital associated with PFLP may be lower as compared to VA-DHS. Also, patients will be able to undergo early weight-bearing resulting in faster overall recovery (Ravi et al., 2017; Subash et al., 2021).

There are, however, certain limitations in the present study. Although the impact models were not validated, it may be argued that a similar mesh structure was employed. Furthermore, the interface condition of the *in silico* model may not appropriately replicate the in vivo condition of the implanted femur.

The bonded interfacial condition assumed for both the implanted construct was to simplify the overall analysis and to have a standard comparison between the implants. The contact modelling of the fracture region though not considered in the present study is recognised as a future scope of work. During measurement, the stiff, flat plate used to transfer the axial load to the femoral head leaves little room for the head to move freely. This may lead to some degree of spurious transverse loading to the femur thereby causing discrepancies in deformation outcome while replicating tests through numerical simulations (Chalise et al., 2012). However, sufficient care was taken to keep the plate as polished as possible such that any frictional loading artefact remains at its bare minimum. Given the high load associated with both normal gait loading (3kN) and for impact sideways fall (peak load of 8.8 kN), a nonlinear material property could have predicted the surface strains and stress values more accurately. In modal analysis, the effect of damping by other bone and soft tissue of musculoskeletal system was not

considered to keep the analysis simple and efficient. Furthermore, the primary objective of this pre-clinical study was to compare the relative merits of different implant types while controlling for all other variables. For this purpose, the above discussed limitations were considered acceptable. The findings of the current study offer new preclinical insights, namely relative strengths of extramedullary plates under dynamic loading, fracture toughness assessment based on impact resistance and energy loss (hysteresis). Future studies will attempt to address influence of bone morphometry on the success of extramedullary fracture plates.

4.5 Summary of the findings

Under dynamic response to the simulated sideways fall, VA-DHS construct was found to predict the least frequency for all modes. PFLP construct predicted identical mode shapes when compared the intact femur suggestive of higher bending stiffness of the fixation. The high stresses for both the intact and implanted femur were observed predominantly around the superior cortex region. PFLP implanted femur predicted the least propensity to adverse stress intensities, thereby demonstrating superior capacity of protecting the fractured femur against fall. The location and magnitude of peak stress, nonetheless, differed significantly in the case of sideways fall as opposed to that predicted under static axial compression (Chapter 3).

Chapter 5

Phenomenological Modelling of Secondary Bone Healing in Comminuted Fracture Treated with Locking and Dynamic Compression Plates

5.1 Introduction

Incidences of femoral fracture can be the outcome of traumatic (e.g., traffic accidents or fall etc.) or non-traumatic conditions (e.g., osteoporosis, geriatric population, cancer in bone etc.) (Moroni et al., 2006). Biological fixations are used to bridge the fracture site and impart stability to promote bone healing. Primary bone healing involves direct union of two broken bones, often seen in case of very small fracture gap (10-100 μm) and strain below 2% (George et al., 2005). On the contrary, secondary bone healing is the most prevalent one and involves classical stages of healing, i.e., injury, haemorrhage, inflammation, primary soft callus formation, callus mineralization and callus remodelling. This type of healing is primarily observed in fracture gaps with larger micromotion. Major proportion of the femoral fractures are treated with internal plate fixations that differs primarily in the screw design. Conventional plating technique is based on the fixation of DCP (Gardner et al., 2004). The introduction of newer type of plate, LP, has expanded the ways of screw-plate fixation. LP involves locking screws having threaded head that allow the screw to fasten into the plate as well as into the bone (Perren, 2002).

A number of numerical models of the bone fracture healing were developed over the last few decades to predict tissue differentiation both quantitatively and qualitatively. These models can be broadly classified as mechanoregulatory healing model, bioregulatory healing models, and coupled mechano-bioregulatory healing models. In mechanoregulatory models, the mechanical stimulus regulated the tissue differentiation in the callus region. Claes et al. (1998) and Claes and Hiegele (1999) correlated strains and hydrostatic pressure to callus tissue differentiation using elastic FE models. Few other studies also used FE models to predict stress and strain distribution at particular healing stages of the fracture callus region (Carter et al., 1988;

Blenman et al., 1989; Cheal et al., 1991). Their results suggested that hydrostatic stresses have an effect on revascularisation and tissue differentiation. Various studies have adopted dynamic models to simulate the healing as a time dependent feedback regulation system (Ament and Hofer, 2000; Bailón-Plaza and van der Meulen, 2003, Isaksson et al., 2008; Doblare et al., 2004; Lacroix and Prendergast, 2002; García-Aznar et al., 2007; Kuiper et al.). Most of these studies used strain invariants as mechanical signals to predict tissue differentiation (Bailón-Plaza and van der Meulen, 2003; Doblare et al., 2004; García-Aznar et al., 2007) while a few others, in addition, used fluid velocity (Isaksson et al., 2008; Lacroix and Prendergast, 2002) and fluid shear stress (Kuiper et al.). On the other hand, bioregulatory and coupled mechano-bioregulatory healing models include activities (migration, proliferation, differentiation and death) of different cells participating in the callus region. Few of these models included growth factors to regulate tissue differentiation (Bailón-Plaza and van der Meulen, 2001; Geris et al., 2008) while others used concentration of different cell types (Isaksson et al., 2008; Lacroix and Prendergast, 2002). Fuzzy logic-based algorithms have successfully been employed in determining tissue differentiations. Amnet and Hofer, simulated kinetics of the healing process using linear elastic FE simulation in combination with their fuzzy logic model (Ament and Hofer, 2000). Simon et al. (2003) used fuzzy logic-based algorithm to predict diaphyseal fracture healing. Also, Shefelbine et al. (2005) used fuzzy approach in their study to determine trabecular fracture healing. Later in another work, Simon et al. (2011) incorporated blood perfusion as a spatio-temporal state variable to simulate revascularisation process. Whener et al. (2011) employed the fuzzy logic algorithm developed by Simon and Shefelbine to study the influence of fixation stability on the healing time.

Several experimental (Yánez et al., 2010; Uhl et al., 2008; Kim et al., 2007; Seide et al., 2007) and computational studies (MacLeod et al., 2015; Kim et al., 2010; Ferguson et al.,1996; Beaupré et al., 1988) have compared and evaluated locking and compression screws based on their mechanical performances. However, no modelling approach addressed the influence of screw type in determining the overall progression of fracture healing. Furthermore, most of these investigations relied on 3D primitive models instead of realistic bone and implant geometries.

The objective of the present study, therefore, was to apply a 3D dynamic fracture healing scheme modelled on a subtrochanteric femur fracture, regulated by both FE analysis and fuzzy logic control in order to understand the spatio-temporal healing

phenomena for both LP and DCP. The study was based on a hypothesis that fuzzy logic controls could actually be used to predict tissue transformation in a realistic and non-invasive manner for secondary healing in plated bone. We further hypothesized that the screw fixation mechanisms herein might bear a significant influence on the healing outcome.

5.2 Materials and method

The simulation of the healing phenomenon in the callus region can be described as an initial value problem involving two mechanical (invariants of strain tensor) and five biological state variables (local tissue composition and vascularisation). The mechanical stimuli were firstly calculated using the finite element analysis (ANSYS)

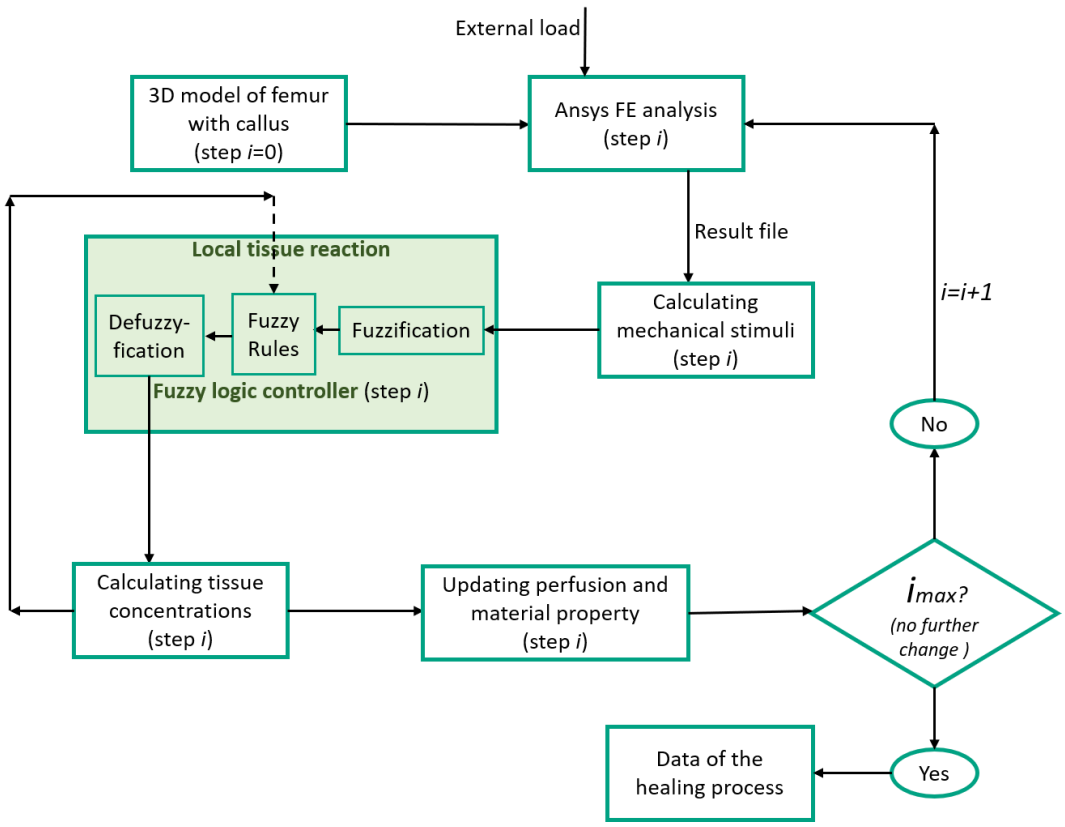

Fig. 5.1: Flow-chart of simulation of dynamic fracture healing model with fuzzy controller.

after properly stating the initial condition in the pre-processor along with loading and boundary conditions. All seven state variables were taken as input to predict the tissue differentiation and vascularisation in the bone healing region using linguistic rule based fuzzy logics (MATLAB) with 32 single rules. Accordingly, the local tissue concentration and material properties were updated. The problem was solved iteratively in several healing step (Fig. 5.1) running in loop.

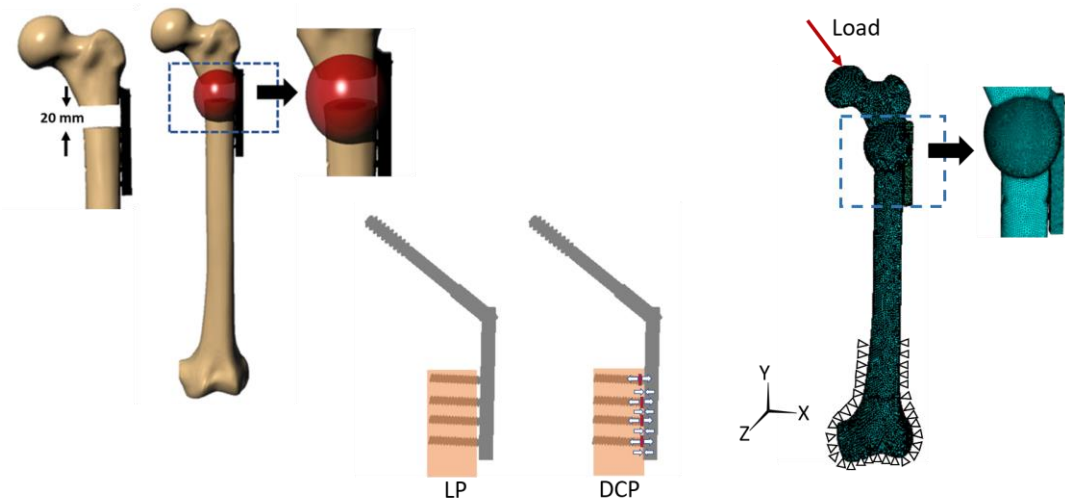

Fig. 5.2: Virtual models of the bone constructs and experimental validation: a) CAD model of femur showing fracture gap of 20 mm along with formed callus (b) CAD model of LP and DCP with depiction of preloads. The red regions indicating preload and white arrows specifying the direction of the preloads (c) 3D FE model of the femur under compressive loading.

Table 5.1: Material Property data of bones, tissues and implant based on ASTM D638***, D695**, D1621* & 308#.

Material	Young's Modulus (MPa)	Poisson's Ratio
Cancellous	155*	0.3
Cortical	16,700(*compressive*)**	0.3
	10,000(*transverse tensile*)***	
Woven bone	4000	0.3
Fibrocartilage	200	0.45
Connective tissue	3	0.3
Plate & screw (Stainless Steel)	193,000#	0.3

5.2.1 Mechanical part: Calculation of mechanical stimuli

For both compression plating and locked plating, the 3D FE models of femur were generated using the manufacturer supplied CAD model of the left femur (Sawbones Europe AB, Malmo, Sweden, model# 3406). A 20mm fracture gap in the subtrochanteric region of the CAD femur was simulated followed by virtual implantation in the NURBS modelling environment of Rhinoceros v14.0 (Rhinoceros, Robert McNeel & Associates, Seattle, USA) (Fig. 5.2). Thereafter the callus region representing the initial fracture haematoma, was modelled in the implanted femur to capture the tissue composition resulting from biological tissue characterization. This

potential healing region was shaped as an ellipsoid around the fracture site (Simon et al., 2011) (Fig. 5.2 a).

The tessellated surface models were then imported into Ansys ICEM CFD v19.0 (ANSYS Inc., PA, USA) to generate volumetric meshing comprising of 4-noded tetrahedral elements (Fig. 5.2 c). After that the volumetric meshing was imported into Ansys mechanical v19.0 (ANSYS Inc., PA, USA) for further analysis. A mesh convergence analysis was carried out with three different mesh size of 0.5 mm, 1.0 mm, and 1.5 mm constituting 427113, 303869 and 262362 elements respectively in the callus region. For mesh sizes 0.5 mm, 1.0 mm and 1.5 mm, the values of distortional strain were predicted to be 0.1309, 0.1311 and 0.1050. Thus, doubling the mesh size from 0.5 mm (fine sized mesh) to 1.0 mm (medium sized mesh) in the callus region resulted in change of the distortional strain by 0.1% whereas the change was almost 20% from medium sized mesh to coarse sized mesh (1.5 mm) Similarly, the variation of the peak von Mises stress between fine and medium mesh was less than 5% at identical location of callus region. Therefore, in view of computational efficiency, the medium sized mesh was considered to be sufficiently accurate. The meshing parameters of the rest of the implanted femur was carried forward from Chapter 2.

A static load of 2.1kN was applied through the femoral head in such a way that it induces the effect of physiological femur i.e., femur being oriented laterally by 10° in the frontal plane and dorsally by 10° in the sagittal plane as described for fatigue testing (ISO 7206-4:2010). The physiological load cases replicated maximum load during stance phase of normal walking for a body weight of 80 kg (Bergmann et al., 2001; Heller et al., 2001). A condition of zero displacement was applied at distal femoral surface nodes sufficiently away from the point of application of load. The screw fastening preload was simulated using ‘pretension load’ by defining the pretension section in APDL for the compression plating. On application of screw-tightening preload, the first thread is found to carry major proportion of load (Gefen et al., 2002). Therefore, the preload was applied on a slice of the first thread in the screw shaft. The pretension load typically involves normal stresses in the axial direction of the screws. The value of the pretension load was chosen as 500N based on average of some previous studies (Perren, 2002; Kim et al., 2010; Ya'ish et al., 2011; Zand et al., 1983). As preload is likely to be present for the proximal locking screw for both plating techniques it was not included to highlight the variation between the two plating systems.

The material property assigned to bone, callus and implant are presented in Table 5.1 (Biomechanical products catalog Sawbones; Simon et al., 2011; Ament and Hofer, 2000). Linear elastic, isotropic and homogenous material properties were considered for cancellous bone, plate and screws. Orthotropic material property was applied to the cortical bone based on the data provided by the manufacturer. The material for the implant was considered to be stainless steel. Poisson's ratio was set as 0.3 for all materials except fibrocartilage (0.45). All interfaces of the FE model for locked type plating were assumed to be bonded under all conditions, whereas for compression plating technique the interface of the distal dynamic screws with plate and bone, and also that between plate and cortical bone was assumed to be in contact with coefficient of friction set as 0.3.

Each callus element comprises its own characteristic material property that were updated after each iteration based on current tissue concentrations. For determination of elements Young's modulus (E) and poison's ratio (ν), a mixture rule is applied using the weighted sum of the material properties of the basic tissue types as shown in equations 1 and 2 (Lacroix and Prendergast, 1999).

$$E_{el} = 4000\text{MPa}\ C_{el,bone} + 40\text{MPa}\ C_{el,cartilage} + 3\text{MPa}\ C_{el,connective\ tissue} \quad \ldots(5\text{-}1)$$

$$\nu_{el} = 0.3\ C_{el,bone} + 0.45\ C_{el,cartilage} + 0.3\text{MPa}\ C_{el,connective\ tissue} \quad \ldots(5\text{-}2)$$

Two independent strain invariants (mechanical stimuli) namely hydrostatic strain (ε_{hyd}) (equation no. 3) and distortional strain (ε_{dis}) (equation no. 4) were calculated from the principal strains (ε_1, ε_2, ε_3) of each element inside the healing region (Pauwels, 1960). The hydrostatic strain represents the volumetric change while the distortional strain denotes change in shape. Initially, the callus region was assumed to consist of 100% connective tissue (0% Cartilage and 0% bone).

$$\varepsilon_{hyd} = 1/3\ (\varepsilon_1 + \varepsilon_2 + \varepsilon_3) \quad \ldots(5\text{-}3)$$

$$\varepsilon_{dis} = 1/(\sqrt{2})\ ((\varepsilon_1-\varepsilon_2)^2 + (\varepsilon_2-\varepsilon_3)^2 + (\varepsilon_3-\varepsilon_1)^2)^{1/2} \quad \ldots(5\text{-}4)$$

Table 5.2: Tissue differentiation rules describing biological processes within the callus region implemented in the fuzzy controller (Shefelbine et al., 2005; Simon et al., 2011).

Rule	ε_{hyd}	ε_{dis}	$C_{perfusion}$	$C_{perfusion,\ neighbour}$	C_{bone}	$C_{bone,\ neighbour}$	$C_{cartilage}$	$\Delta C_{perfusion}$	ΔC_{bone}	$\Delta C_{cartilage}$	Process
1	Not neg. destructive	About zero	Low	Not low	-	-	-	Increase	-	-	Angiogenesis
2	Not neg. destructive	About zero	Not low	high	-	-	-	Increase	-	-	Angiogenesis
3	Not neg. destructive	Low	Low	Not low	-	-	-	Increase	-	-	Angiogenesis
4	Not neg. destructive	Low	Not low	high	-	-	-	Increase	-	-	Angiogenesis
5	Neg. low	Low	High	-	-	High	Low	-	Increase	-	Intramembranous ossification
6	Pos. low	Low	High	-	-	High	Low	-	Increase	-	Intramembranous ossification
7	Neg. medium	Not destructive	-	-	-	-	-	-	-	Increase	Chondrogenesis
8	Neg. low	Not destructive	-	-	-	-	-	-	-	Increase	Chondrogenesis
9	Neg. medium	Not destructive	-	-	-	Not low	Not low	-	Increase	Decrease	Cartilage calcification
10	Neg. low	Not destructive	-	-	-	Not low	Not low	-	Increase	Decrease	Cartilage calcification
11	About zero	Not destructive	-	-	-	Not low	Not low	-	Increase	Decrease	Cartilage calcification
12	Pos. low	Not destructive	-	-	-	Not low	Not low	-	Increase	Decrease	Cartilage calcification
13	Neg. low	Zero	Not low	-	High	High	Low	-	Increase	Decrease	Endochondral ossification
14	Neg. low	Low	Not low	-	High	High	Low	-	Increase	Decrease	Endochondral ossification
15	Pos. low	Zero	Not low	-	High	High	Low	-	Increase	Decrease	Endochondral ossification
16	Pos. low	Low	Not low	-	High	High	Low	-	Increase	Decrease	Endochondral ossification
17	Neg. destructive	-	-	-	-	-	-	Decrease	Decrease	Decrease	Tissue destruction
18	Pos. destructive	-	-	-	-	-	-	Decrease	Decrease	Decrease	Tissue destruction
19	-	Destructive	-	-	-	-	-	Decrease	Decrease	Decrease	Tissue destruction

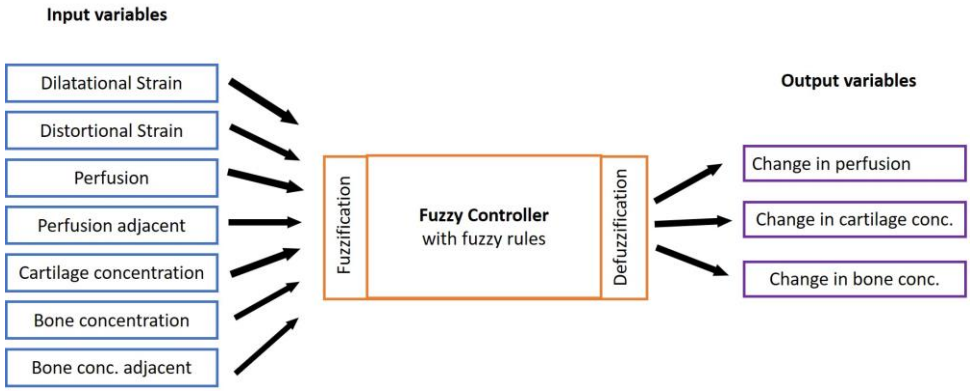

Fig. 5.3: Fuzzy logic controller of tissue differentiation with 7 input and 3 output variables.

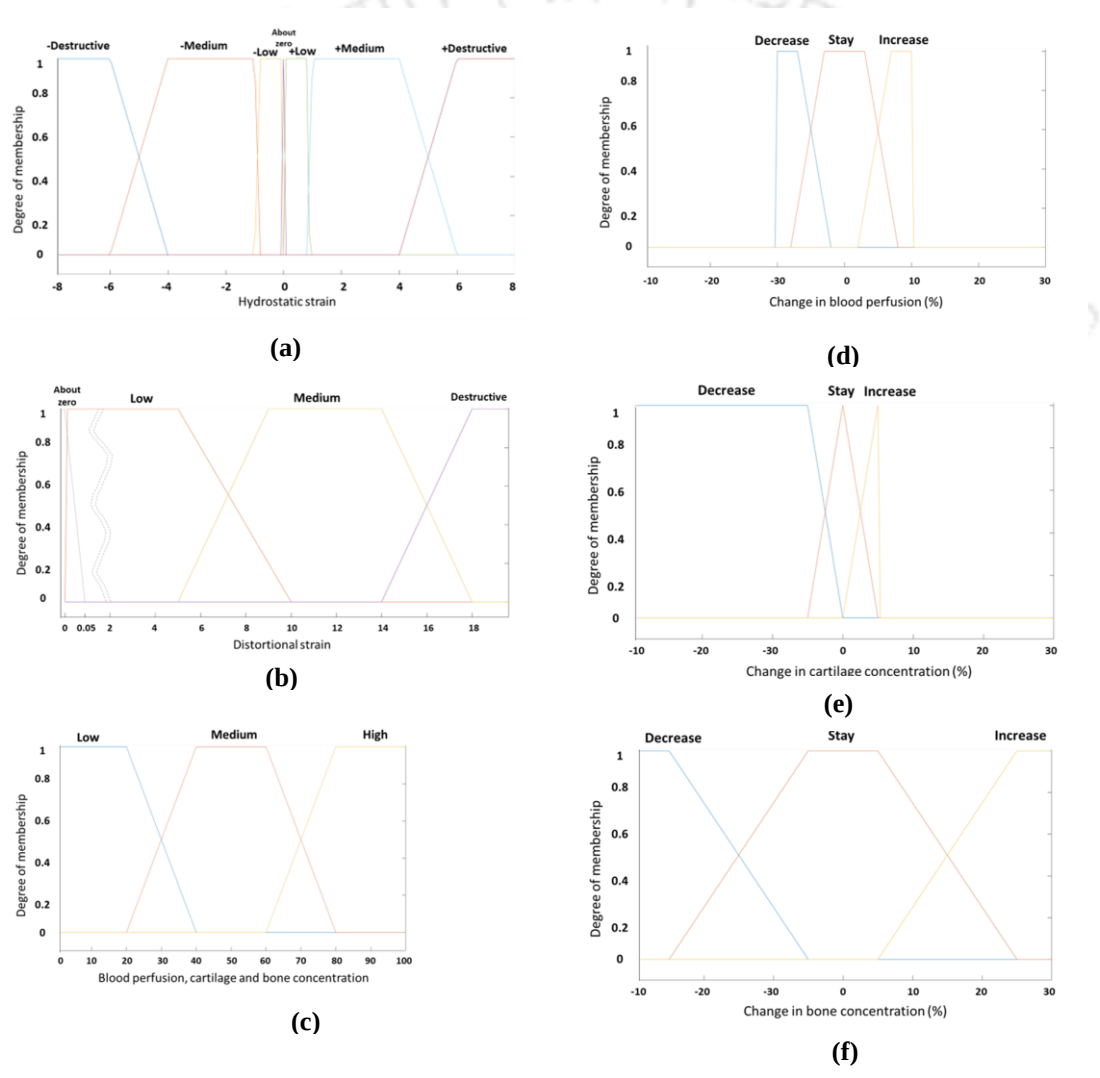

Fig. 5.4: Membership functions of the seven input variables: (a) hydrostatic strain, (b) distortional strain, (c) perfusion, perfusion in neighbour elements, cartilage concentration, bone concentration and bone concentration in neighbour elements. Membership functions of output variables: (d)change in perfusion, (e) change in cartilage concentration, (f) change in bone concentration.

5.2.2 Biological part: simulation of tissue differentiation using Fuzzy logic controller

A linguistic fuzzy rule-based algorithm was used to simulate the tissue differentiation phenomenon inside the callus region. Fuzzy inference engine was developed using the Fuzzy Toolbox in MATLAB R2019A (The Math Works, Inc., Natick, MA, USA) to predict the tissue differentiation and revascularisation. Mamdani fuzzy inference was introduced to build a control system by incorporating a set of linguistic control rules obtained from experienced human operators Mamdani (Mamdani et al., 1975). Mamdani type fuzzy logic controller was employed to link the seven input state variables using some linguistic rules to predict (deterministically) the change in three output state variables (Fig. 5.3). The seven input variables include two mechanical stimuli – hydrostatic strain and distortional strain and five biological variables – perfusion, perfusion in adjacent element, cartilage concentration, bone concentration and bone concentration in adjacent elements. The output variable was change in perfusion, change in cartilage concentration and change in bone concentration.

The fuzzy controller is comprised of 19 linguistic if-then rules that takes into account the process of angiogenesis, intramembranous ossification, chondrogenesis, cartilage calcification, endochondral ossification and tissue destruction (Table 5.2). Rules no. 1-4 describe the process of angiogenesis, that depends on the local mechanical stimuli and perfusion condition of adjacent elements. Good vascularisation assists direct osteogenesis i.e., intramembranous ossification (Rules 5 and 6) and poor vascularisation distant from the bony tissue favours chondrogenesis (Rules 7 and 8). Rules no. 9-12 describes the process of cartilage calcification which requires high mechanical stimuli irrespective of perfusion. Rules no. 13-16 represents endochondral ossification that happens under medium or high blood perfusion and results in increase in bone concentration and decrease of cartilage concentration. Rules no. 17-19 modelled the overloading condition in bone fracture healing. Destruction of bone and cartilage is observed if the tissue is pathologically overloaded. When active, this rule rapidly decreases the perfusion, cartilage and bone concentration.

The membership function of a fuzzy set is apparently the indicator function in classical sets. In fuzzy logic, it describes the degree of truth as an extension of valuation (Zadeh, 1965). Membership function characterizes the information of the fuzzy set and assigns each object a grade of membership ranging between zero and one. Membership

function of seven input variables (Fig. 5.4 a-c) and three output variables (Figs. 5.4 d-f) were defined as trapezoidal functions based on theory of Claes and Heigele (1999). Also, the work of Kaspar et al. (2000) on cell culture experiments served as the fundamentals for defining the membership functions. These membership functions related the quantitative values (strain, concentration, perfusion) to linguistic values (e.g., low, medium, high) and vice versa. The centroid method was used while defuzzification i.e., the final output prediction was an average sum of the weighted single output of the active rules.

The initial perfusion condition was defined in accordance with the work of Simon et al. (2011). Cortex element was assumed to have intact vascularity (100% blood perfusion) excluding the areas adjacent fracture gap. The remaining end of these fragments were defined as initially avascular i.e., 0% blood perfusion. Perfusion was allowed from cortical bone fragment as well as from the peripheral and medullary boundaries to the callus region (Rhinelander, 1974). At the peripheral boundary of the callus, the perfusion was set to 30% which represents the 'extraosseous blood supply' from adjacent soft tissues (Rhinelander, 1974). After 10 days, the perfusion B.C. in the medullary channel was set to 30% to represent potential revascularisation from the marrow.

5.3 Results

The computational work demonstrated the stages of callus healing in two types of plating techniques, namely locking and dynamic compression plate. Bone concentration, cartilage concentration, blood perfusion and change of modulus in the callus region were predicted over space and time, for both cases of LP and DCP, using FE analysis and fuzzy logic-based simulation scheme. The tissue concentrations and distortional strain are predicted based on the outcomes of iterative simulation steps taking each iteration as one day. The simulation was continued iteratively till 60 healing steps running in loop. The connective tissue concentration is calculated by taking the complement to bone and cartilage concentration to attain 100%. The magnitude of strain experienced by the fracture region primarily depends on the applied load and the stiffness of the device, and in turn determines the tissue differentiation pattern of the region. The qualitative predictions of tissue differentiation patterns and other healing parameters in the callus region are showcased through contours in the longitudinal cross-section, considered hereinafter as the ROI.

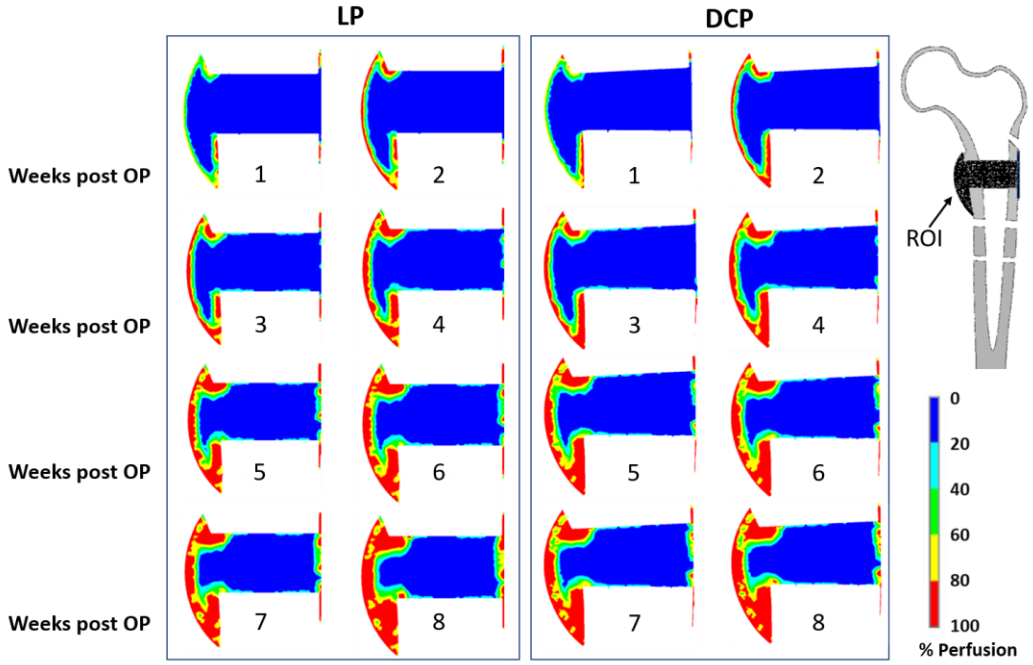

Fig. 5.5: Predicted variation in the perfusion of the callus region for both case of LP and DCP at an interval of 1 week (post operative).

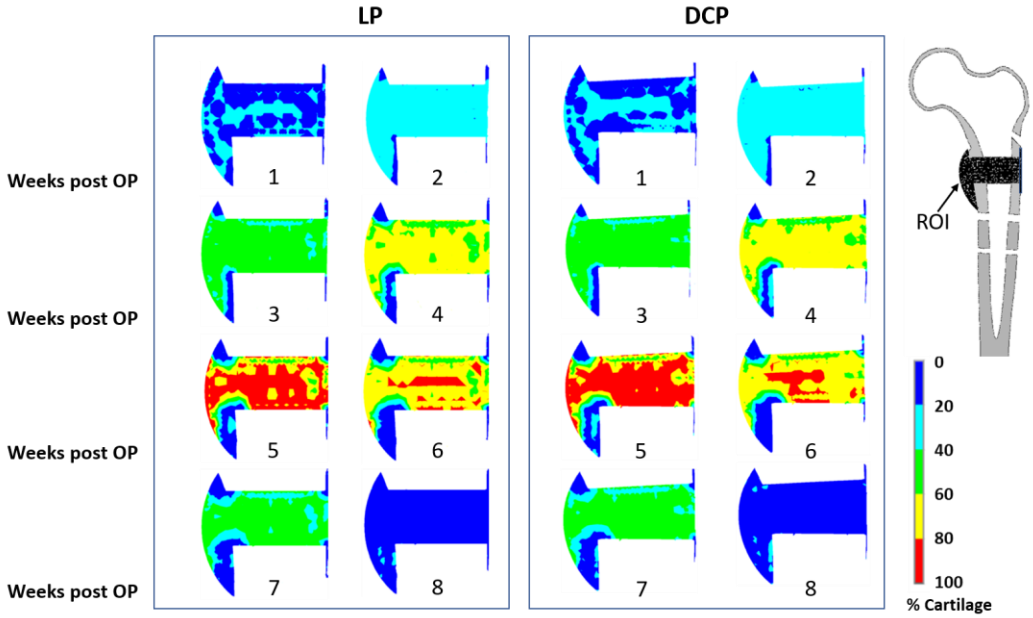

Fig. 5.6: Predicted variation in the cartilage concentration of the callus region for both case of LP and DCP at an interval of 1 week (post operative).

Blood perfusion started at the cortex away from the fracture gap at peripheral side for both cases of LP and DCP, as shown in the ROI (Fig. 5.5). Gradually the blood perfused towards the gap centre. At the beginning of the 4th week, blood perfusion at the periosteum callus was completed for both the cases. Conversely, no revascularisation at the mid-callus was predicted till the end of 8th week. In the early phases, cartilage formation was observed in the areas with high mechanical stimuli and

low blood perfusion for both LP and DCP (Fig. 5.6). Around the 5th week the cartilage concentration was found at the highest for both cases (~73%). High mechanical stimuli in the middle of fracture gap activated endochondral ossification where cartilage formation takes place, which later transformed into woven bone, resulting in delayed healing. At the early stages of healing, bone formation can be observed at the surfaces of cortical bone away from the fracture gap (Fig. 5.7).

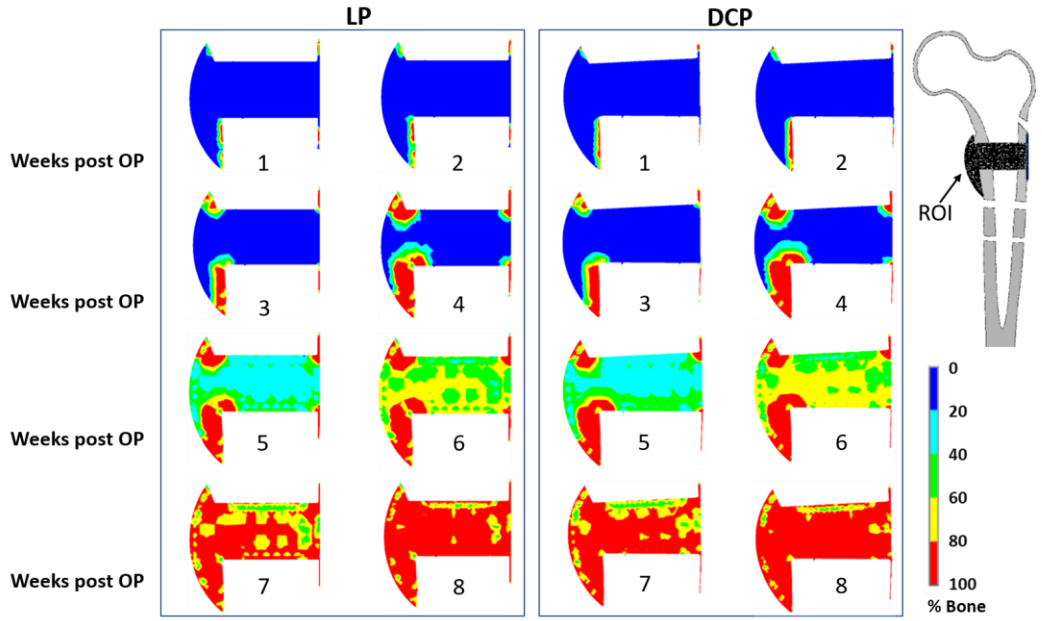

Fig. 5.7: Predicted variation in the bone concentration of the callus region for both case of LP and DCP at an interval of 1 week (post operative).

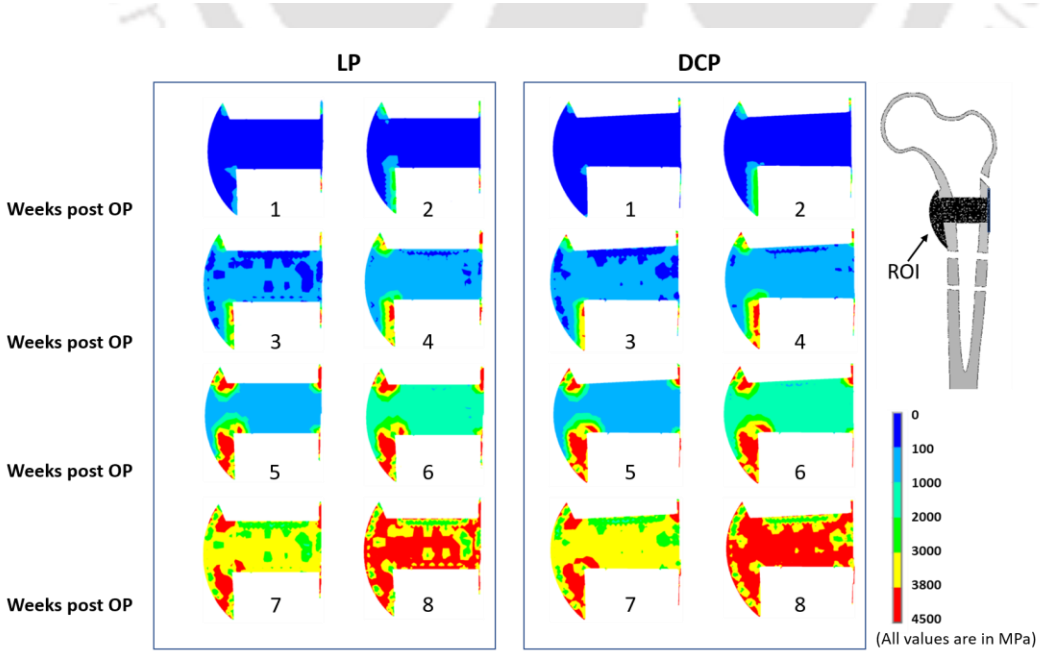

Fig. 5.8: Predicted variation in the modulus of the callus region for both case of LP and DCP at an interval of 1 week (post operative).

Gradually from the 6th week onwards, bone formation propagated into the peripheral healing region where bony bridging occurred. Finally, the entire callus gets transformed into newly formed woven bones (8th week). For both LP and DCP, the initial commencement of bone formation was through intramembranous ossification. However, as the healing progressed, endochondral ossification was dominant between fractured bone and external to periosteal callus. In contrast, intramembranous ossification occurred in the callus directly in contact to the distal and periosteal end of the cortex. The overall change in modulus of the callus region is presented in Fig. 5.8.

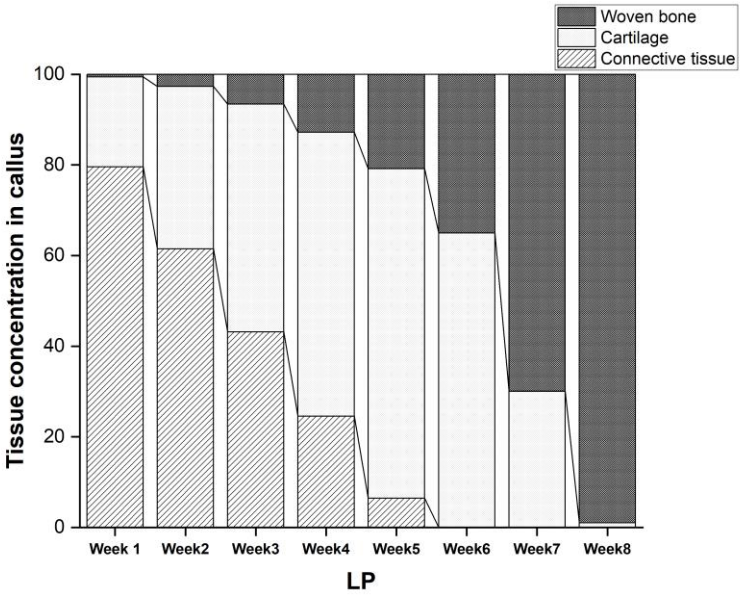

(a)

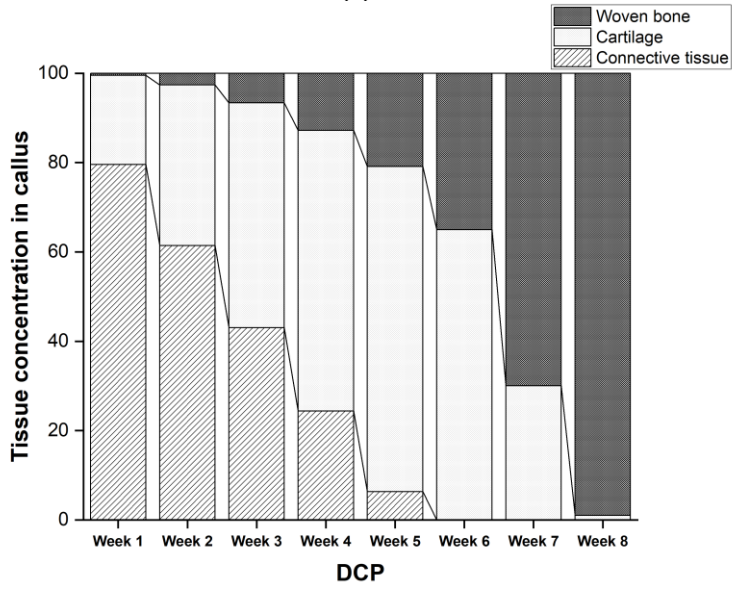

(b)

Fig. 5.9: Post operative variation of tissue concentration in the callus region from week 1-8 (a) LP, (b) DCP.

For both cases of LP and DCP, the modulus increased around same time and no significant variation was observed. However, callus modulus increased more for LP as

compared to DCP at the early phases of healing (10.38%). Nonetheless, in the later stages, i.e., 4th week onwards, DCP was associated with a greater callus modulus. The simulations predicted an overall similar trend in bone healing as well (Fig. 5.8).

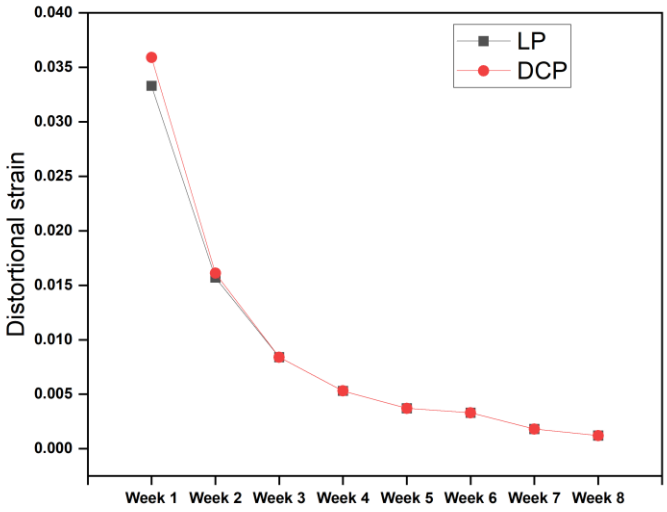

(a)

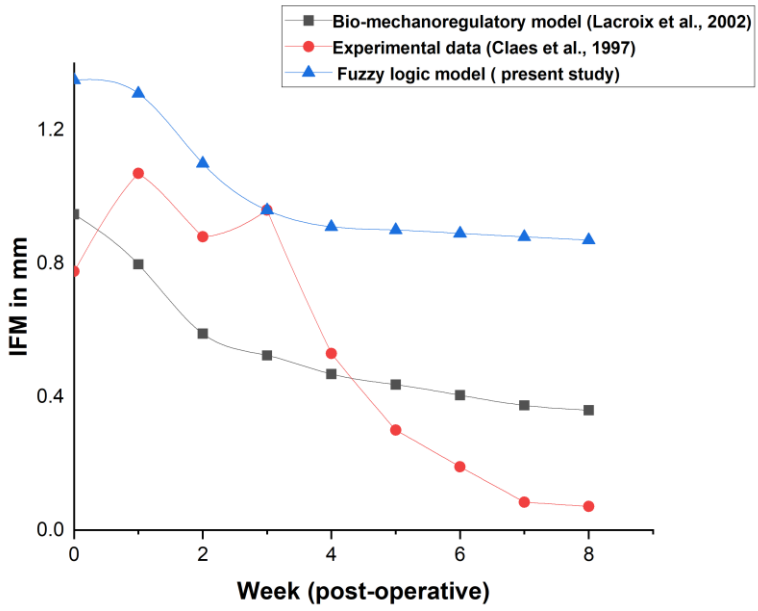

(b)

Fig. 5.10: Distortional strain and interfragmentary movement (IFM) assessment: (a) Distortional strain associated to LP and DCP constructs in the callus region as predicted by the present study (b) Interfragmentary movement (IFM) predicted by the present fuzzy logic scheme as compared to a bio-mechanoregulatory model (Lacroix and Prendergast, 2002) and animal experiment (Claes et al., 1997).

By the end of 5th week, there were almost no trace of connective tissues for both the cases (Fig. 5.9 a,b). Also, woven bone concentration for both cases at the end of 4th week was around 13% which reached almost 99% after 8th week (Fig. 5.9 a,b). Higher

distortional strain was predicted initially in the case of DCP as compared to LP (Fig. 5.10 a). From 3rd week onwards, the callus strains gradually decreased, and no significant difference was observed at the later stages between LP and DCP.

5.4 Discussion

The present study employed a biomechanical model to predict tissue transformation during different stages of secondary fracture healing associated with subtrochanteric femur fracture. The purpose of this study was to understand the difference in fracture healing scenarios at the callus region for two implantation techniques, namely LP and DCP. Fuzzy rules acquired from medical observations were implemented to describe biological phenomena of angiogenesis, intramembranous or endochondral ossification and cartilage calcifications. The entire simulation was carried out in batch mode using a workstation (Model: HP Z2 TWR G4 / OS: Windows 10 Pro / Proc: Intel® Core™ i7-9700 3.0 GHz 8-core CPU / RAM: 32 GB), where each iteration took roughly 1 hour to complete.

The overall blood perfusion patterns (Fig. 5.5) were predicted to be similar for both cases of LP and DCP, and were consistent with the earlier histological observations of Rhinelander et al. (1974). A large area of the mid-callus inside the endosteum remained avascular for a long computational time due to the experience of high distortional strain. Within the simulated time frame of the 8th week, the blood perfusion did not fill the interfragmentary gap completely, which agrees with some of the previous observations (Schweiberer et al., 1977). The delay in revascularisation in the gap region resulted in slowing down of the ossification process. This region was found to be dominated by formation of cartilages instead of woven bone owing to high mechanical stimuli and low blood perfusion (Fig. 5.6). Claes et al. (2002) also reported similar observations in the interfragmentary regions. In those areas, connective tissue persisted as late as in the 4th week primarily due to high mechanical stimuli (Figs. 5.7 and 5.8). The new woven bone formation occurred about two weeks later at the periosteal surface away from the fracture gap (Fig. 5.7). This perhaps may be ascribed to the direct formation of woven bone through the biological process of intramembranous ossification, which requires adequate blood perfusion and the presence of existing bony surfaces.

As the healing process continued, the dominant type of ossification shifted to endochondral ossification from intramembranous ossification. Once the peripheral bone formation was completed, the strains in the middle of the interfragmentary gap

decreased significantly, and bridging started almost at the 6th week. The bridging occurred mainly through endochondral ossification. Various studies also reported occurrences of endochondral ossification in the far cortex zone of callus, while intramembranous ossification occurred in the near cortex zone (Einhorn, 1998; Marsell and Einhorn, 2011). This accorded well with our findings. Further, the degree of calcification predicted in the present study in the near cortex is different from that of the far cortex (Fig. 5.8). This is in accordance with the clinical findings of Lujan et al. (2010), wherein they reported asymmetrical callus formation in distal femur fracture implanted with LP.

The present study further predicted that compressive strength imparted by the DCP helps in the endochondral ossification at the later stages of healing and facilitates faster solidification of callus as compared to the LP (Figs. 5.7 and 5.8). In DCP technique, the physiological load experienced by the femur is transferred as frictional load at the plate-bone interface, whereas in LP, it is transferred through the screw-bone interfaces. Thus, the local environment in the bone fracture healing region around screws is influenced by a mix of effects, unlike the straightforward mechanism related to LP. Also, DCP requires a relatively extensive surgical approach and contributes to necrosis, consequently enhancing the risk of delayed callus formation (Perren, 1988).

In the present study, the rapid development of callus was observed between week 4 and week 8 postoperatively (Figs. 5.9 a,b) for both the cases of LP and DCP , which agreed well with the findings of Gardener et al. (2003). The initial distortional percentage strain associated with LP and DCP in the callus region was found to be 3.2% and 3.6%, respectively (Fig. 5.10 a), which is ideal for callus growth. Strain ranging from 2% to 10% was also reported to facilitate effective generation and development of callus in the fracture site (Gardner et al., 2004). The gradual decrease of the distortional strain for both the cases in the present study (Fig. 5.10a) matches the trend of the gradual decrease of interfragmentary movement reported in the in vivo experiments of Claes et al. (1997). The difference of initial distortional strain in the callus region of LP and DCP fixated femur was primarily responsible for the characteristic variation in the healing responses. Hence, an initial delay in healing associated with DCP was predicted when compared with LP (Fig. 5.8). However, at later stages after the initial calcification were achieved, healing was predominant for DCP fixated femur owing to the compressive stress environment in the callus region.

Although identical progression of healing for both the cases was predicted after the 8th week, early stabilisation of the callus for LP was observed. Ghimire et al. reported that the increase of flexibility in the LP system potentially promotes uniform bone formation across the fracture gap, resulting in better healing outcomes (Ghimire et al., 2020). Various other studies also advocated using flexible fixation to induce the fast formation of callus (Tayton et al., 1982; Goodship et al., 1985). It may be noted that the LP technique tolerates some degree of mobility in the interface of the fracture essential for quick healing. The interfragmentary movements (IFM) at different healing intervals were compared with that reported by two different studies – one numerical mechanobiology based study Lacroix and Prendergast (2002) and the other an animal experiment carried out by Claes et al. (1997) (Fig. 5.10b). Whereas the numerical model (Lacroix and Prendergast, 2002) demonstrated identical trend in bone healing progression as predicted by our scheme, a significant drop in IFM was measured in the animal experiment (Claes et al., 1997) as the bone healing progressed beyond 4th week post-operatively. It may, however, be noted that the starting point of the IFM characteristics varied significantly owing perhaps to the differences in model and mechanical input parameters (stimulation). This further illustrates the dependence of the bone healing progression on the input parameters, e.g., mechanical strain.

The above similarities notwithstanding, the study had certain limitations. The musculoskeletal load applied in the present study was assumed to be static and full weight-bearing over the entire healing time in contrast to the dynamic and partial weight-bearing nature as seen in reality. However, this assumption can be justified considering the predicted distortional strain was in the safe range, indicating that the maximum movement was reached in early weeks in both cases. The future scope of study may include the cyclic nature of loading. Bone resorption and cortical remodelling had not been considered to accurately predict callus shape and size in the later phase of healing. These processes were ignored since the primary focus was on the healing process during the early phases till callus bridging. Moreover, the poroelastic material properties were not considered in the current study. The reason for this was the application of axial load in the model. Consequently, considering hydrostatic strain as mechanical stimulus was more appropriate as compared to flow parameters. The material properties assigned to biological soft tissue were assumed to be linear instead of viscoelastic and nonlinear. However, not enough experimental data are available for such implementations.

FE analysis is an approximate method which is sensitive to parameters like loading, material properties and boundary conditions. Output results may vary considerably, thereby necessitating experimental validation of the FE scheme, like the one the present study has conducted. Also, there exists no precise relationship between the iterative time steps involved, and actual time in days or weeks. Therefore, animal study is warranted at the least, with precise estimation of the loading regime such that a full-fledged validation of the present scheme can be contemplated.

Nevertheless, the present preclinical scheme is robust enough to predict bone healing for different implantation techniques, and thus can serve as a non-invasive tool for evaluating the relative merits of these implants. Rule-based models, e.g., fuzzy logic tools are relatively easier to implement and require less computational time as compared to the equation-based mechanoregulatory models. Furthermore, such techniques provide additional flexibility of incorporating any new rule without disruption of the original model. After incorporating various biological and patient-specific parameters, the fuzzy logic-based iterative model can further account for different clinical phenomena, such as smoking, diabetes, etc. Additionally, the linguistic rules can easily be altered as per the understanding of the medical experts for a more rigorous preclinical assessment. While plan of action for traditional treatment of fractures depends primarily on the experience of the orthopaedist, the present tool can act as a platform to predict post-surgery effects in advance and, thereby help clinicians strategize the best implantation technique for a patient. The model can also be explored/applied in veterinary fractures which are, physiologically and in various aspects, similar to those occurring in human patients.

5.5 Summary of the findings

The overall blood perfusion patterns were predicted to be similar for both cases of LP and DCP, and were consistent with the earlier histological evidences. However, the difference of initial distortional strain in the callus region of LP and DCP constructs was primarily responsible for the characteristic variation in the healing responses. The study further predicted that compressive strength imparted by DCP helps in the endochondral ossification at later stages of healing and facilitates faster solidification of callus as compared to the LP. In DCP, the physiological load experienced by the femur is transferred as frictional load at the plate-bone interface, whereas in LP, it is transferred through the screw-bone interfaces. This suggests that the local environment

in the bone fracture healing region around screws is influenced by a mix of effects in DCP. Rapid development of callus was predicted between week 4 and week 8 postoperatively for both the cases. It may, however, be noted that the predicted outcome is expected to vary significantly depending on the variations in model parameters and mechanical input parameters.

Chapter 6

Forecasting Post-operative Bone Changes for Extramedullary Plates Based on External Bone Adaptation Algorithm

6.1 Introduction

Any metallic implant has a considerably higher modulus and consequently, bears bulk amount of the physiological load. Stress shielding is a direct fall out of such discrepancy of load sharing between the implant and bone, resulting in the bone being deprived of essential mechanical stimulus required for its maintenance (Sommer et al., 2003; Ferguson et al., 1996; Tonino et al., 1981). Bone apposition or resorption is directly related to the stress variations of the implanted construct. Bone being a living tissue adapts its internal (material properties) and external (shape) characteristics according to the mechanical environment. However, for extramedullary implants, external adaptation is more detrimental, especially for patients suffering from non-union or needing more bone union time (Ferguson et al., 1996; Tonino et al., 1981). Different mechanical stimuli have been theorized to induce trigger for bone remodelling, including strain (Cowin and Hegedus, 1976), SED (Huiskes et al., 1987; Weinans et al., 1992), daily stress stimulus (Carter et al., 1996; van Der Meulen et al., 1993) and different other forms of stress (Doblaré and García, 2002). Majority of the mathematical models used a general evolution equation to study the remodelling of external cortical bone (Cowin and Hegedus, 1976; Huiskes et al.,1987; van Der Meulen et al., 1993; Prendergast and Taylor, 1994). While most of these studies address external adaptation in simple geometrical models, no longer term assessment on femur bone due to plate fixation have been undertaken based on commercially viable plating techniques. Moreover, to the best of authors knowledge, there is hardly any in silico study of plating techniques that addresses implant induced cortical thinning. FE based in silico methods have emerged over last few decades as reliable technique to model adaptive evolution of bone geometry and morphology consequent to post-surgery implant induced stress shielding.

Notwithstanding the prevalence of clinical and experimental studies related to the biomechanics of femur fractures and plated construct, the computational modelling of supporting osteotomies with regard to stress shielding and consequent bone remodelling has been scarce. Although such approaches are extensively employed in hip arthroplasties, there is a significant dearth in its use for modelling fracture fixated femur. A few studies, however, included FE based numerical models, albeit simplistic, to assess the outcome of various fixation plates. Using a hierarchical nonlinear hyperelastic FE analysis Latifi et al. (2012) predicted higher stability and durability with PFLP fixation for subtrochanteric fracture, as compared to a few other fixation techniques. In another study, the effect of stress shielding was assessed using a 3D, quarter-symmetric FE model based on a canine femur diaphysis plated with a metal/polymer hybrid design (Ferguson et al., 1996).

The present FE based in silico assessment makes for a comparative longer term performance evaluation of the two extramedullary fixation techniques, i.e., PFLP and DHS, on the basis of relative extent of external remodelling. The remodelling of the cortex was predicted using suitable adaptation law and the results were compared qualitatively with findings from previous clinical investigations.

6.2 Materials and Method

The present remodelling study is in extension to the stability assessment of the intact and implanted femur under static physiological load regime for subtrochanteric femoral fracture as described in Chapter 2. The 3D FE CAD models as mentioned in section 2.2 were re-employed here to carry out the *in silico* estimation of external remodelling. Hence, only a detailed description of the external remodelling scheme is given under the following subsection.

6.2.1 External remodelling of cortical bone

External bone adaptation clinically corresponds to the change in cortex geometry through bone hypertrophy or atrophy. In the present in silico scheme, this external remodelling was carried out by calculating the change in displacement of the surface node at the ROI of the FE model using an adaptation law similar to:

$$\frac{dbi}{dt} = A(S_i - S_{\text{ref}}) \qquad \ldots(6\text{-}1)$$

where b_i is the normal displacement of the surface node i, S_i is the strain energy density of the i^{th} node, S_{ref} is the reference strain energy density and A is a proportionality

constant (Huiskes et al., 1987). The nodes were allowed to displace exclusively in the normal direction. Both resorption and apposition of bone were assumed to be happening simultaneously. The value for constant A was determined by numerical methods and set as 1×10^{-10} m^3 N^{-1} $timestep^{-1}$ (Chennimalai Kumar et al., 2012). The remodelling rates were integrated, to determine the external geometrical changes, using forward Euler integration with a constant computational time-step Δt (Eq. iii)

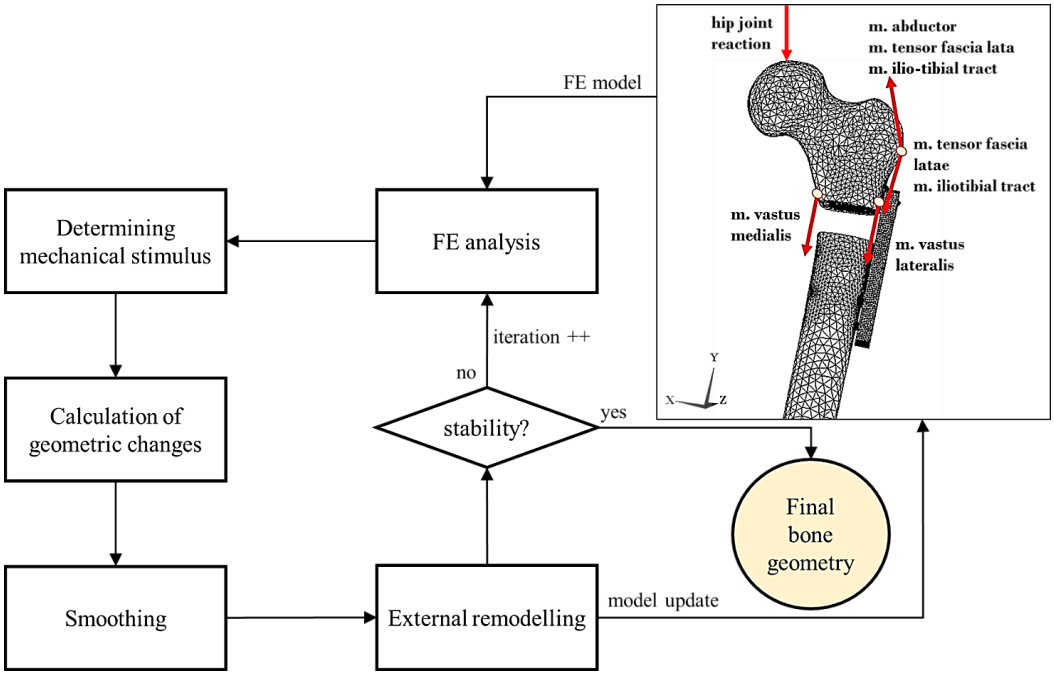

Fig. 6.1: Flowchart for FE based external remodelling simulation. The inset displays a representative FE template for a fixated bone with all muscle forces along with hip joint reaction force considered for the simulation study. For details regarding all force values, see Table 2.2.

$$b_i^{t+\Delta t} = b_i^t + \frac{dbi}{dt}\Delta t \qquad \text{...(6-2)}$$

To avoid undesirable distortion in the surface of the updated mesh, appropriate smoothing was done in the form of distance weighted average displacement bi′t+Δt given by:

$$b_i'^{t+\Delta t} = w\, b_i^{t+\Delta t} + (1\text{-}w)\left[\frac{\sum_{n=1}^{Nneigh} \frac{b_n^{t+\Delta t}}{|Xi-Xn|}}{\sum_{n=1}^{Nneigh} \frac{1}{|Xi-Xn|}}\right] \qquad \text{…(6.3)}$$

where N_{neigh} is the total number of nearest neighbors of node i and |xi-xn| is the distance between the surface node i and a neighboring node ‘n’ (Chennimalai Kumar et al., 2010). The value for w is set as 50%, meaning an equal weightage was considered both for the displacement of a given node and the contribution from its neighboring nodes.

The position xi of each surface node i is then updated using the corresponding normal component of the weighted average displacement, as per following:

$$X_{i,j}^{t+\Delta t} = X_{i,j}^{t} + (n.\varepsilon^{j})\, b_i^{'t+\Delta t} \quad ...(6.4)$$

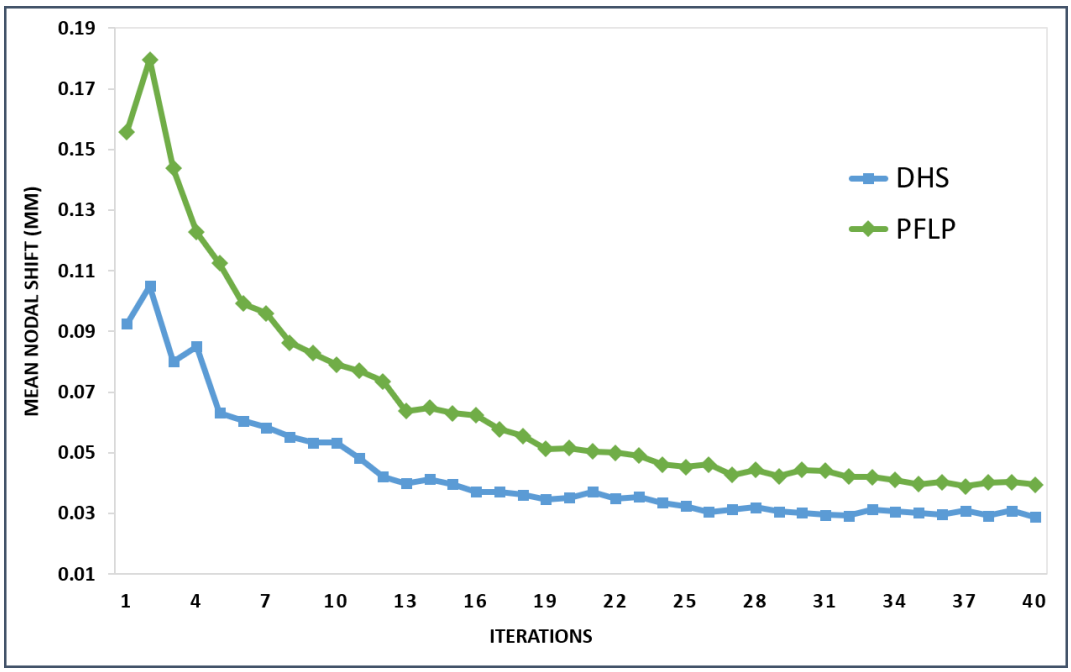

Fig. 6.2: Stability analysis of the external remodelling algorithm: the progression characteristics of mean nodal displacements (mm) over 40 iterations for both DHS and PFLP constructs.

where the subscript j denotes individual components of the position vector xi in three mutually perpendicular directions (x, y and z) and ε_j is the corresponding unit vector. The entire remodelling scheme, along with an FE template for a fixated bone subjected to physiological loading, is presented in Fig. 6.1.

6.3 Results

For prediction of external remodelling of femur, the distal cortical shaft beneath the fracture gap was considered. The remodelling simulation was run for 40 iterations, as shown in Fig. 6.2, both for DHS and PFLP fixated models until the mean nodal shift of the corresponding nodes reached below 4% of 1 mm. This ensured reasonable accuracy in prediction of the adaptation. Nonetheless, the associated error in the mean nodal displacement beyond equilibrium point may be accredited to the noise resulting from high stress concentration at the screw holes. Fig. 6.3 shows the initial (post-operative) and post-adaptation contours of nine distinct cross-sections for DHS and PFLP fixated femur, respectively, which roughly encompass the distal bridging area for both implants. The external remodelling was predicted to be more pronounced in the proximal sections as compared to the distal sections of the bone in both cases. Sections

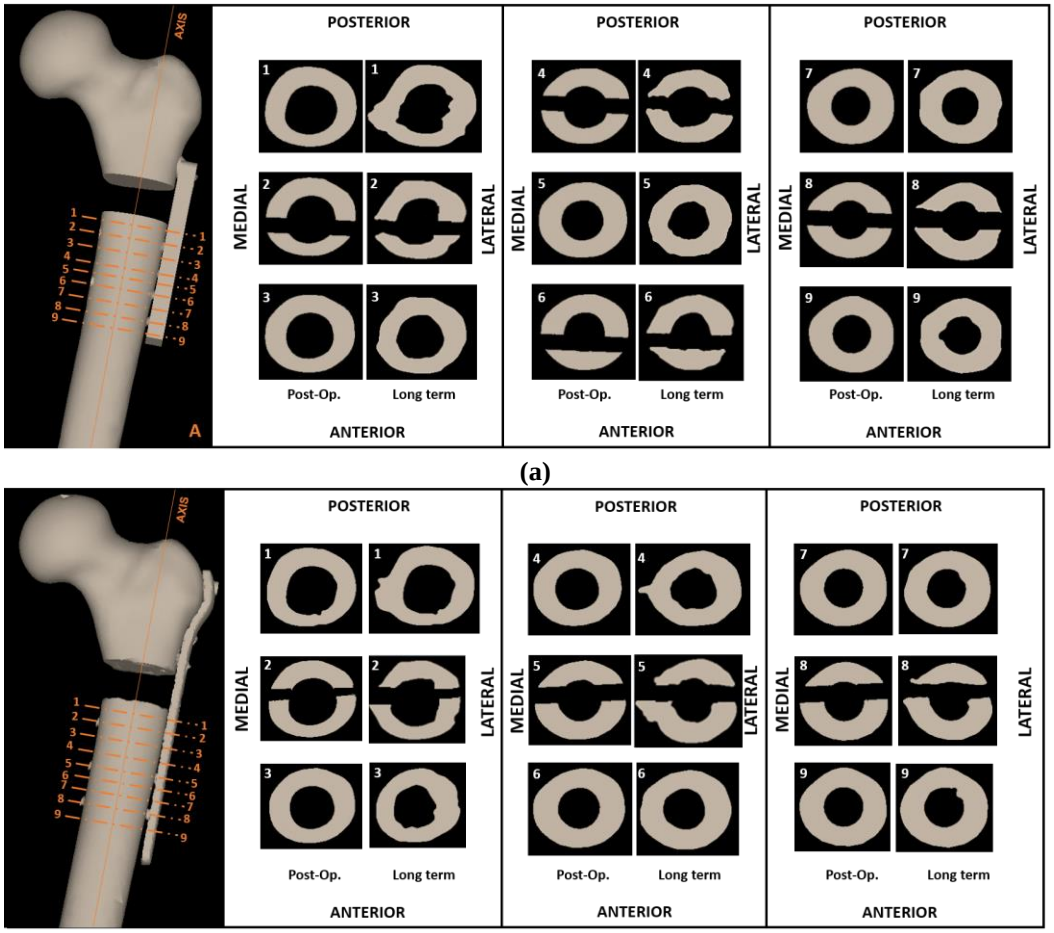

Fig. 6.3: Post-operative and long term (post adaptation) cross-sectional profiles of femoral cortex at nine distinct sections (as shown on the left side) corresponding to (a) DHS and (b) PFLP fixation, respectively, considering body weight of 80 kg.

with screws were found to predict incidences of ossification (see sections 2, 4, 6 and 8 for DHS and 2, 5 and 8 for PFLP in Fig. 6.3), resulting in medio-lateral bulging. Anterior-posterior thinning of the cortex is noted to a certain degree especially for DHS (section 4 and 6). However, both in case of DHS and PFLP, no significant post-adaptation change in bone contour was predicted distally, away from the implant.

In order to estimate the directional change of the nine cross-sectional profiles, the relative shifts in the corresponding centroids were marked for DHS and PFLP constructs, respectively, as depicted in Fig. 6.4. The normalized values of the centroidal shift (Δs) were further calculated based on the degree of shift with respect to the initial profile of the cortex, where C(old) and C(new) are centroids of the initial and the final profile, and ΔCx and ΔCy are the shifts in x and y directions, respectively (Fig. 6.5). It is evident from normalized Δs values that the sections associated with screws (or adjoining sections) demonstrated comparatively higher magnitude of centroidal shift

(Fig. 6.5). However, the peaks (>10%) were predicted in the proximal sections (section 1 and 2) for DHS construct, whereas the same was observed in the mid-section (section 4) for PFLP. From overall consideration, the former predicted more uniform progression of centroidal shift (sections 1-9) as compared to the latter.

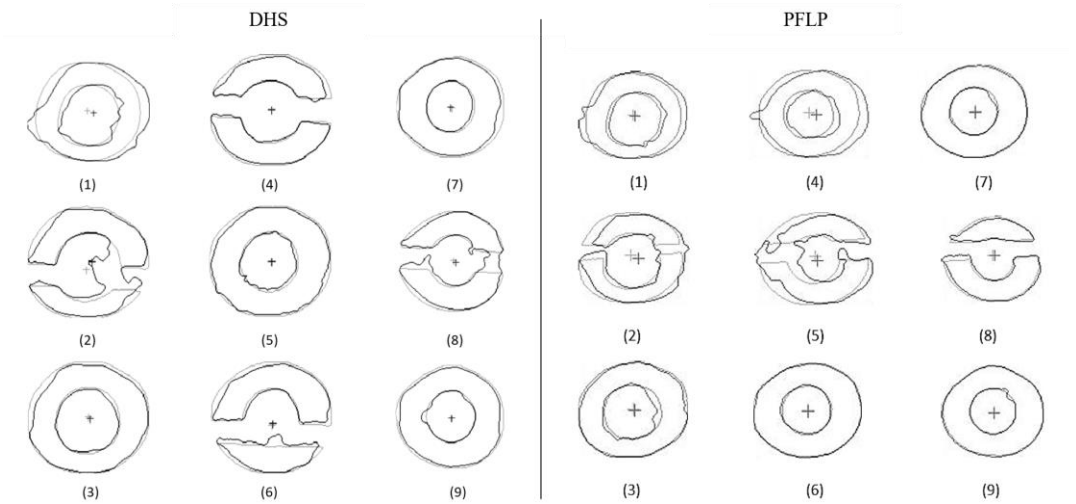

Fig. 6.4: Mapped pre- and post-adaptation cortical contours of the nine distinct sections, along with the relative position of associated centroids, for DHS and PFLP implants. The initial and the final profiles are shown in GREY and BLACK, respectively.

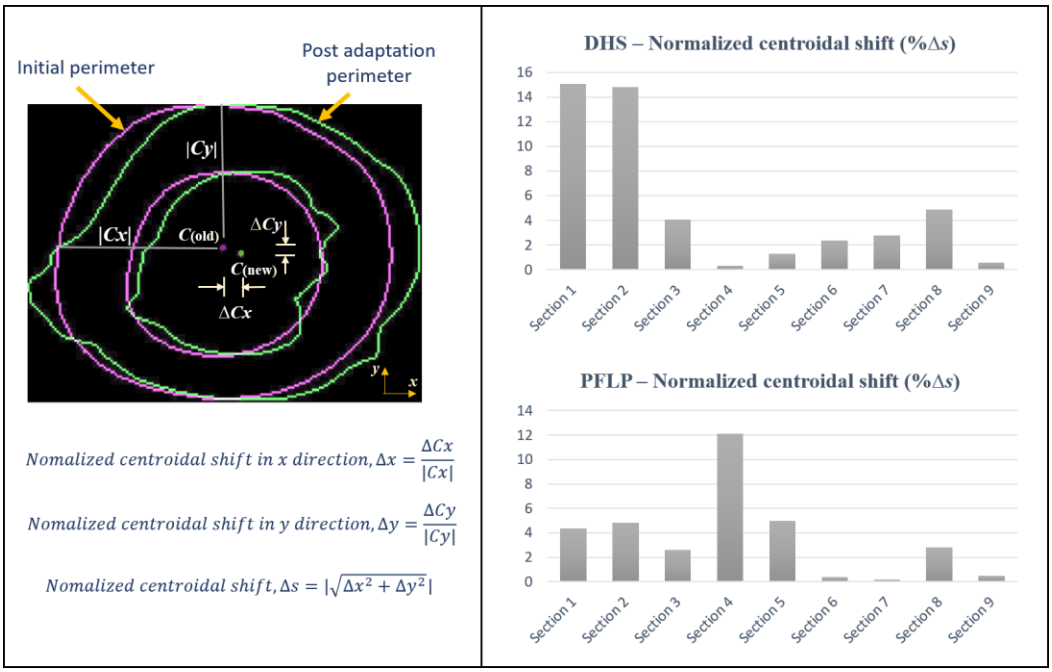

Fig. 6.5: Normalized centroidal shift (Δ*s*) at pre-designated nine sections of cortical bone for DHS and PFLP fixation, respectively. The values of Δs were calculated based on the degree of shift with respect to the initial profile of the cortex, where $C_{(old)}$ and $C_{(new)}$ are centroids of the initial and the final profile, and ΔC_x and ΔC_y are the shifts in *x* and *y* directions, respectively.

The extent of cortical thinning (hypotrophy) and thickening (hypertrophy) were estimated based on relative changes in the cross-sectional area of the cortex after remodelling, as shown in Fig. 6.6. Negative change in area indicates cortical thinning, whereas any positive change in cross-sectional area signifies incidence of ossification. It is evident from the plots that DHS introduced greater thinning of bone (>5% decrease in sections 3 to 7) as compared to PFLP. However, section 1 predicted higher incidences of ossification (~10% increase in area) for both implants.

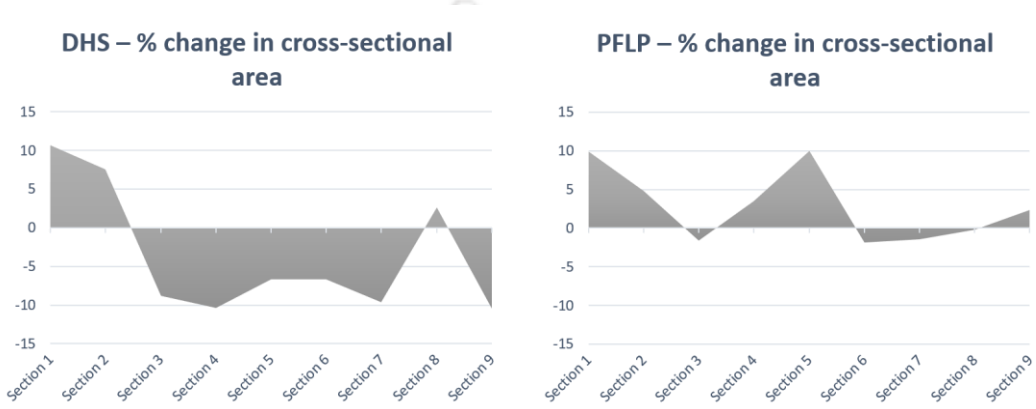

Fig. 6.6: Percentage change in cross-sectional area at the nine distinct sections of the cortical bone fixated with (a) DHS and (b) PFLP implant, respectively.

6.4 Discussions

6.4.1 Clinical significance of the predicted remodelling

There is scarcity of clinical study to validate the longer-term effect of rigid extramedullary devices on cortical thickness. However, an investigation by Terjesen et al. (1985) reflects the nature of external remodelling based on computed tomography (CT) data after osteosynthesis of femoral shaft treated with rigid plate fixation. They observed prominent reduction in cortical thickness (~11% averaged over 12 patients) on the lateral side just beneath the plate, which is similar to our present predictions. A few experimental studies also reported site-specific new bone formation due to localised maximal stress or strain magnitude in canine femur (Rubin and Lanyon, 1985) and mice tibia (Sugiyama et al., 2012). The present study also predicted similar trend of contralateral bulging of cortex due to ossification especially at the screw ends (Fig. 6.3). However, the reported associated reduction in density (osteopenia) of the thickened bone may be predicted based on morphometric remodelling algorithms [44]. In all sections of DHS fixated bone, a clear lateral reduction in cortical contour can be noted (Fig. 6.4), with the exception of the sections associated with screws. From Fig.

6.6a, it can also be deduced that the thinning is more pronounced in the mid-sections (section 3-7). The predicted thinning was not as prominent though, in case of PFLP (Fig. 6.4). Opposite to the site of the plate, i.e., in the medial quadrant, the cortical thickness of the plated segment was reported to have increased (Avval et al., 2016).

The lateral thinning beneath the plate and medial thickening of the cortex at screw ends can be attributed to the post-surgery altered load transfer mechanism in femur. Rigid metal plate fixation protects the bone from normal stress, resulting in considerable bone atrophy, which is clearly documented in animal studies (Latifi et al., 2012; Wang et al., 2014; Weinans et al., 1992). As such, a laterally fixed plate shields the cortex significantly from lateral tensile stresses due to bending, which is otherwise available sufficiently in an intact femur. Moreover, contrary to the overall uniform load distribution in the intact bone, the load flow pattern in a laterally plated bone is predominantly mediolateral. Consequently, distal to the fracture site, the load is passed on from the plate to screw and then finally to the bone. Such load sharing culminates into excessive stress concentration at the screw ends of the medial cortex, thereby leading to hypertrophy (thickening).

6.4.2 The iterative time step and limitations thereof

The iterative time step t and the proportionality constant A in Eq. ii were intertwined to ensure that the remodelling results were independent of scaling. The iterative time step could be viewed as pseudo time step. The iterations were continued until no significant change in the mean distortion of the nodes was observed. Clinically, this is considered as longer term response as the distortion reached a stable condition. Terjesen et al. (1985), in their follow-up study also reported that femoral bone property (cortical density) reaches a stationary stage in less than 1-3 years of plate fixation. A previous study on plated tibiae also found no substantial increase in stress-shielding with increasing duration of plating beyond 1-2 years (Terjesen et al., 1986). This further corroborates well with the equilibrium scenario predicted in the present study (Fig. 6.2). Nevertheless, there exists no clear relationship between the iterative time steps involved in external remodelling, and actual time in months or years. This is a known limitation of most in silico analyses involving bone remodelling (Avval et al., 2016; Chennimalai Kumar et al., 2010; Huiskes et al., 1987). Furthermore, consideration of homogeneous material properties in the model may lead to an overestimation of bone stiffness (Blanchard et al., 2013). However, the primary goal of this study was to conduct a

comparative biomechanical assessment between two different plating techniques. Hence, the absolute nature of the material properties of bone was of secondary importance to the differences observed between the two constructs subjected to identical loading conditions (Ferguson et al., 1996).

6.5 Summary of the findings

Although no adverse external remodelling was noted for either implant, DHS predicted admissible cortical thinning beneath the bone plate. This occurs since a laterally fixed plate shields the cortex significantly from lateral tensile stresses due to bending. Moreover, the load flow pattern in a laterally plated bone is predominantly mediolateral. Hence, a notable degree of contralateral bulging of cortex due to ossification, especially at the screw ends, was predicted for both implants. Nevertheless, tissue regeneration and post-operative fracture healing scenarios need to be addressed and further clinical validation is warranted for conclusive remark on this. The proposed external remodelling scheme may, however, be employed in future studies involving novel fracture plate design, optimization of several influencing factors, e.g., plate thickness, plate shape, screw positioning and alignments etc.

Chapter 7

Novel Design of Minimally Invasive Double Oblique Device for Osteosynthesis (DODO) of Hip: an Extramedullary Plate for NE Population of India

7.1 Introduction

The aging of the world population due to the rise in life expectancy has resulted in increased incidences of hip fracture, especially in the geriatric population. The continuously growing number of motor vehicle accidents in the present age of globalisation has equally contributed to the trauma cases involving proximal femoral fractures in younger adults. Intertrochanteric femoral fracture, most notably, accounts for up to 50% of all such fractures (Rog et al., 2017). These fractures are commonly associated with a significant rate of morbidity and mortality (White et al., 1987). Intertrochanteric fractures involve the upper end of the femur between the greater and lesser trochanter with or without extension in the upper femoral shaft. This kind of fracture is classified as either stable or unstable intertrochanteric fracture. The primary aim of treatment usually comprises stable fixation and early weight bearing. It may be noted that early weight bearing helps in reducing the morbidity and mortality of the patients.

A general observation reveals that the success of such implants, by and large, relies on ethnic, demographic and morphometric variations. Proximal femoral geometry is determined by genetic and environmental factors, e.g., age, race, sex and also lifestyle (Najjar et al., 1978; Ericksen et al., 1979). Tribes of NE India belong to the Mongoloids, characterised by short and wide face, broad nose, projecting cheek bones and relatively shorter stature (Saikia et al, 2008). In contrast, the Caucasoids are characterised by a long head, high forehead, long and narrow nose and taller stature compared to Mongoloids. Most of the commercially available implants in the market are developed based on the data of the Caucasian population of the western countries, and thus they may not be an ideal fit for Indian patients due to anatomic/anthropometric variations.

Siwach et al. (2003) suggested the use of modified implants according to Indian anthropometry to lessen the incidences of intraoperative complications such as fractures and splintering. Few other complications owing to such geometric and morphometric mismatch include aseptic loosening, improper load distribution and discomfort leading to long-term surgical failure (Rawal et al., 2012; Khang et al., 2003). Agarwala et al. (2020) noted that there exist significant differences in anthropometric parameters of hip joints among the population of southern Assam (NE, India) when compared to that of the western population. Pushparthna et al. (2019) observed that femoral length is proportional to the average height of a race. Therefore, in order to achieve an optimum surgical outcome, the geometry of the implant should closely match with that of the femora of the target population.

Metallic implants have considerably higher modulus and consequently bears a bulk amount of the physiological load. Stress shielding is a direct fallout of such discrepancy of load sharing between implant and bone, resulting in the bone being deprived of the essential mechanical stimulus required for its maintenance (Ferguson et al. 1996; Tonino et al., 1976). Larger-sized implants, typically designed for Caucasian patients, have higher structural stiffness, which may further aggravate the adverse effect of implant induced stress shielding, especially on smaller bones of the NE population. Therefore, it is crucial to design an implant through which adequate loads can be transferred to the bone thereby considerably reducing the effect of stress shielding. Although a significant number of experiments and computational studies assessing modifications of intramedullary fixations can be found in the literature (Rawal et al., 2012; Pathrot et al., 2016), very few have focussed on the lengths of the side plates (Rog et al., 2017; McLoughlin et al., 2000; Bolhofner et al., 1999; Wang et al., 2020).There is hardly any study that has incorporated inclined screw orientation with shorter side plates considering regional morphometry, in addition to an anti-rotation screw.

The primary objective of the study is to biomechanically compare a new device for hip osteosynthesis to that of conventional commercially available implants, e.g., PFLP and DHS, using FE analysis. The new design, to be called henceforward as Double Oblique Device for Osteosynthesis of hip (DODO), features a shorter side plate to address the anthropometric requirement of the NE population. We hypothesized that the new design is biomechanically comparable, if not superior, to the commercial designs of EM fixation devices typically used to treat Evans type-I intertrochanteric

femur fractures. Thus, DODO was compared with the conventional implants in terms of stress shielding and axial stability under static load consideration as discussed in Chapter 2, dynamic and impact energy strength assessment for sideways fall as was carried out in Chapter 4, and further secondary bone healing progression was evaluated in DODO implanted NE femur similar to the phenomenological model detailed in Chapter 5.

7.2 Materials and Method

7.2.1 3D model generation of the implanted femur

The 3D FE models of the PFLP and VA-DHS implanted femur were identical to those described in Chapter 3 (section 3.2). However, for this part of the study, three different FE models corresponding to DODO implanted bone were generated as shown in Fig. 7.1. The first one (Model A) was generated using the manufacturer supplied CAD model of the left femur (Sawbones, model# 3406). As opposed to the 48.5 cm Sawbones model for the large femur typical of a Caucasian male, the length of the femur model was scaled down to 37 cm to represent the NE population of India (Pushparthna et al., 2019; Wang et al., 2020; Chansa et al., 2019). This is based on a formula that assumes femur length to be a quarter of the total height of an adult (Mamidi et al., 2011). The 3D scale down ensured a proportional downsizing of all parameters in the entire femur model. Additionally, two more 3D femur models namely Model B and Model C were developed from CT-scan data of one NE patient and one Caucasian patient, respectively. An intertrochanteric fracture,

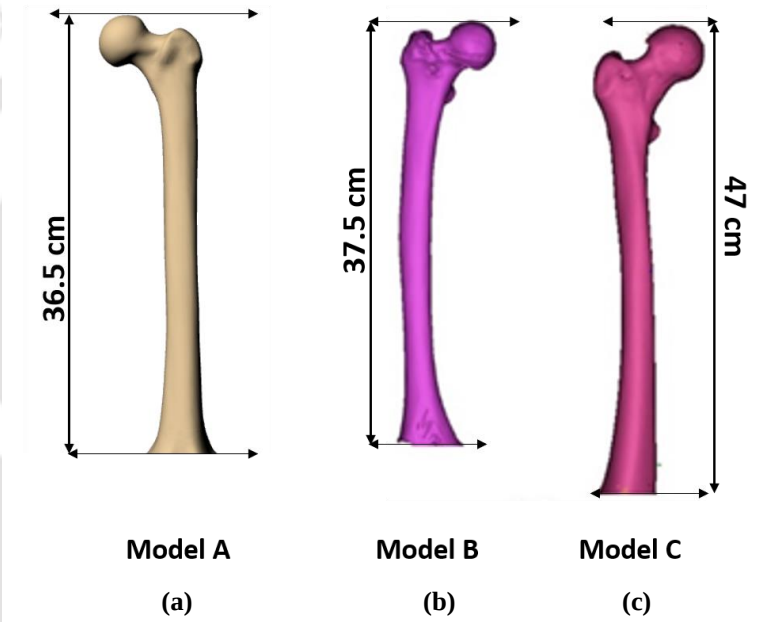

Fig. 7.1: CAD models of femur: (a) manufacturer supplied CAD model of left femur modified for NE patients according to the height of NE patient, (b) NE patient specific femur developed from CT-scan data, (c) Caucasian patient specific femur developed from CT-scan data.

simulated as a two-part fracture with a gap of 1 mm, was created by mimicking the fracture of the PFLP fixated femur (section 3.2).

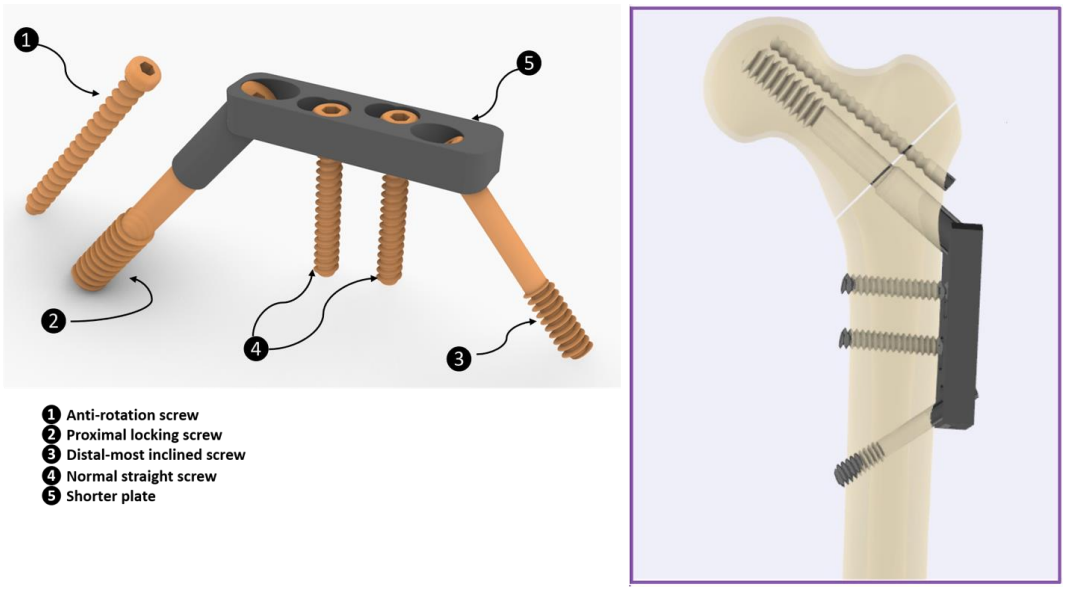

(a) (b)

Fig. 7.2: CAD models of the implant and the implanted femur with a simulated intertrochanteric fracture gap of 10 mm: (a) DODO, (b) DODO fixated femur

Table 7.1: Specifications corresponding to DODO, PFLP and VA-DHS.

		DODO	**PFLP**	**VA-DHS**
Screw	proximal locking	1	3	1
	distal dynamic	3	4	4
Profile (*l*,*b*,*t*) (mm)		58,14,9	195,19,6	109,19,5.8
Holes		3 (Combi)	6 (Combi)	5
Angulation screw	proximal locking	130º		
	distal oblique	50º		
Auxiliary		One anti-rotation screw		

The DODO was modelled and virtually implanted in all the three femurs in the NURBS modelling environment of Rhinoceros v14.0 (Rhinoceros, Robert McNeel & Associates, Seattle, USA) (Fig. 7.2 a). A total of four screws were fixed virtually: one proximal locking (cancellous screw) and three distal dynamic (cortical screws). Tip apex distance (TAD) was kept below 25 mm while fixating and designing both the implants to prevent screw cut out (Abdulkareem, 2012). The distal most screw was obliquely oriented at an angle of 50º such that bone screw anchorage is maximum. Additionally, one anti-rotation screw was attached proximally at the top of the locking

Table 7.2: Material property of cortical and cancellous bone (MPa).

	NE femur	**Caucasian femur**
Cancellous	150	200
Cortical	11,000	15,000

screw for enhanced rotational stability in the proximal femur (Fig. 7.2 b). The overall length of DODO was reduced to the extent of ~50% of the conventional implants. Complete specifications of the DODO, PFLP, and VA-DHS implants are given in Table 7.1.

7.2.2 FE modelling of the intact and implanted femur

The 3D models were then imported into Ansys ICEM CFD v15.0 (ANSYS Inc., PA, USA) to generate a volumetric mesh comprising of 4-noded unstructured tetrahedral elements. After that, the volumetric mesh was imported into Ansys Mechanical v15.0 (ANSYS Inc., PA, USA) and converted into the 10-noded tetrahedral mesh for better accuracy and further analysis. However, the meshing parameters were borrowed from sections 2.2 and 3.2.

Three different types of analyses were performed with DODO implanted femurs according to the morphometry of both NE and Caucasian population. Static load analysis, considering hip joint reaction force, was performed to compare DODO implanted shortened Sawbones femur (37 cm, Model A) with PFLP and VA-DHS implanted long Sawbone (48.5 cm, Caucasian) femur. Load of 1.5 kN and 2 kN was applied vertically downward through the femoral head of the 37 cm and 48.5 cm bone, respectively (Fig. 3 a). The reason for giving different maximum static and dynamic load was that DODO femur should describe physiological loading of native NE population of India having low body weight (60 kg in avg.), whereas PFLP and VA-DHS fixated large femur is meant to describe the loading condition of Caucasian patients having higher body weight (80 kg in avg.) A condition of zero displacement was applied at distal femoral nodes sufficiently away from the point of application of load. Further to assess the strength, dynamic impact analysis mimicking the sideways fall scenario was conducted for both NE (Model B) and Caucasian (Model C) patient specific femur that were developed from the CT data (Fig. 7.3 b). The description of

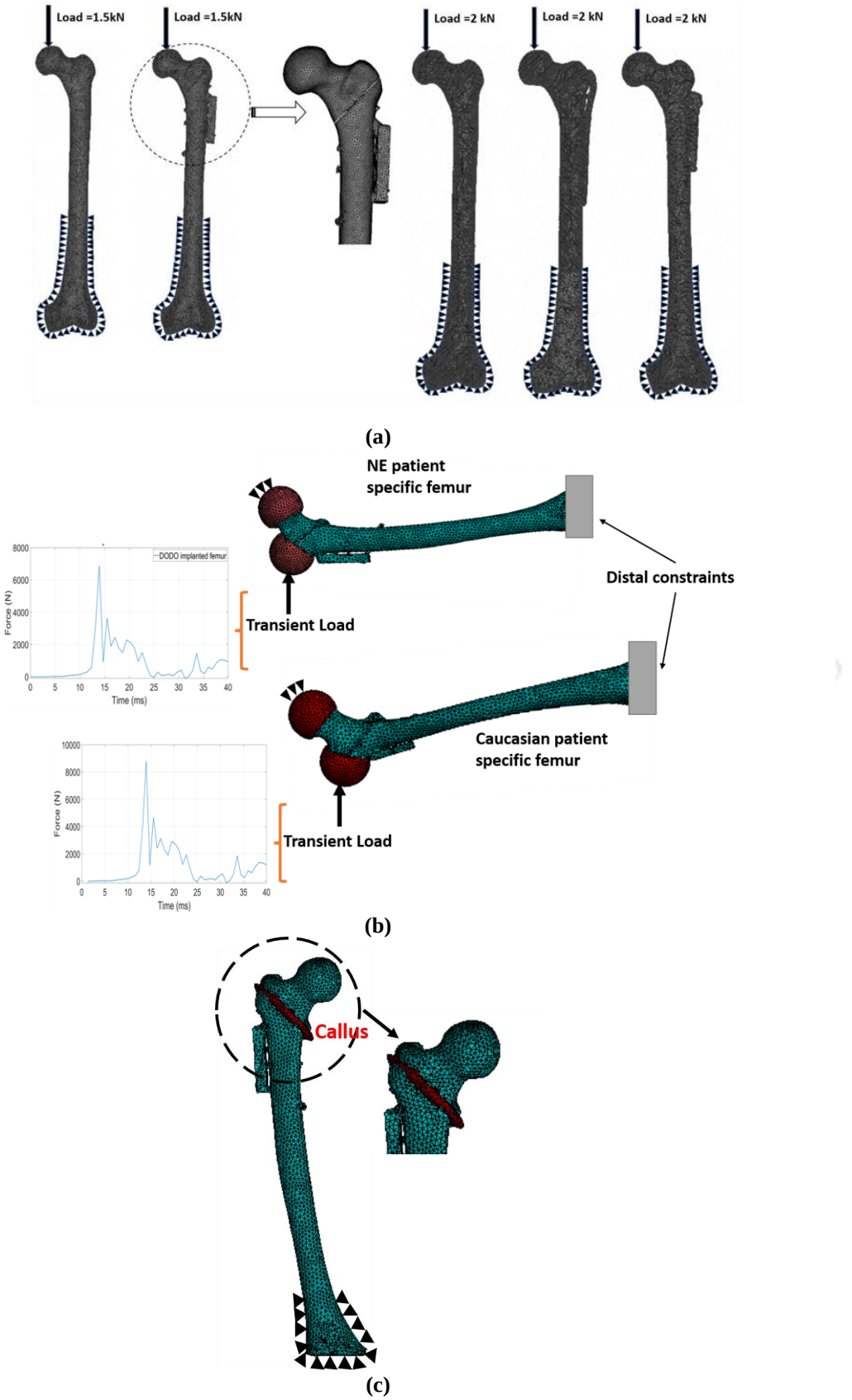

Fig.7.3: FE models of intact and implanted femurs: (a) static loading considering only the hip-joint reaction force, (b) dynamic impact sideways fall loading configuration, (c) callus modelling to predict the secondary bone healing.

this FE analysis is given in details in Chapter 4, section 4.2. The peak load for fall was

~6.6 kN for NE femur and ~8.8 kN for the Caucasian femur depending on the weight of both the patients (Lotz et al., 1995; Robinovitch et al., 1991)). Finally, the Fuzzy logic-based bone heling algorithm developed in Chapter 5 was applied in the DODO implanted NE femur (Model B) to predict the tissue differentiation in the callus region (Fig. 7.3 c).

7.2.3 Material properties

The material model for the Sawbones femur was considered as per Table 2.2. Linear elastic, isotropic, and homogeneous material properties were applied to the cancellous bone, whereas orthotropic material properties were applied to the cortical bone based on the data provided by the manufacturer (Biomechanical products catalog Sawbones). For patient specific femurs, bone modulus was estimated from the Hounsfield Unit (HU) of the CT data of the patient. The apparent density (ρ in g.cm-3) for bone element was computed from corresponding CT number in HU using the following relationship:

$$\rho = \rho 1 + [(\rho 2 - \rho 1) / (HU2 - HU1)] \times [HU - HU1] \quad \ldots (7.1)$$

where (ρ1, HU1) represented the apparent density and CT number of water, i.e., no bone condition (0.022 g.cm-3, 0 HU), and (ρ2, HU2) were the apparent density in the hardest cortical region and corresponding CT number value (1.73 g.cm-3, 1700 HU), respectively. The negative CT grey value was considered to 0 HU (no bone condition). The Young's moduli (E in MPa) of bone elements were related to the apparent density (ρ in g·cm-3) according to the following relation:

$$E = C \rho^{D} \quad \ldots (7.2)$$

The values of constants in Eq. 7.2 were taken from the study of Morgan et al. (2003) and Helgason et al. (2008). The average elastic modulus was considered for both cortical and cancellous bone (Table 7.2). The material for plate and screw were considered to be titanium (Ti) alloy (Young's Modulus, E = 110 GPa). Poisson's ratio was set as 0.3 for all materials. All interfaces between bone and plate were assumed to be bonded under all conditions.

7.3 Results

Fig. 7.4 illustrates the von Mises stress distribution in the femur cortex for both intact and implanted cases. The average von Mises stress at the calcar region of the NE femur (37 cm long femur) for the DODO implant was found to be ~11.0 MPa, and that in the femoral shaft was ~18.0 MPa. The corresponding average stress values in the intact NE

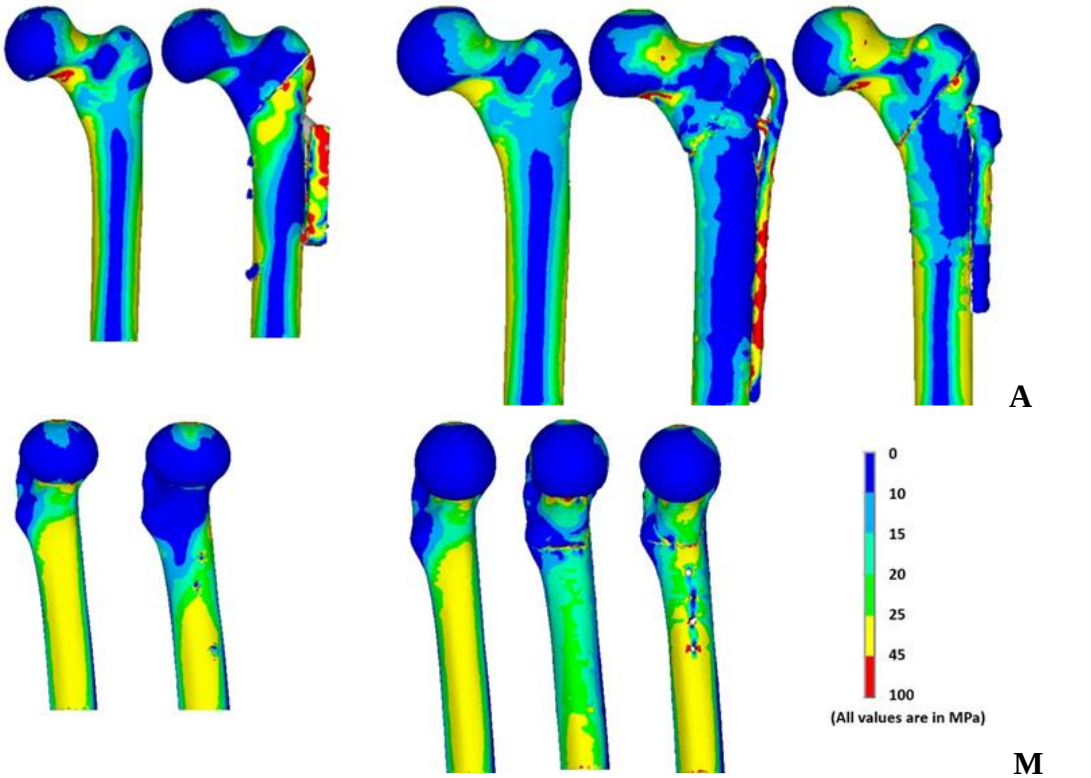

Fig. 7.4. The von Mises stress distribution in anterior (A) and medial (M) aspects of intact and DODO fixated 37 cm femur (first two, considering body weight of 60 kg); intact and DHS fixated 48.5 cm femur (last three, considering body weight of 80 kg).

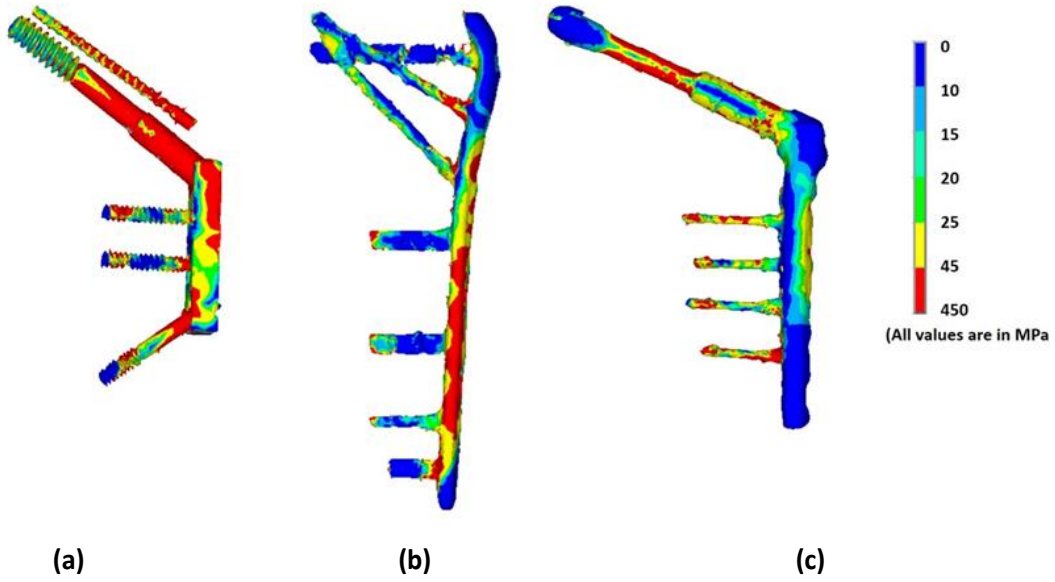

Fig. 7.5: von Mises stress distribution contour for (a) DODO, (b) PFLP and (c) VA DHS implants.

femur was found to be ~16.0 MPa. No significant difference was noted in von Mises stresses for identical calcar sites for PFLP and VA-DHS implanted Caucasian femur (48.5 cm long femur), clocking average values of ~13.0 MPa and ~18.6 MPa, respectively. For the femoral shaft, the respective average stress values were ~10.0 MPa

and ~14.2 MPa. The predicted average von Mises stress for the corresponding 48.5 cm intact femur was 15.0 MPa. In the case of DODO, maximum stress was found to be in the first point of intersection between the lateral plate and proximal locking screw (Fig. 7.5). Stress concentration was also predicted at the intersection area of the screws with the lateral plate in all the implants.

The implant induced stress shielding on the femur demonstrated a similar pattern (Fig. 7.6 a). In all the three femoral constructs, i.e., DODO, PFLP, and VA-DHS fixated femur, a significant portion of the proximal femoral head and the region adjoining to the plate were stress shielded. The stress shielding was substantially high for the PFLP and VA-DHS in the distal bone fragment (lateral aspect) and for DODO in the femoral head. Proximally in the femoral head, stress shielding was predicted to be 46% for DODO implanted NE femur, 37% for PFLP implanted Caucasian femur, and 24% for VA-DHS implanted Caucasian femur. However, the corresponding values were found to be 37%, 44%, and 41%, respectively, in the distal femur (Fig. 7.6 a).

In order to assess post-implantation stability, the maximum axial displacement of the DODO femur construct was compared with that for PFLP and VA-DHS fixated femoral constructs (Fig. 7.6 b). Axial displacement for the DODO construct was

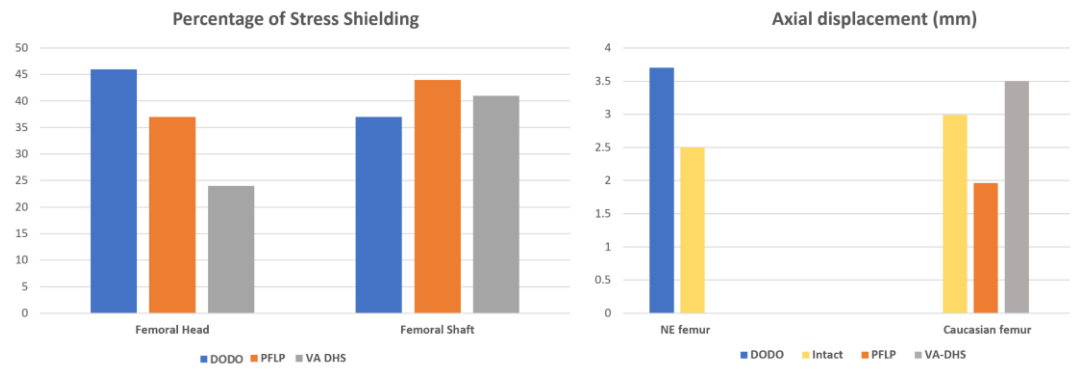

(a) **(b)**

Fig. 7.6: Bar Chart: (a) Percentage of stress shielding in the region of the femoral head and femoral shaft due to various implants. (b) Axial displacement of various implant fixed femurs and corresponding intact bone.

predicted to be 3.7 mm compared to 2.5 mm for the intact NE femur. For PFLP and VA-DHS fixated Caucasian femur, the predicted axial displacement values were 1.9 mm and 3.5 mm as opposed to 2.9 mm in the corresponding intact Caucasian femur. The conventional implants showed high rigidity and higher degree of stress shielding in NE population femur. The intensity of stress shielding on PFLP implanted NE femur

was predicted to be 48% and 45% at femoral head and femoral shaft, respectively. For

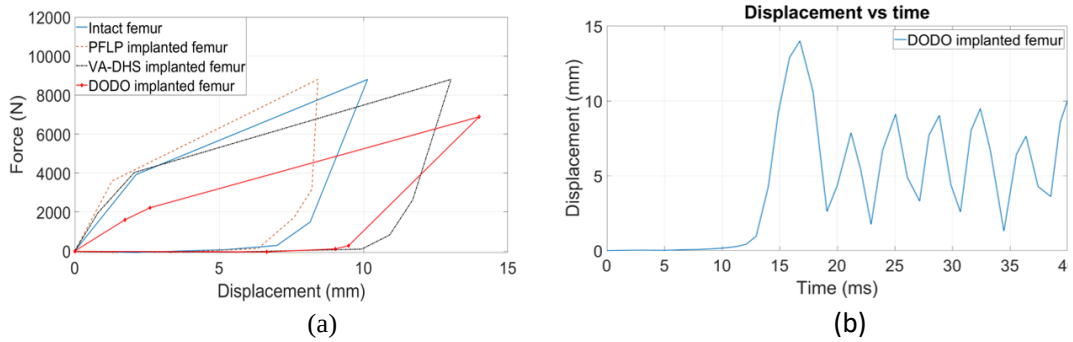

Fig. 7.7: Dynamic impact response: (a) Comparison of Force-displacement loop (energy absorbed) corresponding to intact, PFLP and VA-DHS implanted femur (Fig. 4.5) and DODO implanted NE patient specific femur; (b) displacement-time response of DODO implanted NE patient specific femur.

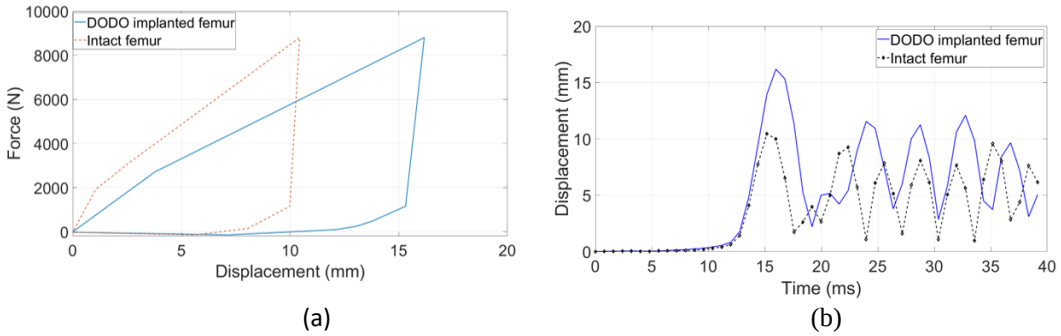

Fig. 7.8: Comparison of dynamic impact response of intact and DODO implanted patient specific Caucasian femur: (a) Force-displacement loop (energy absorbed); (b) displacement-time response

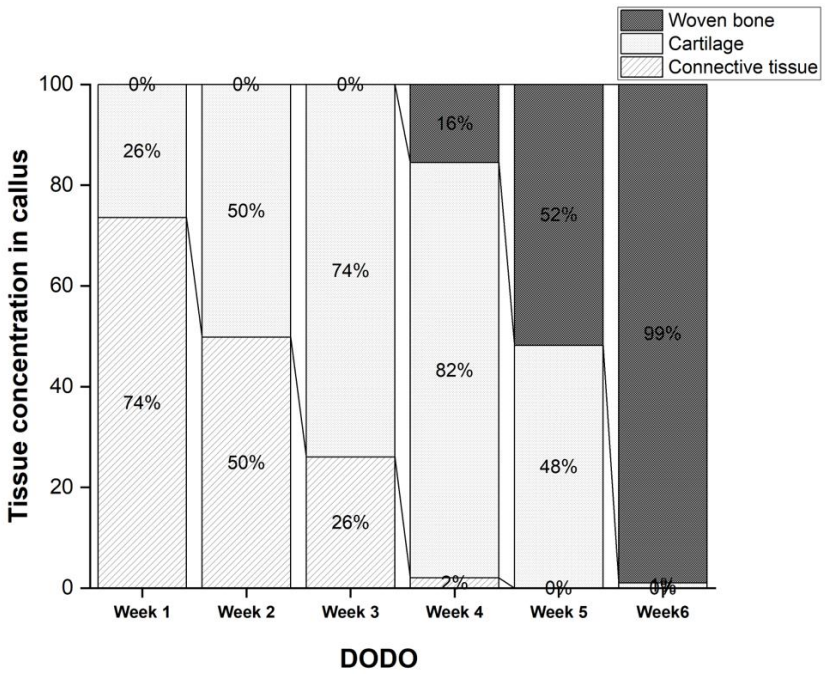

Fig. 7.9: Post operative variation of tissue concentration in the callus region from week 1-8 as predicted in the DODO implanted patient specific NE femur.

VA-DHS, the values were found to be 35% and 43%, respectively. The percentage bone volume stress shielded on NE femur due to implantation was found to be 69% for PFLP, and 60% for VA-DHS, whereas it was only 54% on DODO implanted NE femur. On implanting DODO on Caucasian femur intensity of stress shielding was found to be 43% on femoral head and 36% on femoral shaft. However, DODO implanted on Caucasian femur was found to have high axial displacement of 4.8 mm as compared to 2.9 mm in intact bone. The energy losses were estimated by calculating the area of the stress versus strain loops using trapezoidal integration (Matlab v2019) as described in section 4.3. Energy absorbed by DODO implanted NE patient specific femur was found to be 39 J (Fig. 7.7 a). For easy reference, energy absorbed curves of the commercial implanted femurs in Caucasian femur are incorporated in Fig. 7.7 (a) from Section 4.3, Fig. 4.5. The same values for PFLP implanted femur were 43 J, 44 J for intact femur and for VA-DHS construct it was 66 J. The displacement versus time curve corresponding to DODO implanted NE patient specific femur for the sideways fall is presented in Fig. 7.7b. Maximum displacement corresponding to peak load of fall case was predicted to be ~13 mm. On the contrary, for intact and DODO implanted patient specific Caucasian femur the energy absorbed was 48.7J and 71.3J respectively (Fig. 7.8 a). And the displacement against the peak load was ~10mm for intact femur and ~15mm for DODO implanted patient specific Caucasian femur (Fig. 7.8 a). The secondary bone healing model predicted almost 99% of woven bone formation by the end of 6th week (Fig. 7.9). At the end of 4th week, cartilage formation was predicted to be the highest.

7.4 Discussion

Intertrochanteric fractures can be fixated with various implants, which can either be IM or EM type devices. While the outcomes of the two techniques are still debatable, there is hardly any consensus on their relative superiority. Fracture severity, osteoporosis, cost, intra- and post-operative complications, and, above all, femoral geometry and morphometry make the selection of the implant a difficult task. The present study offers a noble design of implant for stable intertrochanteric fracture considering the regional morphometry of the NE population of India. To establish the suitability and biomechanical stability of the new design, the DODO fixated femoral construct representing regional geometry was compared with conventional PFLP and VA-DHS fixated femur of Caucasian geometric variation. FE analysis based on in-silico models

was employed to predict the stress and displacement patterns for the biomechanical comparison.

It may be observed that, for all implanted models, the laterally fixed plate shields the cortex significantly from lateral tensile stress arising from bending (Fig. 7.4). Contrary to the overall uniform load distribution in the intact bone, the load flow pattern in a laterally plated bone is predominantly medio-lateral, i.e., the load flows from the bone to the implant in the proximal segment and from the implant to the bone in the distal segment of the fractured femur. The above-mentioned load transfer justifies the greater intensity of stresses in the proximal locking screw and distal-most dynamic screw in all models (Fig. 7.5). The length of DODO is kept almost 50% less compared to the other two plates. The former thus predicted almost similar stress distribution, especially at the distal femur when compared with the intact model, unlike the PFLP and VA-DHS fixated femur. Therefore, DODO induced a lower level of stress shielding as compared to the other implants and also explains the compromised rigidity (Fig. 7.6). The displacement-time plot (Fig. 7.7 b), nonetheless, depicted an identical dynamic response to fall for DODO implanted NE femur and VA-DHS implanted Caucasian femur (Fig. 4.4). However, the corresponding value was slightly more in the DODO implanted patient specific Caucasian femur (Fig. 7.8 b). Absorption of energy may be a desirable characteristic in case of flexible components, but not so much in case of rigid structures or where rigidity is desirable (Chansa et al., 2019). Implanted bone should act as a rigid construct in order to avoid dislocation from joints. DODO implanted NE patient specific femur showed the least energy absorption among the PFLP, VA-DHS implanted Caucasian femur and DODO implanted patient specific Caucasian femur. In the present study, the rapid development of callus was observed between week 4 and week 6 postoperatively (Fig. 7.9). The dominant type of ossification shifted to endochondral ossification from intramembranous ossification which was also observed in Chapter 5. Implanting DODO in Caucasian femur resulted in lesser stress shielding intensity albeit with a compromised mechanical stability of the bone-implant construct. This further corroborates the hypothesis that DODO is tailor made for shorter femur and hence may be unsuitable for longer, Caucasian femur. On the other hand, PFLP and VA-DHS, as much as they continue to be in use on NE femurs, impart higher axial stability albeit with a slight compromise on greater amount of stress shielding. Owing to large lengths of PFLP and VA-DHS as compared to

DODO, continuous stress shielding in longer terms can lead to cortical thinning especially underneath the plate (Nag et al., 2021).

The diameter of the proximal locking screw in DODO was purposefully kept large as compared to that for VA-DHS. This was done to compensate for the reduced number of distal screws and increase the overall strength of the modified implant. Moreover, the addition of the anti-rotation screw increased the stability of the overall construct. Previous studies also found that the addition of an anti-rotation screw provides significantly greater biomechanical resistance (Freitas et al., 2014) and reduced lag screw migration rate (Kim et al., 2019). Also, a higher level of stress shielding imparted by DODO in the proximal femur may provide a major biomechanical advantage to reduce complications like varus collapse. However, long-term exposure to high stress shielding in proximal femur may increase varus collapse for osteoporotic geriatric patients.

The phenomenon of screw pull-out at the distal end of the plate leading to plate lift off from the femur shaft is a major cause of failure in the plating techniques (Sperner et al., 1989; Zdericet al., 2018). This occurs due to lack of screw pull-out strength in the distal end of the plate. To counter this, the distal screw in DODO was inserted at an inclined orientation of 50º with respect to the plate. Such inclination of the distal dynamic screw provides an advantage in the form of longer bone to screw interface, thereby enhancing the bone-implant anchorage and overall compressive strength of the construct. Screws inserted at an inclined angle were found to provide superior mechanical stability in spinal instrumentation (Rodriguez-Olaverri et al., 2005). Perren et al. (2005) observed the highest pull-out forces in constructs with 40º divergent angulated screws, whereas inclined screw did not improve the fixation strength when angulated up to 30º, regardless of whether in diverging or converging fashion. Stoffel et al. (2004) also asserted that oblique screws at the end of the plate increase fixation strength. Furthermore, it is worth noting that the DODO has been designed considering the salient features of Ti alloys. Post implantation CT and MRI images of Ti-alloy implants have fewer interferences as compared to “blurring” with stainless steel implants. Lightweight, high strength to weight ratio, lower modulus of elasticity, and excellent resistance to corrosion make it an ideal choice as implant material (Ratner et al., 2004).

It may be noted here that a few biomechanical studies have also supported the use of shorter DHS for intertrochanteric fracture fixations. Rog et al. (2017), in their study, demonstrated that a DHS with a two- or four-hole side plate is biomechanically comparable with regards to the axial and torsional stiffness of the construct. McLouglin et al. (2000) compared the strength and stiffness of a DHS with a two-hole and four-hole side plate and found that the two-hole side plate to be biomechanically comparable to the four-hole side plate, with paradoxically less fracture movement in the two-hole side plate. Various clinical studies have also supported the use of shorter plates for intertrochanteric hip fractures. Bolhofner et al. (1999), in a clinical study involving 69 patients with intertrochanteric fractures, found the use of 135º sliding hip screw with a two-hole side plate to be producing satisfactory healing with relatively less blood loss and shorter surgical time without the loss of side plate fixations.

The proof-of-concept DODO design, however, is not without some limitations. The axial stiffness of the construct, though at par with some other conventional implants, is marginally compromised if compared with the intact bone (Fig. 7.6 b). The present analysis considered only the femur length aspect of the NE population. FE analysis of DODO, implanted on the averaged patient-specific femur of the NE population, would have been more appropriate. Also, the intra-racial variation of the femur length within the NE population is not considered. Moreover, there is ample scope to evaluate different parametric variations (e.g., angling of distal screws for traditional implants, altering plate/screw dimensions etc.) in the design. That being said, the present in-silico work is primarily meant for prototyping and hence warrants in-vitro assessment and ethical clearance before contemplating implantation in real bone. Stress concentration at some locations in the implant could be seen (Fig. 7.5), which potentially can be the region of implant failure. However, in a few locations of the implant and femur, stress singularities are encountered. A stress singularity is a location in an FE model where stress values become unbounded (Prukvilailert et al., 2005). This typically happens near screw holes, sharp edges in screws, etc., and it requires specially curated, sufficiently fine tetra mesh to attain reasonable accuracy. Needless to mention, such meshing techniques may compromise the efficiency of the program significantly. Nevertheless, a supporting in-vitro and, if possible, in-vivo validation can render further insight into the region-specific design efficacies of the novel implant.

7.5 Summary of the findings

DODO appeared to be a viable alternative to the conventional plating techniques, especially for the NE population of India, and predicted better to comparable biomechanical characteristics, especially for Evans type-I intertrochanteric fracture. The use of a large diameter proximal locking screw along with the anti-rotation screw predicted enhanced stability of the implanted construct under a physiologically representative static compressive load. The inclined orientation of the distal screw may help reduce the chances of the plate lift-off phenomenon. Moreover, the stress shielding in the distal femur was reduced significantly, thus providing a more uniform stress distribution. The use of a shorter plate for short-femora patients further enables less invasive surgery as the amount of skin-cut is reduced, thereby facilitating shorter surgical time.

Chapter 8

Conclusions

The femur bone is the longest and largest bone that supports the entire body weight. The ageing population of the world and the increasing number of trauma cases, such as car accidents, falling from height, or sports injury, have resulted in rising incidences of hip fracture. It requires immediate medical attention in the form of orthopaedic surgery, generally involving the implantation of a device, e.g., bone plates, screws, pins, etc. Both extramedullary and intramedullary implants are used to treat patients suffering such fractures. Traditional fixation devices provide stable initial post-operative restoration of the fractured bones allowing early mobilization. However, the primary disadvantage associated with them is the need for a secondary surgical removal of the implant, which otherwise may lead to adverse bone remodelling. A preclinical assessment thus can be helpful in finding out a suitable implant. The popularity of FE analysis has increased over time due to its application in diverse engineering and healthcare fields. Moreover, owing to its low financial cost and high precision predictions, FE analysis has been regarded widely as a reliable preclinical tool to optimize treatment strategies by addressing various biomechanical failure scenarios. It further reduces the complexity in case of clinical situations without worrying about the real model and experimental setup. The present work attempts to preclinically explore the design rationale of extracapsular femoral fixation devices based on physiologically viable FE models. This will lead to the development of improved fracture plate that addresses not only geometric but also morphometric variation in patients.

In the present study, at the very onset, post-operative implant stability was predicted for two different types of bone plates, fixated to a subtrochanteric fractured femur. Further, the implants were fixed to a femur having an intertrochanteric fracture for stability assessment under both static and dynamic loading conditions. The results of FE predicted strain from the intact and implanted femurs (intertrochanteric fracture) were further validated with the DIC strain measurements to gain confidence with the

FE models. Thereafter, bone healing predictive models based on Fuzzy logic were established to find out the healing time associated with different fixation techniques. Also, FE predictive models were developed to determine the post-operative longer-term cortical thinning associated to other implants. Finally, a novel design of implant based on femur morphometrics of the Northeast Indian population is proposed. The present work of this thesis can serve as a rationale for developing a preclinical platform to choose the optimized implantation strategy for a patient.

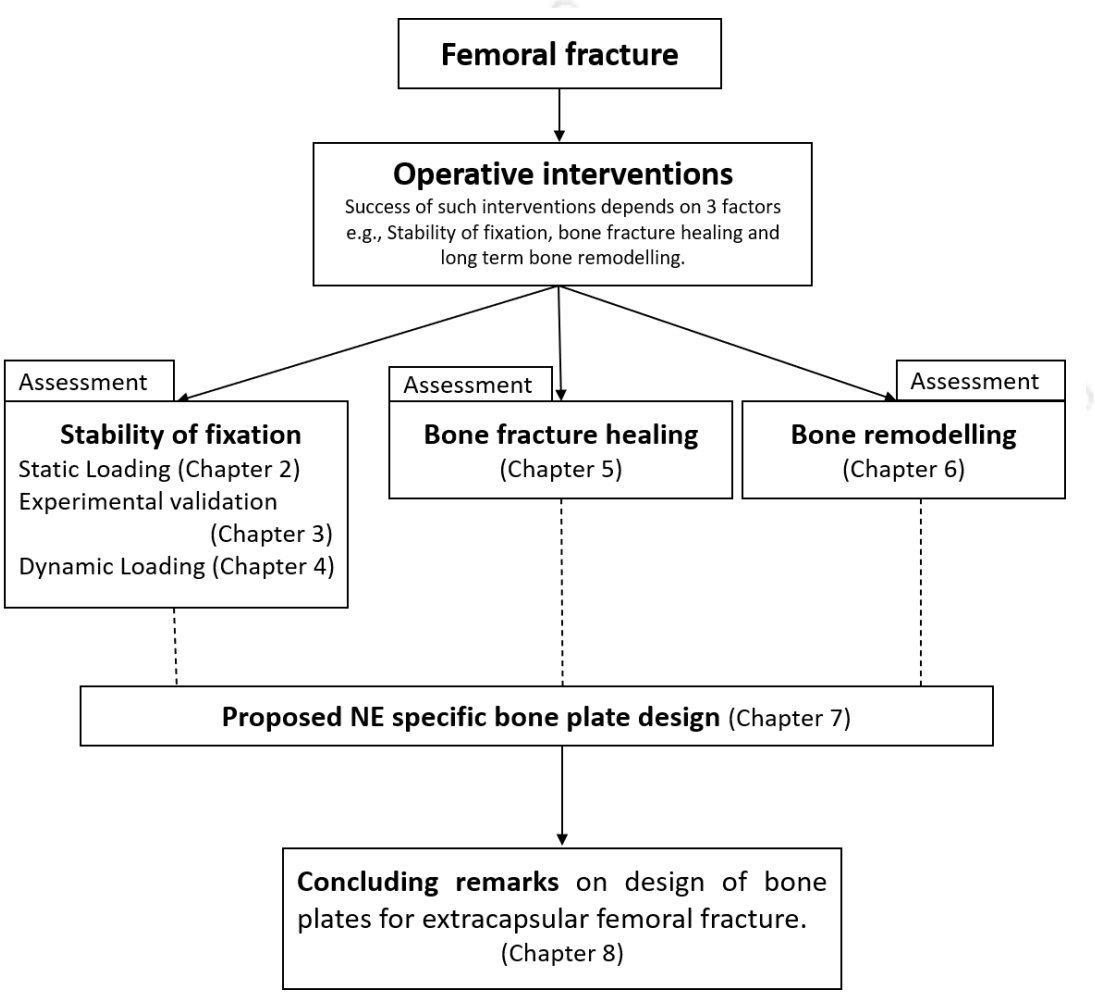

Fig. 8.1: Schematic illustration of the work done in the present thesis.

The specific conclusions and findings of the study are discussed below chapter wise.

- The load flow pattern in a laterally plated fractured bone is identified for subtrochanteric fracture. Linear regression analysis indicated close agreement between the measured average and FE predicted values with a high correlation coefficient (R^2 = 0.9989), low PE in the regression slope (0.3%) and statistically

significant results ($P < 0.0001$). The findings indicated that, any plating strategy may fail unless the screws are not placed judiciously and in sufficient numbers and at proper distance from the fracture gap. Chapter 2 also helped in understanding the stress shielding effects related to particular implant. The post-operative von Mises stress distribution was predicted to be non-uniform for both DHS and PFLP fixated cortical bone as opposed to an intact femur. However, stress shielding was marginally higher for DHS in the distal bone fragment (by ~6%) in the case of subtrochanteric fracture. The Hoffman analysis predicted the possible debonding nature of the bone-screw arrangement further suggesting risk of mechanical failure. Thus, for subtrochanteric fracture, DHS implanted femur showcased superior rigidity as compared to the PFLP implanted femurs.

- In order to develop and validate reasonably accurate 3-D FE models of intact and implanted composite femurs, a DIC-based experimental study was carried out. The FE models of the intact and implanted femurs were developed by mimicking the orientation, loading and boundary conditions of the tested specimens (prepared by orthopaedic registrar). The FE models of supporting osteotomies were also validated based on force-displacement characteristics obtained under in vitro loading. The regression analysis and student's t-test, considering 16 data points, revealed a significant correlation between measured and FE predicted curves. Further, under peak axial load of 3kN, the axial stiffness of the VA-DHS femur construct was found to be lesser than PFLP construct for intertrochanteric fracture. Experimental validation of such *in silico* models impart confidence before prediction models are employed in surgical decision-making or implant selection.

- The implanted femurs were analyzed for impact loading conditions replicating sideways fall scenarios. PFLP implanted femur was found to have higher resistance to bear the fall as compared to VA-DHS implanted femur owing predominantly for its greater length and greater number of screws. The PFLP implanted femur predicted the least propensity to adverse stress intensities, suggesting better structural rigidity and higher capacity in protecting the fractured femur against falls. Moreover, PFLP implanted femur was found to have almost similar frequency distribution to that of the intact femur, though the frequency of intact femur was slightly greater for all the modes except mode 2.

On the other hand, VA-DHS implanted femur was found to have the least frequency for all modes. For mode 2, which corresponds to the effect of bending in the X-Y plane (frontal plane), the frequency of the PFLP construct was found to be higher. The peak von Mises stress in the intact cortex was predicted to be ~130 MPa, whereas the corresponding values were ~103 MPa and ~172 MPa, respectively, for PFLP and VA-DHS construct. The displacement-time plot, nonetheless, depicted an identical dynamic response to fall for intact and PFLP implanted femur. Conversely, VA-DHS predicted larger displacement throughout the loading period. A similar trend could be observed in the force-displacement loop. PFLP and intact femur were associated with low energy loss, whereas in VA-DHS, the energy loss was the highest. The findings are of clinical importance as well since this essentially means LOS at hospitals for PFLP implanted patients will be less as compared to VA-DHS implanted patients. The former patients can initiate partial load-bearing exercise first.

- In order to understand the spatiotemporal secondary bone healing phenomena associated with a fracture, a 3D dynamic fracture healing scheme was modelled on a subtrochanteric femur fracture, regulated by both FE analysis and fuzzy logic control. Tissue transformation in a realistic and non-invasive manner for secondary healing is predicted for LP and DCP. The problem was solved iteratively in several healing steps running in a loop, and accordingly, the local tissue concentrations and material properties were updated. The predicted results accorded well with various previous experimental observations. The study found an initial delay in healing associated with DCP. However, as the healing progressed, there was no significant difference in the overall callus modulus. The presented preclinical scheme may further help predict bone healing for different implantation techniques and thus can serve as a non-invasive tool for evaluating the relative merits of extramedullary plating techniques. Rule-based models e.g., fuzzy interpretations are relatively easy to implement and requires less computational time as compared to the equation based mechanoregulatory models. Furthermore, such techniques provide additional advantage of incorporating any new rule based on the individuality of patient's pathogenic conditions.

- Cortical thinning is a fallout of the discrepancy of load sharing that gets altered on implantation. The post-operative cortical thinning prediction holds a

significant role in the overall success of the implant in the long term. The study developed an iterative model that updated the material property of the cortical bone based on SED values. Depending on the updated value of the elastic modulus of the cortical bone relative to a reference value, it is to be decided whether the phenomenon of bone atrophy or hypertrophy will commence. The remodelling simulation was run for 40 iterations, both for DHS and PFLP fixated models, until the mean nodal displacements of the corresponding nodes reached below 4% of 1 mm. The external remodelling was predicted to be more pronounced in the proximal sections than the distal sections of the bone in both cases. Although no adverse external remodelling was noted for either implant, DHS predicted admissible cortical thinning beneath the bone plate in a subtrochanteric fracture. Thus, the design of implants can be altered depending on such preclinical assessments to find the best implant for a patient.

- In Chapter 7, a novel design, Double Oblique Device for Osteosynthesis of the hip (DODO), is proposed while considering the regional morphometry of the NE population of India. The study employed FE analysis to compare the biomechanical outcome of the new device with that of PFLP and VA-DHS on a femur having an Evans type-I intertrochanteric fracture. The results showed stress shielding was substantially high for the PFLP and VA-DHS in the distal bone fragment (lateral aspect) and for DODO in the femoral head. The difference in axial displacement between the post-implanted DODO-fixed femur and its respective intact femur was predicted to be almost the same as that of the PFLP-fixed femur and its respective intact femur. The computational results found the new device to be a viable alternative to the conventional plating techniques, especially for the NE population of India and predicted better comparable biomechanical characteristics.

Recommendations for future research

There is a great deal of further research scope that may be derived from the present work. Consideration of homogeneous material properties in the cancellous bone model may lead to an overestimation of bone stiffness. Study involving heterogeneous material property can be explored in future. Varying patient specific parameters e.g., subject weight and bone conditions can be further examined for a particular fracture type. The effect of changing mesh density and exploring specialized element types,

based on the anatomy of the bone, on the biomechanical parameters can be explored. Moreover, there exists no clear relationship between the iterative time steps involved in external remodelling, and actual time in months or years. This is a known limitation of most *in silico* analyses involving bone remodelling.

The intermittent load relaxation during experimental method may arouse problem in measuring the exact strain at that moment. Although the load profile was kept similar in the numerical analysis for validation study to keep the effect to minimum still the input loading can be further improved. Though the experiments were performed quasi-statically, but when a material are subjected to high strain rates their response may be different than low strain rates due to phenomena such as strain hardening, dynamic effect etc. The present study was carried out using dry bones where the strain rate affect will be less as compared to real bone specimens. Nevertheless, the validation of the FEA can be conducted in a better way by using different strain rate to analyse strain rate dependence response. The bonded interfacial condition assumed for both the implanted construct was to simplify the overall analysis and to have a standard comparison between the implants. The contact modelling of the fracture region though not considered in the present study is recognised as a future scope of work. During measurement, the stiff, flat plate used to transfer the axial load to the femoral head leaves little room for the head to move freely. This may lead to some degree of spurious transverse loading to the femur thereby causing discrepancies in deformation outcome while replicating tests through numerical simulations. An experimental assessment of VA-DHS, nonetheless, would have led to more insights into study and can be explored. During sideways fall, considering the effects of healing of the fracture zone in the FE model can be further investigated.

The fracture healing model can also be improved upon. It may be noted that FE analysis is an approximate method which is sensitive to parameters like loading, material properties and boundary conditions. Also, there exists no precise relationship between the iterative time steps involved, and actual time in days or weeks with regards to secondary healing. Output results may thus vary considerably, thereby necessitating clinical validation of the FE scheme. Further, animal study is warranted with precise estimation of the loading regime such that a full-fledged validation of the present bone healing scheme can be contemplated. The future scope of study may also include the cyclic nature of loading. Moreover, bone resorption and cortical remodelling was not considered so as to accurately predict callus shape or size in the later phase of healing.

Further, by using FEA results as input for machine learning algorithms valuable outcomes beyond the range of FEA simulations can be predicted and useful insights into bone mechanics can be deduced. Moreover, Machine Learning (ML) can be used in combination with FEA. ML is a data driven approach which requires pre-processing the data, training a machine learning model, validating the model and then using the model for predictions. Data generated from the FEA results will go as input for ML algorithms. Thus, valuable outcomes beyond the range of FEA simulations can be predicted and useful insights into bone mechanics can be deduced.

A clinical evaluation of DODO, implanted on the averaged patient-specific femur of the NE population, can be treated as a scope for future study. Also, the intra-racial variation of the femur length within the NE population can be addressed. There is ample scope to evaluate different parametric variations (e.g., angling of distal screws for traditional implants, altering plate/screw dimensions etc.) in the design. That being said, the present *in-silico* work is primarily meant for prototyping, and hence it warrants *in-vitro* assessment and ethical clearance before contemplating implantation in real bone.

References

Abdulkareem IH. A review of tip apex distance in dynamic hip screw fixation of osteoporotic hip fractures. *Niger Med J*. 2012;53(4):184-191. doi:10.4103/0300-1652.107550

Abe, S., N. Narra, R. Nikander, J. Hyttinen, R. Kouhia, H. Sievänen. Impact loading history modulates hip fracture load and location: A finite element simulation study of the proximal femur in female athletes. Journal of biomechanics, 76, 136–143, 2018.

Agarwala V, Paul A, Daolagupu AK. Anthropometric analysis of the hip joint in Southern Assam population using computed tomography. Int J Orthop Sci 2020;6(1):1133-1139. DOI: 10.22271/ortho.2020.v6.i1o.1971

Ahn, J., J. Bernstein. Fractures in brief: intertrochanteric hip fractures. Clinical orthopaedics and related research, 468(5), 1450–1452, 2010.

Ajovalasit A, Fragapane S, Zuccarello B (2010) Local reinforcement effect of embedded strain gauges. EPJ Web of Conferences.

Aldieri, A., Terzini, M., Osella, G., Priola, A. M., Angeli, A., Veltri, A., Audenino, A., & Bignardi, C. (2018). Osteoporotic hip fracture prediction: is T-score based criterion enough? A Hip Structural Analysis based model. Journal of biomechanical engineering, 10.1115/1.4040586. Advance online publication. https://doi.org/10.1115/1.4040586.

Allied Market Research: Report: A00536, Orthopaedic device market (2019-2026) (https://www.alliedmarketresearch.com/orthopedic-implants-market)

Ament C, Hofer EP. A fuzzy logic model of fracture healing. *J Biomech*. 2000;33(8):961-968.

Aminian A, Gao F, Fedoriw WW, Zhang LQ, Kalainov DM, Merk BR. Vertically oriented femoral neck fractures: mechanical analysis of four fixation techniques. J Orthop Trauma. 2007 Sep;21(8):544-8. doi: 10.1097/BOT.0b013e31814b822e.

Aneja A, Yang E, Briscoe M, Graves ML, Porter SE, Bergin P and Russell GV. Intramedullary Nailing of Femur Fractures in the Obese: A Retrospective Comparison of Patients with Normal Weight versus the Obese. Austin J Trauma Treat. 2014;1(1): 5.

Avval PT, Samiezadeh S, Bougherara H (2016) Long-term response of femoral density to hip implant and bone fracture plate: Computational study using a mechano-biochemical model. Med Eng Phys 38:171–180. https://doi.org/10.1016/j.medengphy.2015.11.013

Bailón-Plaza A, van der Meulen MC. A mathematical framework to study the effects of growth factor influences on fracture healing. *J Theor Biol*. 2001;212(2):191-209.

Bailón-Plaza A, van der Meulen MC. Beneficial effects of moderate, early loading and adverse effects of delayed or excessive loading on bone healing. *J Biomech*. 2003;36(8):1069-1077. doi:10.1016/s0021-9290(03)00117-9.

Barreto S, Clausen CH, Perrault CM, Fletcher DA, Lacroix D.(2013). A multi-structural single cell model of force-induced interactions of cytoskeletal components. Biomaterials, 34(26):6119–6126, ISSN 0142-9612. doi:10.1016/j.biomaterials. 2013.04.022.

Beatty MF, Chewning SW (1979) Numerical analysis of the reinforcement effect of a strain gage applied to a soft material. Int J Eng Sci 17(7):907–915.

Beaupré GS, Carter DR, Orr TE, Csongradi J. Stresses in plated long-bones: the role of screw tightness and interface slipping [published correction appears in J Orthop Res 1988;6(3):466]. *J Orthop Res*. 1988;6(1):39-50.

Bel J. C. Pitfalls and limits of locking plates. Orthopaedics & traumatology, surgery & research: OTSR. 105(1S), S103–S109, 2019

Bergmann G, Deuretzbacher G, Heller M, Graichen F, Rohlmann A, Strauss J, Duda G. (2001). Hip contact forces and gait patterns from routine activities. J Biomech 34(7):859−871.

Berkes MB, Little MT, Lazaro LE, et al. Catastrophic failure after open reduction internal fixation of femoral neck fractures with a novel locking plate implant. J Orthop Trauma 2012; 26:170–176.

Bernakiewicz M, Viceconti M, 2002. The role of parameter identification in finite element contact analysis w.r.t orthopaedic biomechanics applications. Journal of Biomechanics 35: 61-67.

Bettamer A, Allaoui S, Hambli R (2017) Using 3D digital image correlation to visualise the progress of failure of human proximal femur, Computer Methods in Biomechanics and Biomedical Engineering: Imaging & Visualization, 5:4, 233-240, doi: 10.1080/21681163.2015.1067152

Biomechanical products catalog Sawbones: Test materials and composite bones. (https://www.sawbones.com/media/assets/product/documents/biomechanical_catalog 2020.pdf) Accessed 7 Dec 2020

Bishnoi M, Kirmani TT, Huda N, Chahal G, Bishnoi S. (2018). Epidemiological analysis of hip fractures at a tertiary care center: a retrospective study. International Journal of Research in Orthopaedics; 4(4):568-571.

Blair HC. How the osteoclast degrade bone. Bioessays, 20(10): 837-846.1998, February 2001. ISSN 1523-4681.

Blanchard R, Dejaco A, Bongaers E, Hellmich C (2013) Intravoxel bone micromechanics for microCT-based finite element simulations. Journal of Biomechanics. 46(15):2710-2721. DOI: 10.1016/j.jbiomech.2013.06.036.

Blenman PR, Carter DR, Beaupré GS. Role of mechanical loading in the progressive ossification of a fracture callus. *J Orthop Res*. 1989;7(3):398-407.

Blomfeldt R, Törnkvist H, Ponzer S, Söderqvist A, Tidermark J.(2005). Comparison of internal fixation with total hip replacement for displaced femoral neck fractures. Randomized, controlled trial performed at four years. J Bone Joint Surg Am ; 87: 1680-1688.

Bolhofner BR, Russo PR, and Carmen B. Results of intertrochanteric femur fractures treated with a 135-degree sliding screw with a two-hole side-plate. J Orthop Trauma 1999;13: 5–8.

Bombaci H, Gorgec M. Difficulty in removal of a femoral intramedullary nail: the geometry of the distal end of the nail. Yonsei Med J. 2003 Dec 30;44(6):1083-6. doi: 10.3349/ymj.2003.44.6.1083.

Borgström F, Karlsson L, Ortsäter G, Norton N, Halbout P, Cooper C, et al. Fragility fractures in Europe: burden, management and opportunities. Arch Osteoporos. 2020;15:59. https://doi.org/10.1007/s11657-020-0706-y.

Braithwaite, R.S., N.F. Col, J.B. Wong. Estimating Hip Fracture Morbidity, Mortality and Costs. Journal of the American Geriatrics Society, 51, 364-370, 2003.

Burge R, Dawson-Hughes B, Solomon DH, Wong JB, King A, Tosteson A . Incidence and economic burden of osteoporosis-related fractures in the United States, 2005-2025. J Bone Miner Res. 2007; 22: 465–475.

Burstein A.H., V.H. Frankel. A standard test for laboratory animal bone. J Biomech. 4,155–158, 1971.

Carpintero P, Caeiro JR, Carpintero R, Morales A, Silva S, Mesa M.(2014). Complications of hip fractures: A review. World J Orthop.; 5(4): 402-411.ISSN 2218-5836.

Carter D, Orr TE, Fyhrie D (1989) Relationships between loading history and femoral cancellous bone architecture. J Biomech 22(3):231–244

Carter DR (1984) Mechanical loading histories and cortical bone remodelling. Calcif Tissue Int 36(Suppl):S19–S24

Carter DR, Blenman PR, Beaupré GS. Correlations between mechanical stress history and tissue differentiation in initial fracture healing. *J Orthop Res*. 1988;6(5):736-748.

Carter DR, Hayes WC (1977) The compressive behaviour of bone as a two-phase porous structure. J Bone Jt Surg Am 59-A:954–962

Carter DR, Van Der Meulen MCH, Beaupré GS (1996) Mechanical factors in bone growth and development. In: Bone. Elsevier Inc., pp S5–S10

Chaim, S. H., D.P. Mukherjee, A.L. Ogden, R.H. Mayeux, K.K. Sadasivan, J.A. Albright. A biomechanical study of femoral neck fracture fixation with the VHS Vari-Angle Hip Fixation System. American journal of orthopedics (Belle Mead, N.J.) vol. 31(1 Suppl), 22–24. 2002.

Chalise PK, Mishra AK, Shah SB, et al. Outcome of pertrochantric fracture of the femur treated with proximal femoral locking compression plate. Nepal Med Coll J. 2012; 14:324–327.

Chalise, P. K., A.K. Mishra, S.B. Shah, V. Adhikari, R.P. Singh. Outcome of pertrochantric fracture of the femur treated with proximal femoral locking compression plate. Nepal Medical College journal: NMCJ. 14(4), 324–327, 2012.

Chanda, S., Dickinson, A.S., Gupta, S., Browne, M., Full-field in vitro Measurements and in silico Predictions of Strain Shielding in the Implanted Femur after Total Hip Arthroplasty, 2015, Journal of Engineering in Medicine, Proc. IMechE, Part-H, 229(8):549–559.

Chansa M. A Cross - Section Study to Determine Human Height Using Femur Length in Zambian Population. Acta Scientific Microbiology 2.11 (2019):57-61.

Cheal EJ, Mansmann KA, DiGioia AM 3rd, Hayes WC, Perren SM. Role of interfragmentary strain in fracture healing: ovine model of a healing osteotomy. *J Orthop Res*. 1991;9(1):131-142.

Chen X. Parametric design of patient-specific fixation plates for distal femur fractures. Proc Inst Mech Eng H. 2018 Sep;232(9):901-911. doi: 10.1177/0954411918793668. Epub 2018 Aug 13. PMID: 30101650.

Chennimalai Kumar N, Dantzig J, Jasiuk I. 2012. Modeling of cortical bone adaptation in a rat ulna: effect of frequency. Bone 50, 792–797. (doi:10.1016/j.bone.2011.12.008).

Chennimalai Kumar N, Dantzig JA, Jasiuk IM (2012) Modeling of cortical bone adaptation in a rat ulna: Effect of frequency. Bone 50:792–797. https://doi.org/10.1016/j.bone.2011.12.008

Chennimalai Kumar N, Dantzig JA, Jasiuk IM, et al (2010) Numerical modeling of long bone adaptation due to mechanical loading: Correlation with experiments. In: Annals of Biomedical Engineering. Ann Biomed Eng, pp 594–604

Childs SG. 2003. Stimulators of bone healing: Biologic and biomechanica. Orthopaedic Nursing 22: 421-8.

Claes L, Augat P, Suger G, Wilke HJ. Influence of size and stability of the osteotomy gap on the success of fracture healing. *J Orthop Res*. 1997;15(4):577-584.

Claes L, Eckert-Hübner K, Augat P. The effect of mechanical stability on local vascularization and tissue differentiation in callus healing. *J Orthop Res*. 2002;20(5):1099-1105.

Claes L, Recknagel S, Ignatius A. 2012. Fracture healing under healthy and inflammatory conditions. Nature Reviews Rheumatology 8: 133-43.

Claes LE, Heigele CA, Neidlinger-Wilke C, Kaspar D, Seidl W, Margevicius KJ et al. Effects of mechanical factors on the fracture healing process. Clinical Orthopaedics and Related Research. 1998 Oct(355 Suppl):S132-47.

Claes LE, Heigele CA. Magnitudes of local stress and strain along bony surfaces predict the course and type of fracture healing. *J Biomech*. 1999;32(3):255-266.

Cofaru C, Philips W, van Paepegem W. Pixel-level robust digital image correlation. Optics Exp. 2013; 21:29979–29999.

Cooper C, Campion G, Melton LJ 3rd. Hip fractures in the elderly: a world-wide projection. Osteoporos Int. 1992;2:285–9.

Courtney, A. C., E.F. Wachtel, E. R. Myers, W.C. Hayes. Effects of loading rate on strength of the proximal femur. Calcified tissue international, 55(1), 53–58, 1994.

Cowin SC, Hegedus DH (1976) Bone remodeling I: theory of adaptive elasticity. J Elast 6:313–326. https://doi.org/10.1007/BF00041724

Crist BD, Khalafi A, Hazelwood SJ, et al. A biomechanical comparison of locked plate fixation with percutaneous insertion capability versus the angled blade plate in a subtrochanteric fracture gap model. J Orthop Trauma 2009; 23:622–627.

Crist BD, Khalafi A, Hazelwood SJ, Lee MA. A biomechanical comparison of locked plate fixation with percutaneous insertion capability versus the angled blade plate in a subtrochanteric fracture gap model. J Orthop Trauma. 2009 Oct;23(9):622-7. doi: 10.1097/BOT.0b013e3181a2a31d.

Crist, B. D., A. Khalafi, S.J. Hazelwood, M.A. Lee. A biomechanical comparison of locked plate fixation with percutaneous insertion capability versus the angled blade plate in a subtrochanteric fracture gap model. Journal of orthopaedic trauma. 23(9), 622–627, 2009.

Crob M.2006. Finite element analysis of bone remodelling. Implantation of a Remodelling algorithm in MATLAB and ANSYS.

Dalstra M, Huiskes R, van Erning L (1995) Development and validation of a three-dimensional finite element model of the pelvic bone. Trans ASME J Biomech Eng 117:272–278

Davis TR, Sher JL, Horsman A, Simpson M, Porter BB, Checketts RG Intertrochanteric femoral fractures. Mechanical failure after internal fixation. J Bone Joint Surg Br 1990;72:26–31.

Devika D, Gupta NS (2012) Finite element analysis and validation of the critical parameters influencing the mechanical behaviour of tibia bone with patient-specific implant for proximal end fracture. Trends in Biomaterials & Artificial Organs 26(1):10–15

Diaz FV, Kaufmann GH, Galizzi GE. 2000. Determination of residual stresses using hole drilling and digital speckle pattern interferometry with automated data analysis. Opt Lasers Eng. 33:39–48.

Dickinson A., Taylor A., Brown M., The influence of acetabular cup material on pelvis cortex surface strains, measured using digital image correlation, Journal of Biomechanics, 2012, 45(4), 719–723.

Dickinson A., Taylor A., Ozturk H., Browne M., Experimental validation of a finite element analysis model of the proximal femur using digital image correlation and a composite bone model, Journal of Biomechanical Engineering, 2011, 133, 14504.

Dickinson AS, Taylor AC, Ozturk H, Browne M (2011) Experimental validation of a finite element model of the proximal femur using digital image correlation and a composite bone model. Trans ASME J Biomech Eng 133(1):1–6.

Doblaré M, García JM (2002) Anisotropic bone remodelling model based on a continuum damage-repair theory. J Biomech 35:1–17. https://doi.org/10.1016/S0021-9290(01)00178-6

Doblare M, Garcia JM, Gomez MJ. Modelling bone tissue fracture and healing: a review. Eng Fract Mech. 2004;71(1): 1809–1840

Eberle S, Augat P (2007) Preventing contact convergence problems in bone- implant contact models, Materials Science

Einhorn TA. The cell and molecular biology of fracture healing. *Clin Orthop Relat Res*. 1998;(355 Suppl):S7-S21.

Ericksen MF. Ageing changes in the medullary cavity of the proximal femur in American black and whites. Am J Phys Anthropol. 1979;51:563–9

Everts V, Delaissé JM, Korper W, Jansen DC, Tigchelaar-Gutter W, Saftig P, Beertsen W. The bone lining cell: its role in cleaning Howship's lacunae and initiating bone formation. J Bone Miner Res. 2002 Jan;17(1):77-90. doi: 10.1359/jbmr.2002.17.1.77. PMID: 11771672.

Ferguson SJ, Wyss UP, Pichora DR. Finite element stress analysis of a hybrid fracture fixation plate. Med Eng Phys. 1996; 18:241–250.

Ferolke JP, Patka P, (2007). Definition and classification of fractures non-unions. Injury 38 [Suppl 2]: s19-s22.

Floyd JC, O'Toole RV, Stall A, et al. Biomechanical comparison of proximal locking plates and blade plates for the treatment of comminuted subtrochanteric femoral fractures. J Orthop Trauma 2009; 23:628–633.

Floyd JC, O'Toole RV, Stall A, Forward DP, Nabili M, Shillingburg D, Hsieh A, Nascone JW. Biomechanical comparison of proximal locking plates and blade plates for the treatment of comminuted subtrochanteric femoral fractures. J Orthop Trauma. 2009 Oct;23(9):628-33. doi: 10.1097/BOT.0b013e3181b04835. PMID: 19897983.

Floyd MW, France JC, Hubbard DF. Early experience with the proximal femoral locking plate. Orthopedics 2013; 36:1488–1494.

Fogagnolo F, Kfuri M Jr, Paccola C (2004) Intramedullary fixation of pertrochanteric hip fractures with the short AO-ASIF proximal femoral nail. Arch Orthop Trauma Surg 124:31–37

Fortune business insight: Report ID: FBI102586, Orthopaedic device market (2020-2027) (https://www.fortunebusinessinsights.com/orthopedic-devices-market)

Forward DP, Doro CJ, O'Toole RV, et al. A biomechanical comparison of a locking plate, a nail, and a 95 degrees angled blade plate for fixation of subtrochanteric femoral fractures. J Orthop Trauma 2012; 26:334–340.

Freitas A, Torres GM, Souza AC, Maciel RA, Souto DR, Ferreira GN. Analysis on the mechanical resistance of fixation of femoral neck fractures in synthetic bone, using the dynamic hip system and an anti-rotation screw. *Rev Bras Ortop*. 2014;49(6):586-592. Published 2014 Oct 27. doi:10.1016/j.rboe.2014.01.016

Frost, H.M. (1990) Skeletal Structural Adaptations to Mechanical Usage (Satmu), Redefining Wolff Law—The Re- modeling Problem. Anatomical Record, 226, 414-422. http://dx.doi.org/10.1002/ar.1092260403

García JM, Doblaré M, Cegoñino J (2002) Bone remodelling simulation: a tool for implant design. Comput Mater Sci 25:100–114

García-Aznar JM, Kuiper JH, Gómez-Benito MJ, Doblaré M, Richardson JB. Computational simulation of fracture healing: influence of interfragmentary movement on the callus growth. *J Biomech*. 2007;40(7):1467-1476.

Gardner MJ, Helfet DL, Lorich DG. Has locked plating completely replaced conventional plating? *Am J Orthop (Belle Mead NJ)*. 2004;33(9):439-446.

Gardner MJ, Helfet DL, Lorich DG. Has locked plating completely replaced conventional plating? *Am J Orthop (Belle Mead NJ)*. 2004;33(9):439-446.

Gardner TN, Mishra S. The biomechanical environment of a bone fracture and its influence upon the morphology of healing. *Med Eng Phys*. 2003;25(6):455-464.

Gautier E, Sommer C. Guidelines for the clinical application of the LCP. Injury 2003; 34(Suppl. 2): B63–76.

Gefen A. Optimizing the biomechanical compatibility of orthopedic screws for bone fracture fixation [published correction appears in Med Eng Phys. 2003 Jun;25(5):43]. Med Eng Phys. 2002;24(5):337-347.

George C. Babis, Panayotis N. Soucacos, Bone scaffolds: The role of mechanical stability and instrumentation, Injury, Volume 36, Issue 4, Supplement,2005, Pages S38-S44, ISSN 0020-1383, https://doi.org/10.1016/j.injury.2005.10.009.

Geraldes DM, Phillips AT. (2014). A comparative study of orthotropic and isotropic bone adaptation in the femur. Int J Numer Method Biomed Eng 30(9):873–889.

Geris L, Gerisch A, Sloten JV, Weiner R, Oosterwyck HV. Angiogenesis in bone fracture healing: a bioregulatory model. *J Theor Biol*. 2008;251(1):137-158.

Ghimire S, Miramini S, Edwards G, et al. The investigation of bone fracture healing under intramembranous and endochondral ossification. *Bone Rep*. doi:10.1016/j.bonr.2020.100740

Ghosh R., Gupta S., Dickinson A., Browne M., Experimental validation of finite element models of intact and implanted composite hemipelvises using digital image correlation, J. Biomech. Eng., 2012, 134(8), 081003.

Gibson L (1985) The mechanical behaviour of cancellous bone. J Biomech 18(5):317–328

Gilchrist S, Guy P, Cripton PA (2013) Development of an inertia-driven model of sideways fall for detailed study of femur fracture mechanics. Trans ASME J Biomech Eng 135(12):121001.

Gilchrist S., K.K. Nishiyama, P. de Bakker, P. Guy, S.K. Boyd, T. Oxland, P.A. Cripton. Proximal femur elastic behaviour is the same in impact and constant displacement rate fall simulation. Journal of biomechanics vol. 47(15), 3744-3749, 2014.

Glassner PJ, Tejwani NC (2011) Failure of proximal femoral locking compression plate: a case series. J Orthop Trauma 25:76– 83. https://doi.org/10.1097/BOT.0b013e3181e31ccc

Gokhale N.S., Deshpande S.S., Bedekar S.V., Thite A.N., Book- *practical finite element analysis*, 1(445), 2008.

GOM Correlate. GOM—Precise Industrial 3D Metrology. Braunschweig, Germany. Available online: https://www.gom.com (accessed on 7 September 2019).

Goodship AE, Watkins PE, Rigby HS, Kenwright J. 1993. The role of fixator frame stiffness in the control of fracture healing. An experimental study. Journal of Biomechanics 26: 1027-35.

Government of India (2015) The Registrar General & Census Commissioner, India, New Delhi, Ministry of Home Affairs, Government of India 2015

Grassi L, Väänänen SP, Amin Yavari S, et al. Experimental validation of finite element model for proximal composite femur using optical measurements. J Mech Behav Biomed Mater. 2013; 21:86–94.

Grassi L, Väänänen SP, Yavari SA, Jurvelin JS, Weinans H, Ristinmaa M, Zadpoor AA, Isaksson H (2014) Full-field strain measurement during mechanical testing of the human femur at physiologically relevant strain rates. Trans ASME J Biomech Eng 136(11) doi:10.1115/1.4028415.

Grassi, L., S.P. Väänänen, M. Ristinmaa, J.S. Jurvelin, H. Isaksson. How accurately can subject-specific finite element models predict strains and strength of human femora? Investigation using full-field measurements. Journal of Biomechanics. 49(5), 802-806, 2016

Grisso, J.A., J.L. Kelsey, B.L. Strom, G.Y. Chiu, G. Maislin, L.A. O'Brien, S. Hoffman, F. Kaplan. Risk factors for falls as a cause of hip fracture in women. The Northeast Hip Fracture Study Group. The New England journal of medicine vol. 324(19), 1326-31, 1991.

Gullberg B, Johnell O, Kanis JA. World-wide projections for hip fracture. Osteoporos Int. 1997;7(5):407–13.

Guo XE, Kim CH. Mechanical consequence of trabecular bone loss and its treatment: a three-dimensional model simulation. *Bone*. 30: 404-11. doi: 10.1016/S8756-3282(01)00673-1

Gupta, S., van der Helm, F.C.T., Sterk, J.C., van Keulen, F. and Kaptein, B.L., 2004, "Development and Experimental Validation of a Three-Dimensional Finite Element Model of the Human Scapula,", Proc. IMechE Pt. H.: J. Eng. Med., 218, pp. 127-142

Haapasalo H, Kontulainen S, Sievänen H, Kannus P, Järvinen M, Vuori I. Exercise-induced bone gain is due to enlargement in bone size without a change in volumetric bone density: a peripheral quantitative computed tomography study of the upper arms of male tennis players. Bone. 2000 Sep;27(3):351-7. doi: 10.1016/s8756-3282(00)00331-8.

Haentjens P, Casteleyn PP, Opedecam P. Hip arthroplasty for failed internal fixation of intertrochanteric and subtrochanteric fractures in the elderly patient. Arch Orthop Trauma Surg 1994;113(4):222–227.

Haentjens, P., P. Autier, M. Barette, K. Venken, D. Vanderschueren, S. Boonen, Hip fracture study group. Survival and functional outcome according to hip fracture type: a one-year prospective cohort study in elderly women with an intertrochanteric or femoral neck fracture. Bone vol. 41(6), 958-64, 2007.

Hart RT, Davy DT, Heiple KG (1984) Mathematical modelling and numerical solutions for functionally dependent bone. Calc Tissue Int 36(Suppl):S11–S18

Harwood PJ, Newman JB, Michael ALR. 2010. (ii) An update on fracture healing and non-union. Orthopaedics and Trauma 24: 9-23.

Hasenboehler, Erik A., J.F. Agudelo, S.J. Morgan, W.R. Smith, D.J. Hak, P.F. Stahel. Treatment of complex proximal femoral fractures with the proximal femur locking compression plate. Orthopedics vol. 30(8), 618-623, 2007.

Hefzy MS, Singh SP, 1997. Comparison between two techniques for modellong interface condition in a porous coated hip endoprosthesis. Medical Engineering & Physics 19, 50-62.

Helgason B, Gilchrist S, Ariza O, Chak JD, Zheng G, Widmer RP, Ferguson SJ, Guy P, Cripton PA (2014) Development of a balanced experimental-computational approach to understanding the mechanics of proximal femur fractures. Med Eng Phys 36(6):793–799.

Helgason B, Gilchrist S, Ariza O, Chak JD, Zheng G, Widmer RP, Ferguson SJ, Guy P, Cripton PA (2014) Development of a balanced experimental-computational approach to understanding the mechanics of proximal femur fractures. Med Eng Phys 36(6):793–799

Heller M, Bergmann G, Deuretzbacher G, Durselen L, Pohl M, Claes L, Duda GN. (2001). Musculo-skeletal loading conditions at the hip during walking and stair climbing. J Biomech 34(7):883−893

Hensley, S., M. Christensen, S. Small, D. Archer, E. Lakes, R. Rogge. Digital image correlation techniques for strain measurement in a variety of biomechanical test models. Acta of bioengineering and biomechanics. 19(3), 187–195, 2017.

Hodel S, Beeres FJP, Babst R, Link BC. Complications following proximal femoral locking compression plating in unstable proximal femur fractures: medium-term follow-up. Eur J Orthop Surg Traumatol. 2017 Dec;27(8):1117-1124. doi: 10.1007/s00590-017-1981-1.

Hoffman O (1967) The brittle strength of orthotropic materials. J Compos Mater 1:200–206. https://doi.org/10.1177/ 002199836700100210

Huang, H.M., L.C. Pan, S.Y. Lee, C.L. Chiu, K.H. Fan, K.N. Ho. Assessing the implant/bone interface by using natural frequency analysis. Oral surgery, oral medicine, oral pathology, oral radiology, and endodontics vol. 90(3), 285-91, 2000.

Huiskes R, Boeklagen R (1989) Mathematical shape optimization of hip prosthesis design. J Biomech 22(8−9):793−804

Huiskes R, Weinans H, Grootenboer HJ, Dalstra M, Fudala B, Slooff TJ (1987) Adaptive bone-remodelling theory applied to prosthetic-design analysis. J Biomech 20(11−12):1135−1150

Huiskes R, Weinans H, Grootenboer HJ, et al (1987) Adaptive bone-remodeling theory applied to prosthetic-design analysis. J Biomech 20:1135–1150. https://doi.org/10.1016/0021-9290(87)90030-3

Isaksson H, van Donkelaar CC, Huiskes R, Ito K. A mechano-regulatory bone-healing model incorporating cell-phenotype specific activity [published correction appears in J Theor Biol. 2008 Oct 7;254(3):717]. *J Theor Biol*. 2008;252(2):230-246.

Islam, A.B.M.S., Jameel M., Jumaat, M.Z., Seismic isolation in buildings to be a practical reality: Behavior of structure and installation technique. Journal of Engineering and Technology Research Vol. 3(4), pp. 99-117, 2011.

ISO - ISO 7206-4:2010 - Implants for surgery — partial and total hip joint prostheses — part 4: determination of endurance properties and performance of stemmed femoral components. https://www. iso.org/standard/42769.html. Accessed 14 Apr 2020

Issekutz B, JJ B, Birkhead N, Rodahl K (1966) Effect of prolonged bed rest on urinary calcium output. J Appl Physiol 21:1013–1020

Jazinizadeh, F., H. Mohammadi, C.E. Quenneville. Comparing the fracture limits of the proximal femur under impact and quasi-static conditions in simulation of a sideways fall. Journal of the mechanical behavior of biomedical materials. 103, 103593,2020

Jee WSS (2008) Integrated bone tissue physiology: anatomy and physiology. In: Bone Mechanics Handbook Ed: Cowin SC New York Informa Healthcare 2nd edition 11–168

Jetté, B., V. Brailovski, C. Simoneau, M. Dumas, P. Terriault. Development and in vitro validation of a simplified numerical model for the design of a biomimetic femoral stem. Journal of the Mechanical Behavior of Biomedical Materials. 77, 539-550, 2018.

Johnell O, Kanis JA . An estimate of the worldwide prevalence and disability associated with osteoporotic fractures. Osteoporos Int. 2006; 17:1726–1733.

Johnson B, Stevenson J, Chamma R, et al. Short-term follow-up of pertrochanteric fractures treated using the proximal femoral locking plate. J Orthop Trauma 2014; 28:283–287.

Johnson, B., J. Stevenson, R. Chamma, A. Patel, S-J. Rhee, C. Lever, I. Starks, P.J. Roberts. Short-term follow-up of pertrochanteric fractures treated using the proximal femoral locking plate. Journal of orthopaedic trauma vol. 28(5), 283-287, 2014.

Jonnes C, Shishir SM, Najimudeen S (2016) Type II intertrochanteric fractures: proximal femoral nailing (PFN) versus dynamic hip screw (DHS). Arch Bone Jt Surg 4:23–28. https://doi. org/10.22038/abjs.2016.5268

Kahn-Jetter ZL, Chu TC. Three-dimensional displacement measurements using digital image correlation and photogrammic analysis. Exp Mech. 1990; 30:10–16.

Kahn-Jetter, Z. and Chu, T., 1990, "Three-Dimensional Displacement Measurements using Digital Image Correlation and Photogrammetric Analysis," Experimental Mech., 30(1), pp. 10-16

Kanis A, Johansson H, Oden A, et al. A family history of fracture and fracture risk: a meta-analysis. Bone. 2004;35(5):1029–1037. doi: 10.1016/j.bone.2004.06.017.

Kaspar D, Seidl W, Neidlinger-Wilke C, Ignatius A, Claes L. Dynamic cell stretching increases human osteoblast proliferation and CICP synthesis but decreases osteocalcin synthesis and alkaline phosphatase activity. *J Biomech*. 2000;33(1):45-51.

Katz Y, Yosibash Z. New insights on the proximal femur biomechanics using Digital Image Correlation. J Biomech. 2020 Mar 5;101:109599. doi: 10.1016/j.jbiomech.2020.109599. Epub 2020 Jan 8.

Keyak, J. H., S.A. Rossi, K.A. Jones, C.M. Les, H.B. Skinner. Prediction of fracture location in the proximal femur using finite element models. Medical engineering & physics. 23(9), 657–664, 2001.

Khalil, T.B., D.C. Viano, L.A. Taber. Vibrational characteristics of the embalmed human femur. Journal of Sound and Vibration. 75(3), 417-436, 1981.

Khang G, Choi K, Kim CS, Yang JS, Bae TS. A study of Korean femoral geometry. Clinical Orthopaedics and Related Research (1976-2007). 2003;406(1):116-22.

Kim SH, Chang SH, Jung HJ. The finite element analysis of a fractured tibia applied by composite bone plates considering contact conditions and time-varying properties of curing tissues. Compos Struct. 2010;92(9):2109– 2118

Kim T, Ayturk UM, Haskell A, Miclau T, Puttlitz CM. Fixation of osteoporotic distal fibula fractures: A biomechanical comparison of locking versus conventional plates. *J Foot Ankle Surg*. 2007;46(1):2-6.

Kim, C., Chang, J.S. & Kim, J.W. Clinical outcomes of dynamic hip screw fixation of intertrochanteric fractures: comparison with additional anti-rotation screw use. *Eur J Orthop Surg Traumatol* 2019; 29,1017–1023. https://doi.org/10.1007/s00590-019-02397-4

Koval KJ, Zuckerman JD, Joseph D (2006) Handbook of fractures. Lippincott Williams & Wilkins

Kraus M, Krischak G, Weidmann K. (2011). Clinical evaluation of PFNA(R) and relationship between the tip-apex distance and mechanical failure. J Der Unfallchirurg;114(6): 470-478.

Kuiper JH, Ashton BA, Richardson JB. Computer simulation of fracture callus formation and stiffness restoration. In: Proceedings of the 12th Conference of the European Society of Biomechanics; Dublin. p. 61.

Lacroix D, Prendergast PJ. A mechano-regulation model for tissue differentiation during fracture healing: analysis of gap size and loading. *J Biomech*. 2002;35(9):1163-1171.

Lacroix D, Prendergast PJ. Prediction of tissue differentiation during fracture healing-influence of mechanical loading. Proceedings of the American Society of Biomechanics. Pittsburgh. PA. 1999. p.276.

Lacroix D, Prendergast PJ. Three-dimensional simulation of fracture repair in the human tibia. *Comput Methods Biomech Biomed Engin*. 2002;5(5):369-376.

Latifi MH, Ganthel K, Rukmanikanthan S, et al (2012) Prospects of implant with locking plate in fixation of subtrochanteric fracture: Experimental demonstration of its potential benefits on synthetic femur model with supportive hierarchical nonlinear hyperelastic finite element analysis. Biomed Eng Online 11:1. https://doi.org/10.1186/1475-925X-11-23

Latifi MH, Ganthel K, Rukmanikanthan S, et al. Prospects of implant with locking plate in fixation of subtrochanteric fracture: experimental demonstration of its potential benefits on synthetic femur model with supportive hierarchical nonlinear hyperelastic finite element analysis. Biomed Eng Online 2012; 11:2

Lavini F, Carità E, Dall'oca C, Bortolazzi R, Gioia G, Bonometto L, Sandri A, Bartolozzi P. Internal femoral osteosynthesis after external fixation in multiple-trauma patients. Strategies Trauma Limb Reconstr. 2007 Apr;2(1):35-8. doi: 10.1007/s11751-007-0012-x.

Lewis G. Properties of acrylic bone cement: state of the art review. Journal of biomedical materials research. 38(2), 155–182, 1997.

Link, T.M., V. Vieth, R. Langenberg, N. Meier, A. Lotter, D. Newitt, S. Majumdar. Structure Analysis of High Resolution Magnetic Resonance Imaging of the Proximal Femur: in Vitro Correlation with Biomechanical Strength and BMD. Calcif Tissue Int 72. 156–165, 2003.

Lorich DG, Geller DS, Nielson JH.(2004). Osteoporotic pertrochanteric hip fractures: management and current controversies.Instr Course Lect.; 53: 441-454

Lotz, J. C., E.J. Cheal, W.C. Hayes. Fracture prediction for the proximal femur using finite element models: Part II--Nonlinear analysis. Journal of biomechanical engineering. 113(4), 361–365, 1991.

Lotz, J. C., E.J. Cheal, W.C. Hayes. Stress distributions within the proximal femur during gait and falls: implications for osteoporotic fracture. Osteoporosis international: a journal established as result of cooperation between the European Foundation for Osteoporosis and the National Osteoporosis Foundation of the USA. 5(4), 252–261, 1995.

Lujan TJ, Henderson CE, Madey SM, Fitzpatrick DC, Marsh JL, Bottlang M. Locked plating of distal femur fractures leads to inconsistent and asymmetric callus formation. *J Orthop Trauma*. 2010;24(3):156-162.

Lu-Yao GL, Keller RB, Littenberg B, Wennberg JE. (1994).Outcomes after displaced fractures of the femoral neck. A meta-analysis of one hundred and six published reports. J Bone Joint Surg Am ; 76: 15-25

MacLeod AR, Simpson AH, Pankaj P. Reasons why dynamic compression plates are inferior to locking plates in osteoporotic bone: a finite element explanation. Comput Meth Biomech Biomed Eng. 2015; 18:1818–1825.

Madsen JE, Næss L, Aune AK, Alho A, Ekeland A, Strømsøe K (1998) Dynamic hip screw with trochanteric stabilizing plate in the treatment of unstable proximal femoral fractures: a comparative study with the gamma nail and compression hip screw. J Orthop Trauma 12:241–248. https://doi.org/10.1097/00005131- 199805000-00005

Mahaisavariya B, Sitthiseripratip K, Tongdee T, Bohez EL, Vander SJ, Oris P. Morphological study of the proximal femur: A new method of geometrical assessment using 3-dimensional reverse engineering. Med Engg Phys. 2002;24(9):617-22

Malachanne E, Dureisseix D, Jourdan F. Numerical model of bone remodeling sensitive to loading frequency through a poroelastic behavior and internal fluid movements. Journal of the mechanical behavior of biomedical materials, Elsevier, 2011, Bone remodeling, 4 (6), pp.849-857. ff10.1016/j.jmbbm.2011.03.004

Mamdani, E.H., and S. Assilian. 'An Experiment in Linguistic Synthesis with a Fuzzy Logic Controller'. International Journal of Man-Machine Studies 7, no. 1 (January 1975): 1–13. https://doi.org/10.1016/S0020-7373(75)80002-2.

Mamidi RS, Kulkarni B, Singh A. Secular Trends in Height in Different States of India in Relation to Socioeconomic Characteristics and Dietary Intakes. *Food and Nutrition Bulletin*. 2011;32(1):23-34. doi:10.1177/156482651103200103

Mardani-Kivi M, Mirbolook A, Khajeh-Jahromi S, et al. Fixation of intertrochanteric fractures: dynamic hip screw versus locking compression plate. Trauma Mon. 2013; 18:67–70.

Marsell R, Einhorn TA. 2011. The biology of fracture healing. Injury 42: 551-5

Marsell R, Einhorn TA. The biology of fracture healing. *Injury*. 2011;42(6):551-555.

Martini FH, Bartholomew EF (2000) Essentials of anatomy and physiology. Upper Saddle River New Jersey Prentice-Hall Inc. 2nd edition.

Mayhew, P. M., C.D. Thomas, J.G. Clement, N. Loveridge, T.J. Beck, W. Bonfield, C.J. Burgoyne, J. Reeve. Relation between age, femoral neck cortical stability, and hip fracture risk. Lancet (London, England) vol. 366(9480), 129-35, 2005.

McLoughlin SW, Wheeler DL, Rider J, et al. Biomechanical evaluation of the dynamic hip screw with two- and four-hole side plates. J Orthop Trauma 2000;14: 318–323.

Medda S, RARHP (2020) Subtrochanteric femur fractures - StatPearls - NCBI Bookshelf

Miller SC, de Saint-Georges L, Bowman BM, Jee WS. Bone lining cells: structure and function. Scanning Microsc. 1989 Sep;3(3):953-60; discussion 960-1. PMID: 2694361

Moazen M, Jones AC, Leonidou A, et al. Rigid versus flexible plate fixation for periprosthetic femoral fracture – Computer modelling of a clinical case. Med Eng Phys. 2012; 34:1041–1048

Moerman KM, Holt C, Evans SL, Simms CK (2009) Digital image correlation and finite element modeling as a method to determine mechanical properties of human soft tissue in-vivo. J Biomech 42(8):1150–1153.

Morgan EF, Bayraktar HH, Keaveny TM (2003) Trabecular bone modulus-density relationships depend on anatomic site. J Biomech 36(7):897−904

Moroni A, Hoang-Kim A, Lio V, Giannini S. Current augmentation fixation techniques for the osteoporotic patient. Scand J Surg. 2006;95(2):103-9. doi: 10.1177/145749690609500205. MID: 16821653

Morris A, Zuckerman J (2002) National consensus conference on improving the continuum of care of patients with hip fracture. J Bone Joint Surg 84:670–674. https://doi.org/10.2106/00004623- 200204000-00027

Nag, P., S. Chanda. Biomechanical design prognosis of two extramedullary fixation devices for subtrochanteric femur fracture: a finite element study. Medical & biological engineering & computing. 59(2), 271–285, 2021.

Naiyer A, Sohail A, Owais A, Tariq J (2016) Unstable intertrochanteric fracture fixation: is proximal femoral locked compression plate better than dynamic hip screw. J Clin Diagn Res. doi:10.7860/JCDR/2016/11179.7084

Najjar EI, McWilliams ER. Forensic anthropology: The structure, Morphology and variations of human bone and dentition. Springfield, IL: Charles C Thomas; 1978.

Nevitt MC, Cummings SR, Kidd S, Black D. Risk factors for recurrent nonsyncopal falls. A prospective study. JAMA. 1989;261(18), 2663-2668.

Nieves, J.W., J.P. Bilezikian, J.M. Lane, T.A. Einhorn, Y. Wang, M. Steinbuch, F. Cosman. Fragility fractures of the hip and femur: incidence and patient characteristics. Osteoporosis international: a journal established as result of cooperation between the European Foundation for Osteoporosis and the National Osteoporosis Foundation of the USA vol. 21(3), 399-408, 2010.

Nishiyama, K.K., S. Gilchrist, P. Guy, P. Cripton, S.K. Boyd. Proximal femur bone strength estimated by a computationally fast finite element analysis in a sideways fall configuration. Journal of biomechanics. 46(7), 1231–1236, 2013.

Nordin M, Frankel VH. (2001). Basic biomechanics of the musculoskeletal system. Williams & Wilkins Baltimore Philadelphia Lippincott (3rd edition)

Nowotarski PJ, Ervin B, Weatherby B, et al. Biomechanical analysis of a novel femoral neck locking plate for treatment of vertical shear Pauwel's type C femoral neck fractures. Injury 2012; 43:802–806.

Op Den Buijs J, Dragomir-Daescu D (2011) Validated finite element models of the proximal femur using two-dimensional projected geometry and bone density. Comp Meth Prog Biomed 104(2):168–174

Özkaya N, Nordin M (1999) Fundamentals of biomechanics: equilibrium motion and deformation. New York Springer Verlag 2nd edition

Pape HC, Tscherne H (2000) Early definitive fracture fixation, pulmonary function and systemic effects. In: Baue AE, Faist E, Fry M (eds) Multiple organ failure. Springer Verlag, New York, pp 279–290

Parker MJ, Pryor GA. (1996).Gamma versus DHS nailing for extracapsular femoral fractures. Meta-analysis of ten randomised trials. Int Orthop.; 20: 163-168 [PMID: 8832319].

Pathrot D, Haq RU, Aggarwal AN, Nagar M, Bhatt S. Assessment of the geometry of proximal femur for short cephalomedullary nail placement: An observational study in dry femora and living subjects. Indian journal of orthopaedics. 2016;50(3):269.

Pauwels F. Eine neue Theorie über den Einfluß mechanischer Reize auf die Differenzierung der Stützgewebe. Zeitschrift für Anatomie und Entwicklungsgeschichte. 1960. 121, 478-515.

Pérez, M. A., B. Seral-García. A finite element analysis of the vibration behaviour of a cementless hip system. Computer methods in biomechanics and biomedical engineering. 16(9), 1022–1031, 2013.

Perren SM, Cordey J, Rahn BA, Gautier E, Schneider E. Early temporary porosis of bone induced by internal fixation implants. A reaction to necrosis, not to stress protection? Clin Orthop Relat Res. 1988;(232):139-151.

Perren SM, Linke B, Schwieger K, Wahl D, Schneider E. Aspects of internal fixation of fractures in porotic bone. Principles, technologies and procedures using locked plate screws. Acta Chir Orthop Traumatol Cech 2005;72(2):89-97

Perren SM. Evolution of the internal fixation of long bone fractures. The scientific basis of biological internal fixation: choosing a new balance between stability and biology. *J Bone Joint Surg Br*. 2002;84(8):1093-1110. doi:10.1302/0301-620x.84b8.13752

Perren SM. Evolution of the internal fixation of long bone fractures. The scientific basis of biological internal fixation: choosing a new balance between stability and biology. *J Bone Joint Surg Br*. 2002;84(8):1093-1110. doi:10.1302/0301-620x.84b8.13752

Perren SM. Physical and biological aspects of fracture healing with special reference to internal fixation. *Clin Orthop Relat Res*. 1979;(138):175-196.

Perry CC (1986) Strain-gage reinforcement effects on orthotropic materials. Exp Tech 10(2):20–24

Peters W H , Ranson W F . Digital imaging techniques in experimental stress analysis . Optical Engineering, 1982, 21(3): 427-431.

Peters W H, Ranson W F, Sutton M A, et al. Application of Digital Correlation Methods To Rigid Body Mechanics. Optical Engineering, 1983, 22(6).

Prendergast PJ, Taylor D (1994) Prediction of bone adaptation using damage accumulation. J Biomech 27:1067–1076. https://doi.org/10.1016/0021-9290(94)90223-2

Prukvilailert, M., and H. Koguchi. Stress singularity analysis around the singular point on the stress singularity line in three-dimensional joints. *Int. J. Solids Struct.* 2005, 42:3059–3074.

Pushparathna SB, Sangeetha S, Premavathy D. Determination of height using femur length in adult population. 2019. Drug Invention Today.2019;12(4):834-35.

Ramachandra S, Dayanand M, Deepak S, Narasimha Murthy, Hanumantharaju. Outcome of proximal femoral locking compression plate (PFLP) in intertrochanteric femur fracture. Int J Orthop Sci 2019;5(3):677-680 doi: https://doi.org/10.22271/ortho.2019.v5.i3l.1612.

Rapp K, Büchele G, Dreinhöfer K, Bücking B, Becker C, Benzinger P. Epidemiology of hip fractures. Z Gerontol Geriatr. 2019;52(1):10–6.

Ratner D, Hoff man S, Schoen J, Lemons E. Biomaterials science—an introduction to materials in medicine. New York: Elsevier; 2004.

Ravi G.O., S. Saheb, Study of proximal femoral locking compression plate in extra capsular fracture neck of femur. International Journal of Research in Medical Sciences, 3(12), 3726-3733, 2017.

Rawal BR, Ribeiro R, Malhotra R, Bhatnagar N. Anthropometric measurements to design best-fit femoral stem for the Indian population. Indian journal of orthopaedics. 2012;46(1):46

Reilly DT, Burstein AH (1975) The elastic and ultimate properties of compact bone tissue. J Biomech 8:393–405. https://doi.org/10. 1016/0021-9290(75)90075-5

Reina-Romo, E., J. Rodríguez-Vallés, J.A. Sanz-Herrera. In silico dynamic characterization of the femur: Physiological versus mechanical boundary conditions. Medical engineering & physics. S1350-4533(18), 30090-0, 2018.

Rhinelander FW. Tibial blood supply in relation to fracture healing. *Clin Orthop Relat Res*. 1974;(105):34-81.

Roberts MD, Santner TJ, Hart RT. 2009. Local bone formation due to combined mechanical loading and intermittent hPTH-(1-34) treatment and its correlation to mechanical signal distributions. *J. Biomech*. **42**, 2431–2438. (10.1016/j.jbiomech.2009.08.030)

Robinovitch, S. N., W.C. Hayes, T.A. McMahon. Prediction of femoral impact forces in falls on the hip. Journal of biomechanical engineering, 113(4), 366–374, 1991.

Rodriguez-Olaverri JC, Hasharoni A, DeWal H, Nuzzo RM, Kummer FJ, Errico TJ. The effect of end screw orientation on the stability of anterior instrumentation in cyclic lateral bending. Spine J 2005;5(5):554-57

Roesler H (1981) Some historical remarks on the theory of cancellous bone structure (Wolff's law). In: The mechanical properties of bone. Ed: Cowin SC New York The ASME (AMD) 45:27–42

Rog D, Grigsby P, Hill Z, Pinette W, Inceoglu S, Zuckerman L. A biomechanical comparison of the two- and four-hole side-plate dynamic hip screw in an osteoporotic composite femur model. J Orthop Surg (Hong Kong). 2017 May-Aug;25(2):2309499017717199. doi: 10.1177/2309499017717199.

Rossman T, Uthamaraj S, Rezaei A, McEligot S, Giambini H, Jasiuk I, Yaszemski MJ, Lu L, Dragomir-Daescu D. A Method to Estimate Cadaveric Femur Cortical Strains During Fracture Testing Using Digital Image Correlation. J Vis Exp. 2017 Sep 14;(127):54942. doi: 10.3791/54942.

Roux W (1881) Der ziichtende kampf der teile oder die 'tei/auslese' imorganismus (theorie der 'finktionellen unpassung') Leipzig Wilhelm Engelmann

Ruben RB, Folgado J, Fernandes PR (2012) On the optimal shape of hip implants. J Biomech 45(2):239−246

Rubin CT, Lanyon LE (1985) Regulation of bone mass by mechanical strain magnitude. Calcif Tissue Int 37:411–417. https://doi.org/10.1007/BF02553711

Saarenpaa I, Heikkinen T, Ristiniemi J, Hyvonen P, Leppilahti J, Jalovaara P (2009) Functional comparison of the dynamic hip screw and gamma locking nail in trochanteric hip fractures: a matched pair study of 268 patients. Int Orthop 33:255–260. doi:10.1007/s00264-007-0458-y

Sadowski C, Lübbeke A, Saudan M, Riand N, Stern R, Hoffmeyer P. (2002).Treatment of reverse oblique and transverse intertrochanteric fractures with use of an intramedullary nail or a 95 degrees screw-plate: a prospective, randomized study. J Bone Joint Surg Am ; 84-A: 372-381.

Saikia KC, Bhuyan SK, Rongphar R. Anthropometric study of the hip joint in northeastern region population with computed tomography scan. *Indian J Orthop*. 2008;42(3):260-266. doi:10.4103/0019-5413.39572

Saini, P., R. Kumar, V. Shekhawat, N. Joshi, M. Bansal, S. Kumar. Biological fixation of comminuted subtrochanteric fractures with proximal femur locking compression plate. Injury vol. 44(2), 226-231, 2013

Sartori CG, Rodrigues C, Armond JE, Armond RE, Górios C, et al. Femoral Fracture in Elderly: An Avoidable Cause?. Med Case Rep. 2017;4(1):54. doi: 10.21767/2471-8041.100089.

Sathguru Management Consultant Reports: Indian Orthopaedic Device Market, 2016 (http://www.sathguru.com)

Sathish Kumar T, Senthilnathan A, Prabhakar R, Harri Vishnu M. Implant of choice in the management of intertrochanteric fractures in south Indian rural population - A comparative study. Nat J Clin Orthop 2017;1(3):05-12.

Schileo, E., L. Balistreri, L. Grassi, L. Cristofolini, F. Taddei. To what extent can linear finite element models of human femora predict failure under stance and fall loading configurations? Journal of biomechanics. 47(14), 3531–3538, 2014.

Schileo, E., Taddei, F., Malandrino, A., Cristofolini, L. and Viceconti, M., 2007, "Subject-Specific Finite Element Models can Accurately Predict Strain in Long Bones," J. Biomech., 40, pp.2982-2989.

Schweiberer L, Schenk R. Histomorphologie und Vaskularisation der sekundären Knochenbruchheilung, unter besonderer Berücksichtigung der Tibiaschaftfraktur [Histomorphology and vascularization of secondary healing of bone fractures with emphasis on tibial shaft fractures (author's transl)]. *Unfallheilkunde*. 1977;80(7):275-286.

Sehat K, Baker RP, Pattison G, Price R, Harries WJ, Chesser TJ (2005) The use of long gamma nail in proximal femoral fractures. Injury 36:1350–1354

Seide K, Triebe J, Faschingbauer M, et al. Locked vs. unlocked plate osteosynthesis of the proximal humerus - a biomechanical study. *Clin Biomech (Bristol, Avon)*. 2007;22(2):176-182.

Setiobudi T, Ng YH, Lim CT, Liang S, Lee K, Das De S. Clinical outcome following treatment of stable and unstable intertrochanteric fractures with dynamic hip screw. Ann Acad Med Singap. 2011 Nov;40(11):482-7.

Sharma A, Sethi A, Sharma S. Treatment of stable intertrochanteric fractures of the femur with proximal femoral nail versus dynamic hip screw: a comparative study. *Rev Bras Ortop*. 2017;53(4):477-481. Published 2017 Nov 8. doi: 10.1016/j.rboe.2017.07.008

Shefelbine SJ, Augat P, Claes L, Simon U. Trabecular bone fracture healing simulation with finite element analysis and fuzzy logic. *J Biomech*. 2005;38(12):2440-2450.

Simon U, Augat P, Utz M, Claes L. A numerical model of the fracture healing process that describes tissue development and revascularisation. Comput Methods Biomech Biomed Engin. 2011;14(1):79-93.

Simon U, Augat P, Utz M, Claes L. Simulation of tissue development and vascularization in the callus healing process. Transactions ORS, New Orleans, Louisiana, 2003.

Siwach, R. and S. Dahiya. "Anthropometric study of proximal femur geometry and its clinical application." *Indian Journal of Orthopaedics* 37 (2003):247.

Sommer C, Gautier E, Müller M, Helfet DL, Wagner M (2003) First clinical results of the locking compression plate (LCP). Injury 34:43–54. https://doi.org/10.1016/j.injury.2003.09.024

Sowmianarayanan S, Chandrasekaran A, Kumar RK (2008) Finite element analysis of a subtrochanteric fractured femur with dynamic hip screw, dynamic condylar screw, and proximal femur nail implants–a comparative study. Proc Inst Mech Eng H 222:117–127. https://doi.org/10.1243/09544119JEIM156

Sperner G, Wanitschek P, Benedetto KP, Glotzer W. Technical errors and early complications of osteosynthesis of pertrochanteric femoral fractures using the dynamic hip screw. Der Unfallchirurg 1989;92(12):571e6.

Stiffler KS. Internal fracture fixation. Clin Tech Small Anim Pract. 2004 Aug;19(3):105-13. doi: 10.1053/j.ctsap.2004.09.002.

Stoffel K, Stachowiak G, Forster T, Gachter A, Kuster M. Oblique screws at the plate ends increase the fixation strength in synthetic bone test medium. J Orthop Trauma 2004;18(9): 611-16

Streubel PN, Moustoukas MJ, Obremskey WT (2013) Mechanical failure after locking plate fixation of unstable intertrochanteric femur fractures. J Orthop Trauma 27:22–28. https://doi.org/10.1097/ BOT.0b013e318251930d

Streubel PN, Moustoukas MJ, Obremskey WT (2013) Mechanical failure after locking plate fixation of unstable intertrochanteric femur fractures. J Orthop Trauma 27:22–28. https://doi.org/10.1097/ BOT.0b013e318251930d

Su XY, Zhao JX, Zhao Z, Zhang LC, Li C, Li JT, et al. Three-dimensional analysis of the characteristics of the femoral canal isthmus: an anatomical study. Biomed Res Int. 2015;2015. doi: 10.1155/2015/459612

Subash Y., Vishnu, S., Damodharan. Management of Unstable Intertrochanteric Fractures with Proximal Femoral Locking Plate- A Prospective Study of 30 Patients. International Journal of Research in Pharmaceutical Sciences. 12(1), 274-279, 2021.

Sugiyama T, Meakin LB, Browne WJ, et al (2012) Bones' adaptive response to mechanical loading is essentially linear between the low strains associated with disuse and the high strains associated with the lamellar/woven bone transition. J Bone Miner Res 27:1784–1793. https://doi.org/10.1002/jbmr.1599

Sutton, M.A., J.H. Yan, V. Tiwari, H.W. Schreier, J.J. Orteu. The effect of out-of-plane motion on 2D and 3D digital image correlation measurements. Optics and Lasers in Engineering. 46(10), 746-757, 2008.

Swift C, Chesser T, Field A, et al (2010) The management of hip fracture in adults - NICE guideline 27

Sztefek P, Vanleene M, Olsson R, Collinson R, Pitsillides AA, Shefelbine S (2010) Using digital image correlation to determine bone surface strains during loading and after adaptation of the mouse tibia. J Biomech 43(4):599–605

Tayton E, Evans S, O'Doherty D (2010) Mapping the strain distribution on the proximal femur with titanium and flexible-stemmed implants using digital image correlation. J Bone Jt Surg Br 92-B(8):1176–1181

Tayton E, Evans S, O'Doherty D. 2010. Mapping the strain distribution on the proximal femur with titanium and flexible-stemmed implants using digital image correlation. J Bone Joint Surg Br. 92:1176–1181.

Terjesen T, Nordby A, Arnulf V (1985) Bone atrophy after plate fixation: Computed tomography of femoral shaft fractures. Acta Orthop 56:416–418. https://doi.org/10.3109/17453678508994361

Terjesen T, Nordby A, Arnulf V (1986) The extent of stress-protection after plate osteosynthesis in the human tibia. Clin Orthop Relat Res 108–12

Thompson, M.S., Schell, H., Lienau, J. and Duda, G.N., 2007, "Digital Image Correlation: a Technique for Determining Local Mechanical Conditions within Early Bone Callus," Med. Eng. and Phys., 39, pp. 820-823

Thrun, M., C. Finfrock, A. Clarke, K. Clarke. Effects of Unloading on Subsequent Yielding Behavior in 304 Stainless Steel. Frontiers in Materials, vol. 7, 2021. doi:10.3389/fmats.2020.615361.

Tomaszewski, P. K., N. Verdonschot, S.K. Bulstra, G.J. Verkerke. A comparative finite-element analysis of bone failure and load transfer of osseointegrated prostheses fixations. Annals of biomedical engineering, 38(7), 2418–2427, 2010

Tonino AJ, Davidson CL, Klopper PJ, Linclau LA.(1984). Protection from stress in bone and its effects: experiments with stainless steel and plastic plates in dogs. J.Bone joint surg.; 58-B: 107-113.

Treherne RW (1981) Review of Wolff's law and its proposed means of operation. Orthop Rev 10:35–47

Uhl JM, Seguin B, Kapatkin AS, Schulz KS, Garcia TC, Stover SM. Mechanical comparison of 3.5 mm broad dynamic compression plate, broad limited-contact dynamic compression plate, and narrow locking compression plate systems using interfragmentary gap models. *Vet Surg*. 2008;37(7):663-673.

Uhl JM, Seguin B, Kapatkin AS, Schulz KS, Garcia TC, Stover SM. Mechanical comparison of 3.5 mm broad dynamic compression plate, broad limited-contact dynamic compression plate, and narrow locking compression plate systems using interfragmentary gap models. *Vet Surg*. 2008;37(7):663-673.

Uhthoff HK, Bardos DI, Liskova-Kiar M.(1981). The advantages of titanium alloys over stainless steel plates for the internal fixation of fractures. J. Bone joint surg.; 63-B: 427-34.

Väänänen SP, Amin Yavari S, Weinans H, Zadpoor AA, Jurvelin JS, Isaksson H. Repeatability of digital image correlation for measurement of surface strains in composite long bones. J Biomech. 2013 Jul 26;46(11):1928-32. doi: 10.1016/j.jbiomech.2013.05.021.

van Der Meulen MCH, Beaupré GS, Carter DR (1993) Mechanobiologic influences in long bone cross-sectional growth. Bone 14:635–642. https://doi.org/10.1016/8756-3282(93)90085-O

Viceconti M, Bellingeri L, Cristofolini L, Toni A (1997) A comparative study on different methods of automatic mesh generation of human femurs. Med Eng Phys 20(1):1–10

Villette, C.C., A.T.M. Phillips. Rate and age-dependent damage elasticity formulation for efficient hip fracture simulations. Medical Engineering & Physics. 61, 1-12, 2018.

Wagner M, Frenk A, Frigg R. New concepts for bone fracture treatment and the Locking Compression Plate. Surg Technol Int. 2004;12:271-7.

Wagner M. General principles for the clinical use of the LCP. Injury 2003; 34(Suppl. 2): B31–42.

Wang CC, Lee CH, Chin NC, et al. Biomechanical analysis of the treatment of intertrochanteric hip fracture with different lengths of dynamic hip screw side plates. Technology and Health Care: Official Journal of the European Society for Engineering and Medicine. 2020:28(6):593-602. DOI: 10.3233/thc-202248.

Wang J, Ma JX, Lu B, Bai HH, Wang Y, Ma XL (2020) Comparative finite element analysis of three implants fixing stable and unstable subtrochanteric femoral fractures: proximal femoral nail antirotation (PFNA), proximal femoral locking plate (PFLP), and reverse less invasive stabilization system (LISS). Orthop Traumatol Surg Res 106:95–101. https://doi.org/10.1016/j.otsr. 2019.04.027

Wang J, Ma X, Ma J, et al (2014) Biomechanical Analysis of Four Types of Internal Fixation in Subtrochanteric Fracture Models. Orthop Surg 6:128–136. https://doi.org/10.1111/os.12109

Wang J, Ma XL, Ma JX, et al. Biomechanical analysis of four types of internal fixation in subtrochanteric fracture models. Orthop Surg. 2014; 6:128–136.

Wehner T, Claes L, Niemeyer F, Nolte D, Simon U. Influence of the fixation stability on the healing time--a numerical study of a patient-specific fracture healing process. *Clin Biomech (Bristol, Avon)*. 2010;25(6):606-612.

Weinans H, Huiskes R, Grootenboer HJ (1992) The behavior of adaptive bone-remodeling simulation models. J Biomech 25:1425–1441. https://doi.org/10.1016/0021-9290(92)90056-7

Weinans H, Huiskes R, van Rietbergen B, Sumner DR, Turner TM, Galante, JO (1993) Adaptive bone remodelling around bonded noncemented total hip arthroplasty: a comparison between animal experiments and computer simulation. J Orthop Res 11(4):500−51

White BL, Fisher WD, Lauren CA. Rate of mortality for elderly patients after fracture of the hip in the 1980's. J Bone Joint Surg 1987; 69A:1335-1340.

Wieser K, Babst R. Fixation failure of the LCP proximal femoral plate 4.5/5.0 in patients with missing posteromedial support in unstable per-, inter-, and subtrochanteric fractures of the proximal femur. Arch Orthop Trauma Surg. 2010; 130:1281–1287

Wilson RT, Wallace RB. (2007). Trends in hip fracture incidence in young and older adults American Journal of Public Health;97(10):1734–5.

Wirtz C, Abbassi F, Evangelopoulos DS, et al. High failure rate of trochanteric fracture osteosynthesis with proximal femoral locking compression plate. Injury 2013; 44:751–756.

Wirtz C, Abbassi F, Evangelopoulos DS, et al. High failure rate of trochanteric fracture osteosynthesis with proximal femoral locking compression plate. Injury 2013; 44:751–756.

Wolff J (1892) Das gesetz der transformation der knochern. Translated as: The law of bone remodelling by Maquet P Furlong R 1986 Berlin Springer Verlag

Ya'ish FM, Nanu AM, Cross AT. Can DCP and LCP plates generate more compression? The effect of multiple eccentrically placed screws and their drill positioning guides. Injury.2011;42(10): 1095-100.

Yamaguchi I. Laser-speckle strain gauge. J Physics E: Scientific Instrument, 1981, 14(11): 1270-1273.

Yánez A, Carta JA, Garcés G. Biomechanical evaluation of a new system to improve screw fixation in osteoporotic bones. *Med Eng Phys*. 2010;32(5):532-541.

Yánez A, Carta JA, Garcés G. Biomechanical evaluation of a new system to improve screw fixation in osteoporotic bones. *Med Eng Phys*. 2010;32(5):532-541

Yang L, Zhang P, Liu S, Samala PR, Su M, Yokota H. 2007. Measurement of strain distributions in mouse femora with 3D-digital speckle pattern interferometry. Opt Lasers Eng. 45:843–851.

Yeganeh A, Taghavi R, Moghtadaei M. Comparing the Intramedullary Nailing Method Versus Dynamic Hip Screw in Treatment of Unstable Intertrochanteric Fractures. Med Arch. 2016 Feb;70(1):53-6. doi: 10.5455/medarh.2016.70.53-56.

Yong CK, Tan CN, Penafort R, Singh DA, Varaprasad MV (2009) Dynamic hip screw compared to condylar blade plate in the treatment of unstable fragility intertrochanteric fractures. Malays Orthop J 3:13–18. Doi:10.5704/MOJ.0905.001

Yuasa M, Mignemi NA, Barnett JV, Cates JMM, Nyman JS, Okawa A, et al. 2014. The temporal and spatial development of vascularity in a healing displaced fracture. Bone 67: 208-21.

Zadeh LA, Fuzzy sets, Information and Control, Volume 8, Issue 3, 1965, Pages 338-353, ISSN 0019-9958, https://doi.org/10.1016/S0019-9958(65)90241-X.

Zand MS, Goldstein SA, Matthews LS. Fatigue failure of cortical bone screws. J Biomech. 1983;16(5):305-311.

Zderic I, Willhuber GC, Ahrend MD, et al. Biomechanical comparison between standard and inclined screw orientation in dynamic hip screw side-plate fixation: The lift-off phenomenon. *J Orthop Translat*. 2018;18:92-99. Published 2018 Nov 17. doi:10.1016/j.jot.2018.10.005

Zha GC, Chen ZL, Qi XB, et al. Treatment of pertrochanteric fractures with a proximal femur locking compression plate. Injury 2011; 42:1294–1299.

Zhang, Z., Zhang, X., Chen, W., et al. A high-efficient energy regenerative shock absorber using supercapacitors for renewable energy applications in range extended electric vehicle. Applied Energy 178, 177–188, 2016.

Zhong B, Zhang Y, Zhang C, et al. A comparison of proximal femoral locking compression plates with dynamic hip screws in extracapsular femoral fractures. Orthop Traumatol Surg Res. 2014; 100:663–668.

Zuckerman JD. Hip fracture. N Engl J Med. 1996 Jun 6;334(23):1519-25. doi: 10.1056/NEJM199606063342307.

Appendix

Significance of nonlinearity consideration in pre-clinical strength assessment of extramedullary bone plates

A.1 Introduction

Nonlinear analysis demonstrates a real scenario by considering kinematic and/or material nonlinear effects. Nonlinearities may be classified into three types of geometric, material, and contact. Geometric nonlinearities are due to kinematic quantities like strain-displacement relations. Contact can also be classified as geometric nonlinearity because the area of contact is a function of deformation. Thus, whenever high accuracy is needed, a nonlinear analysis may play a vital role in simulating actual material behaviour, establishing the cause of failure, and designing high-performance components. However, a nonlinear analysis may be computationally expensive compared to linear analysis.

The appendix aims to understand the significance of nonlinearity consideration in FE analysis. The investigation employed the previously generated model, used in Chapter 2, PFLP and VA-DHS implanted in a femur having intertrochanteric fracture and was analysed dynamically for entire walking gait cycle. The results were further compared with that of the intact femur. Also, the severity of sideways fall impact force on intact and implanted were analysed under dynamic conditions for both linear and nonlinear analyses. Three analyses approaches were performed on all the models: linear analysis, geometric nonlinear analysis and total (geometric & material) nonlinear analysis for the loading conditions of quasi-static and dynamic scenario.

A.2 Materials and method

The effect of walking gait cycle, sideways fall and different types of nonlinearity considerations in FE analysis were studied by performing numerical simulations on intact femur, PFLP implanted femur and VA-DHS implanted femur. In all the analyses the loads applied were compressive in nature. The intact synthetic femur was validated with the available literature (Villette et al., 2018; Gardner et al., 2010; Schileo et

al.,2008). It is worth noting that the validation was conducted based on three studies, among which one of the studies had performed biomechanical experiment on the manufacturer supplied model (Sawbones, Europe AB, Malmo, Sweden, model# 3406), the same model which was used for this study. The material properties considered for the analyses and methodology followed is delineated bit by bit in the following subsections.

The material models considered up to elastic portion along with yield stress for the bone, implant, and PMMA (polymethylmethacrylate) are presented in Table 1. Isotropic material properties were applied to cancellous bone, implants, and PMMA cap. The implants and their screws were assigned the material properties of steel. Orthotropic material properties were considered for cortical bone based on the data provided in the manufacturer's manual (Sawbones, Europe AB, Malmo, Sweden) . In the cortical bone, Young's modulus in the longitudinal direction was higher compared to transverse directions. Poisson's ratio was set as 0.3 for all materials.

In the analyses wherever material nonlinearity was taken into consideration, elasto-plastic material properties were assigned to bone and implants, while PMMA cap was assigned elastic material properties in all the analyses. The material properties of cortical bone for the plastic region in three anatomical directions (longitudinal, transverse, and radial) were acquired from the literature by Novitskaya et al. (2011). The plastic region properties of cancellous bone were acquired from Sierpowska et al. (2005). The material properties for the elastic region given in the literature were found to be corroborated with the material properties of the synthetic femur considered in our analysis. Also, the loading conditions used in the experimental procedures mentioned in the literature were compressive in nature.

The FE analysis for the present study was performed using the 'OptiStruct' solver of HyperMesh 2019.1. For the present study, all the analyses were simulated using three approaches namely linear analysis, geometric nonlinear analysis and geometric & material nonlinear analysis. In the first approach of linear analysis, stiffness was constant and values of engineering stress and strain were used during simulation. In second approach of geometric nonlinear analysis, stiffness was a function of displacement. The nonlinear analysis is performed in the FE software packages by performing piecewise linearity so the load is split into small increments and stiffness matrix is updated after each incremental load application. The iterations are performed

to ensure that equilibrium is satisfied at every load increment. In the process, Newton's Raphson method is used to solve the equations. In the third approach, both geometric and material nonlinearity was taken into consideration where true stress and strain values were used. This type of analysis approach took all the nonlinearity into consideration during simulation. For the analysis approach, 'Radioss Integration' solver was used, which combined the capability of 'Radioss' solver with 'Optistruct' solver, and data was transferred to and fro between the two solvers during simulation to take the material nonlinearity consideration of orthotropic material along with geometric nonlinearity. Radioss is a structural analysis solver for highly nonlinear problems [54]. The computation time associated with this analysis was high as compared to linear and geometric nonlinear analyses.

A.3 Results

In order to understand the effect of nonlinearity consideration, the intact femur and implanted femurs were analysed for stress and displacement occurring during loading conditions of quasi-statically increasing load, walking cycle and sideways fall. The results of total nonlinear (geometric and material) analysis of intact femur for the loading condition of quasi-statically increasing load were validated against the experimental data and FE analysis data, as shown in Table A.1 and Figure A.1. The values of ultimate axial strength, corresponding displacement and axial stiffness of intact femur obtained through total nonlinear (geometric and material) analysis are shown in Table A.1. The intact femur did not show any sign of failure in case of linear analysis and geometric nonlinear analysis, as material nonlinearity was not considered in those two analysis approaches. The axial stiffness of intact femur in case of linear analysis was found to be 1.53 N/µm and in case of geometric nonlinear analysis, it was found to be 1.27 N/µm.

Table A.1. Validation of nonlinear (geometric & material) analysis with experimental data adapted from Gardner et al. 2010. (Experiment was performed on the femur model #3406 adapted from Sawbones, Sweden)

	Ultimate Axial Strength (KN)	Displacement (at ultimate axial load) (mm)	Axial Stiffness (N/µm)
Nonlinear analysis	7.68	7.93	1.18
Gardner et al. 2010 (Experiment)	7.59	7.70	1.23

The force vs displacement graphs for intact femur for the quasi-statically increasing load in three approaches of analysis are shown in Fig. A.2. The slope of force vs displacement curve in case of linear analysis was found to be highest compared to nonlinear analyses. The slope of force vs displacement in case of total nonlinear (geometric and material) analysis was found to be lowest although the slope of geometric nonlinear analysis was found to be nearly equal to the slope of total nonlinear analysis. The curve of linear analysis was a straight line while the curve of total nonlinear (geometric and material) was found to be nonlinear curve. The curve of total

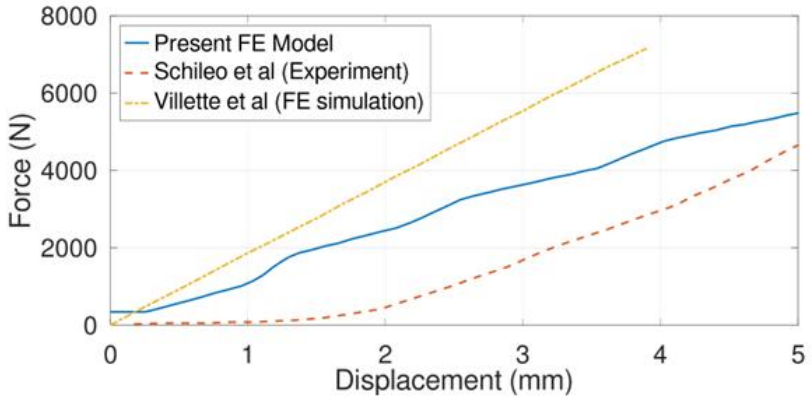

Fig. A.1: Validation of nonlinear (geometric & material) FE simulation with available literature

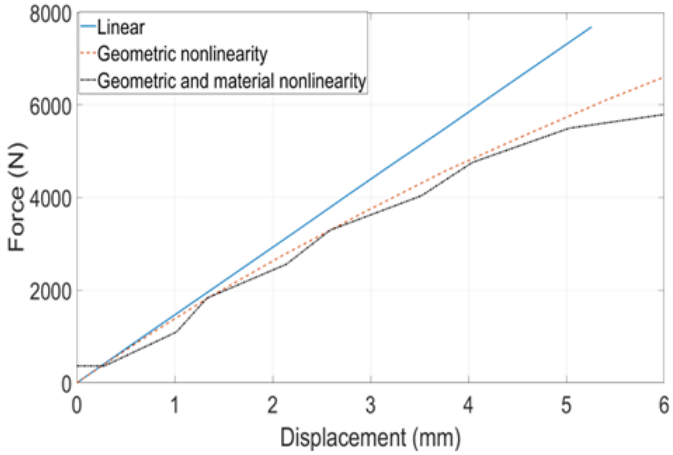

Fig. A.2: Comparison of force vs displacement of intact femur for linear, geometric nonlinearity and geometric & material linearity FE simulations.

nonlinear (geometric and material) was found to be flattened out after crossing the load of 5000N while the curve of linear analysis and geometric nonlinear analysis was found to be maintaining upward tendency.

Stress vs axial load of intact femur for quasi-statically increasing load for isotropic and orthotropic material properties and for the three approaches of analysis in case of orthotropic material properties are shown in Fig. A.3. The slope of stress vs force for

isotropic material was found to be slightly lower compared to orthotropic material consideration but there was large difference found in the failure load of isotropic material and orthotropic material. The failure load for isotropic material consideration was found to be nearly 11 kN while for orthotropic material consideration, it was only 7.68 kN. The ultimate stress for the isotropic material consideration was found to be 157 MPa while for orthotropic material consideration it was found to be nearly 138 MPa (Fig. A.3a). The slope of stress vs force was found to be highest in case of total nonlinear (geometric and material) analysis while it was found to be lowest in case of

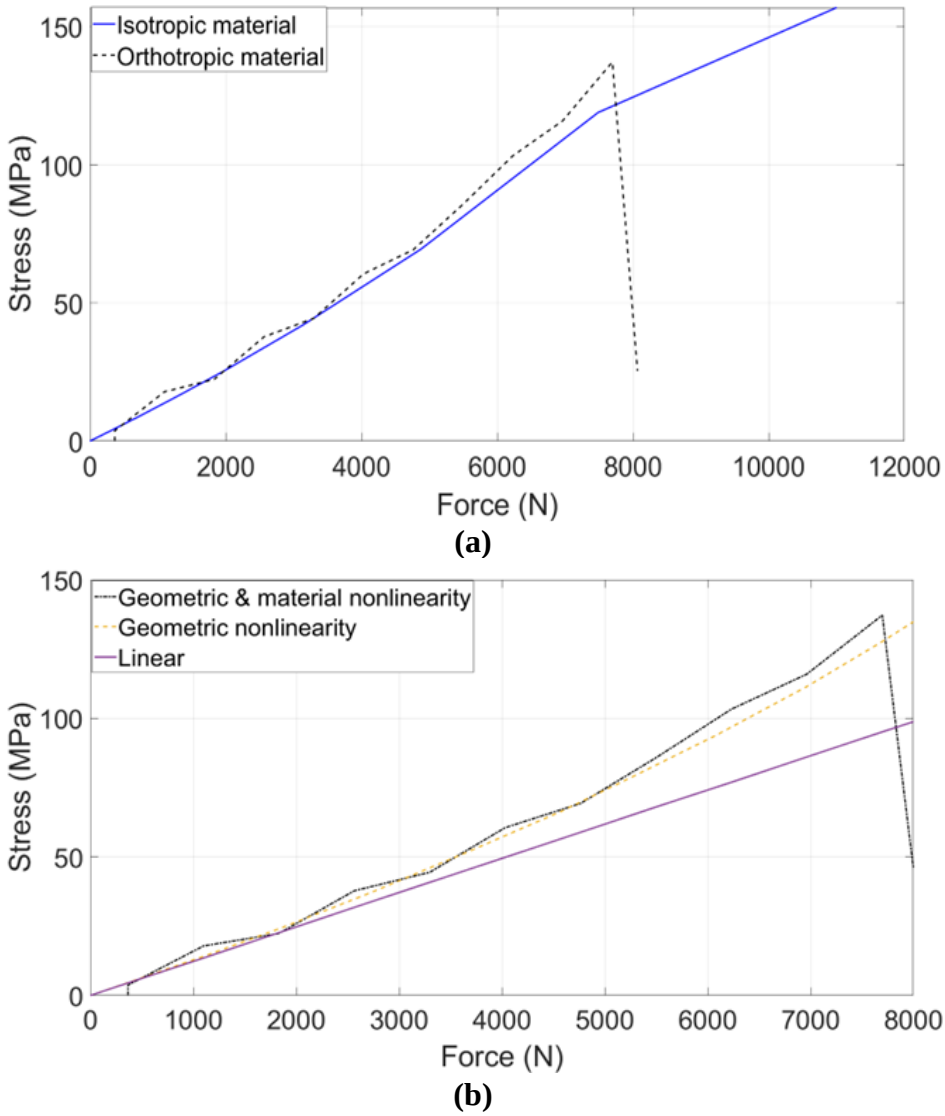

Fig. A.3: Stress vs Axial load of intact femur (a) Comparison of nonlinear (geometric & material) FE analysis for isotropic material property and orthotropic material property (b) Comparison of Linear, Geometric nonlinearity and Geometric & material nonlinearity FE simulations. (Here, all the simulations were performed for orthotropic material property)

linear analysis. The stress was found to be continuously increasing with increasing load in case of linear analysis and geometric nonlinear analysis while after the attainment of

ultimate stress in total (geometric and material) nonlinear analysis, there was found to be drastic decrease in stress with further increase in load (Fig. A.3b).

The displacement versus time curve over a complete walking gait cycle (duration 1s) for intact femur and implanted femurs for three approaches of analysis are shown in Fig. A.4. The results of total nonlinear (geometric and material) analysis illustrated higher displacement compared to linear analysis and geometric nonlinear analysis in all the models of intact femur and implanted femurs. During the stance phase, the geometric nonlinear analysis predicted higher displacement while during the swing phase the curves of linear analysis and geometric nonlinear analysis overlapped each other.

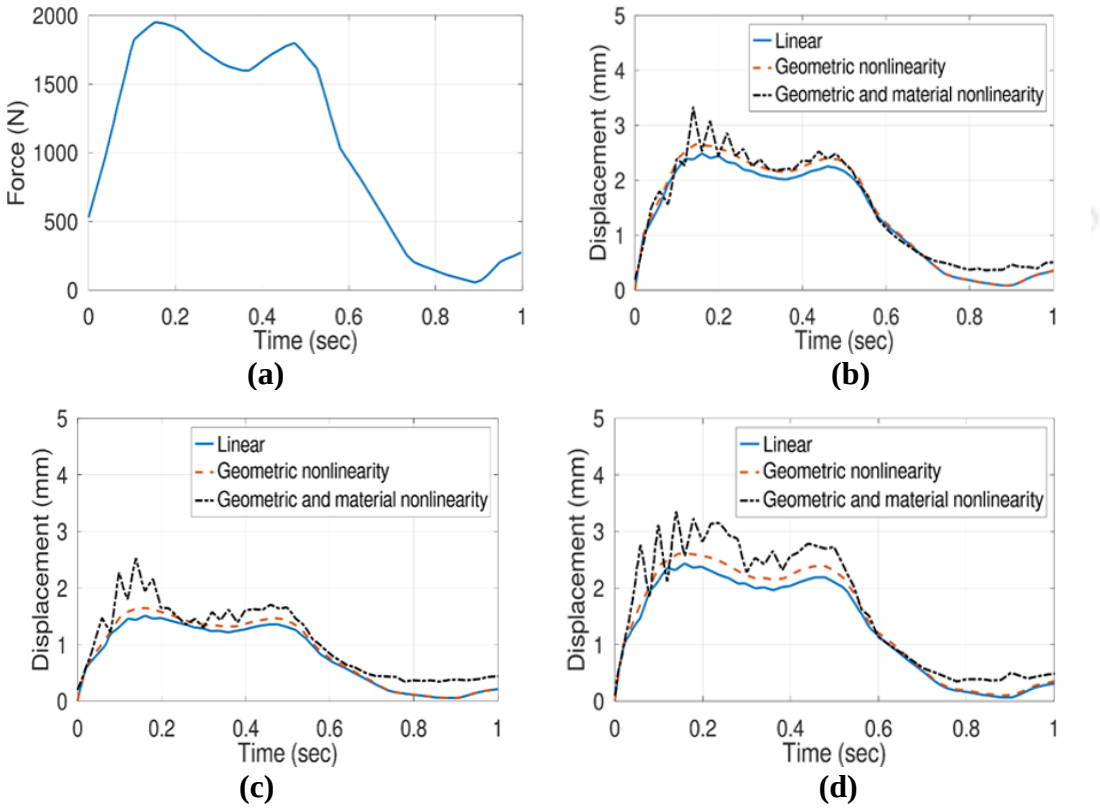

Fig. A.4: Comparison of displacement vs time during walking cycle in the case of linear, geometric nonlinearity and geometric & material nonlinearity analysis: (a) The hip contact resultant force corresponding to normal walking corresponding to a body weight of 750N (Hellar et al., 2005) that was given as input load; (b) (b) intact femur (c) PFLP implanted femur (d) VA-DHS implanted femur.

The displacement corresponding to PFLP implanted femur was found to be lesser compared to intact femur while intact femur and VA-DHS implanted femur were found to be closely associated with each other. The curves of total nonlinear (geometric and material) was found to be fluctuating compared to linear and geometric nonlinear analysis. The maximum displacement occurring during gait cycle analysis by total

nonlinear approach for intact femur, PFLP implanted femur and VA-DHS implanted femur were found to be 3.33 mm, 2.53 mm and 3.36 mm respectively. The maximum

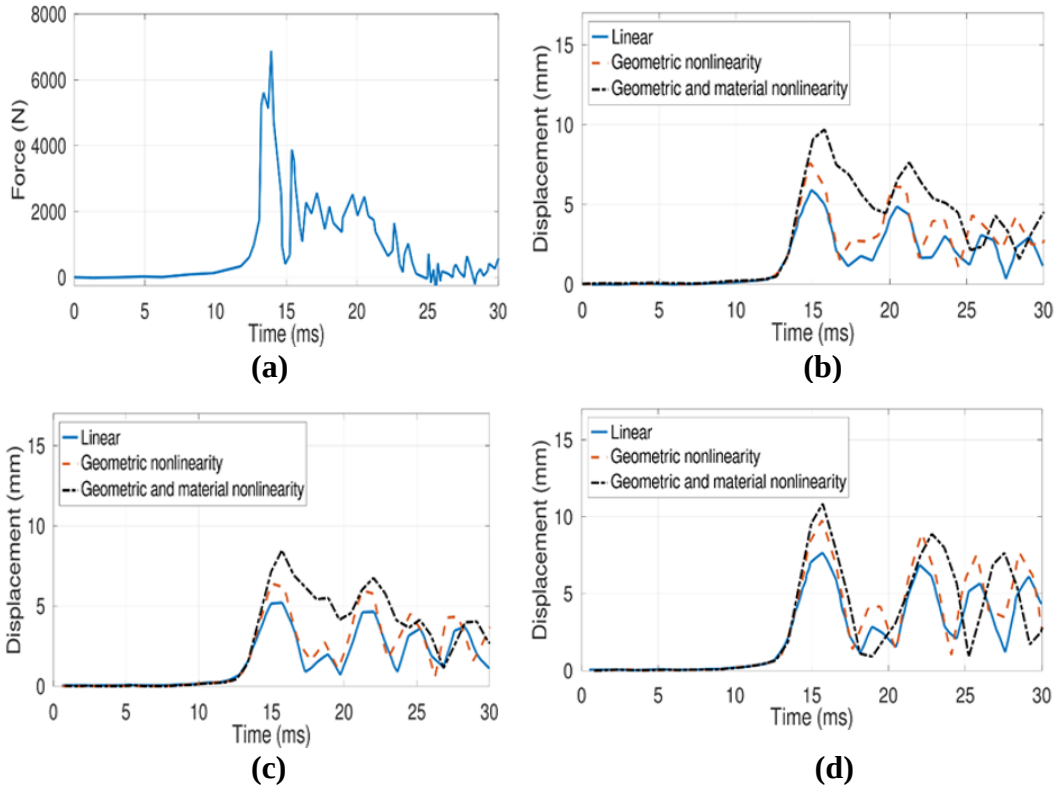

Fig. A.6: Comparison of displacement vs time during impact in the case of linear, geometric nonlinearity and geometric & material nonlinearity analysis: (a) The impact force vs time for sideways fall adapted from Fleps et al.; (b) Intact femur (c) PFLP implanted femur (d) VA-DHS implanted femur

values obtained from the linear analysis were 2.48mm, 1.51mm & 2.43 mm and the values in case of geometric nonlinear analysis were 2.65 mm, 1.65mm & 2.61mm for intact femur, PFLP implanted femur & VA-DHS implanted femur respectively.

The displacement versus time curves of sideways fall for three analysis approaches performed on intact femur and implanted femurs are shown in Fig. A.5. Here, the total nonlinear analysis was found to be displaying highest displacement, the linear analysis was found to be displaying lowest displacement and the displacement predicted by geometric nonlinear analysis was between the above two. The displacement measured in case of VA-DHS implanted femur was highest and the displacements measured in case of intact femur and PFLP implanted femur was found to be closely associated with each other. The maximum displacement occurred due to impact force of sideways fall in total nonlinear analysis approach for intact femur, PFLP implanted femur and VA-DHS implanted femur were found to be 9.71 mm, 8.47 mm & 10.85 mm respectively.

The corresponding maximum values in case of linear analysis were 5.91 mm, 5.20 mm & 7.67 mm and in the case of geometric nonlinear analysis were 7.62 mm, 6.40 mm & 9.77 mm respectively.

A.4 Discussion

This study investigated the significance of nonlinearity consideration in FE simulation under two physiological loading regimes, normal walking gait cycle and sideways fall. The displacement results of the FE simulation by Villete et al. (2018) were found to be increasing linearly with increasing load while the results of present study were found to be closely following the curve of experimental data (Fig. A.1). For a small load the results obtained through linear analysis, geometric nonlinear analysis and total nonlinear analysis were same as shown in force vs displacement curve shown in Fig. 4. For higher load, the consideration of nonlinearity in FE analysis, only can give accurate results. Till the load of 5.5 kN, both geometric nonlinearity and total nonlinearity was found to be displaying the same result but beyond the load of 5.5 kN the accuracy of geometric nonlinearity was reduced and found to be deviated from the curve of total nonlinearity. At the load of 5.76 kN, the displacements obtained from linear analysis, geometric nonlinear analysis and total nonlinear analysis were found to be 3.83mm, 4.98mm and 5.8mm respectively. Thus, at very high load both geometric and material nonlinearity should be taken into consideration in the FE analysis to get accurate results. The study also shown the effect of consideration of isotropic and orthotropic material properties in FE analysis (Fig. A.3a). A large difference in failure load was observed in the case of isotropic and orthotropic, and failure load was higher in isotropic case by an amount of nearly 3.5 kN. The value of ultimate stress in case of isotropic material was 157 MPa while the value in case of orthotropic material it was 138 MPa, which was found to be higher than the yield stress in transverse direction (93 MPa) and lower than the yield stress in longitudinal direction (157 MPa). Thus, consideration of isotropic properties instead of orthotropic may not reveal real physics in the FE analysis. The stress vs force for three analysis approaches performed for orthotropic material revealed that for small load all the three approaches produce the same result but as the load increases, the discarding of nonlinearity may lead to error in result (Fig. A.3b), as it was observed in force vs displacement curve (Fig. A.2). Here, the results of geometric nonlinear and total nonlinear analysis were found to be closely associated with each other, but linear analysis approach was found to be predicting lesser stress at higher load. Thus, the geometric nonlinear analysis can predict the stress with reasonable

accuracy, in the elastic region, but to predict the failure inclusion of material nonlinearity (plastic region) is required (Fig. A.3b).

The dynamic walking gait cycle analysis performed on intact femur and the implanted femurs have given an estimation of effect for using two types of implants namely PFLP and VA-DHS over a realistic scenario, it has also demonstrated the effect of nonlinearity in dynamic cases. The time varying walking gait cycle load were applied on the femoral head which included the numerically averaged resultant force of hip joint reaction and muscle forces. The inclusion of muscle forces may provide a more realistic approach in pre-clinical investigation by subtracting the opposite direction muscle forces from hip joint reaction, as its exclusion may lead to increased bending of proximal femur. The maximum displacement (3.33 mm) occurring during gait cycle of intact femur through total nonlinear analysis approach was found to be approximate to the experimental value of 3.1 mm reported by Rakib et al. (2014). The percentage difference in results of maximum displacement obtained through total nonlinear analysis and geometric nonlinear analysis of intact femur, PFLP implanted femur and VA-DHS implanted femur were ~20%, ~34% & ~22%, while the percentage difference in values between the results of total nonlinear analysis and linear analysis were found to be ~25%, ~40% & ~27% respectively. Thus, in dynamic analysis the error percentage was found to be increased significantly as compared with static analysis.

Simulation of sideways fall revealed the effect of two extramedullary plates (PFLP and VA-DHS) in severe cases of impact force and importance of direction of loading was promulgated. The displacement of intact femur at peak load during sideways fall from De bakker et al experiment [25] on different specimens of cadaver bone was found to be nearly 10mm, which was found to be in corroborate with this study. The percentage difference in maximum displacement obtained through total nonlinear analysis and geometric nonlinear analysis for intact femur, PFLP implanted femur and VA-DHS implanted femur were found to be ~21%, ~24% and ~9% respectively. While the corresponding percentage difference in the results of total nonlinear analysis and linear analysis were found to be ~39%, ~38% & ~29% respectively. Here, the displacement in case of intact femur and PFLP implanted femur was found to be closely associated with each other while the higher displacement was observed in case of VA-DHS implanted femur (Fig. A.5). This may be due to distal screws in case of VA-DHS and presence of screws throughout the length in case of PFLP . Thus, PFLP imparted

higher stiffness compared to VA-DHS and so it can provide high rigidity and protect from fall.

However, the present study has certain limitations. Although the total nonlinear analysis approach in FE analysis was found to be delivering accurate results but the computation time was found to be increased 7-8 times of linear analysis and in the geometric nonlinear analysis, the computation time was found to be 3-4 times of linear analysis. The present study was performed on synthetic femur. In gait cycle analysis, the muscle forces were used but it was numerically averaged to single point of load application that may not represent actual condition of loading at multiple points. In sideways fall scenario, the muscle forces were not considered in analysis and loading data was collected from literatures of in-vitro study.

A.5 Summary

The study revealed that at small load linear analysis can predict accurate results, but as the load is increased higher and higher, discarding of nonlinearity can lead to reduction in the accuracy of results. The error percentage while discarding nonlinearity was found to be increased in dynamic analysis compared to static analysis. Total nonlinear (geometric & material) analysis can reduce the error percentage of less than 5% as compared with experimental procedure.

A.6 Additional References

Novitskaya E, Chen P-Y, Lee S, et al. Anisotropy in the compressive mechanical properties of bovine cortical bone and the mineral and protein constituents. Acta Biomaterialia 2011; 7: 3170-3177.

Rakib M, Choudhury I and Osman NAA. Development of a prefabricated and user-friendly stance-control orthosis. 3rd International Conference on Environmental Energy and Biotechnology IPCBEE 2014; vol. 70.

Sierpowska J, Hakulinen MA, Töyräs J, et al. Prediction of mechanical properties of human trabecular bone by electrical measurements. Physiological Measurement 2005; IOP Publishing Ltd,Volume 26, Number 2.

About the Author

Pratik Nag was born on the sixteenth day of October, 1994, in Agartala, Tripura, India. In the year 2013, he passed the Higher-Secondary (10+2) Examination with first division, under Central Board of Secondary Education with 92% in science group. From 2013 until 2017, he studied his Bachelor's course in Mechanical Engineering at the National Institute of Technology Agartala, India and passed out with a first-class distinction (CGPA: 9.1). In 2016, he was selected as an Indian Academy of Sciences summer research fellow. In 2017, he joined the Indian Institute of Technology Guwahati, India to pursue Ph.D. research in the field of Biomechanics at the Department of Bioscience and Bioengineering. In December 2018, he was awarded the prestigious Prime Minister Research Fellowship (PMRF) by the Govt. of India in the broad area of Interdisciplinary Sciences and Engineering. His doctoral research study is on the topic of 'Biomechanical Design Prognosis and Preclinical Assessment of Bone Plates used to Treat Extracapsular Femoral Fractures'.

List of publications from the present thesis

Patent

1. Double Oblique Device for Osteosynthesis (DODO) of Hip (Filed, Indian patent application ref. no: 348843-001)

Journal

1. **Nag, P.**, Chanda, S. (2021) Biomechanical Design Prognosis of Two Extramedullary Fixation Devices for Subtrochanteric Femur Fracture: A Finite Element Study, 2021, Medical & Biological Engineering & Computing, Springer, 59, 271–285. https://doi.org/10.1007/s11517-020-02306-6

2. **Nag, P.**, Borgohain, B. & Chanda, S. (2021) Novel Design of Minimal Incision Double Oblique Device for Osteosynthesis (DODO) of Hip: Results of an In-silico Study Based on the Femur Morphometrics of the Northeast (NE) Indian population. Indian Journal Orthopaedics, Springer;55(Suppl. 2):385-394. https://doi.org/10.1007/s43465-021-00408-3

3. **Nag, P.**, Borgohain, B., Ahmed, K. A., Phukan, P., Kumar, N., Borjali, A., Varadarajan, K. M., & Chanda, S. (2022). The Influence of Static Load and Sideways Impact Fall on Extramedullary Bone Plates Used to Treat Intertrochanteric Femoral

Fracture: A Preclinical Strength Assessment. Annals of Biomedical Engineering, https://doi.org/10.1007/s10439-022-03013-z

4. **Nag, P.**, Chanda. S. (2022) A preclinical model of post-surgery secondary bone healing for subtrochanteric femoral fracture based on fuzzy interpretations. PLoS ONE 17(7): e0271061. https://doi.org/10.1371/journal.pone.0271061

5. **Nag, P**., Banik, P., Borgohain, B., Chanda, S., Need of patient specific implant: a design rationale based on femur morphometrics of two different population (to be communicated).

Conferences

1. **Nag, P.**, Chanda, S., Proximal Femoral Locking Plate: The Effect of Interface Conditions on Implant-induced Stress Shielding. 1st IEEE International Student Conference, Bangalore. (2019)

2. **Nag, P.**, Chanda, S., A comparison of Proximal Femoral Locking Plate (PFLP) and Dynamic Hip Screw (DHS) based on the effect of stress shielding in subtrochanteric femoral fracture. (2019) Research Conclave, IIT Guwahati. (Poster)

3. **Nag, P.**, Chanda, S., Proximal Femoral Locking Plate (PFLP): in silico assessment of external bone remodelling under static loading. International conference on smart materials for sustainable technology (SMST 2020), 22nd – 25th February, 2020, Goa, India. (Poster)

4. **Nag, P.**, Chanda, S., in silico assessment of bone healing using finite element analysis and fuzzy logics. 26th congress of European Society of Biomechanics (ESB 2021), July 11-14, 2021, Politecnico Milano, Italy. (Poster)

5. **Nag, P.**, Borgohain. B., Chanda, S., Double Oblique Device for Osteosynthesis (DODO) of Hip: an indigenous implant for the northeast (NE) population of India. 66th Annual Conference of Indian Orthopaedic Association (IOACON 2021), December 21-25th, 2021, Goa, India. (Poster)

6. **Nag, P.**, Biomechanical design prognosis and pre-clinical assessment of extramedullary femoral plates. 1st Prime Minister Research Fellow Symposium (PMRF symposium 2022), January 15th, 2022, IIT Delhi, India. (Poster)

7. **Nag, P.**, Kumar, N., Chanda, S., Dynamic impact analysis on implanted femur having intertrochanteric preclinical study to assess implant behaviour on sideways fall, World Congress of Biomechanics (WCB 2022), 10-14, July, 2022, Taiwan (Oral presentation).